UNIVERSITY OF SOUTHAMPTON

FACULTY OF PHYSICAL SCIENCES AND ENGINEERING

SCHOOL OF ELECTRONICS AND COMPUTER SCIENCE

Noncoherent Fusion Detection in Wireless Sensor Networks

by

Fucheng Yang

B. Eng., MSc.

A doctoral thesis report submitted in partial fulfilment of

the requirements for the award of Doctor of Philosophy

at the University of Southampton

September 2013

SUPERVISOR:

Professor Lie-Liang Yang

BEng, MEng, PhD, Senior Member IEEE

Professor of Communications, Signal Processing and Control Group

Department of Electronics and Computer Science

University of Southampton

Southampton SO17 1BJ

United Kingdom

Dedicated to my family

UNIVERSITY OF SOUTHAMPTON

ABSTRACT

FACULTY OF ENGINEERING AND APPLIED SCIENCE

School OF ELECTRONICS AND COMPUTER SCIENCE

Doctor of Philosophy

Noncoherent Fusion Detection in Wireless Sensor Networks

by Fucheng Yang

The main motivation of this thesis is to design low-complexity high efficiency noncoherent fusion rules for the parallel triple-layer wireless sensor networks (WSNs) based on frequency-hopping M-ary frequency shift keying (FH/MFSK) techniques, which are hence referred to as the FH/MFSK WSNs. The FH/MFSK WSNs may be employed to monitor single or multiple source events (SEs) with each SE having multiple states. In the FH/MFSK WSNs, local decisions made by local sensor nodes (LSNs) are transmitted to a fusion center (FC) with the aid of FH/MFSK techniques. At the FC, various noncoherent fusion rules may be suggested for final detection (classification) of the SEs' states.

Specifically, in the context of the FH/MFSK WSNs monitoring single M-ary SE, three noncoherent fusion rules are considered for fusion detection, which include the benchmark equal gain combining (EGC), and the proposed erasure-supported EGC (ES-EGC) as well as the optimum posterior fusion rules. Our studies demonstrate that the ES-EGC fusion rule may significantly outperform the EGC fusion rule, in the cases when the LSNs' detection is unreliable and when the channel signal-to-noise ratio (SNR) is relative high. For the FH/MFSK WSNs monitoring multiple SEs, six noncoherent fusion rules are investigated, which include the EGC, ES-EGC, EGC assisted N-order IIC (EGC-NIIC), ES-EGC assisted N-order IIC (ES-EGC-NIIC), EGC assisted ρ-order IIC (EGC-ρIIC) and the ES-EGC assisted ρ-order IIC (ES-EGC-ρIIC). The complexity, characteristics as well as detection performance of these fusion rules are investigated. Our studies show that the ES-EGC related fusion rules are highly efficient fusion rules, which have similar complexity as the corresponding EGC related fusion rules, but usually achieve better detection performance than the EGC related fusion rules. Although the ES-EGC is a single-user fusion rule, it is however capa-

ble of mitigating the multiple event interference (MEI) generated by multiple SEs. Furthermore, in some of the considered fusion rules, the embedded parameters may be optimized for the FH/MFSK WSNs to achieve the best detection performance.

As soft-sensing is often more reliable than hard-sensing, in this thesis, the FH/MFSK WSNs with the LSNs using soft-sensing are investigated associated with the EGC and ES-EGC fusion rules. Our studies reveal that the ES-EGC becomes highly efficient, when the sensing at LSNs is not very reliable. Furthermore, as one of the applications, our FH/MFSK WSN is applied for cognitive spectrum sensing of a primary radio (PR) system constituted by the interleaved frequency-division multiple access (IFDMA) scheme, which supports multiple uplink users. Associated with our cognitive spectrum sensing system, three types of energy detection based sensing schemes are addressed, and four synchronization scenarios are considered to embrace the synchronization between the received PR IFDMA signals and the sampling operations at cognitive spectrum sensing nodes (CRSNs). The performance of the FH/MFSK WSN assisted spectrum sensing system with EGC or ES-EGC fusion rule is investigated. Our studies show that the proposed spectrum sensing system constitutes one highly reliable spectrum sensing scheme, which is capable of exploiting the space diversity provided by CRSNs and the frequency diversity provided by the IFDMA systems.

Finally, the thesis summarises our discoveries and provides discussion on the possible future research issues.

Declaration of Authorship

I, **Fucheng Yang**, declare that the thesis entitled **Noncoherent Fusion Detection in Wireless Sensor Networks** and the work presented in it are my own and has been generated by me as the result of my own original research. I confirm that:

- This work was done wholly or mainly while in candidature for a research degree at this University;
- Where any part of this thesis has previously been submitted for a degree or any other qualification at this University or any other institution, this has been clearly stated;
- Where I have consulted the published work of others, this is always clearly attributed;
- Where I have quoted from the work of others, the source is always given. With the exception of such quotations, this thesis is entirely my own work;
- I have acknowledged all main sources of help;
- Where the thesis is based on work done by myself jointly with others, I have made clear exactly what was done by others and what I have contributed myself;
- Parts of this work have been published.

Signed: ..... Date: .....

Acknowledgements

Firstly, I would like to thank my supervisor Professor Lie-Liang Yang for his substantial supporting and generous guidance, from the bottom of my heart. His guidance and advice always bring me a brainstorm or help me overcome some complicated problems. All in all, this report would never gone this far without him. I am also grateful to other faculty members and researchers of the department, in particular of Prof. Lajos Hanzo, Prof. Sheng Cheng, Dr. Soon Xin Ng, Dr. Rober Maunder, Dr. Mohammed El-Hajjar and Dr. Rong Zhang, who have made my learning experience at the University of Southampton more than enjoyable.

I also owe many personal thanks to all my other colleagues in the Communication, Signal Processing and Control Group, particularly to Chen-Dong, for his help. I am also deeply indebeted to many friends of mine both in and outside Southampton for sharing my joys and sorrows.

Finally, I would like to dedicate this report to my beloved parents in China for their endless love, care and support.

List of Publications

1. **F. Yang and L.-L. Yang**, “A single-user noncoherent combining scheme achieving multiuser interference mitigation for FFH/MFSK systems ”, *IEEE Transactions on Communications*, Accepted 2013.

2. **F. Yang and L.-L. Yang**, “Low-complexity noncoherent fusion rules for WSNs monitoring multiple events ”, has been submitted to *IEEE Transactions on Aerospace and Electronic Systems*. (Revised)

3. **F. Yang and L.-L. Yang**, “Energy-Based Cooperative Spectrum Sensing of SC-FDMA Systems ”, has been submitted to *IEEE Transactions on Vehicular Technology*.

4. **F. Yang and L.-L. Yang**, “Frequency-hopping/M-ary frequency-shift keying for wireless sensor networks: Noncoherent detection and performance”, *The Seventh International Symposium on Wireless Communication Systems (ISWCS’10)*, pp. 135-139, 19th-22nd September 2010, York,UK. (Best Paper)

5. **F. Yang and L.-L. Yang**, “Frequency-hopping/M-ary frequency-shift keying wireless sensor network monitoring multiple source events”, *IEEE 75th Vehicular Technology Conference (VTC’12 Spring)*, pp. 1-5, 2012.

6. **F. Yang and L.-L. Yang**, “Frequency-hopping/M-ary frequency-shift keying wireless sensor networks with soft-sensing”, *First IEEE International Conference on Communications in China (ICCC’12)*, pp. 751-756, 2012.

Contents

List of Symbols

General Conventions

- $\boldsymbol{A} \otimes \boldsymbol{B}$ indicates the Kronecker product operation between $\boldsymbol{A}$ and $\boldsymbol{B}$.
- $\boldsymbol{A} \boxplus \boldsymbol{B}$ indicates the element-wise addition of $\boldsymbol{A}$ and $\boldsymbol{B}$ in the Galois field $GF(M)$.
- $\boldsymbol{A} \boxminus \boldsymbol{B}$ indicates the element-wise subtraction of $\boldsymbol{A}$ and $\boldsymbol{B}$ in the Galois field $GF(M)$.
- $\oplus$ indicates the addition operation in the Galois field $GF(M)$.
- $\ominus$ indicates the subtraction operation in the Galois field $GF(M)$.
- $|\ |^2$ denotes the square-law operation
- The superscript * indicates complex conjugation. Hence, X^* represents the complex conjugate of the variable X.
- The superscript ^{T} indicates transpose operation. Hence, $\mathbf{X}^T$ represents the transpose of the matrix $\mathbf{X}$.
- The superscript ^{H} indicates complex conjugate transpose operation. Hence, $\mathbf{X}^H$ represents the hermitian of the matrix $\mathbf{X}$.

Special Symbol

$\boldsymbol{r}$: The received signals at the fusion center

$\mathbb{E}[\mathcal{L}]$: The expected lifetime of wireless sensor networks

$\mathbb{E}[E_\omega]$: The expected energy wasted

$\mathbb{E}[E_r]$: The expected reporting energy

ε_0: The the total initial energy

$\mathcal{P}_c$: The constant continuous power consumption

ν: The average local sensor nodes reporting rate

H_m: The mth state of the observed source event (SE)

P_m: The probability of occurrence of hypothesis H_m

D_i: The decision made by the fusion center (FC)

C_{ij}: The cost associated with the decision D_i given that the true hypothesis is H_j

R: The average cost function

P_d: The local detection probability

P_m: The local missing probability

P_f: The local false-alarm probability

P_e: The local error probability

P_c: The local correct probability

P_D: The overall detection probability

P_M: The overall missing probability

P_F: The overall false-alarm probability

P_E: The overall error probability

P_B: The overall error probability per bit

P_C: The overall correct probability

$P(D_i, H_j)$: The joint probability of deciding D_i while H_j is true

$\Lambda(\boldsymbol{y})$: The likelihood ratio

$\mathcal{L}\Lambda(\boldsymbol{r})$: The log-likelihood ratio

M: The number of the observed SE's states

L: The number of LSNs

K: The number of SEs

I: The number of erasured elements per row

N: The number of iterative interference cancellation operations

r_l: The observation for the lth LSN

A_m: The amplitude corresponding to the mth state

n_l: The observation noise for the lth LSN

γ_s: The observation SNR at the LSNs

$Q_{(x)}$: The Gaussian Q-function

$\boldsymbol{F}$: The frequency band used by MFSK modulation

$\boldsymbol{a}$: The FH address of single SE

$\boldsymbol{s}$: The local estimations of single SE by L LSNs

$\boldsymbol{m}$: The results after FH operation with single SE

T_s: The total transmission time of L LSNs

T_h: The transmission time of each of the L LSNs

$\tilde{s}_l(t)$: The signal transmitted by the lth LSN during one time-slot

P: The transmission power

f_c: The main carrier frequency

ϕ_l: The initial phase introduced by carrier modulation of the lth LSN

$\psi_{T_h}(t)$: The pulse-shaped signalling waveform

$r_l(t)$: The received signal at the FC from the lth LSN during one time-slot

h_l: The channel gain with the respect to the lth LSN

$n(t)$: The Gaussian noise process presenting at the FC

$\boldsymbol{R}$: The received matrix after square-law operations

R_{ml}: The element of matrix $\boldsymbol{R}$ with respect to the lth LSN and the mth decision variable before frequency-dehopping operations

Ω: The average channel power

$\mathbf{1}$: An all-one column vector of M-length

N_{ml}: The complex Gaussian noise sample collected from the mth frequency band over the lth time-slot

E_s: The total energy per symbol

E_h: The transmitted energy by each of the LSNs per symbol

$\boldsymbol{D}$: The decision matrix after of single SE

$\bar{\boldsymbol{D}}$: The decision matrix of single SE after erasure operations

X: A given state of the observed SE

$\mathcal{X}$: A set containing the M possible states

$\mathcal{X}_W$: The range of possible states of SE based on EGC fusion rule

W: The number of possible states of SE based on EGC fusion rule.

M': The number of possible LSN's decisions

$\lfloor L/2 \rfloor$: The smaller or equal to $L/2$ nearest integer operation

A_i: The probability that i out of L LSNs make correct detections

$\bar{\gamma}_s$: The average SNR per symbol

$\bar{\gamma}_L$: The average SNR per symbol over each LSN

ψ: The characteristic function

I_L: The Lth-order modified Bessel function of the first kind

$\boldsymbol{A}$: The FH address used by the WSN with multiple SEs

$\boldsymbol{S}$: The local estimations of multiple SEs

$\boldsymbol{M}$: The results after FH operation with multiple SEs

$\boldsymbol{a}_k$: The FH address for the kth SE

$\boldsymbol{s}_l$: The local estimations of the K SEs by the the lth LSN

$\tilde{s}_{k,l}(t)$: The signal transmitted by the lth LSN for the kth SE during one symbol-duration

$h_{k,l}$: The channel gain corresponding to the MFSK frequency band activated for the kth SE by the lth LSN.

$\boldsymbol{D}_k$: The detection matrix for the kth SE

$\bar{\boldsymbol{D}}_k$: The modified detection matrix for the kth SE after erasure operation

$\hat{s}_k$: The overall estimation of the kth SE

L_k: The reliability measurement of the kth SE based on the detection matrix $\boldsymbol{D}_k$

$\boldsymbol{R}^{(i)}$: The updated received matrix after $(i-1)$ times IIC operations

$\boldsymbol{D}_k^{(i)}$: The detection matrix for the kth SE after $(i-1)$ times IIC operations

$\bar{L}_k$: The reliability measurement of the kth SE based on the modified detection matrix $\bar{\boldsymbol{D}}_k$

$U+1$: The number of multipaths of communication channels

$\boldsymbol{\mathcal{F}}_N$: The N-point FFT matrix

List of Figures

Chapter 1

Introduction

1.1 Research Background

Wireless sensor networks (WSNs) have become increasingly important and relevant to research communities as well as military and civilians [1]. Briefly, there are two main reasons behind driving the researches and applications of WSNs. The first one is the advancement of technologies, which enables WSNs to have low-cost sensors, reliable wireless communications and rapid single-chip computation capability [2, 3]. The second one is the wide-range applications of WSNs, such as surveillance, health-care, disaster recovery, home automation, etc., which may influence our daily life comprehensively [2, 4].

WSNs are the result of rapid convergence of various technologies: digital circuitry, wireless communications, micro-electromechanical systems (MEMS), and ad hoc networks. Based on the resemblance of the existing techniques, WSNs work with unique characteristics as follows. Typically, the tiny local sensor nodes (LSNs), which consist of sensing, data processing and communicating components, leverage the idea of WSNs [5]. Usually, WSNs are composed of a large number of LSNs that are densely deployed either inside the phenomenon or very close to it [6]. Owing to their self-organizing capability of WSNs' protocols and algorithms, the positions of LSNs need not to be predetermined [7]. The low-cost LSNs are usually prone to failures. However, the WSNs are robust to failures, when a big number of LSNs are densely deployed. The topology of WSN's framework may be changed without significant change on protocols and fusion rules. In the most widespread parallel WSN model, LSNs do not communicate with each other, but communicate us-

ing broadcast paradigm. The tiny LSNs have the limits on size, power consumption, computation capacity and memory [8, 9]. Furthermore, in large-scale WSNs, LSNs may not have their global identification (ID) because of the large amount of overhead generated by the large number of LSNs.

To achieve optimal performance in a WSN system, many aspects should be carefully considered [10–16], which include the topology structure, medium access control (MAC), sensing capacity, energy efficiency, signal processing at LSNs, fusion rules, applications, etc. In the following sections of this chapter, some of the above mentioned aspects will be discussed in detail. The reminder of this chapter is organized as follows. In Section 1.2, we introduce some basic topology structures used in WSNs. In Section 1.3, some MAC protocols are reviewed. In Section 1.4, we consider the energy-efficient communication in WSNs as well as the definition of lifetime of WSNs, which is followed by a summary of some applications of WSNs in Section 1.5. Finally, the organization of this thesis is given in Section 1.7.

1.2 Topology Structures of WSNs

The topology of WSNs defines the process of data collection and signal detection [1, 7, 17, 18]. Meanwhile, the topology structure of a WSN imposes significantly influence on the signal processing, life-time and detection performance of the WSN. Before choosing a suitable topology of a WSN, many constraints should be considered, including the communication among LSNs, the link quality between LSNs and fusion center (FC), the robustness of signal processing algorithms, etc. Typically, there are four different topology frame works, which include the parallel topology with FC, parallel topology without FC, serial topology and tree topology [10]. Below we briefly describe these four topologies, as well as their advantages and disadvantages.

1.2.1 Parallel Topology with Fusion Center

Fig 1.1 shows the WSN structure with parallel topology with a FC [10], where L LSNs are used to simultaneously observe the source event(s) (SE(s)). Note that, we assume that the quantifications are carried out at the LSNs, as the observed SEs are always analogue. In Fig 1.1, $H_0,\ H_1, \cdots, H_{M-1}$ denote the M hypotheses or possible states about the SE, $\mathcal{D}_1,\ \mathcal{D}_2, \cdots, \mathcal{D}_L$ denote the local detection rules, while $\mathcal{D}$ represents the fusion rule used by the FC. $r_1,\ r_2, \cdots, r_L$ are the observations

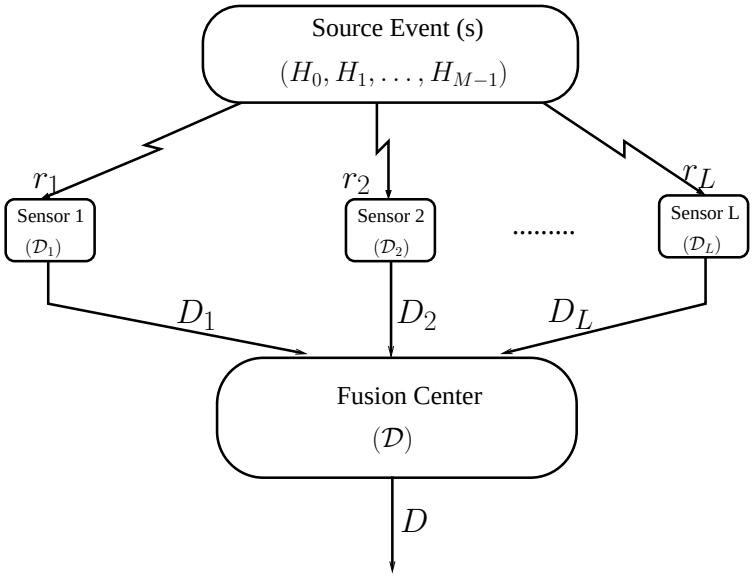

Figure 1.1: Basic structure of parallel WSN with fusion center.

obtained by the L LSNs, based on which the detection outputs $D_1,\ D_2, \cdots, D_L$ are obtained with the aid of $\mathcal{D}_1,\ \mathcal{D}_2, \cdots, \mathcal{D}_L$. Finally, D represents the detection of the FC. In this structure, the identical LSNs do not communicate with each other and the FC does not feed back any information to the LSNs. Based on their own observations, the L LSNs make their local detections independently and then transmit their local decisions to the FC separately. Specifically, in the case of using hard local detection, each local decision may take corresponding value, which is dependent on the LSN's decision about which state the observed SE is in. In the case of using soft local decision, the local observation space is partitioned into more nuanced regions so as to yield more accurate local decisions. Finally, at the FC, the received signals from all the L LSNs are combined based on various fusion rules, in order to make a global decision. In this type of WSN, when one or several LSNs make erroneous local decisions, or some links between LSNs and FC are failed, detection performance of final decision may not degrade significantly, provided that there are a sufficient number of LSNs left. Usually, the WSNs with FC is capable of achieving a better detection performance than the WSNs without FC, but at the cost of higher complexity and delay.

1.2.2 Parallel Topology without Fusion Center

Fig 1.2 shows a parallel topology WSN without FC [10, 19], which is similar as Fig 1.1 but without a FC. In Fig 1.2, there are L individual LSNs monitoring single or multiple SEs independently. The

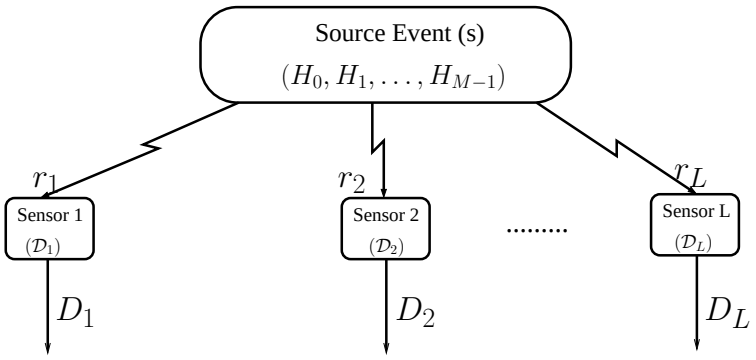

Figure 1.2: Basic structure of parallel WSN without FC.

local decisions are made by the L LSNs based on their separate local observations. The LSNs do not communicate with each other. However, their operations are coupled, due to the fact that the cost of decision making is coupled and that a system-wide optimization is usually performed [19]. In this structure, the decisions by the LSNs are not corrected to make further decision. This kind of topology enables WSNs to work with low-complexity and low-delay. However, this type WSNs without FC are hard to satisfy the requirement of high detection performance.

1.2.3 Serial Topology

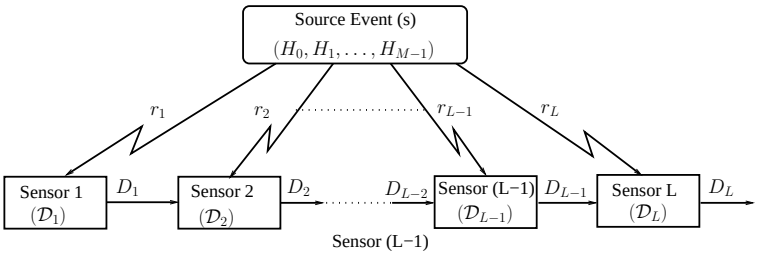

Figure 1.3: Basic structure of serial topology WSN.

In a WSN with serial topology [10, 19], as shown in Fig 1.3, L LSNs are used to observe single or multiple SEs. As shown in Fig 1.3, one LSN makes its local estimation based on its own observation and the information received from the previous LSN. In more detail, the first LSN does not receive any information from the other LSNs and hence its local decision is made solely based on its own observation. This local decision from the first LSN is then transmitted to the second LSN, which uses it in conjunction with its direct observation to make its decision, which will be sent to the next LSN. This process is repeated at each of the LSNs in the serial network. Finally,

the Lth LSN makes the final decision based on the aggregated information received directly from the $(L-1)$th LSN and its own observation received from the SE.

Compared with the WSNs with parallel topology, as shown in Fig 1.1 and Fig 1.2, WSNs with serial structure are prone to generate erroneous propagation, if the previous LSNs make erroneous local decisions. For this structure, the computation delay accumulates, because a LSN has to wait for decisions of the previous LSNs. Furthermore, the delay may become unacceptable for some LSNs in a large scale serial WSN system. Additionally, the serial topology WSN is sensitive to the failures of one or several LSNs.

1.2.4 Tree Topology

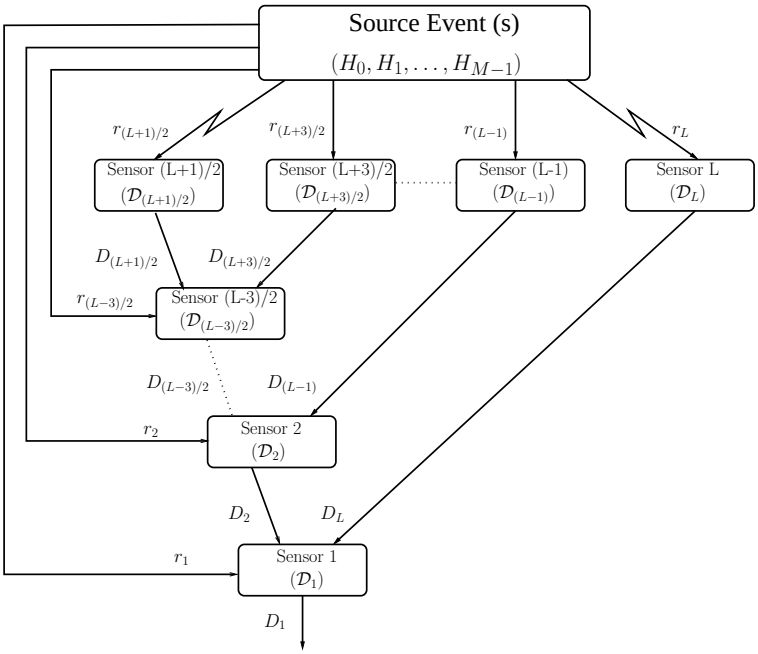

Figure 1.4: Basic structure of tree topology WSN.

Thus far, we have introduced the structures for the parallel WSNs and the serial WSNs. As indicated earlier, the topology of WSNs can be organized in a variety of configurations. One typical example is the tree topology [10]. In a WSN with tree topology, LSNs form a directed acyclic graph, where the first LSN is the root of the tree and information from all the other LSNs flows on a unique path toward it [19]. As shown in Fig 1.4, L LSNs are applied to observe single or multiple SEs. Among these L LSNs, some of them monitor the SEs directly and transmit their local decisions to some other LSNs. As shown in Fig 1.4, there are some LSNs, which do not directly observe the

SEs but get information from the other LSNs, in order to make their decisions.

In comparison with the previous serial topology, in this tree topology, the ith $(1 \leq i \leq \frac{L-3}{2})$ LSN makes its local decision based on its own observation and two other LSNs' estimations. While, for the other LSNs, local decisions are made just based on their own observations. On the other hand, in comparison with the WSNs with parallel topology or serial topology, the WSNs with tree topology rely more on the reliability of the whole WSN system. The links existing among different LSNs make the WSN system more complex and generate more delay. The local detection performance of some of the LSNs are affected by by their own observations as well as the other LSNs' decisions.

1.3 Medium Access Control Protocols for WSNs

In some applications, WSNs consisting of a large number of miniaturized batter-powered LSNs are required to operate for years without human intervention [12]. Hence, there has been a growing interest on optimization of WSNs, so that the limited resource carried by a WSN is capable of maintaining it in efficient operation for a long time. Typically, the optimization is involved with novel signal processing algorithms, energy-efficient MAC protocols, self-organizing and reliable data aggregation algorithms, etc. [13, 20]. In WSNs, the design of MAC protocols glues and integrates these optimization facets, by considering the constraints imposed by the limited energy budget of LSNs together with the requirement of long lifetime [21]. To satisfy the unique requirements of WSNs, many MAC protocols have been designed or modified from the existing ones for the other purposes. As some examples, the MAC protocols used by WSNs include the gateway MAC (G-MAC) [22], self-organizing MAC for sensor networks (SMACS) [23], traffic adaptive medium access (TRAMA) [24], flow-aware medium access (FLAMA) [25], energy efficient MAC (EMAC) [26], position-enabled MAC (PMAC) [27], mobility adaptive MAC (MMAC) [28], multi-frequency MAC for WSNs (MMSN) [29], ect. All these MAC protocols are modified based on the existing canonical ones. In this section, two typical multiple-access schemes used by the MAC protocols are discussed, which are the time-division multiple-access (TDMA) and carrier sense multiple-access (CSMA).

1.3.1 Time Division Multiple Access

TDMA belongs to the typical category of reservation-based protocols [26], which requires the knowledge of network topology to establish a schedule, so that each of the nodes is capable of accessing the channel and communicating with the other nodes, while avoids interference from the other nodes. Under the TDMA principles [30], time is divided into frames and each frame is further divided into time-slots. In WSNs, operated in TDMA, each LSN is assigned a unique time-slot during which it has the priority to communicate. In the TDMA protocol, the transmission does not suffer from collisions. The scheduling delay is usually acceptable.

TDMA scheme is very efficient, when the source requirements are predictable and each of the nodes always has data to send. However, it is inefficient, when traffic is light. In this case, some time-slots might be wasted as there is no data to transmit. Under TDMA, the throughput is hard-limited. Hence, it cannot undertake bursty traffic beyond utilization of all the available time slots. For this sake, it is essential for the TDMA-based schemes to have the knowledge of network topology and time synchronization. However, the estimation of topology and implementation of time synchronization require a big overhead or/and expensive hardware. For this reason, TDMA scheme becomes less attractive in large scale WSNs.

1.3.2 Carrier Sense Multiple Access

In order to reduce the requirements of TDMA and make efficient use of time-slots, the CSMA is introduced, which does not need global synchronization and topology knowledge of WSNs [20]. Under the principles of CSMA, each of the LSNs first senses the channel before transmission. If the channel is found to be busy, the LSN then postpones the transmission to avoid collision. By contrast, when the LSN finds the channel is not being occupied, it then starts transmission.

The CSMA scheme has the following characteristics. First, the operation of CSMA does not rely on the knowledge of topology structure and is robust to LSNs' mobility. Therefore, CSMA is a good candidate for WSNs with mobility. Second, the capability of avoiding collision reduces interference by preventing transmission on occupied channels, yielding a better detection performance. In comparison with the TDMA, the throughput of CSMA may decrease significantly, when traffic load is heavy, in this case, a lot of resource needs be used for channel sensing. Additionally,

in terms of energy-efficiency, CSMA may not perform as well as TDMA. This shortcoming makes the CSMA not very useful for the WSNs that require high energy-efficiency.

1.4 Energy-Efficient Communication and Law of Lifetime

Some WSNs, such as distributed WSNs, with hundreds of LSNs promising a continuous and maintenance-free observation of the environment [31] have several unique characteristics, including high LSN density, low data rate and stringent energy limit. Battery-powered WSNs may be applied indoor or outdoor without maintenance for a couple of years. Therefore, during the research of WSNs, a significant focus has been put on high energy-efficiency to extend the life-time of WSNs.

Design an energy-efficient protocol for WSNs demands a throughout investigation of the interactions among the sensor application, network protocol, MAC layer and RF communication, etc. Some energy-efficient upper layer protocols and algorithms have been proposed, such as, the energy-efficient MAC protocol [21], low duty cycle sleeping scheduling [32, 33], energy-aware routing protocol [14], etc. Generally speaking, energy control and energy management are two major techniques used in WSNs, even though they appear in various forms at different layers.

On the other hand, lifetime is a crucial factor of large-scale WSNs in many applications, where it is impossible or infeasible to replace or maintain the LSNs once that are deployed [15]. In literatures, various methods have been proposed to maximize the lifetime of WSNs [15, 17, 34, 35]. In WSNs, the lifetime depends on many factors, including network architecture, specific application, various parameters of protocol, etc. In [34], a simple law that reflects WSNs' lifetime for any applications under any network configurations has been provided. This law of lifetime not only identifies the two key physical layer parameters that affect WSNs' lifetime, but also plays as a guidance for maximization of WSNs' lifetime. Below we consider the energy-efficient communication in WSNs as well as the lifetime issues concerned by WSNs.

1.4.1 Energy-Efficient Communication

In a little more detail, the energy consumption of communication subsystem in WSNs can be divided into two parts, the first part is related to the power for signal transmission, while the second

part is the energy consumed by receiver circuit [34]. Hence, minimizing the energy-consumption of both parts is crucial, as receiver may consume as much energy as transceiver. In WSNs, many LSNs may be located in the receiving ranges of some other LSNs. In this case, it is beneficial to shut down the radio receivers of the idle LSNs. However, most MAC protocols utilize unique addresses to route packets to some specific destinations, with the expectation that these destinations are actively listening to packets. Once some receivers are shut down, the routing among different LSNs may become unstable.

In comparison of the energy-efficiency between multihop transmission and direct transmission WSNs, the result is depended on the scale of the considered WSN. Explicitly, a LSN in a WSN always seeks the nearest LSN as a candidate for its next hop of transmission. However, this will result in multihop transmission. In a multihop WSN, due to the propagation pathloss of wireless signals, it becomes advantageous to increase the number of hops in terms of energy consumption. In practice, there is a range of distances for which direct transmission maybe more energy-efficient than multi-hop transmission. In a direct communication WSN with fusion center (FC), each LSN sends data directly to the FC. When the FC is far away from the LSNs, direct communication will consume a large amount of transmission power. This will deplete the LSNs' power quickly and shorten the lifetime of WSNs significantly. In this case, multihop WSNs outperform direct communication WSNs in term of energy-efficiency. On the other hand, when the transmission distance between LSNs and FC is short and/or the radio electronics energy is high, direct transmission is more energy-efficient than multihop transmission.

1.4.2 Law of WSNs Lifetime

The power constraint of LSNs imposes many fundamental limitations, such as, lifetime on the design of WSNs. The lifetime of a WSN is referred to as the time period that a WSN has the ability to collect data from entire network domain and process the sensing information [34]. Given a WSN, different deployment strategies for LSNs may result in different life time. The most effective approach for deployment for LSNs is placing the LSNs in a controllable manner, so that the maximal lifetime is achievable. Unfortunately, this is not technically feasible in large-scale WSNs. Furthermore, in some applications, the locations of LSNs may not be physically reachable or fixed, due to the limitations of different perspectives.

In designations of WSNs, there are various factors need to be optimized in order to extend the lifetime of WSNs. These factors include network architecture and protocols, data collection initiation, channel characteristics, energy consumption model, etc [34–36]. In literatures, many research has been done in order to estimate the lifetime of WSNs. For example, the upper bounds of lifetime have been derived in [35–38] for various WSNs. Additionally, in [15], formulas for the lifetime of WSNs have been derived based on 2D Gaussian distribution .

In [34], a general formula for the lifetime of WSNs is provided, which holds regardless of the underlying network model. In [34], the lifetime of WSNs is defined as the time span from that the WSN is built up until that the WSN is nonfunctional. Here, the nonfunctional instant may be explained in different ways, such as, when a certain number of LSNs are out of power, the instant when a desired area is impossible to monitor, the instant when LSNs cannot communicate with FC, the instant when the detection performance is unacceptable, etc. According to [34], the average lifetime of WSNs can be expressed as

$$\mathbb{E}[\mathcal{L}] = \frac{\varepsilon_0 - \mathbb{E}[E_\omega]}{\mathcal{P}_c + \nu \mathbb{E}[E_r]} \tag{1.1}$$

where $\mathbb{E}[\mathcal{L}]$ is the expected average lifetime of WSNs, ε_0 is the total initial energy, $\mathbb{E}[E_\omega]$ is the expected energy wasted, $\mathcal{P}_c$ is the constant of continuous power consumption, ν is the average LSN reporting rate defined as the number of data collections per unit time and $\mathbb{E}[E_r]$ is the expected reporting energy consumed by all the LSNs in a randomly chosen data collection. Eq (1.1) is suitable for any WSNs under a general setting: arbitrary network architecture, arbitrary channel and radio models and arbitrary definition of lifetime. According to (1.1), when the total initial energy ε_0 is given, reducing the value of $\mathbb{E}[E_r]$ or $\mathbb{E}[E_\omega]$ will improve the lifetime of the WSN. These two factors reflect the influence of channel condition and residual energy on the WSN's lifetime. Therefore, in order to maximize the lifetime of WSN through minimizing $\mathbb{E}[E_r]$ and $\mathbb{E}[E_\omega]$, a protocol should exploit effectively the channel state information (CSI) and the information about the residual energy of all the LSNs.

1.5 Applications of WSNs

Recently, achievements in micro-sensors technology, energy-efficient electronics and wireless communications make WSN become realities in applications [16, 39]. Proposed applications of WSNs

include environmental monitoring, natural disaster prediction and relief, homeland security, healthcare, manufacturing, transportation, home appliances and entertainment, etc. Each of the proposed applications can be further divided into different categorise of emphasis or measurement. Some previous work on WSN applications on environmental monitoring, health care, military and spectrum sensing in cognitive radio are detailed as follows.

1.5.1 Applications of WSNs in Environment Monitoring

With the significant development of human society, environmental issues have become highly important for manifestation of civilization and life quality. Environment monitoring represents the way of human understanding, foreseeing and utilizing the nature [40, 41]. During a long history, it is restrictive for human being to monitor inaccessible environments such as, ocean, desert and mountain, etc, based on traditional methods. Distributed WSNs are capable of monitoring a large-scale range by deploying small-size LSNs, while without human maintaining. Therefore, the emergence of WSNs builds a bridge between human being and physical world, which is able to extend humans being's capability to cooperate with nature.

In [40], a distributed WSN is proposed, which uses mote hardware to gather data for seven environmental parameters, including barometric pressure, ambient humidity, wind direction, wind speed, underground water level and rainfall. In this proposed WSN, the sensed data is transmitted through multihop transmission to the FC for further decision.

Realizing that there are deficiencies for both fixed and mobile WSNs, researchers are looking for a more formal method of integrating these two kinds of systems to achieve greater spatiotemporal measurement coverage. In [42], one reasonable method is introduced by combining the WSNs and robotic systems together, in which the signals are shared among LSNs and robot. This kind of robotic WSNs have certain capability of improving data quality, measurement certainty, accurate real-time modelling and mapping of large environmental processes.

A framework of WSN has been built in [43] for aquatic environmental monitoring, where many factors are carefully treated during the design of the marine monitoring WSNs, such as, sensing activity, wireless transmission form LSNs to FC, signal processing and battery power, etc. In [43], a power-aware and adaptive TDMA protocol guarantees robust transmissions and adaptability to

topology changes. To optimize energy storage and prolong batteries lifetime, each unit of this WSN is endowed with adaptive solar-energy-harvesting mechanisms and tandem batteries.

1.5.2 Applications of WSNs in Healthcare

It is well known that the aged population in the world is increasing and a considerable percentage of them are suffering from chronic illness [44]. Novel advanced technologies, such as wearable devices and WSNs can help patients and caregivers by providing continuous medical supervision, demotic healthcare control, rapid access to medical data, emergency communication , etc., both at home and at hospital [45–48]. During the past decades, there has been an increasing demand for intelligent devices, which are capable of detecting the vital factors without interfering the daily routine of those who use them [49]. Owing to above-mentioned information, WSNs may find a lot of applications in healthcare by providing monitoring and service to the dependent patients.

Generally, there are mainly three parts of health care WSNs, which include the body sensor network, wireless communication and healthcare devices [50]. In terms of body sensor network, smart wearable devices with sensors have been designed for providing healthcare to the dependent patients [51], such as blood pressure, body temperature, humidity, etc. Furthermore, with the help of smart wearable devices, it is possible to automatically execute healthcare manage and improve the assistance to patients in geriatric facilities. A bridge between body sensor network and the public communication network may be built, through which the collected data is transmitted to the central server. At the central server, diagnosis and healthcare suggestion are made based on the received sensed data [52–54].

Through the realization of WSN healthcare applications, there are still many tasks that should be carefully treated. First, the sensed data from human being is always analogy and complex biological signal, which is difficult to be quantified [52]. Second, transmission and handing with a large scale of data from body sensors consume remarkable communication resource, which brings a burden to the quick and reliable healthcare response [50].

1.5.3 Applications of WSNs in Military

WSNs were originally developed mainly for military surveillance with the features of robustness, self-organizing and fault-tolerance [55]. Typically, radar, sonar, infra-red, etc, may be used for a military WSN to collect the battlefield information and send it to the FC in order to make a more reliable decision [10].

WSNs are widely applied for different military purposes, which are detailed as follows [56–63]. First, WSNs can be employed to prevent the base and headquarters from being attacked [56]. Second, instantaneous information in the battlefield can be used for planning future operations and missions [64]. Third, thousands of low-complexity and low-cost LSNs can be scattered in enemy forces areas indetectablely for sensing and collecting useful information.

During the design of military WSNs, there are many challenges to satisfy the serious requirements of robustness, self-organizing and reliability. First, as a large amount of sensor nodes in remote area cannot be deployed predictably, they must identify their neighbours quickly and build the network automatically. Second, military WSNs are designed of having certain capability of resisting both human and nature influence. Third, since, in most scenarios, the distributed sensor nodes cannot be recharged or maintained, the energy efficiency of sensor nodes should be carefully treated.

1.5.4 Applications of WSNs in Spectrum Sensing

Supporting cognitive radio (CR) users through a collateral WSN to spectrum sensing has recently been proposed as a popular approach to overcome spectrum sensing limitations of wireless communication system [65–69]. Explicitly, there are mainly two reasons for using spectrum sensing [70]. First, radio spectrum is an extremely scarce resource. Over the past years, traditional approaches to spectrum management have been challenged by new insights into the actual use of spectrum. In most countries, all frequencies have been completely allocated to specific operators and users. For examples, the National Telecommunication and Information Administration (NTIA) frequency allocation chart indicates multiple allocations over essentially all of the frequency bands. Thus, within the current regulatory framework, spectrum appears to be a scarce resource. Second, actual measurements indicate low spectrum utilization, which can be found in Spectrum Policy Tast

Force report from Federal Communications Commission (FCC). Conventional radios are regulated by fixed spectrum allocation policies, which are operated in certain time frames, over certain frequency bands and within certain geographical regions. These static spectrum assignment policies have resulted in low-efficiency in usage of the precious spectrum resources. For example, the measurement shows that the average spectrum occupancy from 30 MHz to 3 GHz over six cities is 5.2% and that the maximum total spectrum occupancy is 13.1% in New York City.

Cognitive radio (CR) is introduced to overcome above the mentioned problems, which is a typical spectrum sensing assisted cooperative radio. In CR terminology, primary radio (PR) users have higher priority or legacy rights on the usage of spectrum, while, CR users have lower priority. Hence, it is critically important for CR users to sense the frequency bands assigned to PR users but not used at a particular time and geographic location [65]. However, it is hard for CR users to scan a wide range of frequency bands, due to the scarce resource (energy, hardware limitation, etc.). Furthermore, depending on the PR and CR network location and topologies, the CR users may not sense the spectrum with sufficient accuracy. In this case, WSNs are employed for spectrum sensing in CR systems, which are capable of achieving satisfactory results in terms of efficient use of available spectrum and reducing interference with PR users.

In [67, 68, 71, 72], a WSN is employed to assist the CR network by providing information on the current spectrum occupancy in spatial or time domain. Specifically, in [68], a WSN system is deployed to provide distributed spectrum sensing for cognitive operation, in which the spectrum sensing performance of WSN is evaluated as a function of the network density. Then, the WSN architecture is considered in [73], which is a key issue for spectrum sensing jointly in space and time. Furthermore, [65] proposes a protocol for a WSN supporting CR devices, in which the fundamental trade-off between statistics of the PR traffic, the interference range and transmit power of CR user is studied. It also extends the spectrum sensing problem from the spatial dimension to fast dynamics of primary traffic.

1.6 Novel Contribution

The main contribution of this thesis are as follows:

- A novel triple-layer wireless sensor network (WSN) assisted by M-ary frequency-shift key-

ing (MFSK) modulation and frequency-hopping (FH), referred to as the FH/MFSK WSN is proposed. The FH/MFSK WSN is benefit from the embedded advantages of noncoherent MFSK and FH techniques. First, low-complexity noncoherent detection can be employed, which does not depend on energy-greedy channel estimation and, hence is beneficial to the life-time of energy limited WSNs. Second, FH/MFSK techniques are capable of enhancing the detection performance of the WSN by reducing the correlation among the signals transmitted by different local sensor nodes (LSNs).

- We conceive a novel erasure-supported equal gain combining (ES-EGC) fusion rule, which is first employed by the FH/MFSK WSN monitoring single source event (SE). In comparison with the conventional equal gain combining (EGC) fusion rule, our proposed novel ES-EGC fusion rule may significantly improve the detection (classification) performance of FH/MFSK WSNs, at low-cost of computation increasement. Furthermore, a closed-form union-bound for the average error classification probability (ECP) of the FH/MFSK WSNs using ES-EGC is derived.

- We further extend our research to a FH/MFSK WSN monitoring multiple SEs. As in this case, there is multiple event interference (MEI), iterative interference cancellation (IIC) is introduced to suppress the MEI. Six low-complexity noncoherent fusion rules are studied and compared. In detail, these fusion rules include the benchmark EGC and the proposed ES-EGC, EGC assisted N-order iterative interference cancellation (EGC-NIIC), ES-EGC assisted N-order IIC (ES-EGC-NIIC), EGC assisted ρ-fraction IIC (EGC-ρIIC) as well as the ES-EGC assisted ρ-fraction IIC (ES-EGC-ρIIC). The complexity of these fusion rules is analyzed. Our studies show that the ES-EGC related fusion rules in general outperform the corresponding EGC related fusion rules. The ES-EGC is a high-efficiency single-user fusion rule, which, for some cases, may achieve even better detection performance than some of the noncoherent multiuser fusion rules, such as, the EGC-NIIC fusion rule.

- In order to improve the detection performance of the FH/MFSK WSNs monitoring single SE, we incorporate soft-sensing into LSNs, where soft information is used to scale the transmission power of the MFSK tones sent to the FC. In comparison with hard local decisions, our studies show that using soft-sensing is capable of enhancing the detection performance of the

FH/MFSK WSN. Furthermore, the ES-EGC fusion rule is robust to the errors made by LSNs, which may significantly outperform the EGC fusion rule, especially, when the soft-sensing at LSNs is not very reliable.

- Finally, as one of the applications, a FH/MFSK WSN assisted cognitive spectrum sensing system is proposed specifically for spectrum sensing of an interleaved frequency-division multiple access (IFDMA) primary radio (PR) system supporing multiple users. Associated with our studies, three types of energy-based detections and four synchronization scenarios are considered during the local detections at cognitive radio sensing nodes (CRSNs). Our studies demonstrate that reliable local sensing is achievable at the CRSNs even at very low SNR. We furthermore demonstrate that the ES-EGC fusion rule is a high-efficiency fusion rule, which is capable of attaining much better overall detection performance than the EGC fusion rule.

1.7 Thesis Organization

In this thesis, parallel triple-layer wireless sensor networks (WSNs) assisted by M-ary frequency-shift keying (MFSK) modulation and frequency-hopping (FH), referred to as the FH/MFSK WSN, are investigated for different applications. The report is structured as follows.

In Chapter 2, we first provide a literature overview of the classical binary testing at LSNs. Then, both the channel-aware fusion rules and noncoherent M-ary fusion rules are discussed. Then, existing approaches for local spectrum sensing are reviewed. All the fusion rules and local spectrum sensing approaches are analyzed in the context of their advantages and disadvantages, as well as the requirements and application limits.

In Chapter 3, we investigate the detection performance of FH/MFSK WSNs monitoring single source event (SE) with hard local decisions, when assuming communications over additive white Gaussian noise (AWGN) channels or Rayleigh fading channels. The principle of our proposed FH/MFSK WSN is first introduced, which includes the signal classification at local sensor nodes (LSNs), signal transmission schemes for LSNs and signal classification at fusion center (FC). In this chapter, three different noncoherent fusion rules are considered and their performance is compared. Furthermore, the error classification probability (ECP) of some fusion rules is analyzed and

compared. Finally, some simulation results are provided to illustrate the ECP performance of the proposed FH/MFSK WSN with various fusion rules.

In Chapter 4, a parallel triple-layer FH/MFSK WSN with hard local decisions is proposed to monitor multiple SEs of each having multiple states. In this FH/MFSK WSN, multiple SEs are observed by a number of LSNs, each of which simultaneously observes all the SEs. The LSNs convey their decisions about the SEs' states to the fusion center (FC) with the aid of the FH/MFSK techniques. At the FC, the SEs' states are detected based on noncoherent fusion rules. In this chapter, six low-complexity noncoherent fusion rules are studied. They include the conventional benchmark of equal gain combining (EGC) and five proposed noncoherent fusion rules, namely the erasure-supported EGC (ES-EGC), EGC assisted N-order iterative interference cancellation (EGC-NIIC), ES-EGC assisted N-order IIC (ES-EGC-NIIC), EGC assisted ρ-fraction IIC (EGC-ρIIC) as well as the ES-EGC assisted ρ-fraction IIC (ES-EGC-ρIIC). The complexity of these fusion rules is analyzed and the performance of the FH/MFSK WSN employing, respectively, these fusion rules is investigated and compared, when assuming that the wireless channels from LSNs to FC experience independent Rayleigh fading. Furthermore, the impact of the parameters embedded in the various fusion rules on the design and performance of the FH/MFSK WSN is analyzed.

In Chapter 5, a soft-sensing and signal transmission scheme is proposed for improving the reliability of FH/MFSK WSNs. Associated with the scheme, two low-complexity noncoherent fusion rules are investigated, which are the conventional EGC fusion rule and the proposed ES-EGC fusion rule. The ECP performance of FH/MFSK WSNs employing respectively the EGC and ES-EGC fusion rules is investigated, when assuming that channels from LSNs to FC experience independent Rayleigh fading. Our studies and performance results show that using soft-sensing is able to enhance the ECP performance of FH/MFSK WSNs. Furthermore, ES-EGC fusion rule is robust to the errors made by LSNs and is capable of achieving an enhanced performance over EGC fusion rule, especially, when the sensing of LSNs is not very reliable.

In Chapter 6, as one of the applications WSNs, a FH/MFSK assisted cognitive spectrum sensing system has been proposed for spectrum sensing, specifically, a IFDMA PR system supporting multiple users. Three types of energy-based detection, as well as four synchronization scenarios have been considered during the local detections at cognitive radio sensing nodes (CRSNs). After each of the CRSNs obtains the on/off states of the PR users, it sends the detected states to the FC with

the aid of FH/MFSK. Finally, at the FC, noncoherent detection is carried out, which is based on either the EGC or ES-EGC fusion rule. The performance of the FH/MFSK WSN assisted spectrum sensing system has been investigated by simulations, when assuming communications over multiple Rayleigh fading channels. Our studies and performance results show that reliable local sensing is achievable at the CRSNs even at very low SNR. Furthermore, the ES-EGC fusion rule is a highly efficient fusion rule, which is capable of attaining much better overall detection performance than the EGC fusion rule, especially, when the channel SNR is relative high.

Finally, conclusions are summarized and future work are given at the end of this report.

Chapter 2

Overview of Local Detection and Fusion Rules

In the area of WSNs, a lot of researches have been done in order to attain reliable signal detection at LSNs and FC, while requiring lowest computation complexity and minimum communication traffic between LSNs and FC [4, 6, 10, 74–83]. Numerous fusion rules for the classical distributed detection problems have been obtained during the past decades. Specifically, the optimum fusion rule has been considered in [84] under conditional assumption of independence. Assuming limited resource, the detection performance of distributed WSNs has been investigated, with the objective to optimize the LSNs' allocations or the number of LSNs [85–89]. None of these works, however, tackle the impact of the loss of transmission from LSNs to FC on the detection performance of WSNs.

Many studies have attempted to overcome this impractical assumption [90–95]. Considering nonideal communication channels, WSNs have been optimized through the optimization at FC level or/and LSN level. Specifically, in [96], optimal thresholds are established both at the FC and the LSNs with assumption that signals transmitted through a simple binary symmetric channel. In this presented approach, acceptable detection performance is achievable, however, at the cost of high computation complexity and serious delay, as well as the requirements of channel estimation. Considering restricted energy consumption and limited transmission range of LSNs [5, 31], multi-hop technique has been widely applied for large-scale WSNs for prolong monitoring range, as well as the lifetime. Consequently, corresponding decision fusion rules in multihop WSNs have been

studied in [79].

The main motivation behind the development of opportunistic spectrum access technologies, such as CR, is to increase the spectral efficiency of wireless communication system, in order to achieve high data communication. Spectrum sensing is believed one of the most important components to support CR systems. The main task of spectrum sensing is to determine if a frequency band of interest is occupied by PR users during a time slot within a certain geographical area [97].

In this chapter, we first briefly summarize the principles of classical binary hypothesis testing at LSNs, following by the discussion of some existing binary fusion rules for triple-layers WSNs. Then, we focus on the M-ary noncoherent fusion rules. Finally, some basic local spectrum sensing approaches for cognitive WSNs are addressed.

2.1 Classical Binary Local Detection

In the context of classical binary local detection at LSNs, we assume that the observed SE has two states, corresponding to two hypothesises H_0 and H_1. The local detection is made based on the observation y at each of individual LSNs. As shown in Fig 2.1, the total region of observation Z is divided into two parts, Z_0 and Z_1. Whenever an observation y falls into Z_0, the LSN makes a decision as D_0, otherwise, it chooses D_1. It might be expected that, based on the same received observation y, different decision criteria perhaps yielding different results. Hence, various classic local detection approaches for different purposes are detailed as follows.

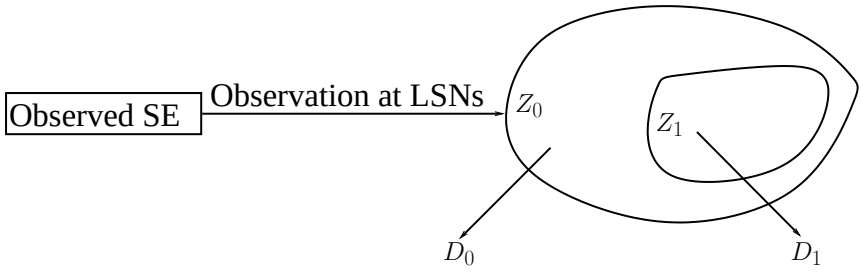

Figure 2.1: Illustration of decision region and decision making.

2.1.1 Bayesian Detection

Under the Bayesian criterion, the decision is made to achieve the average cost R as small as possible [98–101], which is related to the value of the *a-priori* probability and the cost of each decision. Explicitly, for the binary case, the two hypotheses related to the SE can be expressed as H_0 and H_1. The probabilities of occurrence of hypothesis H_0 and H_1 are expressed as P_0 and P_1, respectively, which satisfy $P_0 + P_1 = 1$. Let $C_{ij}, i, j = 0, 1$, be the cost associated with the decision D_i, when given that the true hypothesis is H_j. Then, $P(D_i, H_j)$ denotes the joint probability of deciding D_i while H_j is true.

The average cost can then be expressed as

$$\begin{aligned} R &= \sum_{i=0}^{1}\sum_{j=0}^{1} C_{ij}P(D_i, H_j) \\ &= \sum_{i=0}^{1}\sum_{j=0}^{1} C_{ij}P(D_i|H_j)P_j,\ i = 0, 1;\ j = 0, 1 \end{aligned} \tag{2.1}$$

where, according to [99], $P(D_0|H_1)$ denotes the miss probability, which is expressed as P_M, $P(D_1|H_0)$ is the false-alarm probability expressed as P_F, while $P(D_1|H_1)$ represents the detection probability, which is expressed as P_D. Furthermore, we have

$$P_M = 1 - P_D \tag{2.2}$$

and

$$P(D_0|H_0) = 1 - P_F \tag{2.3}$$

Upon applying the above-defined probabilities into (2.1), the average cost of the detection can be expressed as

$$R = C_{00}(1 - P_F)P_0 + C_{01}(1 - P_D)P_1 + C_{10}P_FP_0 + C_{11}P_DP_1 \tag{2.4}$$

where for a given observation y, (2.4) can be rewritten as [99]

$$R = C_{10}P_0 + C_{11}P_1 + \int_{Z_0} [P_1(C_{01} - C_{11})f(y|H_1)] - [P_0(C_{10} - C_{00})f(y|H_0)]dy \tag{2.5}$$

where Z_0 is the region for making the decision in favour of the hypothesis H_0, as shown in Fig 2.1.

In (2.5), it is easy to find that both the first and second items are always positive and constant, regardless of which decision is made. Furthermore, in Bayesian based detection, it is reasonable [102] to assume that the cost of making a wrong decision is greater than that of making a

correct decision, implying that

$$C_{01} > C_{11},\ C_{10} > C_{00} \tag{2.6}$$

Under these assumptions, in (2.5), both $P_1(C_{01} - C_{11})f(y|H_1)$ and $P_0(C_{10} - C_{00})f(y|H_0)$ are positive. Therefore, in order to minimize the cost, what we need to do is to make the result of the integral in (2.5) as small as possible. Hence, if

$$P_1(C_{01} - C_{11})f(y|H_1) \geqslant P_0(C_{10} - C_{00})f(y|H_0) \tag{2.7}$$

the detector should choose H_1, otherwise, the detector should choose H_0.

Alternatively, the Bayes criterion may be represented as

$$\frac{f(y|H_1)}{f(y|H_0)} \underset{H_1}{\overset{H_0}{\lessgtr}} \frac{P_0(C_{10} - C_{00})}{P_1(C_{01} - C_{11})} \tag{2.8}$$

The left part of (2.8) is called the likelihood ratio and defined as

$$\Lambda(y) = \frac{f(y|H_1)}{f(y|H_0)} \tag{2.9}$$

Because $\Lambda(y)$ is the ratio of two PDF functions, it is a one dimensional variable regardless of the dimensionality of observed signal y. The right part of (2.8) is the threshold, which is denoted as λ

$$\lambda = \frac{P_0(C_{10} - C_{00})}{P_1(C_{01} - C_{11})} \tag{2.10}$$

Then, the Bayes detection can be viewed as a likelihood ratio test (LRT) as

$$\Lambda(y) \underset{H_1}{\overset{H_0}{\lessgtr}} \lambda \tag{2.11}$$

It is clear from (2.11) that the computation of $\Lambda(y)$ is not affected by either the *a-priori* probabilities or cost functions. This invariance of the data processing is of considerable practical importance, as the *a-priori* probabilities and cost functions are merely to get. The Bayes detection enables us to build an entire processor and leave λ as a variable threshold to accommodate changes in our estimates of the *a-priori* probabilities and cost functions.

The Bayesian detection has widely been studied in the context of WSNs. Specifically, it has been applied to the distributed detection problem in WSNs [10, 74, 98, 99]. In [10], the fusion detection in parallel WSNs with FC has been studied by minimizing the Bayesian risk involving basic concepts and properties of Bayesian detection. A person-by-person optimization (PBPO) approach

has been proposed for distributed Bayesian signal detection [74]. With the PBPO approach, the distributed WSN is treated as two separate parts; the first one is the FC and the second one consists of the LSNs invoked. At first, under fixed local decision rules, the fusion rule is optimized in order to minimize the average cost. Then, under a given fusion rule, the individual local decision rules of LSNs are optimized. The decision rules used by LSNs are optimized one LSN at a time, while keeping the transmission maps of the other LSNs fixed. The optimization is carried out iteratively until convergence is achieved [74, 103].

2.1.2 Maximum A-Posteriori and Maximum Likelihood Detection

In Bayesian detection, the average cost is minimized with the aid of the *a-priori* probabilities, as well as the risk values [99, 101, 104]. However, in practice, the risk values or cost functions are quite difficult to get, even through they may exist. In this case, maximum *a-posteriori* (MAP) detection [104] may be employed, which needs only the *a-priori* probabilities regardless of the risk values. The basic principles behind MAP decision are that the LSN chooses the most possible assumption based on its observation or received signal. Under binary Bayesian testing as shown in (2.7), if we make an assumption that

$$C_{10} - C_{00} = C_{01} - C_{11} \tag{2.12}$$

Then, the Bayesian detection is reduced to the MAP detection [99–101]. In more detail, after applying (2.12) into (2.7), we can see that the LSN chooses H_1, if

$$P_1 f(y|H_1) \geqslant P_0 f(y|H_0) \tag{2.13}$$

or it chooses H_0, if

$$P_1 f(y|H_1) < P_0 f(y|H_0) \tag{2.14}$$

Furthermore, when applying the relationship of $P_0 = 1 - P_1$, the LRT of MAP detection can be expressed as

$$\Lambda(y) \underset{H_1}{\overset{H_0}{\lessgtr}} \lambda \tag{2.15}$$

where $\Lambda(y) = \frac{f(y|H_1)}{f(y|H_0)}$ is the likelihood ratio (LR) and λ is the threshold which equals to $P_0/(1-P_0)$.

In (2.15), when $P_0 = P_1 = 0.5$ or when the LSN is unable to obtain the knowledge of P_0 and P_1 and has to assume that $P_0 = P_1 = 0.5$, then the MAP detection is further reduced to the maximum likelihood (ML) detection. Based on (2.15) and using the assumption of $P_0 = P_1$, we can see that the ML detection chooses H_1, if

$$f(y|H_1) \geqslant f(y|H_0) \tag{2.16}$$

Otherwise, it chooses H_0, if $f(y|H_1) < f(y|H_0)$.

In general, the MAP detection is known to minimize the probability of error without considering the costs of various decisions. It works with requirement of the *a-priori* probabilities about H_0 and H_1, which, however, it is sometimes impractical and restricts the applications of the MAP detection [99]. Below we consider the Neyman-Pearson detection, which is not dependent on these *a-priori* probabilities.

2.1.3 Neyman-Pearson Detection

From the previous two subsections, it can be seen that the Bayesian detection requires both the *a-priori* probabilities of H_1 and H_0 and the cost functions for all the possible decisions. By contrast, the MAP detection does not require the cost functions, but needs the knowledge about the *a-priori* probabilities of each hypothesis. In some physical situations, such as, in radar applications, it is sometimes difficult to assign realistic costs and the *a-priori* probabilities [99, 101]. In these cases, Neyman-Pearson (NP) detection might be the best choice, which needs neither the cost functions nor the *a-priori* probabilities [105]. In these applications, we would make the false-alarm probability P_F as small as possible, while make the detection probability P_D as large as possible. However, for most practical applications, these two probabilities $(P_F \text{ and } P_D)$ are conflicting objectives. Specifically, NP detection usually minimizes P_F for a given value of P_D or maximizes P_D for a given value of P_F [103, 106]. Therefore, it is suitable for the cases where the costs or/and the the *a-priori* probabilities are hard to find.

Based on the NP detection [99, 101, 106], the probability of detection expressed by P_D is maximized, when the probability of false-alarm P_F is fixed. The LRT of assisted NP detection can be expressed as

$$\Lambda(y) = \frac{f(y|H_1)}{f(y|H_0)} \underset{H_1}{\overset{H_0}{\lessgtr}} \lambda \tag{2.17}$$

where, λ is a preset threshold for NP detection, motivating the maximum P_D subject to the constraint that P_F is less than some predetermined constant.

A specific statement of NP detection is detailed as follows. Given a false-alarm probability P_F, NP detection may be designed to maximize P_D or minimize P_M under this constraint. Let us construct a function F, which can be expressed as

$$\begin{aligned} F &= P_M + \lambda P_F \\ &= \int_{Z_0} f(y|H_1)dy + \lambda \int_{Z_1} f(y|H_0)dy \end{aligned} \tag{2.18}$$

Clearly, minimizing F is equivalent to minimize P_M. Function F can also be rewritten as

$$F = \lambda + \int_{Z_0} [f(y|H_1) - \lambda f(y|H_0)]dy \tag{2.19}$$

The only variable quantity of (2.19) is the region Z_0. Hence, the minimizing is achievable by including in the region Z_0 only the portion of the domain for which the integrand is negative. In this way, function F is minimized for a given value of P_F, which also gives the minimum of P_M

In [107–109], the fusion detection based on the NP principles has been considered for WSNs, where local decisions are transmitted via wireless channels to the FC. In these NP-based schemes, constraints on the probability of false-alarm are imposed, while the miss probability of the overall system is minimized. Furthermore, the cases of using dependent observations have been addressed in [110], and the problem of energy-efficient routing along with the NP detection has been studied.

Note that, the NP detection represents a special case of the Bayesian detection [99], which has been considered in Subsection 2.1.1, without considering the risks and assuming equal *a-priori* probabilities. In practice, the NP detection has found more applications than the Bayesian and MAP detections. However, the NP detection neglects the risks and the *a-priori* probabilities, which results in that the cost of the decision might be high for some applications.

2.2 Optimum and Sub-Optimum Channel-Aware Fusion Rules

A classical triple-layer WSN is made up of sensor layer, wireless channel layer and fusion center (FC) layer [75, 76]. Each LSN prepossesses and extracts information from its observation and, then, transmits the local decisions to the FC through wireless channels.

In this subsection, we overview a rang of channel-aware fusion rules, which make decisions by considering the state of the channels from LSNs to FC.

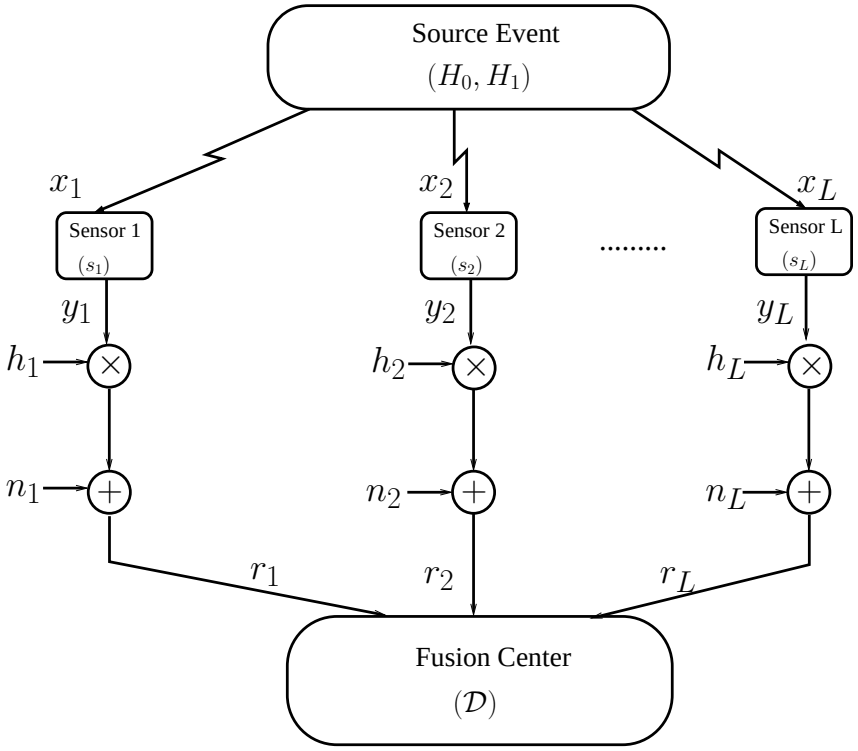

Figure 2.2: Triple-layer system model for the WSNs observing binary source events, in the presence of channel fading and noise.

For convenience of our description, we build a parallel WSN structured by three layers as shown in Fig 2.2. In this proposed WSN system, an binary SE $(H_0 \text{ and } H_1)$ is observed by L individual LSNs. Each LSN processes its observation and makes a local decision about the hypothesis of the SE. Explicitly, the lth local decision can be expressed as

$$\begin{aligned} y_l &= -1, \ \text{if hypothesis } H_0 \text{ is chosen} \\ y_l &= +1, \ \text{if hypothesis } H_1 \text{ is chosen} \end{aligned} \tag{2.20}$$

Correspondingly, the false and detection probabilities of the lth LSN can respectively be written as

$$\begin{aligned} P_{fl} &= P(y_l = +1|H_0) \\ P_{dl} &= P(y_l = +1|H_1) \end{aligned} \tag{2.21}$$

Then, local decisions are transmitted from each of L LSNs to the FC via L independent fading

channels. The received signal at the FC from the lth LSN can be expressed as

$$r_l = y_l h_l + n_l,\ l = 1, 2, \ldots, L \tag{2.22}$$

where y_l is the transmitted local decision of the lth LSN, h_l is the fading channel gain and n_l is a zero-mean Gaussian random variable with variance σ^2. Note that, when channel state information (CSI) is available at the FC, the channel gain h_l in (2.22) is always real and positive, after assuming perfect phase compensation.

Furthermore, for a given y_l, the received signal r_l as shown in (2.22) obeys the independent Gaussian distribution expressed as

$$f(r_l|y_l) = \frac{1}{\sqrt{2\pi}\sigma}\exp\left[-\frac{(r_l - y_l h_l)^2}{2\sigma^2}\right] \tag{2.23}$$

Final decision is made by the FC based on the received signal from all the L LSNs. Therefore, in this type of WSNs, errors may come from two aspects, the first one is the disturbance and noise presenting the LSNs' observations and the second one is from the transmission channels between LSNs and FC, which introduce noise, fading and/or interference. Note that, in the following, we derive the channel-aware fusion rules by incorporating the channel fading between LSNs and the FC, when given fixed local detection performance.

2.2.1 Optimum Likelihood-Ratio Fusion Rule

The optimum likelihood-ratio fusion rule has been studied in [74, 76, 79, 82, 84] for WSNs. Let us assume that, in a WSN system, both the instantaneous channel state information (CSI) regarding the channels from LSNs to FC and the LSNs' detection performance, which is explained by the detection and false alarm probabilities of the LSNs, are available to the FC. The received signal $\boldsymbol{r} = [r_1, r_2, ..., r_L]^T$ at the FC is a vector containing the observations from L LSNs. Then, when given the independence assumption of local observations, the likelihood-ratio (LR) evaluated at the FC, can be expressed as [74]

$$\begin{aligned}
\Lambda(\boldsymbol{r}) &= \frac{f(\boldsymbol{r}|H_1)}{f(\boldsymbol{r}|H_0)} \\
&= \prod_{l=1}^{L} \frac{f(r_l|H_1)}{f(r_l|H_0)} \\
&= \prod_{l=1}^{L} \frac{f(r_l, y_l = +1|H_1) + f(r_l, y_l = -1|H_1)}{f(r_l, y_l = +1|H_0) + f(r_l, y_l = -1|H_0)}
\end{aligned} \tag{2.24}$$

Upon submitting (2.21) and (2.23) into (2.24), the optimum LR testing can be rewritten as

$$\begin{aligned}\Lambda(\boldsymbol{r}) &= \prod_{l=1}^{L} \frac{P_{dl} f(r_l|y_l=+1) + (1-P_{d_l}) f(r_l|y_l=-1)}{P_{fl} f(r_l|y_l=+1) + (1-P_{f_l}) f(r_l|y_l=-1)} \\ &= \prod_{l=1}^{L} \left[\frac{P_{d_l} e^{-\frac{(r_l-h_l)^2}{2\sigma^2}} + (1-P_{d_l}) e^{-\frac{(r_l+h_l)^2}{2\sigma^2}}}{P_{f_l} e^{-\frac{(r_l-h_l)^2}{2\sigma^2}} + (1-P_{f_l}) e^{-\frac{(r_l+h_l)^2}{2\sigma^2}}} \right] \end{aligned} \tag{2.25}$$

where P_{d_l} and P_{f_l} are, respectively, the detection probability and false alarm probability of the lth LSN. If we prefer the logarithmic form, the log-likelihood ration (LLR) testing is [74]

$$\begin{aligned}\mathcal{L}\Lambda(\boldsymbol{r}) &= \log \Lambda(\boldsymbol{r}) \\ &= \sum_{l=1}^{L} \log \left[\frac{P_{d_l} e^{-\frac{(r_l-h_l)^2}{2\sigma^2}} + (1-P_{d_l}) e^{-\frac{(r_l+h_l)^2}{2\sigma^2}}}{P_{f_l} e^{-\frac{(r_l-h_l)^2}{2\sigma^2}} + (1-P_{f_l}) e^{-\frac{(r_l+h_l)^2}{2\sigma^2}}} \right] \end{aligned} \tag{2.26}$$

According to [76], the optimum LR-based fusion rule is capable of achieving the best detection performance. On the other hand, as shown in (2.25) or (2.26), optimum LR-based fusion rule requires both the LSN's performance and complete instantaneous CSI, as well as the noise variance. The optimum LSN's detection is channel-dependent, requires to be adjusted, whenever the channels from LSNs to FC change. Furthermore, the computation complexity of the optimum LR fusion rule is extremely high for WSNs. Due to the stringent constraints of WSNs, the application of the optimum LR-based fusion rule is restricted only to the WSNs that high detection performance is essential.

2.2.2 Sub-Optimum Fusion Rule: Chair-Varshney Fusion Rule

The optimum LR-based fusion rule is capable of achieving the optimal detection performance. However, it demands an extremely high complexity and requires the *a-priori* information, including the instantaneous CSI of all the LSNs to FC channels, as well as the detection and false-alarm probabilities of all the LSNs. In order to relieve from these requirements, Chair-Varshney (CV) fusion rule has been developed [74, 76, 79], which is derived based on the approximation of the optimum LR-based fusion rule within high channel SNR region.

It can be shown that (2.26) can be rewritten as

$$\mathcal{L}\Lambda(\boldsymbol{r}) = \sum_{l=1}^{L} \log \left[\frac{P_{d_l} + (1-P_{d_l}) e^{-\frac{2r_l h_l}{\sigma^2}}}{P_{f_l} + (1-P_{f_l}) e^{-\frac{2r_l h_l}{\sigma^2}}} \right] \tag{2.27}$$

Furthermore, (2.27) can be decomposed into

$$\begin{aligned}\mathcal{L}\Lambda(\boldsymbol{r}) &= \sum_{l=1,\, r_l>0}^{L} \log\left[\frac{P_{d_l}+(1-P_{d_l})e^{-\frac{2r_lh_l}{\sigma^2}}}{P_{f_l}+(1-P_{f_l})e^{-\frac{2r_lh_l}{\sigma^2}}}\right] \\ &+ \sum_{l=1,\, r_l<0}^{L} \log\left[\frac{P_{d_l}+(1-P_{d_l})e^{-\frac{2r_lh_l}{\sigma^2}}}{P_{f_l}+(1-P_{f_l})e^{-\frac{2r_lh_l}{\sigma^2}}}\right] \end{aligned} \tag{2.28}$$

When assuming that the channel SNR is infinite yielding $\sigma^2 \to 0$, the LLR related to the CV fusion rule can be expressed based on (2.28) as

$$\begin{aligned}\mathcal{L}\Lambda(\boldsymbol{r}) &= \sum_{l=1,\, r_l>0}^{L} \log\left(\frac{P_{d_l}}{P_{f_l}}\right) + \sum_{l=1,\, r_l<0}^{L} \log\left(\frac{1-P_{d_l}}{1-P_{f_l}}\right) \\ &= \sum_{l=1,\, \text{sign}(r_l=+1)}^{L} \log\left(\frac{P_{d_l}}{P_{f_l}}\right) + \sum_{l=1,\, \text{sign}(r_l=-1)}^{L} \log\left(\frac{1-P_{d_l}}{1-P_{f_l}}\right) \end{aligned} \tag{2.29}$$

where P_{d_l} and P_{f_l} have the same meaning as the previous explanations.

According to (2.29), CV fusion rule is separated into a two stage process. First, an estimation of observed SE is made in the context of each individual LSN:

$$\hat{y}_l = \text{sign}(r_l),\ l = 1, 2, \ldots, L \tag{2.30}$$

Then, the decision statistic of CV fusion rule can be derived as

$$\mathcal{L}\Lambda(\boldsymbol{r}) = \sum_{l=1,\, \hat{y}_l=1}^{L} \log\left(\frac{P_{d_l}}{P_{f_l}}\right) + \sum_{l=1,\ \hat{y}_l=-1}^{L} \log\left(\frac{1-P_{d_l}}{1-P_{f_l}}\right) \tag{2.31}$$

The LLR expression (2.28) of the CV fusion rule can be viewed as an approximation of the optimum LR-based fusion rule shown in (2.26) within high channel SNR region. It does not require any knowledge regarding the channel statistics but does require the detection probability and false alarm probability of each of the LSNs. The decision rules at the LSNs are optimized under the assumption that the channels from LSNs to FC are ideal. Hence, the CV fusion rule may only be suitable for the WSNs where the communications between LSNs and FC are reliable. It has been shown in [74] that, for high-channel SNR, the CV fusion rule is capable of achieving the performance as good as the optimum LR-based fusion rule. However, in the low channel SNR region, the CV fusion rule suffers significant detection performance loss.

2.2.3 Sub-Optimum Fusion Rule: Maximum Ratio Combining Fusion Rule

In low channel SNR region, maximum ratio combining (MRC) fusion rule approximates the optimum LR-based fusion rule [79,84], which is optimal in terms of the maximum of output SNR [76]. For convenience of reading, here we rewrite the simplified optimum LLR decision statistic of (2.27) as

$$\mathcal{L}\Lambda(\boldsymbol{r}) = \sum_{l=1}^{L} \log\left[\frac{P_{d_l} + (1-P_{d_l})e^{-\frac{2r_l h_l}{\sigma^2}}}{P_{f_l} + (1-P_{f_l})e^{-\frac{2r_l h_l}{\sigma^2}}}\right] \tag{2.32}$$

For low channel SNR, i.e., for $\sigma^2 \to \infty$, we have $e^{-\frac{2r_l h_l}{\sigma^2}} \to 1$, which can be approximated by the first term of the Taylor series expansion, i.e., $e^{-\frac{2r_l h_l}{\sigma^2}} \approx 1 - \frac{2r_l h_l}{\sigma^2}$. Therefore, we have

$$\begin{aligned}
\mathcal{L}\Lambda(\boldsymbol{r}) &= \sum_{l=1}^{L} \log\left[\frac{P_{d_l} + (1-P_{d_l})\left(1-\frac{2r_l h_l}{\sigma^2}\right)}{P_{f_l} + (1-P_{f_l})\left(1-\frac{2r_l h_l}{\sigma^2}\right)}\right] \\
&= \sum_{l=1}^{L} \log\left[\frac{1-(1-P_{d_l})\frac{2r_l h_l}{\sigma^2}}{1-(1-P_{f_l})\frac{2r_l h_l}{\sigma^2}}\right] \\
&\approx \sum_{l=1}^{L} \left\{\log\left[1-(1-P_{d_l})\frac{2r_l h_l}{\sigma^2}\right] - \log\left[1-(1-P_{f_l})\frac{2r_l h_l}{\sigma^2}\right]\right\}
\end{aligned} \tag{2.33}$$

Using the fact that, for $x \to 0$

$$\log(1+x) \approx x \tag{2.34}$$

Hence, (2.34) can be further simplified to

$$\begin{aligned}
\mathcal{L}\Lambda(\boldsymbol{r}) &\approx \sum_{l=1}^{L} \left\{\left[-(1-P_{d_l})\frac{2r_l h_l}{\sigma^2}\right] - \left[-(1-P_{f_l})\frac{2r_l h_l}{\sigma^2}\right]\right\} \\
&= \sum_{l=1}^{L} (P_{d_l} - P_{f_l})\frac{2r_l h_l}{\sigma^2}
\end{aligned} \tag{2.35}$$

Given that $\frac{2}{\sigma^2}$ is a (possibly unknown) constant and, hence, can be neglected, (2.35) can finally be simplified to

$$\mathcal{L}\Lambda(\boldsymbol{r}) \approx \sum_{l=1}^{L} (P_{d_l} - P_{f_l}) r_l h_l \tag{2.36}$$

Furthermore, if the LSNs are identical, i.e., all the LSNs use the same local decision rule and achieve the same detection probability and false-alarm probability, then, $\mathcal{L}\Lambda(\boldsymbol{r})$ of (2.36) reduces to a MRC statistic of

$$\mathcal{L}\Lambda(\boldsymbol{r}) = \sum_{l=1}^{L} r_l h_l \tag{2.37}$$

In essence, the MRC testing statistic as shown above is the first-order approximation of the optimum LLR based fusion rule and is asymptotically accurate as $\sigma^2 \to \infty$.

From (2.37), we can see that the MRC fusion rule does not require the knowledge of P_{d_l} or P_{f_l}. However, it requires that all the LSNs are identical. The CSI is essential for the MRC fusion rule. The MRC fusion rule is optimal, which maximizes the output SNR under the assumption that the observations through multiple independent channels are identical. However, in the context of WSNs, identical observations cannot be guaranteed as the LSNs are prone to erroneous estimations. It has been illustrated that all the LSNs can use the same local decision rule without much performance loss, especially when the number of LSNs is high. In this case, the MRC fusion rule is effective [95]. In essence, the MRC testing statistic as shown in (2.37) is the first-order approximation of the optimum LLR based fusion rule and it is asymptotically accurate as $\sigma^2 \to \infty$. Hence, the MRC fusion rule is not effective in the high channel SNR region.

2.2.4 Sub-Optimum Fusion Rule: Equal Gain Combining Based Fusion Rule

Motivated by the fact that, in some cases, there is no CSI available. In this case, the equal gain combining (EGC) may be employed, which requires minimum amount of information [74, 111–114]. The EGC fusion rule can be expressed as

$$\mathcal{L}\Lambda(\boldsymbol{r}) = \sum_{l=1}^{L} r_l \tag{2.38}$$

In comparison with the optimum LLR-based fusion rule, the EGC fusion rule releases most of the requirements. When considering the detection performance of the three sub-optimum fusion rules (CV, MRC and EGC), the MRC is the best at low SNR region; while at high SNR, CV outperforms the other two. EGC fusion rule can be viewed as a trade-off between the MRC and CV fusion rules.

2.3 Noncoherent M-ary Fusion Rule

In Section 2.2, a range of channel-aware fusion rules have been reviewed in the context of binary WSNs, which are often preferred for the applications demanding high data rate. From Subsection 2.2.1, we can know that channel estimation is essential for implementation of the optimum channel-aware fusion rules, which requires extra bandwidth for transmission of overhead for channel estimation, in addition to their relatively high complexity of implementation. In practice, there

are many applications for WSNs, which emphasise on low-complexity over high data rate. In these types of WSNs, noncoherent fusion rules are preferred, which detect signals without relying on channel estimations. In this section, we provide a summary of existing noncoherent fusion rules suitable for the WSNs.

In relation with our studies in the following chapters, the noncoherent fusion detections are described based on a framework of M-ary frequency-shift keying (MFSK) WSN [115, 116]. Specifically, in the MFSK-assisted WSN, L number of LSNs are used to monitor single SE with M possible states. Observations of L LSNs are transmitted one-by-one to the FC using MFSK modulation with L time-slots. At the FC, the received signals from the L LSNs are first processed in the square-law operation [117]. Then, the detection matrix $\boldsymbol{D}$ of $(M \times L)$ is formed. Let the element in the detection matrix $\boldsymbol{D}$ corresponding to the mth row and the lth column be expressed as $D_{ml},\ m = 0, 1, \cdots, M-1;\ l = 1, 2, \cdots, L$. Based on $\boldsymbol{D}$, noncoherent fusion rules are discussed below.

2.3.1 Equal Gain Combining Fusion Rule

Equal gain combing (EGC) fusion rule, well known as a typical square law combining approach, is an effective mean of combating multipath fading in noncoherent communications [118]. Note that, the EGC fusion rule discussed here is specifically for noncoherent detection, which is not fully the same as that described in Subsection 2.2.4. The EGC fusion rule presents significant practical interest, because, in most cases, it can provide reasonable detection performance, while requires the lowest complexity for implementation [117, 118].

When the EGC fusion rule is employed, the M decision variables formed by the FC can be expressed as

$$D_m = \sum_{l=1}^{L} D_{ml},\ \ m = 0, 1, \ldots, M-1 \tag{2.39}$$

Then the largest one of $\{D_0, D_1, \ldots, D_{M-1}\}$ is selected and, correspondingly, its m index with its value in $\{0, 1, \ldots M-1\}$ represents the estimation of the state that the monitored SE is currently at.

Numerous research has dealt with the performance of noncoherent communication system in conjunction with the EGC fusion rule over AWGN or/and fading channels [119]. For examples,

Proakis has developed a generic BER expression for EGC fusion rule of binary signals over AWGN channels [120]. Then, a close-form expression for average BER of binary frequency-shift keying (BFSK) over independent identically distributed (i.i.d.) Rayleigh fading channels is given [115]. Following, general expressions for the average BER of BFSK signals over Rician or Nakagami-m fading channels have been derived in [121] and [122], respectively.

Considering the application in WSNs, the EGC fusion rule has been employed at the FC of a FH/MFSK WSN system, where an M-ary SE is observed by L individual LSNs [117]. It has been indicated that when communicating over AWGN or Rayleigh fading channels, the WSN systems with EGC fusion rule capable of achieving a promising detection performance, when operated at reasonable SNR. In [118], the detection performance of the WSNs employing EGC fusion rule has been investigated, when assuming communications over correlated fading channels.

2.3.2 Majority Vote Fusion Rule

The majority vote (MV) fusion rule [123–125] can be described by starting from $\boldsymbol{D}$. Let λ (> 0) be a preset threshold in MV fusion rule, a new matrix $\boldsymbol{D}'$ can be formed based on $\boldsymbol{D}$ by comparing each of its elements with the threshold λ. Specially, if $D_{ml} > \lambda$, the corresponding element in $\boldsymbol{D}'$ is set to $D'_{ml} = 1$, otherwise, $D'_{ml} = 0$. Hence, $\boldsymbol{D}'$ is a matrix with its elements taking values of 1 or 0. Based on $\boldsymbol{D}'$, when the MV fusion rule is employed, the FC makes a decision in favour of the particular M-ary symbol, which has a value in $\{0, 1, \cdots, M-1\}$ corresponding to the specific row having the highest number of nonzoroentries in $\boldsymbol{D}'$, which provides an estimation to the state of the SE monitored.

Explicitly, for MV fusion rule, the M decision variables are evaluated based on the new formed matrix $\boldsymbol{D}'$ via EGC fusion rule as

$$D_m = \sum_{l=1}^{L} D'_{ml}, \;\; m = 0, 1, \ldots, M-1 \tag{2.40}$$

The MV fusion rule has attracted much attention in the research on noncoherent combining schemes for its simplicity [126]. The performance of MV fusion rule has been demonstrated in various applications, such as, in WSNs. Under the assumption of independent LSNs, if the individual local correct probability is larger than 0.5 the overall detection performance improves as the number of LSNs increases. In some cases, for simplicity of theoretical analysis of the MV fusion

rule, it is usually assumed that all the LSNs have the same detection performance. In [127], the detection performance has been analysed under the assumption that the local observations are independent. A theoretical framework for combining local decisions has been built which uses distinct pattern representations [128]. It is shown that MV fusion rule can be viewed as a special case of EGC fusion rule, as also shown (2.40).

2.3.3 Selection Combining Fusion Rule

For the selection combing (SC) fusion rule, first, the decision variable for each possible state is formed by selecting the largest one of the corresponding row, given by [90, 129]

$$D_m = \max\{D_{m1}, D_{m2}, \ldots, D_{mL}\}, \;\; m = 0, 1, \ldots, M-1 \tag{2.41}$$

where $\max\{\cdot\}$ represents the maximum of the correspond entries.

Then, the largest one of $\{D_0, D_1, \ldots, D_{M-1}\}$ is selected and its index value in terms of m represents the estimation of the state of the observed SE.

Among the three noncoherent fusion rules EGC, MV and SC, communicating over multipath fading channels, SC is the least complicated algorithm, as it processes only one of the diversity brands [119]. The SC fusion rule chooses the branch with the highest SNR or the strongest signal, then assuming equal noise power of individual channels. In order to achieve better detection performance, independent channel fading is desired. However, this channel fading independence may not always be practical, because, for example, of insufficient space in small-size WSNs and, as a result, the diversity gain may not be guaranteed. Additionally, different wireless channels may experience various average SNRs due to different noise power and transmitting distance. These factors also constrain the application of the SC fusion rule.

2.3.4 Product Combining Fusion Rule

In the context of the product combing (PC) fusion rule [91, 130, 131], the decision variable for each of the possible states of the SE are formed as

$$D_m = \prod_{l=1}^{L} D_{ml}, \;\; m = 0, 1, \ldots, M-1 \tag{2.42}$$

Then, the largest one of these M decision variables is chosen and its index value in terms of m stands for the estimation of the state of the observed SE.

The design of the PC fusion rule is based on an assumption that the received signals corresponding to a non-signal frequency band carries relatively lower power in at least one of the L individual LSNs, with a high probability. Consequently, when the products of (2.42) are computed, the undesired decision variables with just noise yield low values. By contrast, the desired signal contains both signal and noise, the decision variable (formed by the product of (2.42)) has a significantly higher value. Hence, statistically, reliable detection performance may be expected when employing the PC fusion rule [132]. Note that, the PC fusion rule has first been proposed by Viswanathan and Taghizadeh in [133]. Following, the performance of the PC fusion rule is analyzed under different jamming and fading conditions [134]. In [135], the BER performance of the fast frequency-hopping (FFH) binary frequency-shift-keying (BFSK) system employing the PC fusion rule is derived, when multitone jamming and AWGN as well as independent Rician fading channels are considered.

2.3.5 Noise-Normalization Combining

The noise-normalization combing (NNC) fusion rule forms the decision variables based on the received signals, the interference and noise power [92]. In detail, let σ_{ml}^2 be the interference-plus-noise power of D_{ml}. Then, the M decision variables are formed as [92, 136, 137]

$$D_m = \sum_{l=1}^{L} \frac{D_{ml}}{\sigma_{ml}^2}, \quad m = 0, 1, \ldots, M-1 \tag{2.43}$$

The largest one of $\{D_0, D_1, \ldots, D_{M-1}\}$ is then selected and, correspondingly, the m index with the value in $\{0, 1, \ldots M-1\}$ represents the estimation of the state that the SE is currently at.

In the NNC fusion rule (also referred to as adaptive gain control fusion rule), the reciprocal of the noise power is required to normalize the received signal before the L individual received signals are combined [92]. The detection performance of the NNC fusion rule for a FH/BFSK system has been analyzed in [138], when communicating over partial-band Gaussian noise jamming channels. The detection performance analysis is then extended to the Rayleigh fading channels and general Nakagami-m channels in [92] and [139], respectively.

2.3.6 Self-Normalization Combining

Under the self-normalization combing (SNC) fusion rule, the decision variable for the mth state is related to the elements of the other possible states [132,140,141]. The M decision variables formed based on the SNC fusion rule are given by

$$D_m = \sum_{l=1}^{L} \frac{D_{ml}}{D_{0l} + D_{1l} + \ldots + D_{(M-1)l}}, \;\; m = 0, 1, \ldots, M-1 \tag{2.44}$$

Then, the largest one of the M decision variables of $\{D_0, D_1, \ldots, D_{M-1}\}$ is selected and its subscript value represents the estimation for the state of the SE being observed.

In the SNC fusion rule, the reciprocal of the sum of M different elements is used for normalization before combining them to form the decision variable. Hence, it is sensitive to channel fading, yielding, sometimes, a significant performance degradation when compared with its nonfaded performance [141]. In references, the SNC fusion rule has been examined for channels with no fading in [140]. The performance of the SNC fusion rule over Rician and Nakagami-m fading channels has been analyzed in [141] and [132], respectively.

2.3.7 Soft-Limiting Combining

The soft-limiting combining (SLC) fusion rule is also referred to as the clipping combing fusion rule [116]. Under this SLC fusion rule, the elements D_{ml} in the decision matrix $\boldsymbol{D}$ are first clipped by a certain value before the combining operation. Specifically, let λ be the preset threshold, which can be set, for example, as the value achieving the lowest error probability for given conditions, such as local decision probability, channel SNR, etc [93]. Then, by comparing the decision element D_{ml} with the threshold λ, we obtain

$$\begin{aligned} D'_{ml} &= D_{ml}, \;\; \text{if } D_{ml} \leq \lambda \\ D'_{ml} &= \lambda, \;\; \text{if } D_{ml} > \lambda \end{aligned} \tag{2.45}$$

for $m = 0, 1, \cdots, M-1$; $l = 1, 2, \cdots, L$. After the clipping operations, the decision variables are formed based on the EGC principles, yielding

$$D'_m = \sum_{l=1}^{L} D'_{ml}, \;\; m = 0, 1, \ldots, M-1 \tag{2.46}$$

Finally, the largest one among $\{D'_0, D'_1, \ldots, D'_{M-1}\}$ is selected and its index value for m represents the estimate of the state of the monitored SE. In the SLC fusion rule, the preset threshold λ is usually refereed to as a the clipping threshold, which depends on the noise power as well as the number of active users [132], when multiuser communication is the case. The basic principles behind the SLC is that, if more than one interfering user happens to choose the same frequency band, a higher interference power is anticipated by the FC in the corresponding branch. Hence, the clipping operation may be effective to suppress the interference [142, 143]. However, operation of the SLC fusion rule requires the information of noise variance and the number of active users, in order to calculate the accurate threshold. Furthermore, it can be shown that the knowledge of noise power plays a more important role than that of the number of active users , in order to accurately estimate the clipping threshold [143].

2.4 Spectrum Sensing Approaches

Spectrum is now becoming a scarce resource, when licensed spectrum or frequency-band is intended to be only available for primary radio (PR) users. For this sake, a new concept referred to as cognitive radio (CR) has been introduced in order to improve the utilization rate of spectrum by identifying and utilising the spectrum holes. In CRs, the spectrum hole is defined by the Federal Communications Commission (FCC) as a band of frequencies that are not being used by the licensed user of that band at a particular time in a particular geographical area. Hence, the main task of spectrum sensing is to determine whether the frequency band of interest is occupied by PR users during a time slot within a certain geographical area [97]. Explicitly, the deployment of CRs will inevitably create interference to PRs, yielding possibly decrement of communication quality of PRs. Therefore, in order to make efficient user of the spectrum holes of PRs but to keep the interference on PRs at an reasonable level, quick and accurate spectrum sensing in the three dimensions of frequency, time and space is essential.

In this section, some typical spectrum sensing approaches are reviewed in detail. First, we consider the original problem of local spectrum sensing. Then, a comprehensive overview of existing solutions of spectrum sensing is provided.

2.4.1 Spectrum Sensing Model

The general problem of spectrum sensing can be described as binary hypothesis test: H_0 means that PR user is off or the frequency band of interest is available; and H_1 denotes that PR user is active or the frequency band of interest is busy. Hence, the received signal at CR users can be expressed as:

$$\begin{aligned} H_0 :\ & y(t) = n(t), \\ H_1 :\ & y(t) = x(t) + n(t) \end{aligned} \tag{2.47}$$

where $y(t)$ is the received signal at a CR user, $n(t)$ is the AWGN with zero mean and $x(t)$ represents the signal received from PR user. In the context of spectrum sensing, the detection performance is usually measured two parameters: detection probability (P_d) and false-alarm probability (P_f). Hence, P_d can be expressed as

$$P_d \triangleq \Pr(\delta \geqslant \lambda \mid H_1) \tag{2.48}$$

where δ denotes the test statistics and λ is the threshold for detection. By contrast, P_f can be expressed as

$$P_f \triangleq \Pr(\delta \geqslant \lambda \mid H_0) \tag{2.49}$$

There are many spectrum sensing approaches in literature. Below, we provide a brief overview of some spectrum sensing approaches, including energy detection [144–147], matched filter (MF) detection [148–150] and feature based detection approaches [151, 152].

2.4.2 Energy Detection

Energy detection is the simplest and common spectrum sensing approach, which detects the spectrum availability by measuring the energy of received signal in a certain frequency band. Since it is easy to implement, energy detection has widely been studied for detecting PR users. However, the performance of energy detection is highly susceptible to noise power uncertainty. It is difficult to set the threshold properly without the knowledge of the accurate noise level. Furthermore, energy detection is incapable of differentiating between desired signals, noise and interference. The

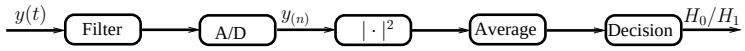

(a) Time-domain energy detection

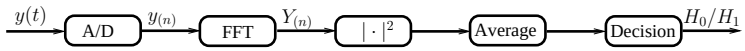

(b) Frequency-domain energy detection

Figure 2.3: Flow chart of energy detection.

detection performance of energy detection degrades significantly in shadowing and fading environments [146, 147].

Energy detection can be operated in either frequency or time domain. As shown in Fig 2.3a, conventional time-domain energy detection consists of a low-pass filter, Nyquist sampling and A/D converter, square-law device and integrator [144]. Correspondingly, the received signal after sampling can be expressed as:

$$\begin{aligned} &H_0 : y(n) = n(n) \\ &H_1 : y(n) = x(n) + n(n), \;\; n = 0,\, 1, \cdots, N-1; \end{aligned} \tag{2.50}$$

where N is the number of sampling, the noise sample $n(n)$ is assumed to be white Gaussian noise with zero mean and variance σ_n^2. The test statistics for energy detection is:

$$\delta_E = \frac{1}{N} \sum_{n=0}^{N-1} \mid y(n) \mid^2 \tag{2.51}$$

Then, the availability of the frequency band of interest using energy approach can be determined according to

$$\delta_E \underset{H_1}{\overset{H_0}{\lessgtr}} \lambda \tag{2.52}$$

where λ is the threshold.

In time-domain energy detection, the bandwidth of filter needs to match with that of a given signal, which is inflexible in practical application. An alternative approach is to estimate the spectrum via squared magnitude of the output of the fast Fourier transform (FFT) of the sampled signals, forming the frequency-domain energy detection, as shown in 2.3b. Compared with the conventional time domain energy detection, the frequency domain energy detection, is capable of monitoring multiple sub-bands simultaneously [145]. Furthermore, an arbitrary bandwidth can be processed by choosing a corresponding number of frequency bins.

In frequency-domain, the detection performance can be improved through increasing either the frequency resolution of FFT or the number of samples. However, increasing the values of these two parameters increases the computation complexity as well as processing delay. In practice, it is common to set a suitable FFT size to meet the desired resolution with a moderate complexity. Then, the trade-off between the detection performance and complexity/delay may be optimized by the number of samples. It has been shown [144] that under the assumption that the number of samples is infinite, an energy detector is capable of achieving any desired P_d and P_f simultaneously. According to [144], the minimum number of samples required is:

$$U = 2\left[Q^{-1}\left(P_f - P_d\right)\gamma^{-1} - Q^{-1}P_d\right]^2 \tag{2.53}$$

where Q^{-1} denotes the inverse Gaussian Q-function and γ is the observation signal to noise ratio (SNR).

In practice, unfortunately, there is a minimum value of SNR, below which energy detection cannot work any more. This minimum value of SNR is called the 'SNR wall' [146, 147]. The reasons behind the 'SNR wall' phenomenon are the two impractical assumptions for the observation noise. First, the noise $n(n)$ in (2.50) is assumed to be the white Gaussian noise with zero mean and variance σ_n^2. However, in practice, the observation noise is an aggregation of thermal noise at receiver and interference due to nearby unintended emissions, etc. Second, the noise variance is assumed to be known perfectly, so that the corresponding threshold can be set accurately. However, CR users usually cannot estimate the noise variance precisely, as noise variance could vary over time due to temperature change, interference, etc.

2.4.3 Matched Filter Detection

Matched filter (MF) detection is a linear filter designed to maximize the output SNR for a given input signal [148]. When the *a-priori* information of PR user is perfectly known by CR user, MF detection is the optimum spectrum sensing approach [149, 150] in stationary Gaussian noise. The main advantage of the MF detection is low complexity and delay. If the conditions are satisfied, MF detection is able to implement fast sensing and meet the desired probability of false-alarm or probability of detection in short time, as it requires only $\mathcal{O}\left(1/\mathrm{SNR}\right)$ samples [153].

Against the above mentioned advantages, MF detection has some major disadvantages. First,

MF detection requires perfect knowledge of all the PR users. Otherwise, the detection performance degrades significantly. Second, there is a security issue, as CR user needs to access to the communication in PR. Third, since the MF is designed to sense all the frequency bands of interest, the implement complexity maybe largely impractical, also due to the requirement of perfect knowledge of all the possible signals. Finally, MF detection is not energy efficient, as all the receiver algorithms needs to be executed for decisions [148].

2.4.4 Feature Detection

From the above discussion, we have know that MF detection is limited for the practical applications requiring perfect knowledge of received signals. Actually, there is always some available information, such as, the type of PR users, regulation of transmitted signal [148], etc., which may be useful for spectrum sensing. In the following, we overview some spectrum sensing approaches, which exploit known features of received signals. Specifically, we focus on two types of feature detections, namely the second order cyclostationarity detection and the eigenvalue based detection.

2.4.4.1 Cyclostationary Detection

The initial work of spectrum sensing with the aid of the second order stationarity analysis can be traced back to the contribution of Dandawate and Giannakis in 1994 [154]. The general principles behind the cyclostationary detection are that, most man-made signals show periodic patterns related to the corresponding symbol rate, chip rate, channel code or cyclic prefix make the received signals present as a cyclostationary random process [151,152]. In a little bit more detail, the time-varying covariance function of received signals $R_y(\tau)$ can be expressed by a Fourier series, where the Fourier coefficients are known as the cyclic covariance with cyclic frequency f_0. By exploiting some of these cyclic characteristics of random process, one can construct the detectors to benefit from the spectral correlation. This method has widely been used for detection of OFDM signals [151].

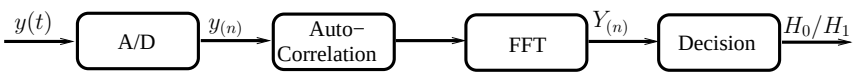

Figure 2.4: Flow chart of second order cyclostationarity detection.

A discrete-time zero-mean stochastic process $y(t)$ is said to be the second-order cyclostation-

ary, if it satisfies $y(t) = y(t+T)$, where the smallest value of T is called as the period. Furthermore, the corresponding autocorrelation function is also periodic with period of T, given by

$$\begin{aligned} R_y(\tau) &= \mathbb{E}[y(\tau)y(t+\tau)] \\ &= \mathbb{E}[y(\tau+T)y(t+\tau+T)] \end{aligned} \tag{2.54}$$

Hence, the autocorrelation function can be expressed as

$$\begin{aligned} R_y(\tau) &= \sum_{k=-\infty}^{\infty} b_k e^{j2\pi f_0 k\tau}, \ \left(f_0 = \frac{1}{T}\right) \\ b_k &= \frac{1}{T}\int_0^T R_y(\tau)e^{-j2\pi f_0 k\tau}d\tau \\ &= \lim_{\bar{T}\to\infty}\frac{1}{\bar{T}}\int_{-\frac{\bar{T}}{2}}^{\frac{\bar{T}}{2}} R_y(\tau)e^{-j2\pi f_0 k\tau}d\tau \end{aligned} \tag{2.55}$$

where $\bar{T} \to \infty$. The power spectrum density (PSD) of $y(t)$ can be obtained through the discrete time Fourier transformation (DTFT) [152]:

$$\begin{aligned} S(f) &= \int_{-\infty}^{\infty} R_y(\tau)e^{-j2\pi f\tau}d\tau \\ &= \sum_{n=-\infty}^{\infty} b_n\delta(f-nf_0) \end{aligned} \tag{2.56}$$

where b_n is given in (2.55). The cyclic autocorrelation function at a given cyclic frequency determines the correlation between two spectral components of the signal separated in frequency by an amount of $\frac{1}{T}$. Hence, if there exists an n such that $f = nf_0$, b_k for some k's are not zero and $S(f) \neq 0$.

Under the cyclostationary detection, it is assumed that noise is a wide-sense stationary (WSS) process with no correlation, resulting in that $b_k = 0$ for any value of k. By contrast, digital modulated signals are cyclostationary with spectral correlation due to signal periodicities, resulting in that the values of some b_k are lager than zero. Hence, in the cyclostationary based spectrum sensing, the detection can be described by comparing the value of b_k with a preset threshold λ, yielding

$$\begin{aligned} &\theta = H_0; \text{ if for all } b_k \ (k = 0, \ \pm 1, \ \pm 1, \cdots), \ b_k < \lambda \\ &\theta = H_1; \text{ if for some } b_k \ (k = 0, \ \pm 1, \ \pm 1, \cdots), \ b_k > \lambda \end{aligned} \tag{2.57}$$

Note that, for the Gaussian random process, the test statistics as shown in (2.57) is irrational, as the received signal is uncorrelated, yielding that

$$b_k = \lim_{\bar{T}\to\infty}\frac{1}{\bar{T}}\int_{-\frac{\bar{T}}{2}}^{\frac{\bar{T}}{2}} R_y(\tau)e^{-j2\pi f_0 k\tau}d\tau = 0; \quad k = 0, \ \pm 1, \ \pm 2, \cdots \tag{2.58}$$

In comparison with the energy based spectrum sensing, the cyclostationary detection is a non-coherent spectrum sensing approach. It is less sensitive to the noise uncertainty, provided that the cyclic frequency of signals is available. Furthermore, it is capable of distinguishing different types of digital modulation signals. On the other hand, when the cyclic frequency is not available at the receiver, the sensing device requires other sources to get the information, which increases the complexity of the cyclostationary detection [155]. Additionally, as shown in (2.58), cyclostationary detection may be completely fail, when the received signal is Gaussian distributed, which might be the result of many interference signals, multiple fading, etc.

2.4.4.2 Eigenvalue-based Detection

To overcome the shortcomings of energy detection, a method using the properties of the eigenvalues of received signal's covariance matrix is introduced [156–158]. The principles behind the eigenvalue-based detection is that the PR signals received at a CR user are usually correlated because of dispersive channels, utility of multiple receive antennas or even oversampling [151]. Such correlation can be utilized for offering highly reliable spectrum sensing.

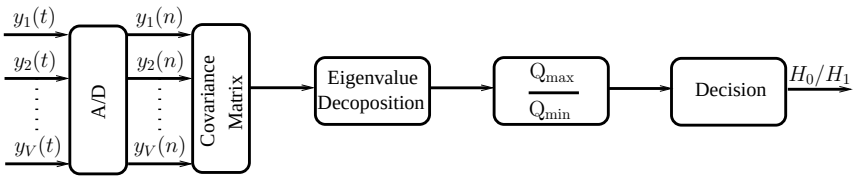

Figure 2.5: Flow chart of eigenvalue based spectrum sensing.

Specifically, with the aid of the eigenvalue-based detection, the vacancy of a frequency band of interest can be determined based on the fluctuation of the covariance matrix's eigenvalue. Let the covariance matrix $\hat{\boldsymbol{R}}_y$ of received signals be expressed as

$$\hat{\boldsymbol{R}}_y = \frac{1}{V}\sum_{v=0}^{V-1} \boldsymbol{y}[v]\boldsymbol{y}^H[v] \tag{2.59}$$

where V is the length of observation and $\boldsymbol{y}[v]$ is a vector of length N, for example, which contains the observation samples. The eigenvalues of $\hat{\boldsymbol{R}}_y$ can then be obtained via eigenvalue-based detection. From the eigenvalues, various test statistics may be formed. For examples, the ratio of the maximum to the minimum eigenvalues [159], the ratio of the maximum to the average eigen-

values [157], etc. In detail, let $\mu_{(0)} \geq \mu_{(1)} \geq \cdots \geq \lambda \geq \mu_{(N-1)}$ be the N eigenvalues of the covariance matrix $\hat{\boldsymbol{R}}_y$. The test statistics of the ratio between the maximum and minimum eigenvalues can be written as

$$\delta = \frac{\mu_{(0)}}{\mu_{(N-1)}} \underset{H_1}{\overset{H_0}{\lessgtr}} \lambda \tag{2.60}$$

Similarly, the test statistics of using the ratio between the maximum and average eigenvalues can be described as

$$\delta = \frac{\mu_{(0)}}{\sum_{i=0}^{N-1} \mu_{(i)}} \underset{H_1}{\overset{H_0}{\lessgtr}} \lambda \tag{2.61}$$

In [158], the asymptotic threshold values for the test statistics of (2.60), and (2.61) have been studied.

From above, the eigenvalue-based detection is based on the autocorrelation matrix $\hat{\boldsymbol{R}}_y$ of received signals, which is a noncoherent detector requiring only energy information. Hence, it is effective for implementation blindly. The eigenvalue-based detection becomes less efficient when signals become less correlated, as, in this case, all eigenvalues have similar values.

2.5 Conclusion

In this chapter, an overview of the detection approaches that may be employed by LSNs and FC, as well as the spectrum sensing approaches in CRs has been presented. Explicitly, each of the detection approaches has its unique advantages, disadvantages and requirements. Therefore, in design of local detection at LSNs and fusion rule for FC, the detection schemes should be carefully chosen based on the objectives and communication environments.

Specifically, the characteristics of the classical local detection, the optimum and sub-optimum channel-aware fusion rules, the noncoherent fusion rules and the spectrum sensing approaches are summarized as follows.

1. **Classical local detections**: In this chapter, we have introduced three types of classical binary local detection approaches. The Bayesian detection aims to minimize the average cost, which requires both the *a-priori* probability and the cost of each decision. When the cost function is

not available, the MAP or ML detection may be employed. The NP detection minimizes P_f for a given value of P_d or maximizes P_d for a given value of P_f without requiring any further information. The design objectives and requirements of these local detection approaches are summarized in Table 2.1.

Local Detection at LSNs	Objective	Requirements
Bayesian Detection	Minimize average cost	*a-priori* probability and cost function
MAP and ML Detection	Maximize the correct probability	*a-priori* probability
NP Detection	Minimize P_f for a given P_d or maximize P_d for a given P_f	None

Table 2.1: Objectives and requirements of local detection at LSNs.

2. **Channel-aware fusion rules**: In this chapter, the channel-aware fusion rules have been discussed based on a classical triple-layer WSN model. From our discussion and comparison, we can know that the LLR fusion rule achieves the best performance, under the stringent requirements including LSN's performance and CSI. To relieve from these requirements, the Chair-Varshney (CV) and the EGC fusion rule have been introduced. These sub-optimum channel-aware fusion rules have different requirements and yield sub-optimum performance. The trade-offs between the detection performance and the required *a-priori* information for optimum and sub-optimum channel-aware fusion rules are summarized in Table 2.2.

Fusion rule	*a-priori* information	Detection performance
Optimum LLR	CSI and LSNs' detection performance	Optimal
Chair-Varshney	LSNs' detection performance	Near-optimal for high SNR
MRC	CSI	Near-optimal for low SNR
EGC	Channel phase	Robust in wide SNR range

Table 2.2: Comparison among optimum and sub-optimum channel-aware fusion rules.

3. **Noncoherent M-ary fusion rules**: Some existing noncoherent M-ary fusion rules have been addressed in Section 2.3, which require no channel estimation nor LSNs' detection performance. All our discussion of the noncoherent M-ary fusion rules are based on a framework of MFSK WSN system. Specifically, the noncoherent M-ary fusion rules have been described based on a so-called detection matrix $\boldsymbol{D}$ formed at the FC. The decision variables for

the introduced noncoherent M-ary fusion rules are summarized in Table 2.3.

Fusion Rule	Decision Variable
EGC	$D_m = \sum_{l=1}^{L} D_{ml}$
MV	$D_m = \sum_{l=1}^{L} D'_{ml}$
SC	$D_m = \max\{D_{m1}, D_{m2}, \ldots, D_{mL}\}$
PC	$D_m = \prod_{l=1}^{L} D_{ml}$
NNC	$D_m = \sum_{l=1}^{L} \frac{D_{ml}}{\sigma^2_{ml}}$
SNC	$D_m = \sum_{l=1}^{L} \frac{D_{ml}}{D_{0l}+D_{1l}+\ldots+D_{(M-1)l}}$
SLC	$D'_m = \sum_{l=1}^{L} D'_{ml}$

Table 2.3: Decision variables of various M-ary noncoherent fusion rules.

4. **Spectrum sensing approaches**: In Section 2.4, a range of local spectrum sensing approaches have been introduced. The main task of spectrum sensing is to determine whether a particular frequency band is free or busy during a time slot within a certain geographical area. In this chapter, three local spectrum sensing approaches, namely, the energy detection, matched filter detection and feature detection have been addressed. The advantages and requirements of these spectrum sensing approaches are summarized in Table 2.4.

Spectrum sensing	Advantages	Requirements
Energy	Easy to implement and low-complexity	Noise variance
Matched Filter	Low-complexity and low-delay	Knowledge for all possible signals
Cyclostationary	Robust to noise uncertainty	Cyclic frequency
Eigenvalue-based	All above	Correlation of signals

Table 2.4: Comparison of local spectrum sensing approaches.

Chapter 3

Noncoherent Detection in FH/MFSK WSN Monitoring Single Event

3.1 Introduction

Due to the great potential for many applications and also due to the advancement of emerging technologies, WSNs have drawn intensive research in recent years. In WSNs, signal detection constitutes one of the very important tasks, and a lot of research effort has been made for design of high-efficiency and low-complexity detection algorithms [10, 74–76, 79–82, 103, 160]. Specifically, for monitoring binary events, optimum and sub-optimum detection algorithms have been derived under various optimization criteria, as shown in Chapter 2. As some examples, detection schemes found in literature include Neyman-Pearson detection [10, 82], Bayes detection [10, 75, 82], maximum likelihood detection [10, 74–76, 79, 82], maximum ratio combining and equal gain combining assisted detection [74–76, 79], Chair-Varshney detection [74, 75, 79], etc. In order to improve spectral efficiency and reduce detection delay, in [78], a multiple-access model has been proposed for transmission of signals from LSNs to FC and corresponding fusion detection rules have been studied. In [80], the fusion detection of M-ary events has been investigated by merging the fusion detection with channel decoding. Furthermore, owing to its low-complexity, in WSNs, noncoherent detection is often preferred to coherent detection, as the noncoherent detection does not require extra complexity and extra resources for channel estimation [115].

In this chapter, a novel wireless sensor network (WSN) framework, namely the frequency-

hopping M-ary frequency shift keying (FH/MFSK) WSN, is proposed, which monitors an M-ary source event (SE) and conveys signals from each local sensor node (LSN) to the fusion center (FC) with the aid of frequency-hopping (FH) and M-ary frequency-shift keying (MFSK) techniques. The SE under observation by LSNs are assumed to have M states occurring with equal-probable. The estimations of LSNs are transmitted to the FC using MFSK modulation aided by FH. Channels from LSNs to FC are modelled either as additive white Gaussian noise (AWGN) channels or Rayleigh fading channels.

In this proposed FH/MFSK WSN, the FH/MFSK technique is introduced for enhancing the detection performance by reducing the correlation among the signals transmitted by different LSNs, so that the FC can benefit from both the space diversity and the frequency diversity. Explicitly, this frequency diversity becomes more important, when the LSNs are closely distributed, making the signals transmitted by different LSNs correlated in space. In WSNs, coherent fusion rules are often preferred for the applications demanding high data rate. However, there are a range of applications, which weight the implementation complexity over the data rate. In these WSNs, noncoherent fusion rules are usually preferred, which achieve the fusion detection without relying on channel estimation. In this chapter, signals are noncoherently detected at the FC based on the square-law principles aided by conventional equal gain combining (EGC), novel erasure-supported equal gain combining (ES-EGC) fusion rule and optimum posterior fusion rule.

In this chapter, we analyze the lower-bound of error classification probability (ECP) performance of the FH/MFSK WSNs with ES-EGC fusion rule over Rayleigh fading channels. Furthermore, the detection performance of the FH/MFSK WSN is investigated by simulation approaches. Our studies show that the FH/MFSK constitutes one of the promising schemes for efficient information delivery in WSNs. Reliable detection can be achieved at reasonable SNR levels for detection at LSNs and at the FC. Compared with the conventional EGC fusion rule, our proposed ES-EGC fusion rule significantly improves the detection performance of FH/MFSK WSNs at low-cost of complexity and delay.

Note that, in our WSN systems, we choose MFSK instead of differential phase-shift keying (DPSK) because of the following considerations. First, it is well known that the MFSK is an energy efficient modulation scheme while the multiple DPSK can be counted as a bandwidth efficient scheme but not an energy-efficient scheme. For WSNs, we prefer to the energy-efficient

schemes in order t o extend the lifetime. Second, in DPSK, at least one pilot symbol is required and the detection is dependent one the one-step channel estimation. By contrast, MFSK can be fully noncoherent detected by depending on energy detection. Furthermore, when using the DPSK, the FH and data modulation have to be operated separately. In contrast, MFSK and FH can be jointly operated, which increases the bandwidth efficiency.

The reminder of this chapter is organized as follows. In Section 3.2, we provide the details of the proposed FH/MFSK WSN, where the observed SE, LSNs' processing are considered. In Section 3.3, signal processing at the FC with various fusion rules is analyzed. The characteristics of FH/MFSK WSN are described in Section 3.4. Section 3.5 provides the detection performance of FH/MFSK WSNs with ES-EGC fusion rules over Rayleigh fading channels. Then, some simulation results and discussions are provided in Section 3.6. Finally, in Section 3.7, our conclusions are derived.

3.2 System Description

The framework of the WSN considered in this chapter is shown in Fig 3.1, which is a typical triple-layer WSN model widely used for research in literature [74, 75, 79–82, 160]. As shown in Fig. 3.1, the L number of LSNs simultaneously observe an SE with M states and convey their observations to the FC using FH/MFSK. The FC finally makes a decision about the state of the observed SE, based on the signals received from the L LSNs. Below we describe in detail the components of the FH/MFSK WSN considered, as well as their operations and corresponding assumptions invoked.

3.2.1 Source Event

As shown in Fig. 3.1, the single SE s is assumed to have M states corresponding to M hypothesises, which are expressed by $H_0, H_1, \ldots, H_{M-1}$. In this chapter, we assume for simplicity that the M hypothesises represent M amplitudes, $A_0, A_1, \ldots, A_{M-1}$, obtained by quantizing a continuous event, such as temperature, pressure, etc. Therefore, given that the SE is at state m, $m = 0, \ldots, M-1$, the lth LSN's observation can be represented as

$$r_l = A_m + n_l, \quad l = 1, 2, \ldots, L \tag{3.1}$$

where n_l is the observation noise.

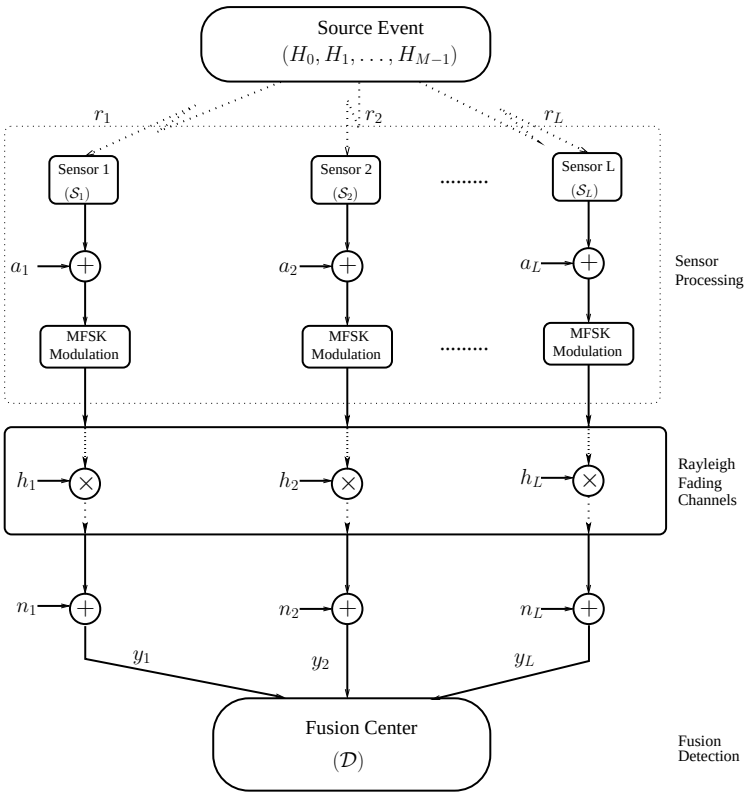

Figure 3.1: Triple-layer system model for the WSNs observing an M-ary event, where information is transmitted to the FC based on FH/MFSK scheme.

3.2.2 Sensor Processing

When the lth, $l = 1, 2, \ldots, L$, LSN obtains an observation in the form of (3.1) for the SE s, it decides the state of s based on the principle of MASK [115]. Let the states estimated by the L LSNs are collected to $\boldsymbol{s} = [s_1, s_2, \ldots, s_L]$, where $s_l = m$, if the lth LSN estimates that the SE's amplitude is A_m. Let us assume that the SE is linearly and uniformly quantized. Then, the decision error probability of each of the LSNs is given by [115]

$$P_e = 2\left(1 - \frac{1}{M}\right) Q\left(\sqrt{\frac{6\log_2 M}{M^2 - 1}\gamma_s}\right) \tag{3.2}$$

where γ_s represents the observation signal-to-noise ratio (SNR) at the LSNs, referred to as the sensor SNR for convenience. In practice, the sensor SNR γ_s is dependent on the SE's characteristics, the specific quantization approach used, the sensing method, etc. In (3.2), $Q(x)$ is the Gaussian Q-function defined as $Q(x) = (2\pi)^{-1/2} \int_x^\infty e^{-t^2/2} dt$. Note that, in our simulations in Section 3.6, we assume that an erroneous observation leads to one of the $(M-1)$ states other than the correct one with the same probability of $P_e/(M-1)$.

Following the sensing to determine a state of the SE, as shown in Fig. 3.1, the L LSNs transmit their observed states to the FC with the aid of the FH/MFSK techniques. The total transmission time is assumed to be T_s seconds, which is referred to as the symbol duration. Let us assume that the WSN system uses M orthogonal frequency bands with their center frequencies forming a set $\boldsymbol{F} = \{f_0, f_1, \ldots, f_{M-1}\}$. These M frequencies are used for both FH and MFSK modulation, which are implemented as follows. Let $\boldsymbol{a} = [a_1, a_2, \ldots, a_L]$ be a FH address used by the WSN, where the integer $a_l \in \{0, 1, \cdots, M-1\}$, $l = 1, 2, \ldots, L$. The purpose of using the FH address is two folds. First, transmitting the information about the SE on different frequency bands is capable of providing frequency-diversity for detection at the FC. This becomes even more important, when some LSNs are located close to each other, resulting in that their signals received by the FC are correlated, in the space domain, if the signals are transmitted on the same frequency band. Second, with the aid of the FH, signals received from the L LSNs can be noncoherently combined, which will become explicit in our forthcoming discourse. Based on the FH address $\boldsymbol{a}$ and the estimates $\boldsymbol{s}$, the LSNs first carry out the operation

$$\begin{aligned} \boldsymbol{m} &= [m_1, m_2, \cdots, m_L] = \boldsymbol{s} \oplus \boldsymbol{a} \\ &= [s_1 \oplus a_1, s_2 \oplus a_2, \cdots, s_L \oplus a_L] \end{aligned} \tag{3.3}$$

where $\oplus$ represents the addition operation in the Galois field ($GF(M)$). Therefore, the value of m_l, $l = 1, 2, \ldots, L$, is within $[0, M-1]$, suitable for MFSK modulation. Following the FH operation shown in (3.3), the components of $\boldsymbol{m}$ are respectively passed to the MFSK modulators of the L LSNs, where they are converted to the MFSK frequencies $\boldsymbol{F}_m = [f_{m_1}, f_{m_2}, \ldots, f_{m_L}]$, where $f_{m_l} \in \boldsymbol{F}$. Finally, the MFSK modulated signals of the L LSNs are transmitted one-by-one to the FC in a time-division fashion using L time-slots of duration T_h, where $T_h = T_s/L$. Specifically, the signal transmitted by the lth LSN during the $iT_s < t \leq (i+1)T_s$ can be expressed in complex form as

$$\begin{aligned} \tilde{s}_l(t) =& \sqrt{P}\psi_{T_h}(t - iT_s - (l-1)T_h) \\ & \times \exp(j2\pi[f_c + f_{m_l}]t + j\phi_l), \ \ l = 1, 2, \ldots, L \end{aligned} \tag{3.4}$$

where P denotes the transmission power, which is assumed the same for all the L LSNs, f_c is the main carrier frequency and ϕ_l is the initial phase introduced by carrier modulation. In (3.4), $\psi_{T_h}(t)$ is the pulse-shaped signalling waveform, which is defined over the interval $[0, T_h)$ and normalized

to satisfy $\int_0^{T_h} \psi^2(t)dt = T_h$.

Assuming that the signal $\tilde{s}_l(t),\ l = 1,2,\ldots,L$, is transmitted over flat Rayleigh fading channels, at the FC, the received signal during $iT_s < t \leq (i+1)T_s$ can be expressed as

$$\begin{aligned} y_l(t) =& h_l\tilde{s}_l(t) + n_l(t) \\ =& \sqrt{P}h_l\psi_{T_h}(t - iT_s - (l-1)T_h) \times \exp(j2\pi[f_c + f_{m_l}]t + j\phi_l) + n(t), \\ l =& 1,2,\ldots,L \end{aligned} \tag{3.5}$$

where $h_l = \alpha_l \exp(j\theta_l)$ denotes the channel gain with respect to the ith symbol and the lth LSN, which is assumed constant over one symbol-duration. Furthermore, when Gaussian channels are assumed, we have $\alpha_l = 1$. In (3.5), $n(t)$ is the Gaussian noise process presenting at the FC, which has zero mean and single-sided power-spectral density (PSD) of N_0 per dimension.

3.3 Fusion Processing

When the FC receives the signals in the form of (3.5), the SE's state is estimated using noncoherent detection approach detailed as follows.

First, corresponding to each of the L LSNs, M decision variables can be formed as

$$\begin{aligned} R_{ml} =& |(\sqrt{\Omega P}T_h)^{-1} \int_{iT_s+lT_h}^{iT_s+(l+1)T_h} y_l(t)\psi^*_{T_h}(t - iT_s - (l-1)T_h) \\ & \times \exp(-j2\pi[f_c + f_m]t)dt|^2, \end{aligned} \tag{3.6}$$

where $m = 0,1,\ldots,M-1$ and $l = 1,2,\ldots,L$, and $\Omega = E[|h_l|^2]$ denotes the average channel power. Since it has been assumed that the M frequency bands invoked are orthogonal to each other, there is no interference between any two frequency bands. Consequently, upon substituting (3.5) into (3.6) and absorbing the carrier phase ϕ_l into h_l, we obtain

$$R_{ml} = \left| \frac{\mu_{mm_l}h_l}{\sqrt{\Omega}} + N_{ml} \right|^2,\ m = 0,1,\ldots,M-1;\ \ l = 1,2,\ldots,L \tag{3.7}$$

where, by definition, $\mu_{mm} = 1$, if $m = m_l$, otherwise $\mu_{mm_l} = 0$. In (3.7), N_{ml} is a complex Gaussian noise sample collected from the mth frequency band over the lth time-slot, which is

given by

$$N_{ml} = (\sqrt{\Omega P}T_h)^{-1} \int_{iT_s+lT_h}^{iT_s+(l+1)T_h} n(t)\psi^*_{T_h}(t - iT_s - (l-1)T_h) \times \exp(-j2\pi[f_c + f_m]t)dt \tag{3.8}$$

which has mean zero and a variance of $\sigma^2 = LN_0/(\Omega E_s) = L/\bar{\gamma}_s$, where $E_s = PT_s$ represents the total energy for transmitting one M-ary source symbol from L LSNs to FC, with each LSN's transmitted energy being $E_h = E_s/L$, $\bar{\gamma}_s = \Omega E_s/N_0$ denotes the average SNR per symbol.

From (3.7), we can see that there are in total ML decision variables, which can be used to form a $(M \times L)$ time-frequency matrix denoted by R. Based on this time-frequency matrix $\boldsymbol{R}$, the FC can carry out the final detection. In this chapter, a range of detection schemes are considered, which include EGC, ES-EGC and posterior fusion rule. Let us first state the EGC fusion rule.

3.3.1 EGC Fusion Rule

In the context of the EGC fusion rule, the FC detects the observed SE's state based on the detection matrix $\boldsymbol{D}$ obtained from frequency de-hopping on $\boldsymbol{R}$. More details are stated as follows.

1. **Frequency De-hopping**:

$$\boldsymbol{D} = \boldsymbol{R} \boxminus (\mathbf{1} \otimes \boldsymbol{a}^T) \tag{3.9}$$

where $\mathbf{1}$ denotes an all-one column vector of M-length and $\otimes$ denotes the Kronecker product operation between two matrices [116]. In (3.9), the operation of $\boldsymbol{A} \boxminus \boldsymbol{B}$ shifts the elements in $\boldsymbol{A}$ based on the values provided by $\boldsymbol{B}$. Specifically, after the operation in (3.9), we have

$$D_{(m \ominus a_l)l} = R_{ml},\ m = 0, 1, \ldots, M-1,\ \ l = 1, 2, \ldots, L \tag{3.10}$$

where $\ominus$ denotes the subtraction operation in the Galois field $GF(M)$. The operation in (3.10) means that the element indexed by m in $\boldsymbol{R}$ is changed to the one indexed by $m' = m \ominus a_l$ in $\boldsymbol{D}$.

2. **EGC Detection**: Finally, the M decision variables for detection of the SE's state can be formed in EGC principle [116] as

$$D_m = \sum_{l=1}^{L} D_{ml}, \quad m = 0, 1, \ldots, M-1 \tag{3.11}$$

Then, the largest one of $\{D_0, D_1, \cdots, D_{M-1}\}$ is selected and mapped to an integer in the range $[0, M-1]$, which represents the estimate to the SE's state.

3.3.2 ES-EGC Fusion Rule

After some close look, we can know that there are mainly two reasons behind the erroneous detections in the SE FH/MFSK WSNs. The first one is that the LSNs are not perfect, which may make erroneous local decisions. Secondly, the local decisions transmitted through wireless channels to the FC experience channel fading and noise. When some LSNs make erroneous decisions, undesired signals will be sent. Statistically, in $\boldsymbol{R}$ and $\boldsymbol{D}$, the entries containing both signals and noise would have relatively higher power than those containing only noise. Based on this observation, before forming the decision variables, the FC can erase a few of entries with the highest values from each row of $\boldsymbol{D}$. In this way, the undesired elements are most probably removed and the detection performance can be improved. Our ES-EGC fusion rule is based on above observation, the detection processing of which can be stated as follows.

1. **Frequency De-hopping**:

$$\boldsymbol{D} = \boldsymbol{R} \boxminus (\mathbf{1} \otimes \boldsymbol{a}^T) \tag{3.12}$$

   which is the same as that in the EGC fusion rule.

2. **Erasure Operation**: In each of the M rows of $\boldsymbol{D}$, I $(0 < I < L)$ elements having the largest values are replaced with zeros, forming a new matrix $\bar{\boldsymbol{D}}$.

3. **EGC Detection**: M decision variables are formed from $\bar{\boldsymbol{D}}$ in the EGC principles [116] as

$$\bar{D}_m = \sum_{l=1}^{L} \bar{D}_{ml}, \quad m = 0, 1, \ldots, M-1 \tag{3.13}$$

   Finally, the largest of $\{\bar{D}_0, \bar{D}_1, \cdots, \bar{D}_{(M-1)}\}$ is selected and its index is mapped to an integer in the range $[0, M-1]$, which represents the estimation to the state of the SE being observed.

3.3.3 Optimum Fusion Rule

Above, we have considered two low-complexity fusion rules, which are not optimum. Let us now consider the optimum rules which are in MAP and ML principles. The optimum fusion rule is

derived based on the observations provided by the square-law devices. Let us assume that the observed SE is at state H_m, where $m = 0, \ldots, M-1$. For a given state value X of the SE and a FH address of $\boldsymbol{a}$, the probability density function (PDF) of the received matrix $\boldsymbol{R}$ can be expressed as $p(\boldsymbol{R}|X, \boldsymbol{a})$. Then, based on the MAP principles, the SE's state can be estimated according to the optimization problem

$$\begin{aligned}\widehat{X} &= \max_{X\in\mathcal{X}} p(X|\boldsymbol{R}, \boldsymbol{a}) \\ &\stackrel{\triangle}{=} \max_{X\in\mathcal{X}}\{P(X)p(\boldsymbol{R}|X, \boldsymbol{a})\}\end{aligned} \tag{3.14}$$

where $\mathcal{X} = \{0, 1, \cdots, M-1\}$ is a set containing the M possible states.

When all the hypotheses for the states of the SE are equal-probability, the influence of $P(X)$ can be ignored in (3.14). Furthermore, using the fact that the ML entries in the received matrix $\boldsymbol{R}$ are independent, $p(\boldsymbol{R}|X, \boldsymbol{a})$ can be then rewritten as

$$p(\boldsymbol{R}|X, \boldsymbol{a}) = \prod_{m=0}^{M-1}\prod_{l=1}^{L} p(R_{ml}|X, \boldsymbol{a}) \tag{3.15}$$

Upon substituting (3.15) into (3.14) and considering the equal-probability of the hypotheses, the MAP-assisted optimization can be modified to

$$\widehat{X} = \max_{X\in\mathcal{X}}\{\prod_{m=0}^{M-1}\prod_{l=1}^{L} p(R_{ml}|X,\boldsymbol{a})\} \tag{3.16}$$

Let the local estimations made by the L LSNs be collected to $\boldsymbol{s} = [s_1, s_2, \ldots, s_L]$. Then, one given SE's state corresponds to M^L possible local estimation vectors $\boldsymbol{s}_n$. Hence, (3.16) can be rewritten as

$$\widehat{X} = \max_{X\in\mathcal{X}}\{\sum_{n=0}^{M^L} P(\boldsymbol{s}_n|X)\prod_{m=0}^{M-1}\prod_{l=1}^{L} p(R_{ml}|\boldsymbol{s}, \boldsymbol{a})\} \tag{3.17}$$

when assuming that the channels from LSNs to the FC are Rayleigh fading channels, the PDF of R_{ml} can be expressed as

$$p(R_{ml}|\boldsymbol{s}, \boldsymbol{a}) = \frac{1}{K_{ml}+\sigma^2}\exp\left(-\frac{R_{ml}}{K_{ml}+\sigma^2}\right) \tag{3.18}$$

where σ^2 denotes the normalized noise variance, $K_{ml} = 1$, if the lth LSN actives the (m,l)th element in the received matrix $\boldsymbol{R}$, otherwise, $K_{ml} = 0$. Finally, when substituting (3.18) into (3.17), the optimization problem can be described as

$$\widehat{X} = \max_{X\in\mathcal{X}}\left\{\sum_{n=0}^{M^L} P(\boldsymbol{s}_n|X)\prod_{m=0}^{M-1}\prod_{l=1}^{L}\frac{1}{K_{ml}+\sigma^2}\exp\left(-\frac{R_{ml}}{K_{ml}+\sigma^2}\right)\right\} \tag{3.19}$$

From the above discussion, it can be seen that, when communicating over Rayleigh fading channels with Gaussian noise, the FC needs to carry out $M \times M^L = M^{L+1}$ tests to find the final decision. Therefore, the complexity of the optimum detection increases exponentially with the value of M, which is prohibitive for practical application. Following, a sub-optimum fusion rule is considered, when the MAP is operated after using the EGC to find some desirable candidates. In brief, when the FC forms the received matrix $\boldsymbol{R}$, EGC fusion rule is first employed to get several possible estimations (candidates) of the SE's state. Then the FC makes further decision among the possible states using the MAP principles. In detail, this sub-optimum fusion rule is stated as follows.

1. **Frequency De-hopping**:

$$D_{(m\ominus a_l)l} = R_{ml},\ m = 0,1,\ldots,M-1,\ \ l = 1,2,\ldots,L \tag{3.20}$$

2. **EGC Estimation**: After the frequency de-hopping, M decision variables are formed in EGC principles [116] as

$$D_m = \sum_{l=1}^{L} D_{ml},\quad m = 0,1,\ldots,M-1 \tag{3.21}$$

3. **Identification of candidates**: W, $W = 1,\ 2,\cdots,\ M$, largest elements of $\{D_0, D_1,\cdots, D_{M-1}\}$ are selected and their indexes represent the W possible states of the SE. The set of the possible states is defined as $\mathcal{X}_W$.

4. **Detection**: Final decision is made according to the optimization:

$$\widehat{X} = \max_{X\in\mathcal{X}_W}\left\{\sum_{n=0}^{M^L} P(\boldsymbol{s}_n|X)\prod_{m=0}^{M-1}\prod_{l=1}^{L}\frac{1}{K_{ml}+\sigma^2}\exp\left(-\frac{R_{ml}}{K_{ml}+\sigma^2}\right)\right\} \tag{3.22}$$

From (3.22), it can be seen that the sub-optimum fusion rule needs $W \times M^L$ tests, in order to make the final decision, which is still exponential with respect to L. Furthermore, when $W = M$, the sub-optimum fusion rule is the same as the optimum fusion rule. By contrast, in the case of $W = 1$, the sub-optimum fusion rule is the same as the conventional EGC fusion rule, as optimization of (3.22) is unnecessary.

The computation complexity can be further slightly reduced by reducing the terms involved in the product, which we refer to as the shrink local decisions aided sub-optimum MAP (SLD-SMAP) fusion rule. Specifically, with the SLD-SMAP, the FC first derives candidate sates that

the SE may be at based on the EGC fusion rule. Then, from the received matrix $\boldsymbol{R}$ the elements possibly activated are identified with the aid of a threshold, say λ, forming a referred matrix $\tilde{\boldsymbol{R}}$. If the value of an element in $\boldsymbol{R}$ is higher than the threshold, the corresponding element in $\tilde{\boldsymbol{R}}$ is set to one. Otherwise, it is set to zero. In this way, the MAP detection only needs to consider those $\boldsymbol{s}_n's$, which activate the elements all matching to the nonzero elements in $\tilde{\boldsymbol{R}}$. Let the set containing such $\boldsymbol{s}_n's$ be expressed as $\mathcal{N}$.

Then the final decision of the SLD-SMAP can be made based on the optimization problem:

$$\widehat{X} = \max_{X \in \mathcal{X}_W} \left\{ \sum_{n \in \mathcal{N}} P(\boldsymbol{s}_n | X) \prod_{m \in (\tilde{R}_{ml}=1)}^{M-1} \prod_{l=1}^{L} \frac{1}{K_{ml}+\sigma^2} \exp\left(-\frac{R_{ml}}{K_{ml}+\sigma^2} \right) \right\} \tag{3.23}$$

From (3.23) we can see that the complexity of the SLD-SMAP is determined by the threshold λ, which can be controlled at a reasonable level according to the practical requirements.

3.4 Analysis of FH/MFSK WSNs Characteristics

First, the FH/MFSK WSNs are in favour of employing noncoherent fusion rules. All the fusion detection schemes described in Section 3.3 are noncoherent detection schemes, which do not require to consume extra energy for channel estimation. This energy-efficient and, typically, low-complexity detection strategies are beneficial to the life-time of battery-powered WSNs. Second, in our proposed FH/MFSK WSNs, the introduction of FH can improve the achievable diversity gain. The FH operation makes the component signals combined at FC become more uncorrelated, in addition to the uncorrelation introduced by the spatial separation of LSNs. It can be known that the FH operation turns out to become more important, if LSNs are located close to each other in space. In this case, signals transmitted by different LSNs may become correlated in space and full space diversity cannot be guaranteed. Additionally, owing to the employment of noncoherent MFSK and FH, the FH/MFSK assisted WSN can benefit from the embedded advantages of noncoherent MFSK and FH techniques [116].

In this chapter, three different fusion rules are introduced, including the EGC, ES-EGC and optimum fusion rules. Among these fusion rules, EGC fusion rule is probably the simplest linear combining and characterized by the property that all the channels are equally weighted. However, as the LSNs are not perfect and make erroneous decisions, EGC fusion rule may experience se-

riously problems from these errors, which may significantly degrade the detection performance, when local detections are not reliable. ES-EGC fusion rule can efficiently mitigate the negative influence generated by the erroneous local decisions. It is also a low-complexity fusion rule. The optimum noncoherent fusion rule considered in Section 3.3.3 is derived based on the MAP principle, which is capable of attaining the optimum performance. However, its complexity is exponentially dependent the value of L, which is prohibitive for practical application. In this case, by reducing the testing spaces, the sub-optimum fusion rule, especially, the SLD-SMAP fusion rule, may have significantly lower complexity than the optimum fusion rule.

Note that, in the FH/MFSK WSNs, the final achievable detection performance is jointly determined by the detection performance of L LSNs and that of FC. If the detection performance of the L LSNs is poor, the overall achievable detection performance will probably be poor, even when the detection at the FC is very reliable. Similarly, the overall achievable detection performance will become worse, if the detection at the FC becomes less reliable. Hence, when considering the optimization in FH/MFSK WSNs, the fusion detection and the LSNs' detection need to be jointly optimized. However, we note that the optimization issue is beyond the scope of this thesis, which, however, constitutes one of our future research topics in the context of the FH/MFSK WSNs.

3.5 Analysis of Detection Performance of FH/MFSK WSNs with Single SE

From the principles of FH/MFSK WSNs, as shown in the previous sections, we can see that the overall performance of the FH/MFSK WSNs is effected by both the L LSNs' detection reliability and the FC's detection reliability. In this section, we assume that the error detection probability of all LSNs are the same and is expressed as P_e. Correspondingly, the correct detection probability of LSNs is expressed as P_d, and $P_d + P_e = 1$. Due to the unreliable observations made by LSNs, the final detection at FC might not be reliable, even though the channel SNR of the wireless channels from LSNs to FC is sufficiently high. In this case, an error-floor of the detection probability at FC may be observed. In this section, we first analyse the error floor of the detection performance of the FH/MFSK WSNs with EGC or ES-EGC fusion rule. Then, a lower-bound for the the error probability of ES-EGC fusion rule over Rayleigh fading channels is investigated.

3.5.1 Error Floor of EGC Fusion Rule

For convenience of our analysis, it is reasonable to assume that all the L LSNs make their local decisions independently. Since it is the error-floor that is considered, the transmission from LSNs to FC is assumed to be ideal without introducing errors. Under the EGC principles, when there are L LSNs and if the transmission from LSNs to FC is ideal, the detection at FC is correct, provided that more than half of the L LSNs make correct local decisions. Hence, for deriving the error-floor, we only need to consider the cases that more than half of the LSNs make their local decisions incorrectly. Let $P_E(i)$ denote the erroneous fusion detection probability, when there are i, $i = 0, 1, ..., \lfloor L/2 \rfloor$, LSNs make correct local detections, while the other $(L-i)$ LSNs make erroneous detections. Here, $\lfloor L/2 \rfloor$ denotes the integer smaller or equal to $L/2$. Then, the average error classification probability (ECP) at FC can be expressed as

$$P_E = \sum_{i=0}^{\lfloor L/2 \rfloor} A_i P_E(i) \tag{3.24}$$

where A_i is the probability that there are i out of L LSNs make correct detections, which can be expressed as

$$A_i = \binom{L}{i} P_d^i P_e^{L-i} \tag{3.25}$$

Furthermore, among the $(L-i)$ LSNs making erroneous detections, if there are no more than $(i-1)$ LSNs choosing the same erroneous state, the fusion detection is still correct when communicating over ideal wireless channels. Hence, $P_E(i)$ for $i = 0, 1, \cdots, \lfloor L/2 \rfloor$ can be expressed as

$$P_E(i) = \sum_{k=i}^{L-i} \binom{M-1}{1} \left(\frac{1}{M-1}\right)^k \left(\frac{M-2}{M-1}\right)^{L-i-k} \tag{3.26}$$

where, for simplicity, we assumed that the FC will make an erroneous decision, if i erroneous LSNs choose the same state. Upon substituting (3.25) and (3.26) into (3.24), the ECP floor can be expressed as

$$P_E = \sum_{i=0}^{\lfloor L/2 \rfloor} \sum_{k=i}^{L-i} \binom{L}{i} P_d^i P_e^{L-i} \left(\frac{1}{M-1}\right)^{k-1} \left(\frac{M-2}{M-1}\right)^{L-i-k} \tag{3.27}$$

Note that, in practice, if i out of the $(L-i)$ erroneous LSNs choose the same state, the FC will make a final decision randomly, which results in an error probability of 0.5. However, when the number of LSNs is big enough, the approximates result of (3.27) is accurate.

3.5.2 Error Floor of ES-EGC Fusion Rule

Again, we assume that A_i of (3.25) is the probability that i out of the L CRSNs make correct local decisions and the other $(L-i)$ CRSNs make erroneous local decision. The FC makes an erroneous decision, when there is at least one undesired row, which contains at least i entries. Let us consider the following two cases.

First, when $1 \leq I \leq \lfloor L/2 \rfloor$, i.e., when at most half of the L elements are removed from each of the L rows, the error-floor of the ES-EGC fusion rule can also be expressed as (3.24). In this case, if $0 \leq i \leq I$, all the i elements in the desired row, which are sent by the i CRSNs making correct local decisions, are removed. Consequently, we can simply approximate $P_E(i) = 1$. By contrast, when $I < i \leq \lfloor L/2 \rfloor$, denoting that, after removing I elements from each of the M rows, there are still $(i-I)$ entries in the desired row. In this case, an error occurs, only if there is at least a undesired row, which has at least $(i-I)$ nonzero elements, or there are at least i entries before the erasure operation. Therefore, we can express $P_E(i)$ for $i = I+1, I+2, \cdots, \lfloor L/2 \rfloor$ as

$$P_E(i) = \sum_{k=i}^{L-i} (M-1) \left(\frac{1}{M-1}\right)^k \left(\frac{M-2}{M-1}\right)^{L-i-k} \tag{3.28}$$

Consequently, when considering the above two cases, we have

$$\begin{aligned} P_E = &\sum_{i=0}^{I} \binom{L}{i} P_d^i P_e^{L-i} + \sum_{i=I+1}^{\lfloor L/2 \rfloor} \sum_{k=i}^{L-i} \binom{L}{i} P_d^i P_e^{L-i} \\ &\times \left(\frac{1}{M-1}\right)^{k-1} \left(\frac{M-2}{M-1}\right)^{L-i-k}, \ 1 \leq I \leq \lfloor L/2 \rfloor \end{aligned} \tag{3.29}$$

The second case is when $\lfloor L/2 \rfloor < I < L$, i.e., when more than half of the L elements per row are removed. Then, if $i \leq I$, we can know that all the i nonzero elements in the desired row will be removed, yielding an approximate erroneous probability $P_E(i) = 1$. By contrast, if $i > I$, meaning that more than I of the L CRSNs send the FC the correct symbol, the desired row still has $(i-I)$ nonzero elements. By contrast, all the nonzero elements in the undesired rows are removed, as the number of nonzero entries in all the undesired rows is less than I. Consequently, the FC always makes correct decision. Therefore, by considering the above cases, we have

$$P_E = \sum_{i=0}^{I} A_i P_E(i) = \sum_{i=0}^{I} \binom{L}{i} P_d^i P_e^{L-i}, \ \lfloor L/2 \rfloor < I < L. \tag{3.30}$$

3.5.3 Errors Probability of ES-EGC Over Flat Rayleigh Fading Channels

Due to the randomness of the TF-elements activated by erroneous local decisions, there are many possible combinations required to be considered when analyzing the error performance of the FH/MFSK WSNs. Furthermore, the erasure operations invoked make the analysis highly involved, as the remaining decision variables after the erasure operations become correlated. For this sake, in this section, we analyse the detection performance of ES-EGC fusion rule with perfect LSNs. This ECP (BER) can be viewed as a lower-bound of the ECP (BER) of the FH/MFSK WSN systems.

Without loss of any generality, we assume that the observed SE belong to state $m = 0$. In this case, the elements D_{ml} obey the exponential distribution with the probability density function (PDF) expressed as [115]

$$\begin{aligned} p_{D_{0l}}(D_{0l}) =& \frac{1}{1+\bar{\gamma}_L}\exp\left(-\frac{D_{0l}}{1+\bar{\gamma}_L}\right),\ m=0 \\ p_{D_{ml}}(D_{ml}) =& \frac{1}{\bar{\gamma}_L}\exp\left(-\frac{D_{ml}}{\bar{\gamma}_L}\right),\ 1\le m\le M-1 \end{aligned} \tag{3.31}$$

for $l = 1,2,\ldots,L$, where $\bar{\gamma}_L = \bar{\gamma}_s/L$ and $\bar{\gamma}_s$ represents the average SNR per symbol. For convenience, let us combine above two equations into one by introducing $\bar{\gamma}_m = 1+\bar{\gamma}_L$ for $m = 0$ and, otherwise, $\bar{\gamma}_m = \bar{\gamma}_L$. In this case, the cumulative distribution function (CDF) of D_{ml} can be expressed as [115]

$$P_{D_{ml}}(D_{ml}) = 1-\exp\left(-\frac{D_{ml}}{\bar{\gamma}_m}\right),\ 0\le m\le M-1 \tag{3.32}$$

As discussed previously in Section 3.3.2, in the ES-EGC fusion rule, I $(I < L)$ largest TF elements are deleted from each of the M rows of $\boldsymbol{D}$. This process is equivalent to ordering the elements of each row from the maximum to the minimum and, then, deleting the I largest, forming the decision matrix $\bar{\boldsymbol{D}}$. Correspondingly, the decision variables of the ES-EGC can be written as

$$\bar{D}_m = \sum_{l=I}^{L}\bar{D}_{ml},\ m=0,1,\ldots,M-1 \tag{3.33}$$

Furthermore, after the ordering, the elements are no long independent and identically distributed (iid). Instead, the PDF of the lth, $l \ge I$, largest in row m of $\bar{\boldsymbol{D}}$ is given by

$$p_{\bar{D}_{ml}}(\bar{D}_{ml}) = \frac{l!}{(l-1)!(L-l)!}P_{D_{ml}}(D_{ml})^{L-l}\left[1-P_{D_{ml}}(D_{ml})\right]^{l-1}p_{D_{ml}}(D_{ml}) \tag{3.34}$$

where the PDF $p_{D_{ml}}(D_{ml})$ and CDF $P_{D_{ml}}(D_{ml})$ are given in (3.31) and (3.32), respectively.

In order to derive the error probability of the ES-EGC scheme, first, we need to derive the PDF of $\bar{D}_m$ for $m = 0, 1, \ldots, M-1$. In this section, we derive the PDFs with the aid of the moment generating function (MGF) [129]. The MGF of the decision variable $\bar{D}_m$ can be expressed as

$$\begin{aligned}\mathcal{M}_{\bar{D}_m}(s) &= E_{\bar{D}_m}\left[\exp\left(s\bar{D}_m\right)\right] \\ &= E_{\bar{D}_{mN},\bar{D}_{m(N+1)},\ldots,\bar{D}_{m(L)}}\left[\exp\left(s\sum_{l=N}^{L}\bar{D}_{ml}\right)\right]\end{aligned} \tag{3.35}$$

where $E[\cdot]$ denotes the expectation operation with respect to the distributions of $\bar{D}_{mN}, \bar{D}_{m(N+1)}$, $\ldots, \bar{D}_{m(L)}$. However, due to the dependence of $\bar{D}_{mN}, \bar{D}_{m(N+1)}, \ldots, \bar{D}_{m(L)}$, the MGF of (3.35) is unable to be directly derived. For solving this dilemma, the Sukhatme's approach [161] is introduced. Let us define the transforms

$$\begin{aligned}&X_{mn} \triangleq \bar{D}_{m(I-1+n)} - \bar{D}_{m(I+n)},\ n = 1, 2, \cdots, L-I-1 \\ &X_{m(L-I)} \triangleq \bar{D}_{m(L)}\end{aligned} \tag{3.36}$$

where $X_{mn} \geq 0$, as the elements in each row of $\bar{\boldsymbol{D}}$ are arranged in decreasing order. Then, we have

$$\bar{D}_m = \sum_{l=I}^{L}\bar{D}_{ml} = \sum_{n=1}^{L-I} nX_{mn} \tag{3.37}$$

According to [161], the random variables X_{mn}, $n = 1, 2, \cdots, L-I$ are independent random variables following the exponential distributions

$$p_{X_{mn}}(x_n) = \frac{I+n}{\bar{\gamma}_m}\exp\left[-\frac{x_n(I+n)}{\bar{\gamma}_m}\right],\ x_n \geq 0,\ n = 1, 2, \cdots, L-I \tag{3.38}$$

Hence, when substituting (3.37) into (3.35), we can express the MGF of the decision variable $\bar{D}_m$ as

$$\begin{aligned}\mathcal{M}_{\bar{D}_m}(s) &= E_{X_{m1},X_{m2},\ldots,X_{m(L-I)}}\left[\exp\left(s\sum_{n=1}^{L-I} nX_{mn}\right)\right] \\ &= \prod_{n=1}^{L-I}\int_0^{\infty} e^{snx_n} p_{X_{mn}}(x_n)\, dx_n\end{aligned} \tag{3.39}$$

Upon substituting (3.38) into the above equation, we obtain

$$\begin{aligned}\mathcal{M}_{\bar{D}_m}(s) &= \prod_{n=1}^{L-I}\int_0^{\infty} e^{snx_n}\frac{I+n}{\bar{\gamma}_m}e^{-\frac{x_n(I+n)}{\bar{\gamma}_m}}dx_n \\ &= \prod_{n=1}^{L-I}\left(\frac{I+n}{I+n-n\bar{\gamma}_m s}\right)\end{aligned} \tag{3.40}$$

From the definitions of the MGF and the Laplace transform, we can readily know that the Laplace transform of the PDF of $\bar{D}_m$ is given by

$$\begin{aligned}\mathcal{L}_{\bar{D}_m}(s) &= \mathcal{M}_{\bar{D}_m}(-s) \\ &= \prod_{n=1}^{L-I}\left(\frac{I+n}{I+n+n\bar{\gamma}_m s}\right) \\ &= \prod_{n=1}^{L-I}\left(\frac{1}{1+\frac{n\bar{\gamma}_m}{I+n}s}\right)\end{aligned} \tag{3.41}$$

Finally, with the aid of the residue theorem [162] for the inverse Laplace transform, the PDF of $\bar{D}_m$ can be expressed in closed form as

$$p_{\bar{D}_m}(z_m) = \sum_{n=1}^{L-I} S(L,I,n)\frac{I+n}{n\bar{\gamma}_m}\exp\left(-\frac{I+n}{n\bar{\gamma}_m}z_m\right), \quad m=0,1,\ldots,M-1 \tag{3.42}$$

where, by definition, $S(L,I,n) = \prod_{u=1,u\neq n}^{L-I}\frac{n(I+u)}{n(I+u)-u(I+n)}$. Note that, (3.42) is not suitable for the case of $I=0$. When $I=0$, the problem is reduced to the conventional one and the corresponding PDF can be found from many text books, such as from [115]. From (3.42), we can readily obtain the CDF of $\bar{D}_m$, which is

$$P_{\bar{D}_m}(z_m) = \sum_{n=1}^{L-I} S(L,I,n)\left(1-\exp\left(-\frac{I+n}{n\bar{\gamma}_m}z_m\right)\right), \quad m=0,1,\ldots,M-1 \tag{3.43}$$

When given the PDFs and CDFs of the decision variables $\bar{D}_m$ for $m=0,1,\ldots,M-1$, the ECP of the FH/MFSK WSNs employing the ES-EGC can be derived from the formula [115]

$$\begin{aligned}P_E =& 1-\int_0^\infty p_{\bar{D}_0}(z_0)\left[\int_0^{z_0} p_{\bar{D}_1}(z_1)dz_1\right]^{M-1} dz_0 \\ =& 1-\int_0^\infty p_{\bar{D}_0}(z_0)\left[P_{\bar{D}_1}(z_0)\right]^{M-1} dz_0\end{aligned} \tag{3.44}$$

After substituting $p_{\bar{D}_m}(z_m)$ of (3.42) with $m=0$ and $P_{\bar{D}_m}(z_m)$ of (3.43) with $m=1$ into the above equation and completing the second integration, we can express of the ECP as

$$\begin{aligned}P_E = 1-&\int_0^\infty \sum_{n=1}^{L-I} S(L,I,n)\frac{I+n}{n(1+\bar{\gamma}_L)}\exp\left(-\frac{I+n}{n(1+\bar{\gamma}_L)}z_0\right) \\ &\times\left[\sum_{m=1}^{L-I} S(L,I,m)\left(1-\exp\left(-\frac{I+m}{m\bar{\gamma}_L}z_0\right)\right)\right]^{M-1} dz_0\end{aligned} \tag{3.45}$$

where $\bar{\gamma}_0 = 1+\bar{\gamma}_L$ and $\bar{\gamma}_1 = \bar{\gamma}_L$ were used.

Additionally, upon following [115], an union-bound for the ECP of (3.44) can be obtained, which can be expressed as

$$\begin{aligned} P_E^{(U)} &= (M-1)\, P\left(\bar{D}_1 > \bar{D}_0\right) \\ &= (M-1) \int_0^{\infty} p_{\bar{D}_1}(z_1) P_{\bar{D}_0}(z_1) dz_1 \\ &= (M-1) \int_0^{\infty} \sum_{n=1}^{L-I} S(L,I,n) \frac{I+n}{n\bar{\gamma}_L} \exp\left(-\frac{I+n}{n\bar{\gamma}_L} z_1\right) \\ &\quad \times \left[\sum_{m=1}^{L-I} S(L,I,m) \left(1 - \exp\left(-\frac{I+m}{m(1+\bar{\gamma}_L)} z_1\right)\right)\right] dz_1 \end{aligned} \tag{3.46}$$

Upon completing the integration and after some arrangement, we arrive at

$$\begin{aligned} P_E^{(U)} = (M-1) \sum_{n=1}^{L-I} \sum_{m=1}^{L-I} & S(L,I,n) S(L,I,m) \\ & \times \left[1 - \left(1 + \frac{n(I+m)\bar{\gamma}_L}{m(I+n)(1+\bar{\gamma}_L)}\right)^{-1}\right] \end{aligned} \tag{3.47}$$

Finally, when assuming that the M possible symbols are transmitted with the same probability, the BER of the FH/MFSK WSNs using ES-EGCD can be evaluated from the formula [115]

$$P_B = \frac{M}{2(M-1)} P_E \text{ and } P_B^{(U)} = \frac{M}{2(M-1)} P_E^{(U)} \tag{3.48}$$

3.6 Simulation Results and Analysis

In this section, the simulation results for the error performance of our FH/MFSK WSNs are depicted and analysed. The ECP performance of the FH/MFSK WSNs is investigated, when assuming that signals observed by LSNs are only disturbed by Gaussian noise, while the channels from LSNs to FC are AWGN or Rayleigh fading channels. Some ECP performance evaluated from the analytical formulas is also shown and compared with the simulation results. Additionally, some comparison on the detection performance of the various fusion rules is carried out.

Fig. 3.2 depicts the ECP performance of the FH/MFSK WSNs employing EGC or ES-EGC fusion rule, when operated over AWGN (Fig. 3.2a) or Rayleigh fading channels (Fig. 3.2b). The local detection probability of each LSN is set as $P_d = 0.95$, and $I = 1$ erasure is used in the ES-EGC fusion rule. The main objective of Fig. 3.2 is to investigate the impact of the number of LSNs on the achievable ECP performance of the FH/MFSK WSNs. From Fig. 3.2, we observed that both

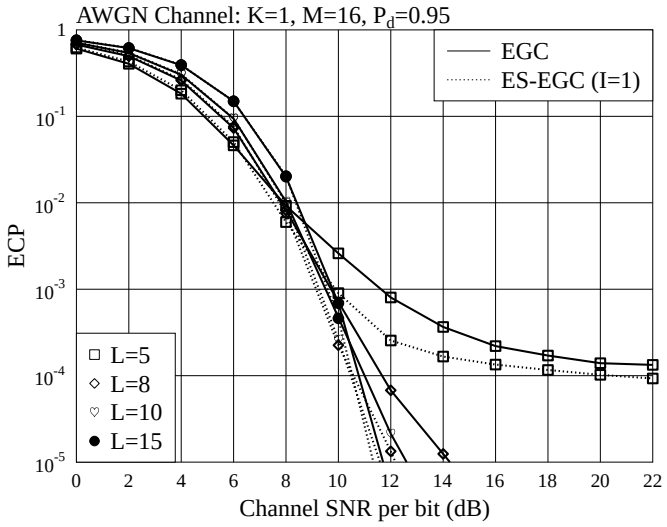

(a) AWGN channel

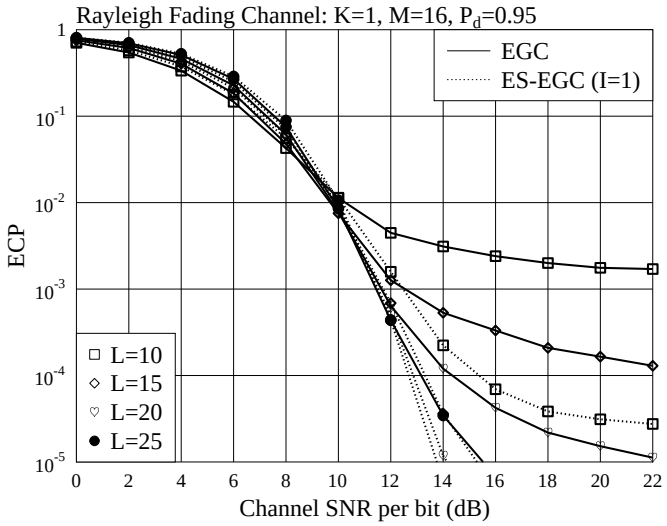

(b) Rayleigh fading channel

Figure 3.2: ECP versus channel SNR per bit performance of the FH/MFSK WSNs, when the WSN employs various number of LSNs with $P_d = 0.95$, when communicating over AWGN or Rayleigh fading channels.

the channel SNR and the number of LSNs have significant influence on the detection performance of the FH/MFSK WSN systems. As shown in Fig. 3.2, when communicating over Rayleigh fading channels, the FH/MFSK WSN system needs a higher channel SNR LSNs to achieve a similar overall ECP performance achieved in AWGN channels. When the number of LSNs is not enough, as seen in Fig. 3.2, error-floor are observed.

As shown in Fig. 3.2, when the channel SNR is sufficiently high, the ECP performance of the FH/MFSK WSN improves, as the WSN employs more LSNs for attaining the space diversity. However, when the channel SNR is not relatively low, using more LSNs may result in degraded ECP performance, which is due to the fact that the total energy for transmission by all the LSNs is a constant and that more errors occur at the LSNs. Furthermore, from Fig. 3.2 we can see that the ES-EGC fusion rule outperforms the EGC fusion rule in both the AWGN channels and Rayleigh fading channels, provided that channel SNR is sufficiently high, make the wireless channels are reasonably reliable.

In Fig. 3.3, we illustrate the effect of the value of M on the ECP performance of the FH/MFSK WSN supporting $K = 1$ SE using $L = 8$ LSNs with $P_d = 0.95$, when communicating over either AWGN channels (Fig. 3.3a) or Rayleigh fading channels (Fig. 3.3b). In the ES-EGC, the number of the erased entry per row is set as $I = 1$. As shown in Fig. 3.3, increasing the value of M improves the overall detection performance of the FH/MFSK WSN systems when either EGC or ES-EGC fusion rule is employed. The ES-EGC fusion rule outperforms the EGC fusion rule for both AWGN channels and Rayleigh fading channels, provided that the channel SNR is reasonable high. As shown in Fig. 3.3(b), when Rayleigh fading channels are assumed between LSNs and FC, the erasure operation is not effective for the improvement of the overall detection performance when the channel SNR is below 10 dB per bit. In fact, if the channel SNR is too low, erasure operation may even degrade the detection performance of the FH/MFSK WSN. This is because, although invoking the erasure operation is capable of mitigating interference, it however reduces the diversity order and the energy for detection. As shown in Fig. 3.3(a) and Fig. 3.3(b), when the value of M increases, significant improvement of the detection performance is possible for both AWGN channels and Rayleigh fading channels, provided that the channel SNR is high enough. When comparing Fig. 3.3(a) and Fig. 3.3(b), we can see that the FH/MFSK WSN over Rayleigh fading channels achieves much worse detection than over AWGN channels.

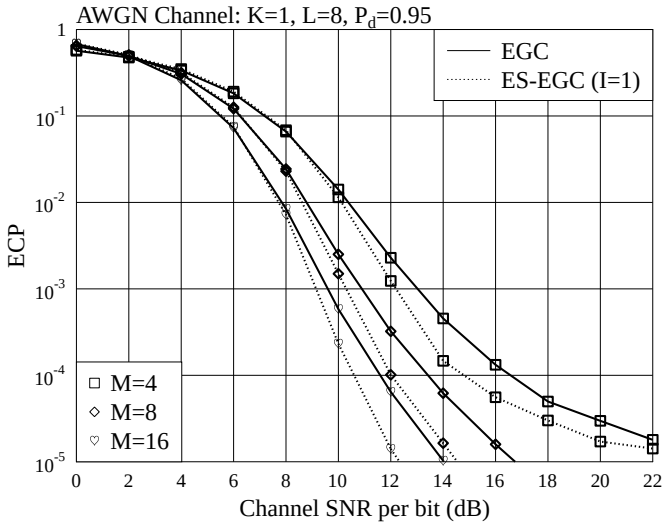

(a) AWGN channel

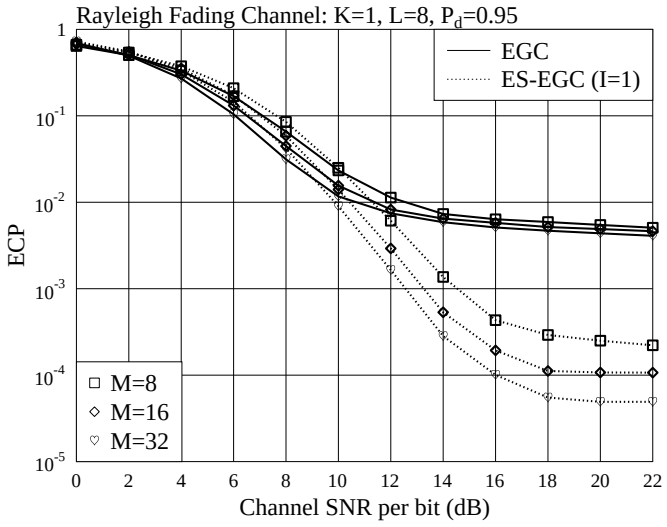

(b) Rayleigh fading channel

Figure 3.3: ECP versus channel SNR per bit performance of the FH/MFSK WSNs, when the WSN employs $L = 8$ LSNs with $P_d = 0.95$ over AWGN or Rayleigh fading channels.

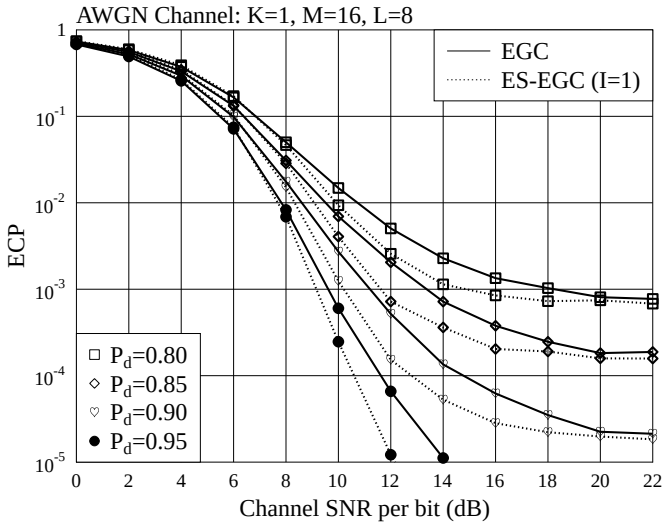

(a) AWGN channel

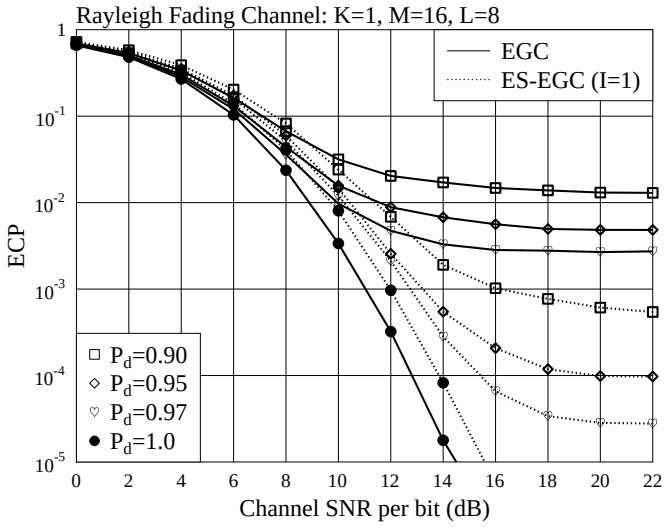

(b) Rayleigh fading channel

Figure 3.4: ECP versus channel SNR per bit performance of the FH/MFSK WSN supporting $K = 1$ SE with $M = 16$ states, when the WSN employs $L = 8$ LSNs with various detection performance over AWGN or Rayleigh fading channels.

Fig. 3.6 shows the ECP performance of the FH/MFSK WSN employing $L = 8$ LSNs monitoring $K = 1$ SE with $M = 16$ states (hypotheses). Two different fusion rules are considered, which are the EGC and ES-EGC fusion rules. From the simulation results shown in Fig. 3.6, we can explicitly observe that both the LSN's reliability and the channel SNR have strong impact on the overall achievable detection performance of the FH/MFSK WSN over either AWGN or Rayleigh fading channels. From Fig. 3.6(a), we can see that the overall detection performance degrades, as the correct detection probability P_d of the LSNs decreases. Furthermore, error floors can be clearly seen in Fig. 3.6(a) or Fig. 3.6(b), which is because of the errors generated at the LSNs. Again, in general, the ES-EGC fusion rule outperforms the EGC fusion rule, provided that the channel SNR is sufficiently high, making the interference dominating the performance. Note that, when the local detection probability $P_d = 1$, i.e., when there are no errors in the detection at the LSNs, the erasure operation will remove some useful information, making the detection performance of the ES-EGC fusion rule worse than that of EGC fusion rule.

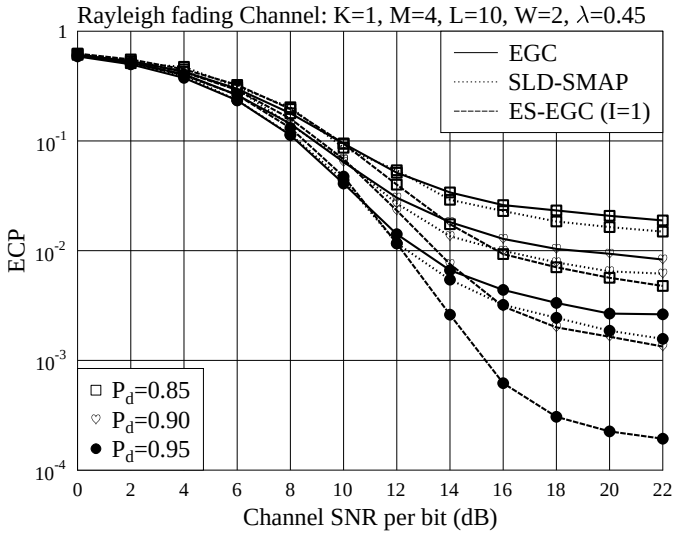

Figure 3.5: ECP versus channel SNR per bit performance of the FH/MFSK WSNs, when $L = 10$ LSNs are employed to monitor $K = 1$ SE with $M = 4$ states, when communicating over Rayleigh fading channels.

Fig. 3.5 shows the ECP performance of the FH/MFSK WSN supporting $K = 1$ SE with $M = 4$ states (hypotheses), where three different fusion rules, including the EGC, SLD-SMAP and the ES-EGC are considered. In the context of the SLD-SMAP fusion rule, the number of possible states based on EGC fusion rule is set as $W = 2$ and the threshold is set as $\lambda = 0.45$. For the

ES-EGC, $I = 1$ entry is removed from each of the rows. From the simulation results we can see that increasing LSN's reliability or channel SNR improves the overall detection performance of the FH/MFSK WSN. In general, the proposed ES-EGC fusion rule yields the best ECP performance among these fusion rules. The SLD-SMAP achieves a slightly better ECP performance than the EGC fusion rule over the channel SNR range considered, but at the expense of higher complexity.

In Fig. 3.6, the ECP versus channel SNR performance of the FH/MFSK WSN systems is investigated with respect to various values of M and I. The ES-EGC fusion rule is applied at the FC. In Fig. 3.6, the simulation results, theoretical results, as well as the theoretical upper-bound are detailed. Note that, the theoretical results and the upper-bounds were evaluated using (3.45) and (3.47), respectively. As shown in Fig. 3.6, the theoretical results match well with the simulation results for $M = 2,\ 4,\ 8$ and $I = 1,\ 2,\ 3$. According to our discussion in Section 3.5, the upper bound equals to the exact detection performance, when $M = 2$. By contrast, a gap between the upper bound and the exact performance is observed when $M = 4$. Moreover, this gap becomes larger, when M is increased to 8. Our simulation results also show that the proposed ES-EGC achieves the lowest ECP, when $I = 1$. Increasing the value of I does not make the detection performance better, but worse. Additionally, from Fig. 3.6, we can see that the upper bound converges to the exact ECP performance, as the channel SNR increases.

3.7 Conclusions

In this chapter, a FH/MFSK WSN framework has been proposed, which monitors an M-ary SE whose states are conveyed to the FC with the aid of FH/MFSK scheme. The FH technique has been introduced to enhance the diversity gain, especially in the case that the LSNs are close to each other, resulting in that their channels to the FC are correlated. The MFSK modulation scheme is employed in favour of noncoherent detection for implementing low-complexity detection. In this chapter, three different noncoherent fusion rules have been considered for fusion detection, which include the EGC, ES-EGC and optimum fusion rules. The error performance of the FH/MFSK WSN has been investigated, when the channels from LSNs to FC are AWGN or Rayleigh fading channels. Our studies and performance results show that, when the LSN's detection is unreliable, and the channel SNR is relatively high, the ES-EGC fusion rule may significantly outperform the

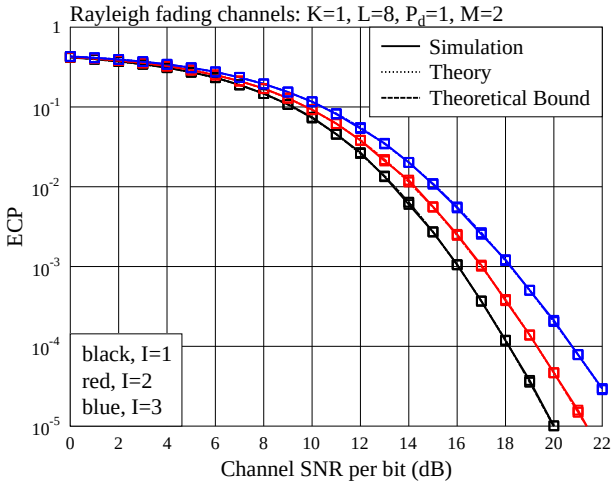

(a) M=2

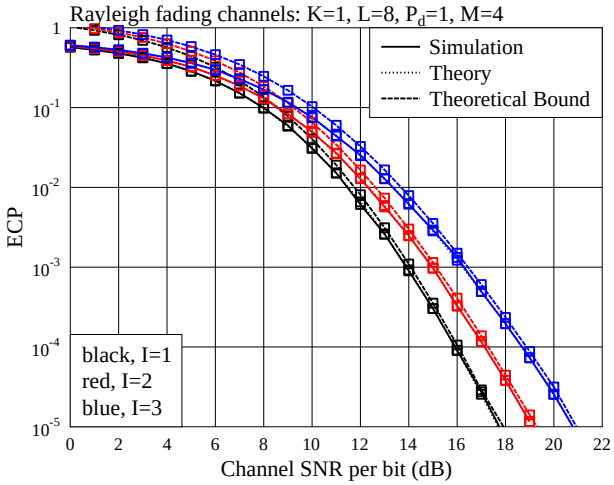

(b) M=4

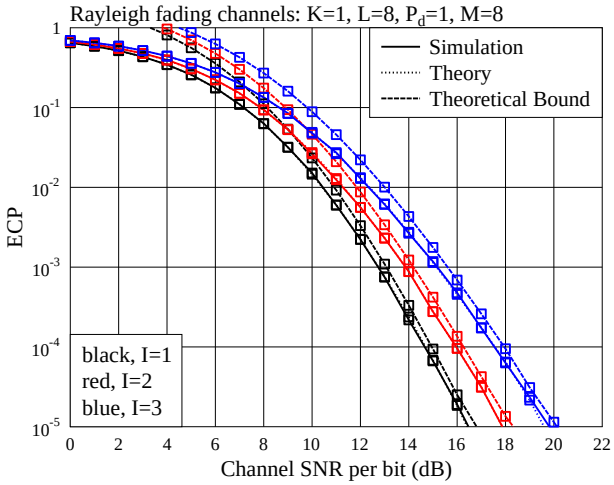

(c) M=8

Figure 3.6: ECP versus channel SNR per bit performance of the FH/MFSK WSN with the ES-EGC fusion rule, when communicating over Rayleigh fading channels.

EGC fusion rule. Therefore, the ES-EGC fusion rule is robust to the errors made by LSNs. By contrast, when the detection at LSNs is highly reliable, making the channel noise dominate the FC's detection performance, then, we may simply use the EGC fusion rule. In fact, the ES-EGC fusion rule may be regarded as an extension of the EGC fusion rule, the number of erasures per row may be determined according to the specific environment where the FH/MFSK WSN is deployed. Our optimum fusion rule has been derived based on the MAP principles. As the optimal MAP fusion rule has extremely high complexity, sub-optimum MAP fusion rule and SLD-SMAP fusion rule have been discussed in Section 3.3.3. These sub-optimum fusion rules have relatively lower complexity than the optimum MAP fusion rule.

Our studies in this chapter show that, our proposed FH/MFSK WSN is capable of achieving promising detection performance for reasonable system setting. However, the achievable detection performance of the FH/MFSK WSN is jointly determined by many factors, including, such as the detection performance of LSNs, the number of LSNs, the number of states of each SE, the wireless channels between LSNs and FC, etc. Apart from the above factors, the computation complexity and signal processing delay should also be jointly considered, when optimizing the overall performance of the FH/MFSK WSNs.

Chapter 4

Noncoherent Detection in FH/MFSK WSN Monitoring Multiple Events

4.1 Introduction

In this chapter, we consider a triple-layer WSN, which uses a number of LSNs to simultaneously monitor multiple SEs of each having multiple states. By contrast, in Chapter 3 as well as in literature [10, 74–76, 79–82, 163–165], the WSNs monitoring only single SE are usually addressed. In our WSN, the frequency-hopping and M-ary frequency-shift keying (FH/MFSK) techniques are employed for transmitting signals from LSNs to FC. Here the FH/MFSK is employed, in order to support multiple SEs, to achieve noncoherent classification at FC as well as to enhance the diversity performance of fusion detection.

It is well-known that EGC is a typical fusion rule for noncoherent detection, and it has low-complexity and low detection delay [115, 116]. Furthermore, the EGC fusion rule is optimum for noncoherent detection over the fading channels only experiencing Gaussian noise [115]. However, it is a very deficient scheme for signal detection over interference channels. In the FH/MFSK WSN considered in this chapter, there are possibly two types of interference, in addition to background Gaussian noise. First, a LSN may make erroneous classifications about the states of SEs. In this case, the corresponding LSN will transmit interference to its FC, instead of conveying positive information to the FC for enhancing the fusion detection. Second, the FH/MFSK signals transmitted by the LSNs for conveying the state information of multiple SEs may interfere with each

other, yielding the so-called multiple event interference (MEI), in parallel with the terminology of multiuser interference (MUI) used, for example, in code-division multiple-access (CDMA) systems [166]. Note that, in this chapter, we choose iterative interference cancellation (IIC) instead of parallel interference cancellation (PIC) to suppress the MEI because of the following main reasons. First, PIC approach cause a rather inefficient reception performance as it is suceptible to errors and the probability for inaccurate detection is quite high [167]. Second, PIC requires precious hardware gear in order to operate in parallel. which makes it unprofitable for numerous practical implementations [168, 169].

In order to improve the fusion detection performance of the FH/MFSK WSN, in this chapter, we propose and investigate five noncoherent fusion rules, in addition to the conventional EGC, which is considered here as a benchmark. Specifically, we first investigate the novel low-complexity fusion rule, namely the erasure-supported equal gain combining (ES-EGC) fusion rule proposed in Chapter 3, in the scenario of supporting multiple SEs. Our studies show that the ES-EGC is a highly efficient fusion rule, which has a similar complexity as the conventional EGC. However, it is capable of achieving much better error performance than the conventional EGC. Furthermore, although it is a single-user fusion rule[1], it employs the capability to effectively mitigate the MEI. Then, by combining and extending the conventional EGC, the ES-EGC as well as the multiuser iterative interference cancellation (IIC) [170] schemes, four multiuser fusion rules are proposed and investigated associated with the FH/MFSK WSN. Specifically, the four multiuser fusion rules are named respectively as the EGC assisted N-order IIC (EGC-NIIC), ES-EGC assisted N-order IIC (ES-EGC-NIIC), EGC assisted ρ-fraction IIC (EGC-ρIIC) as well as the ES-EGC assisted ρ-fraction IIC (ES-EGC-ρIIC). In this chapter, the complexity of the considered fusion rules is analyzed. The error performance of the FH/MFSK WSN associated with various fusion rules is investigated by simulations, when assuming that the communication channels from LSNs to FC experience independent Rayleigh fading. Our studies and performance results show that, in general, the ES-EGC related fusion rules outperform the corresponding EGC related fusion rules. Furthermore, in some cases, the single-user ES-EGC fusion rule may even achieve better error performance than the multiuser EGC-NIIC and multiuser EGC-ρIIC fusion rules, which have much higher complexity than

[1]Single-user fusion rules are referred to as the fusion rules which detect one SE without making use of any information about the other SEs. By contrast, multi-user fusion rules are those fusion rules which detect one SE with the aid of partial or full information about the other SEs.

the ES-EGC fusion rule.

The reminder of this chapter is organized as follows. In Section 4.2, we describe the framework of the proposed FH/MFSK WSN, where the SEs and sensor processing are addressed. Section 4.3 details the operations of the six fusion rules. Section 4.4 considers the complexity of the six fusion rules. In Section 4.5, we discuss the characteristics of the FH/MFSK WSN, while in Section 4.6, we provide a range of performance results obtained by simulations. Finally, in Section 4.7, our conclusions are stated.

4.2 System Description

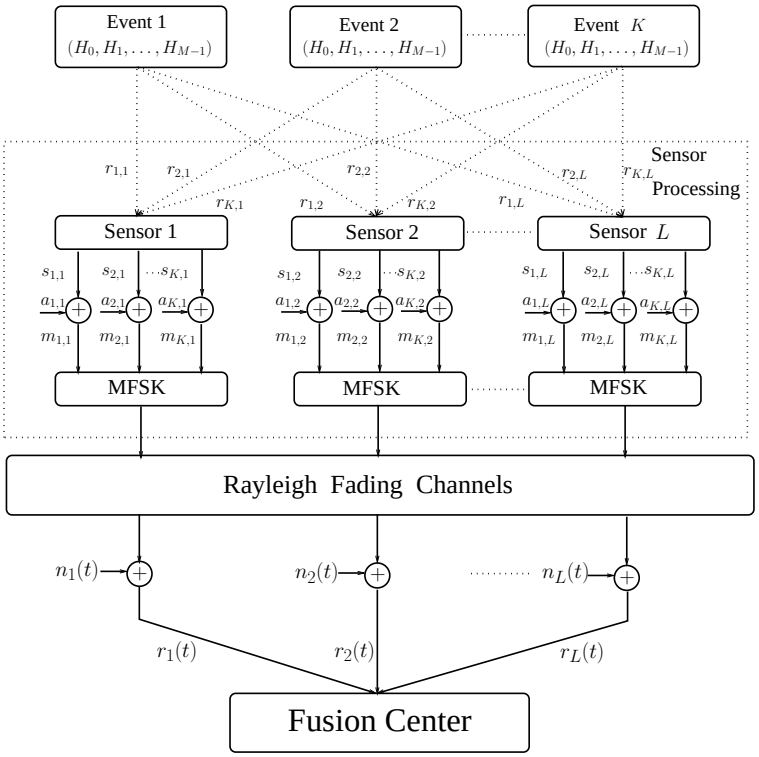

Figure 4.1: Triple-layer system model for the WSNs observing K source events with M states, where information is transmitted to the fusion center based on FH/MFSK scheme.

The framework for our triple-layer FH/MFSK WSN monitoring multiple SEs is shown in Fig. 4.1. In this FH/MFSK WSN, we assume that there are K SEs, each of which may be at one of the M possible states (hypotheses). The K SEs are simultaneously monitored by L number of LSNs. We assume that every LSN is capable of simultaneously observing the K SEs without observation interference. In fact, we can view that each LSN consists of K sub-sensors, each of

which monitors one SE. These K sub-sensors share one common wireless transmitter to send their decisions to the FC. Explicitly, this system arrangement has some advantages, including that: (a) the number of LSNs does not increase with the number of SEs being monitored and, hence, the system may not need to use a big number of LSNs, even when there are many SEs; (b) owing to using a relatively low number of LSNs, synchronization among the LSNs may become relatively easy. From Fig. 4.1, we can see that local decisions are made at the L LSNs in the context of the K SEs. Then, the operations of FH and MFSK are carried out to transmit the local decisions to the FC with the aid of the unique FH addresses assigned to the different LSNs for the K SEs. Finally, at the FC, the received signals are detected noncoherently under different fusion rules. Below, we provide further details about the SEs as well as the operations carried out at the LSNs and FC.

4.2.1 Source Event

In practice, the SEs to be monitored are usually analog signals. For convenience of processing, they are usually digitalized to finite states. In this section, we assume that each of the SEs has M states corresponding to M hypotheses, expressed as $H_0, H_1, \ldots, H_{M-1}$, as shown in Fig. 4.1. Each of the observed SEs has various number of states with different probability. In this chapter, for convince of our analyse, we assume that all the SEs have M states and each of the M states of a SE has the same probability to present. In Fig. 4.1, the K SEs are observed by a total L number of LSNs and every LSN monitors simultaneously all the K SEs. Furthermore, we assume that the K SEs are independent and there is no interference among the observations of a LSN.

4.2.2 Sensor Processing

At a LSN, such as the lth LSN, the observation obtained from the kth SE is denoted by $r_{k,l}$, as seen in Fig. 4.1. Based on $r_{k,l}$, the lth LSN first makes a local decision about the state that the kth SE is currently at, and this state is expressed as $s_{k,l}$, $s_{k,l} \in \{0, 1, \ldots, M-1\}$. We assume that the erroneous and correct detection probabilities with respect to the K LSNs are the same and are expressed as P_e and $P_d = 1 - P_e$, respectively. Furthermore, we assume that, whenever an erroneous decision is made, the erroneous state estimated by a LSN has the same probability to be any of the $(M-1)$ erroneous states.

Let us collect the K estimates of LSN l into the vector $\boldsymbol{s}_l = [s_{1,l}, s_{2,l}, \cdots, s_{K,l}]^T$. Furthermore, let

$$\boldsymbol{S} = [\boldsymbol{s}_1\, \boldsymbol{s}_2\, \cdots\, \boldsymbol{s}_L] \tag{4.1}$$

which collects the local decisions of the K SEs made by the L LSNs. Hence, $\boldsymbol{S}$ is an $(K \times L)$ matrix. As shown in Fig. 4.1, following the detection of the SEs, the LSNs convey their decisions to the FC based on the FH/MFSK principles, which are operated as follows.

Let the symbol duration be expressed as T_s, which is divided into L chips of duration $T_h = T_s/L$. Within every symbol duration of T_s, the L LSNs send their corresponding local decisions of the K SEs to the FC with the aid of the FH/MFSK technique, one LSN uses one of the L chips to transmit their K decisions. We assume that the FH/MFSK WSN system has in total M orthogonal frequency bands, whose center frequencies form the set $\mathcal{F} = \{f_0, f_1, \ldots, f_{M-1}\}$. These M frequencies are used for both the FH and MFSK modulation in the principles of fast frequency-hopping (FFH) [171, 172]. Specifically, let the FH address assigned for transmission of the kth SE's state be expressed as $\boldsymbol{a}_k = [a_{k,1}, a_{k,2}, \ldots, a_{k,L}]^T$, where $a_{k,l}$ is an element in the Galois field $GF(M)$, i.e., $a_{k,l} \in GF(M)$. Based on $\boldsymbol{a}_k$ for $k = 1, 2, \ldots, K$, we form a matrix

$$\boldsymbol{A} = [\boldsymbol{a}_1\, \boldsymbol{a}_2\, \cdots\, \boldsymbol{a}_K]^T \tag{4.2}$$

Then, the FH operations in the context of the K SEs and the L LSNs can be represented as

$$\boldsymbol{M} = [\boldsymbol{m}_1\, \boldsymbol{m}_2\, \cdots\, \boldsymbol{m}_L] = \boldsymbol{S} \boxplus \boldsymbol{A} \tag{4.3}$$

where $\boldsymbol{m}_l = [m_{1,l}\, m_{2,l}\, \cdots\, m_{K,l}]^T$, $l = 1, 2, \ldots, L$, and $\boldsymbol{S} \boxplus \boldsymbol{A}$ carries out the element-wise addition of $\boldsymbol{S}$ and $\boldsymbol{A}$ in $GF(M)$, yielding that $m_{i,j} = S_{i,j} \oplus A_{i,j}$ with $\oplus$ representing the addition operation in $GF(M)$. Explicitly, we have $m_{i,j} \in GF(M)$, which is suitable for MFSK modulation by mapping $m_{i,j}$ to the frequency $f_{m_{i,j}}$. Let us express the corresponding frequencies for transmission of $\boldsymbol{M}$ as

$$\boldsymbol{F}(\boldsymbol{M}) = \begin{bmatrix} f_{m_{1,1}} & f_{m_{1,2}} & \cdots & f_{m_{1,L}} \\ f_{m_{2,1}} & f_{m_{2,2}} & \cdots & f_{m_{2,L}} \\ \vdots & \vdots & \ddots & \vdots \\ f_{m_{K,1}} & f_{m_{K,2}} & \cdots & f_{m_{K,L}} \end{bmatrix} \tag{4.4}$$

where the lth column contains the frequencies to be transmitted within the lth chip-duration by the lth LSN. Consequently, based on the principles of MFSK, the signal transmitted by the lth LSN for the kth SE during the ith symbol-duration $iT_s < t \leq (i+1)T_s$ can be expressed in complex form as

$$\begin{aligned}\tilde{s}_{k,l}(t) =& \sqrt{P}\psi_{T_h}(t - iT_s - [l-1]T_h)\exp\left(j2\pi[f_c + f_{m_{k,l}}]t + j\phi_{k,l}\right), \\ & k = 1, 2, \ldots, K;\ l = 1, \ldots, L\end{aligned} \tag{4.5}$$

where P denotes the transmission power, which is assumed the same with respect to all the L LSNs and K SEs, f_c is the main carrier frequency and $\phi_{k,l}$ is the initial phase introduced by the carrier modulation. In (4.5), $\psi_{T_h}(t)$ is the pulse-shaped signaling waveform, which is defined over the interval $[0, T_h)$ and satisfies $T_h^{-1}\int_0^{T_h}\psi^2(t)dt = 1$.

We assume that the M frequencies used by the FH/MFSK WSN are sufficiently separated, resulting in that each of them experiences independent flat Rayleigh fading. Then, the signal received by the FC from the lth LSN during $iT_s < t \leq (i+1)T_s$ can be expressed as

$$\begin{aligned}r_l(t) &= \sum_{k=1}^{K} h_{k,l}\tilde{s}_{k,l}(t) + n_l(t) \\ &= \sum_{k=1}^{K} \sqrt{P}h_{k,l}\psi_{T_h}(t - iT_s - [l-1]T_h)\exp(j2\pi[f_c + f_{m_{k,l}}]t + j\phi_{k,l}) + n_l(t), \\ & l = 1, \ldots, L,\end{aligned} \tag{4.6}$$

where $h_{k,l}$ denotes the channel gain corresponding to the MFSK frequency band activated for the kth SE by the lth LSN, $h_{k,l}$ obeys the complex Gaussian distribution with zero mean and a variance of 0.5 per dimension. Furthermore, in (4.6), $n_l(t)$ represents the Gaussian noise process presenting at the fusion center, which has zero mean and a single-sided power-spectral density (PSD) of N_0 per dimension.

4.3 Signal Detection at Fusion Center

In the FH/MFSK WSN monitoring multiple SEs, as seen in Fig. 4.1, the signals for conveying the states of different SEs may interfere with each other, generating the so-called multi-event interference (MEI) [116]. The MEI may significantly degrade the detection performance, if it is not treated

properly. In this chapter, some existing and proposed low-complexity noncoherent fusion rules are studied and compared. Specifically, the following six noncoherent fusion rules are considered:

1. EGC [75, 76, 79]: Equal gain combining;
2. ES-EGC: Erasure-supported equal gain combining;
3. EGC-NIIC: Equal gain combining assisted N-order iterative interference cancellation;
4. ES-EGC-NIIC: Erasure-supported equal gain combining assisted N-order iterative interference cancellation;
5. EGC-ρIIC: Equal gain combining assisted ρ-fraction iterative interference cancellation;
6. ES-EGC-ρIIC: Erasure-supported equal gain combining assisted ρ-fraction iterative interference cancellation.

Note that, in the above list, the conventional EGC rule is used as a benchmark, in order to illustrate the advantages and disadvantages of the other five proposed fusion rules. The conventional EGC fusion rule [75, 76, 79] is the simplest but experience severe MEI. The other five fusion rules are proposed in order to mitigate, more or less, the negative influence of MEI. The principles of these noncoherent fusion rules will be detailed in the following subsections.

In our FH/MFSK WSN, the FC starts the detection by forming a time-frequency matrix $\boldsymbol{R}$ of $(M \times L)$-dimensions based on the observations extracted from the signals received from the L number of LSNs. Specifically, when the square-law noncoherent detection is considered, the elements of $\boldsymbol{R}$ have the values

$$R_{ml} = \left| \frac{1}{\sqrt{\Omega P} T_h} \int_{iT_s+(l-1)T_h}^{iT_s+lT_h} r_l(t) \psi_{T_h}^*(t - iT_s - [l-1]T_h) \exp(-j2\pi[f_c + f_m]t) dt \right|^2, \quad (4.7)$$

where $m = 0, 1, \ldots, M-1$ and $l = 1, 2, \ldots, L$, and $\Omega = E[|h_{k,l}|^2]$ denotes the channel power. Since it has been assumed that the M number of frequency bands invoked are orthogonal to each other, there is no interference between two different frequency bands. Consequently, upon substituting (4.6) into (4.7) and absorbing the carrier phase $\phi_{k,l}$ into $h_{k,l}$, we obtain

$$R_{ml} = \left| \sum_{k=1}^{K} \frac{\mu_{k,ml} h_{k,l}}{\sqrt{\Omega}} + N_{ml} \right|^2, \; m = 0, 1, \ldots, M-1; \; l = 1, 2, \ldots, L \quad (4.8)$$

where, by definition, $\mu_{k,ml} = 1$, if $m = m_{k,l}$, while $\mu_{k,ml} = 0$, if $m \neq m_{k,l}$. Let us assume that, for a given set of transmitted symbols of the K SEs, the number of SEs activating the (m,l)th element of $\boldsymbol{R}$ is K_{ml} $(0 \leq K_{ml} \leq K)$. Then, (4.8) can also be written as

$$R_{ml} = \left| \sum_{k=1}^{K_{ml}} \frac{h_{k,l}}{\sqrt{\Omega}} + N_{ml} \right|^2, \; m = 0, 1, \ldots, M-1; \; l = 1, 2, \ldots, L \tag{4.9}$$

In (4.8) and (4.9), N_{ml} represents a complex Gaussian noise sample in terms of the mth frequency band and the lth time-slot, which is given by

$$N_{ml} = \frac{1}{\sqrt{\Omega P} T_h} \int_{iT_s+(l-1)T_h}^{iT_s+lT_h} n_l(t) \psi_{T_h}^*(t - iT_s - [l-1]T_h) \exp(-j2\pi[f_c + f_m]t) dt \tag{4.10}$$

It can be shown that N_{ml} has mean zero and a variance of $LN_0/(\Omega E_s) = L/\bar{\gamma}_s$, where $E_s = PT_s$ represents the total energy for transmitting one M-ary symbol, while $\bar{\gamma}_s = \Omega E_s / N_0$ denotes the average SNR per symbol. Note that, as $T_h = T_s/L$, the transmitted energy for a SE's state by one LSN is $E_h = E_s/L$.

As an example, the time-frequency matrix $\boldsymbol{R}$ for a FH/MFSK WSN using $L = 6$ LSNs to monitor $K = 2$ SEs of $M = 8$ states is given by

$$\boldsymbol{R} = \begin{bmatrix} & \bigcirc & & \square \\ \square & & & \\ & \bigcirc & & \\ & & & \bigcirc \\ & & \square & \\ & \square & & \bigcirc \\ \boxed{\square} & & & \\ & & \bigcirc & \square \end{bmatrix} \tag{4.11}$$

where the empty entries contain only noise, while the marked entries include both signals and noise. For the sake of illustration, in (4.11), the elements with '□' are activated for conveying the state of the first SE, while that with '◯' correspond to the second SE. Furthermore, for (4.11), we assumed that the states of the two SEs were 5, 3 and that there were no observation errors. The corresponding FH addresses were $\boldsymbol{a}_1 = [4,\ 3,\ 7,\ 6,\ 2,\ 5]$, $\boldsymbol{a}_2 = [2,\ 4,\ 6,\ 3,\ 1,\ 7]$.

Note that, in the FH/MFSK WSN scheme, there exist the cases that a given LSN activates the same MFSK frequency for transmitting the states of two or more SEs. In this case, as shown in (4.5),

there will be several terms having the same MFSK frequency and the same initial carrier phase. Consequently, for the element R_{ml} in (4.8) corresponding to this frequency, there will be several $m_{k,l}$'s, which make $\mu_{k,ml} = 1$ but correspond to the same value for their $h_{k,l}$'s. This phenomenon can also be seen in (4.11), where the element marked as '$\textcircled{\square}$' conveys the information of both the first and second SEs.

Based on the time-frequency matrix $\boldsymbol{R}$, the FC then carries out the required processing and makes the final detection based on one of the six proposed fusion rules, which are now detailed as follows.

4.3.1 Equal Gain Combining (EGC)

In the context of the EGC fusion rule [116], the FC detects the kth SE's state by first carrying out the frequency de-hopping to form a detection matrix $\boldsymbol{D}_k$ as

$$\boldsymbol{D}_k = \boldsymbol{R} \boxminus (\mathbf{1} \otimes \boldsymbol{a}_k^T),\ k = 1, 2, \ldots, K \tag{4.12}$$

where $\mathbf{1}$ denotes an all-one column vector of M-length and $\otimes$ denotes the Kronecker product operation between two matrices [116]. In (4.12), the operation of $\boldsymbol{A} \boxminus \boldsymbol{B}$ shifts the elements in $\boldsymbol{A}$ based on the values provided by $\boldsymbol{B}$. Specifically, after the operation in (4.12), we have

$$D_{k,m \ominus a_{k,l},l} = R_{ml},\ m = 0, 1, \ldots, M-1;\ l = 1, \ldots, L \tag{4.13}$$

where $\ominus$ is the subtraction operation in $GF(M)$. In other words, the (m,l)th element in $\boldsymbol{R}$ is mapped to the $(m \ominus a_{k,l}, l)$th element in $\boldsymbol{D}_k$, after the frequency de-hopping operations of (4.12).

Based on (4.12), the EGC fusion rule then forms the M decision variables for detection of the kth SE's state, which are given by

$$D_{k,m} = \sum_{l=1}^{L} D_{k,ml},\ m = 0, 1, \ldots, M-1 \tag{4.14}$$

for $k = 1, 2, \ldots, K$. Finally, for each of $k = 1, 2, \ldots, K$, the largest one of $\{D_{k,0}, D_{k,1}, \ldots, D_{k,M-1}\}$ is selected and, correspondingly, the m index with the value in $\{0, 1, \ldots, M-1\}$ represents the estimate of the state that the kth SE is currently at.

Fig 4.2 shows the operations of the EGC detection in correspondence to the example having the received matrix $\boldsymbol{R}$ of (4.11). After frequency de-hopping of the received matrix $\boldsymbol{R}$ using the FH

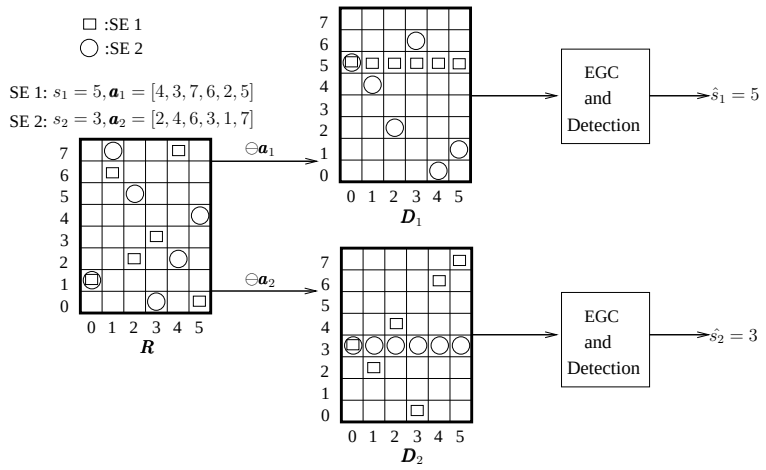

Figure 4.2: An example showing the EGC processing, where squares and circles represent the elements actived by SE 1 and 2, respectively.

address $\boldsymbol{a}_1$, we obtain the detection matrix $\boldsymbol{D}_1$ for SE 1. Based on $\boldsymbol{D}_1$, M decision variables are formed in the EGC principles as shown in (4.14). Then, the largest one of the M decision variables is chosen and, correspondingly, its index represents the detection of the state of SE 1. When the FC makes a correct decision, an estimation of $\hat{s}_1 = 5$ is estimated. Similarly, the state of SE 2 can be detected.

The EGC fusion rule is a linear noncoherent fusion rule, which has very low-complexity. However, the EGC fusion rule may experience severe MEI, the amount of which is dependent on the FH addresses employed and the number of SEs. The error performance of the EGC fusion rule is sensitive to the MEI and may significantly degrade as the number of SEs increases. Below we consider a range of fusion rules, which have certain capability to mitigate MEI. Let us first describe the ES-EGC fusion rule, which is a single-user noncoherent fusion rule with low-complexity, but is capable of efficiently mitigating MEI.

4.3.2 Erasure-Supported Equal Gain Combining (ES-EGC)

From 4.3.1, we can see that, when the LSNs observe the SEs' states without errors, there is a full row with its entries containing both signal and noise. This row is the desired row, corresponding to the desired state of the being detected SE. By contrast, in the $(M-1)$ interfering rows, there are only a few of entries containing both signal and noise, while the other entries contain only noise. Furthermore, in the $(M-1)$ interfering rows, the entries containing both signal and noise

are distributed in a random way over the $(M-1)L$ entries. Straightforwardly, if the SNR per symbol is sufficiently high, we can believe that the entries containing both signal and noise should in general have relatively higher power than those containing only noise. Based on this observation, in the detection matrix, such as $\boldsymbol{D}_1$ shown in Fig 4.2, if a given number of entries having the highest values are removed from each of the M rows , the removed entries will most probably contain both signal and noise. As the result, the rest entries of the desired row still contain both signal and noise, while, in the interfering rows, the number of entries containing both (interfering) signal and noise may be significantly reduced, which in turn reduces the MEI. Our ES-EGC fusion rule is based on the principles as above discussed.

Explicitly, the ES-EGC fusion (or detection) rule is a single-user fusion rule. However, as our simulation results in Section 4.6 show, it is a high-efficiency fusion rule, which, for some cases, may achieve even better error performance than some of the noncoherent multiuser fusion rules [116]. Interestingly but unfortunately, in the long history of noncoherent detection, especially, for the noncoherent multiuser systems, such a simple detection principle has not been realized.

Note furthermore that, for the FH/MFSK WSN, the ES-EGC fusion rule is capable of providing performance improvement, even when single SE is monitored, as evidenced by our simulations results in Chapter 3 as well as in Section 4.6.

The ES-EGC fusion rule starts with the same operations as the EGC fusion rule. First, for the kth SE, the FC removes the FH imposed by the L LSNs by carrying our the frequency de-hopping operation, as shown in (4.12), yielding the detection matrix $\boldsymbol{D}_k$. After obtaining $\boldsymbol{D}_k$, the ES-EGC fusion rule carries out the erasure operations. Specifically, in each of the M rows of $\boldsymbol{D}_k$, I $(0 \leq I < L)$ elements corresponding the I largest values are replaced by the value of zero. Let us denote the modified detection matrix after the erasure operation by $\bar{\boldsymbol{D}}_k$. Then, based on this modified detection matrix, M decision variables formed in EGC principles can be expressed as

$$\bar{D}_{k,m} = \sum_{l=1}^{L} \bar{D}_{k,ml},\ m = 0, 1, \ldots, M-1;\ k = 1, 2, \ldots, K \tag{4.15}$$

Finally, the largest one of the M decision variables of $\{\bar{D}_{k,0}, \bar{D}_{k,1}, \cdots, \bar{D}_{k,M-1}\}$ is selected and its index value in terms of m represents the estimate for the state of the kth SE.

In Fig 4.3, an example showing the principles of the ES-EGC fusion rule with $I = 1$ is illustrated based on the received matrix $\boldsymbol{R}$ of (4.11). After frequency de-hopping, decision matrix

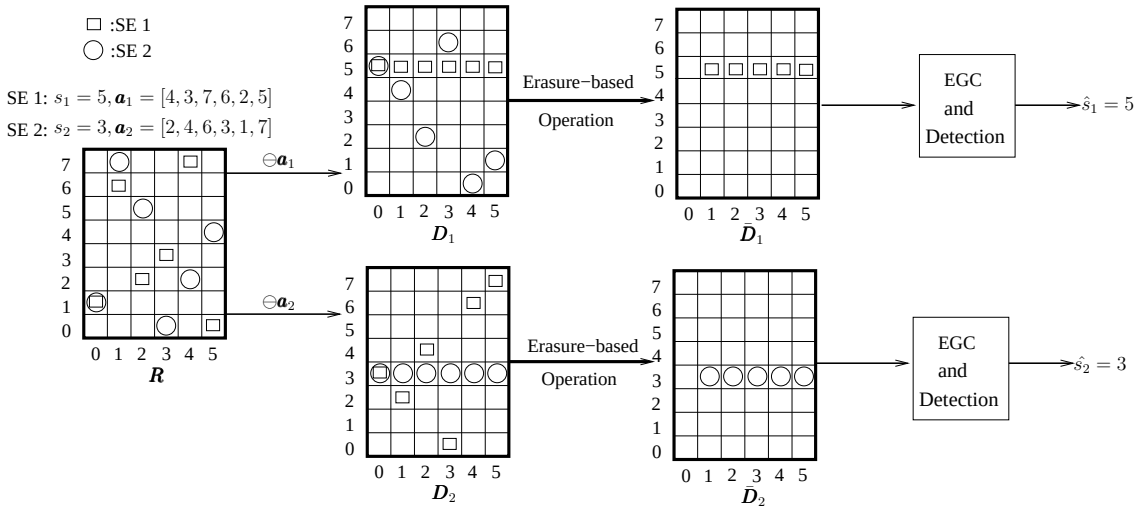

Figure 4.3: An example to illustrate the ES-EGC processing, where squares and circles represent the elements actived by SE 1 and 2, respectively, and $I = 1$ element per row is erasured.

$\boldsymbol{D}_1$ and $\boldsymbol{D}_2$ are obtained respectively by the frequency de-hopping using $\boldsymbol{a}_1$ and $\boldsymbol{a}_2$. Then, erasure operation is carried out to migrate interference. Assuming that the elements containing both signal and noise have higher power than the entries with just noise, after removing $I = 1$ element with the highest value from each row, the corresponding modified detection matrices $\bar{\boldsymbol{D}}_1$ and $\bar{\boldsymbol{D}}_2$ are obtained as shown in Fig 4.3. Explicitly, the interfering entries in the interfering rows are all removed. Hence, the detection will become more reliable.

In literature, the EGC principle has been invoked in some noncoherent multiuser detection schemes [75, 76, 79, 116]. It has been argued and will also be shown by our performance results, the ES-EGC scheme outperforms the conventional EGC scheme. Therefore, the ES-EGC scheme may be applied to some of the noncoherent multiuser detection schemes, in order to improve the error performance. In this chapter, both the EGC and the ES-EGC is applied to the noncoherent iterative interference cancellation (IIC) scheme, forming different noncoherent multiuser fusion rules, which are detailed in our forthcoming discourses.

4.3.3 EGC Assisted N-Order Iterative Interference Cancellation (EGC-NIIC)

The EGC-NIIC fusion rule represents one of the extensions of the noncoherent IIC detection scheme proposed in [170], which uses the majority vote as the basic detection scheme and the symbols of different users are detected one-by-one iteratively until the last one. By contrast, in

our proposed EGC-NIIC fusion rule, the EGC-based detection forms the basic detection rule, and the IIC is only operated associated with the first N most reliable SEs (users), whose symbols are detected one-by-one iteratively from the more reliable ones to the less reliable ones. After the iterative detection of the first N most reliable SEs, the rest $(K-N)$ SEs are simultaneously detected using the EGC fusion rule.

In order to specify the most reliable SE to be detected at a stage, in our EGC-NIIC, a low-complexity reliability measurement method is proposed, which measures the reliability of an EGC-based detection based on the formula

$$L_k = \frac{\max_2 \{D_{k,0}, D_{k,1}, \cdots, D_{k,M-1}\}}{\max_1 \{D_{k,0}, D_{k,1}, \cdots, D_{k,M-1}\}} \tag{4.16}$$

where $\max_1\{\cdot\}$ and $\max_2\{\cdot\}$ represent, respectively, the maximum and 'second' maximum of the decision variables $\{D_{k,0}, D_{k,1}, \cdots, D_{k,M-1}\}$, which are the outputs of the EGC, as shown in (4.14). According to [173–175], statistically, the demodulated M-ary symbols with relatively low values of L_k are more reliable than those with relatively high values of L_k. Hence, in our EGC-NIIC fusion rule, an estimate to the state of the kth SE is rendered the most reliable one, if its corresponding L_k value is lower than any of the others'.

Let us assume that the FC employs the knowledge of the FH addresses in $\boldsymbol{A}$ assigned to the K SEs. Then, the EGC-NIIC algorithm can be stated as follows.

1. **Initialization**: $\boldsymbol{A}$, $N \leq K-1$, $\boldsymbol{R}^{(1)} = \boldsymbol{R}$.

2. **EGC-NIIC detection**: for $i = 1, 2, \ldots, N$, the following steps are executed:

   (a) **Frequency de-hopping**: For those $(K-i+1)$ SEs having not been detected, the detection matrices, $\boldsymbol{D}_1^{(i)}, \boldsymbol{D}_2^{(i)}, \ldots, \boldsymbol{D}_{K-i+1}^{(i)}$, are formed according to

   $$\boldsymbol{D}_k^{(i)} = \boldsymbol{R}^{(i)} \boxminus (\mathbf{1} \otimes \boldsymbol{a}_k^T),\ k = 1, 2, \ldots, K-i+1 \tag{4.17}$$

   (b) **Forming decision variables**: For each of the $(K-i+1)$ SEs, the M decision variables are formed based on the EGC principles as

   $$D_{k,m}^{(i)} = \sum_{l=1}^{L} D_{k,ml}^{(i)},\ m = 0, 1, \ldots, M-1;\ k = 1, 2, \ldots, K-i+1 \tag{4.18}$$

(c) **Reliability Measurement**: The reliabilities with respect to all the $(K-i+1)$ SEs are measured based on (4.16), and are expressed as $L_1^{(i)}, L_2^{(i)}, \ldots, L_{K-i+1}^{(i)}$.

(d) **Detecting the most reliable SE**: The most reliable SE is identified as

$$k' \leftrightarrow L_{k'}^{(i)} = \min\left\{L_1^{(i)}, L_2^{(i)}, \ldots, L_{K-i+1}^{(i)}\right\} \tag{4.19}$$

Correspondingly, the state of the most reliable SE, i.e., of the k'th SE, is detected as the m index value of the largest in $\{D_{k';0}^{(i)}, D_{k';1}^{(i)}, \ldots, D_{k';M-1}^{(i)}\}$. Let the estimated state for the k'th SE be expressed as $\hat{m}_{k'}$.

(e) **Update $\boldsymbol{R}^{(i)}$ to $\boldsymbol{R}^{(i+1)}$**: $\boldsymbol{R}^{(i+1)}$ is updated from $\boldsymbol{R}^{(i)}$ by setting the elements at $(\hat{m}_{k'} \oplus a_{k',l}, l)$ for $l = 1, 2, \ldots, L$ to zero.

3. **Finally**, for the rest $(K-N)$ SEs, they are detected simultaneously based on $\boldsymbol{R}^{(N+1)}$ using the EGC fusion rule, as stated in Section 4.3.1.

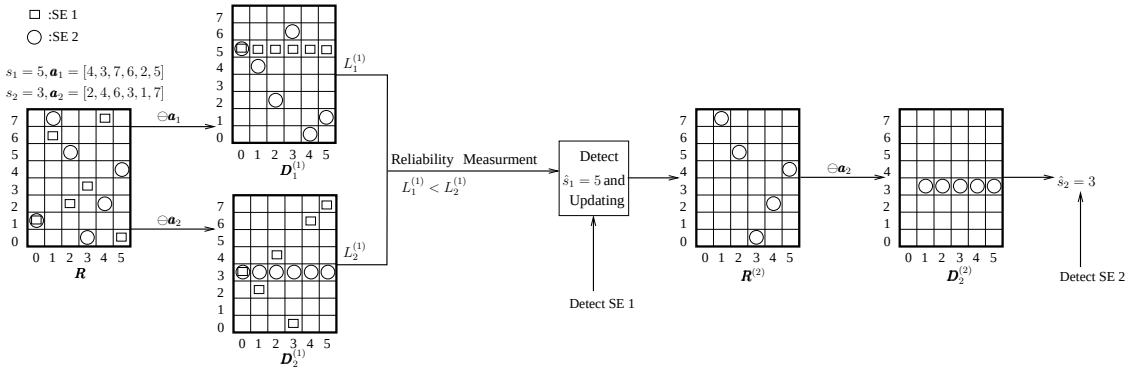

Figure 4.4: An example showing the processing of the EGC-NIIC processing, where squares and circles represent the elements actived by SE 1 and 2 , respectively, and the number of IIC iterations is set as $N = 1$.

Fig 4.4 illustrates the operations of the EGC-NIIC detection when the received matrix $\boldsymbol{R}$ is given by (4.11). After the frequency de-hopping operation, the detection matrices $\boldsymbol{D}_1^{(1)}$ and $\boldsymbol{D}_2^{(1)}$ are obtained. Then, for each of the two SEs, M decision variables are formed under the EGC principles. Then the reliabilities of the detection of SE 1 and SE 2 are measured based on (4.16). If we assume that SE 1 is more reliable than SE 2, SE 1 is then first detected based on $\boldsymbol{D}_1^{(1)}$. Then, based on the detected symbol $\hat{s}_1$ and the FH address $\boldsymbol{a}_1$, $\boldsymbol{R}^{(1)}$ is updated as $\boldsymbol{R}^{(2)}$ by carrying out interference cancellation (IC) [170]. Based on $\boldsymbol{R}^{(2)}$, we then detect SE 2. Specifically, after the

frequency de-hopping operation, $\boldsymbol{D}_2^{(2)}$ is obtained, based on which can be detected in the EGC principles.

From the above-stated EGC-NIIC algorithm, we can see that the IC operations are only implemented with the first N most reliable SEs, while the other $(K-N)$ SEs are detected based on the EGC fusion rule described in Section 4.3.1. The reason behind this proposed EGC-NIIC is that, in the FH/MFSK WSN, there are three factors affecting the performance of fusion detection, which are the detection reliabilities of LSNs, wireless channel and the MEI. Due to the unreliable detection at the LSNs, even a SE measured based on (4.16) with the highest reliability might finally be detected in error. In this case, applying the IC will generate negative effect on the following detections. Furthermore, it can be shown that this negative effect becomes worse as the number of SEs invoked and/or the number of LSNs increase. Note that, for given values of K, L as well as the observation reliability of the LSNs, there usually exists an optimum value for N, which yields the best fusion detection performance, as illustrated by our results in Section 4.6.

4.3.4 ES-EGC Assisted N-Order Iterative Interference Cancellation (ES-EGC-NIIC)

The operations of the ES-EGC-NIIC is very similar as that of the EGC-NIIC, except that the detection matrices $\{\boldsymbol{D}_k^{(i)}\}$ used by the EGC-NIIC are replaced by the modified detection matrices $\{\bar{\boldsymbol{D}}_k^{(i)}\}$, which are obtained based on the principles of ES-EGC, as shown in Section 4.3.2. In detail, in the context of the ES-EGC-NIIC fusion rule, the reliabilities are measured according to

$$\bar{L}_k = \frac{\max_2 \{\bar{D}_{k,0}, \bar{D}_{k,1}, \cdots, \bar{D}_{k,M-1}\}}{\max_1 \{\bar{D}_{k,0}, \bar{D}_{k,1}, \cdots, \bar{D}_{k,M-1}\}} \tag{4.20}$$

where $\bar{D}_{k,0}, \bar{D}_{k,1}, \cdots, \bar{D}_{k,M-1}$ denote the M decision variables provided by the ES-EGC detection.

In summary, the ES-EGC-NIIC algorithm can be described as follows:

1. **Initialization**: $\boldsymbol{A}$, $N \leq K-1$, $0 \leq I < L$, $\boldsymbol{R}^{(1)} = \boldsymbol{R}$.

2. **ES-EGC-NIIC detection**: for $i = 1, 2, \ldots, N$, the following steps are executed:

   (a) **Frequency de-hopping**: For those $(K-i+1)$ SEs having not been detected, the de-

tection matrices, $\boldsymbol{D}_1^{(i)}, \boldsymbol{D}_2^{(i)}, \ldots, \boldsymbol{D}_{K-i+1}^{(i)}$, are formed according to

$$\boldsymbol{D}_k^{(i)} = \boldsymbol{R}^{(i)} \boxminus (\mathbf{1} \otimes \boldsymbol{a}_k^T),\ k = 1, 2, \ldots, K-i+1 \tag{4.21}$$

(b) **Erasure operation**: For each of the detection matrices, $\boldsymbol{D}_1^{(i)}, \boldsymbol{D}_2^{(i)}, \ldots, \boldsymbol{D}_{K-i+1}^{(i)}$, I $(0 \leq I < L)$ number of the largest entries in each row are set to zero, forming the modified detection matrices, $\bar{\boldsymbol{D}}_1^{(i)}, \bar{\boldsymbol{D}}_2^{(i)}, \ldots, \bar{\boldsymbol{D}}_{K-i+1}^{(i)}$.

(c) **Forming decision variables**: For each of the $(K-i+1)$ SEs, the M decision variables are formed based on the EGC principles as

$$\bar{D}_{k,m}^{(i)} = \sum_{l=1}^{L} \bar{D}_{k,ml}^{(i)},\ m = 0, 1, \ldots, M-1;\ k = 1, 2, \ldots, K-i+1 \tag{4.22}$$

(d) **Reliability measurement**: The reliabilities with respect to all the $(K-i+1)$ SEs are measured based on (4.20), and are expressed as $\bar{L}_1^{(i)}, \bar{L}_2^{(i)}, \ldots, \bar{L}_{K-i+1}^{(i)}$.

(e) **Detecting the most reliable SE**: The most reliable SE is identified as

$$k' \leftrightarrow \bar{L}_{k'}^{(i)} = \min\left\{\bar{L}_1^{(i)}, \bar{L}_2^{(i)}, \ldots, \bar{L}_{K-i+1}^{(i)}\right\} \tag{4.23}$$

Correspondingly, the state of the k'th SE is detected as the m index of the largest in $\{\bar{D}_{k';0}^{(i)}, \bar{D}_{k';1}^{(i)}, \ldots, \bar{D}_{k';M-1}^{(i)}\}$. Let the estimated state for the k'th SE be expressed as $\hat{m}_{k'}$.

(f) **Update $\boldsymbol{R}^{(i)}$ to $\boldsymbol{R}^{(i+1)}$**: $\boldsymbol{R}^{(i+1)}$ is updated from $\boldsymbol{R}^{(i)}$ by setting the elements at $(\hat{m}_{k'} \oplus a_{k',l}, l)$ for $l = 1, 2, \ldots, L$ to zeros.

3. **Finally**, for the rest $(K-N)$ SEs, they are detected simultaneously based on $\boldsymbol{R}^{(N+1)}$ using the ES-EGC fusion rule, as stated in Section 4.3.2.

Fig 4.5 considered an example of the ES-EGC-NIIC fusion detection after the FC obtains the received matrix $\boldsymbol{R}$ in the form of (4.11). After the frequency de-hopping operation, the detection matrices $\boldsymbol{D}_1^{(1)}$ and $\boldsymbol{D}_2^{(1)}$ are formed based on (4.21). Then, the erasure operations are carried out, where the largest entry in each row is replaced by zero, forming $\bar{\boldsymbol{D}}_1^{(1)}$ and $\bar{\boldsymbol{D}}_2^{(1)}$. In this example, it is assumed that the element containing both signal and noise has higher power than the element containing only noise. Furthermore, the element actived simultaneously by both SE 1 and SE 2 is assumed to have high power than that actived by single SE. Hence, under these assumptions, the modified detection matrices $\bar{\boldsymbol{D}}_1^{(1)}$ and $\bar{\boldsymbol{D}}_2^{(1)}$ are shown in Fig 4.5. With the aid of $\bar{\boldsymbol{D}}_1^{(1)}$ and

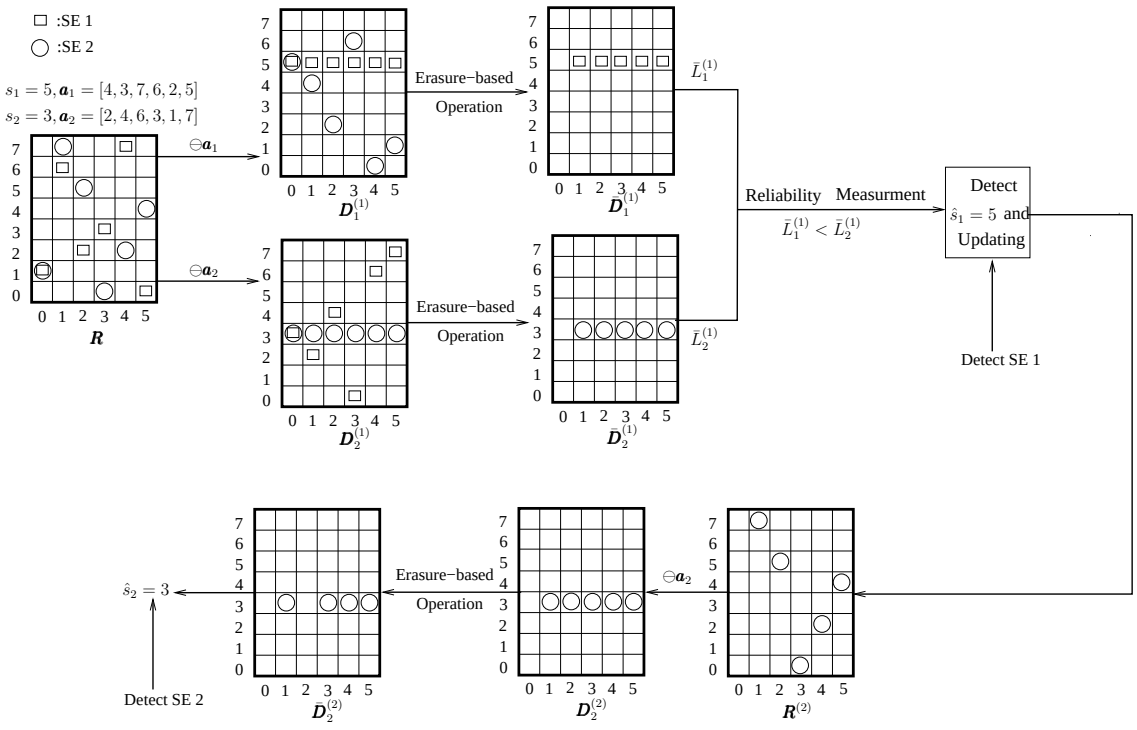

Figure 4.5: An example showing the procedure of the ES-EGC-NIIC, where squares and circles represent the elements actived by SE 1 and 2, respectively. In this example, SE 1 is assumed to be more reliable than SE 2, and $I = 1$ element per row is erasured.

$\bar{\boldsymbol{D}}_2^{(1)}$, for each of the two SEs, the decision variables are formed based one the EGC principles according to (4.22). Then, the reliabilities of SE 1 and SE 2 are measured based on (4.20). As we assumed that SE 1 is more reliable than SE 2, yielding SE 1 is first detected $\hat{s}_1 = 5$. Then, based on the decision $\hat{s}_1$ and the FH address $\boldsymbol{a}_1$, the corresponding elements in $\boldsymbol{R}$ are removed, yielding an updated matrix $\boldsymbol{R}^{(2)}$. Then, after frequency de-hopping on $\boldsymbol{R}^{(2)}$ and erasure operation on $\boldsymbol{D}_2^{(2)}$, we obtain the modified detection matrix $\bar{\boldsymbol{D}}_2^{(2)}$ for SE 2. Finally, based on $\bar{\boldsymbol{D}}_2^{(2)}$, the state of SE 2 is detected, which is $\hat{s}_2 = 3$.

As seen from the algorithm and the above example, in the ES-EGC-NIIC, the IIC operations fully remove nonzero elements from the time-frequency matrix $\boldsymbol{R}$. Hence, the IIC operations at one iteration impose effect on the following iterations of detection and the effect is accumulative, yielding error propagation. By contrast, the erasure operations are only applied to the detection matrices, which are independent iteration-by-iteration. Hence, the effect of the erasure operations at one iteration of detection does not (or, at least, not directly) propagate to the following iterations of detection.

Note furthermore that, as in the EGC-NIIC fusion rule, when given the values of K, L and I as well as the observation reliability of the LSNs in the ES-EGC-NIIC, there usually exists a value for N, which yields the best fusion detection performance, as illustrated by our results in Section 4.6.

4.3.5 EGC Assisted ρ-Fraction Iterative Interference Cancellation (EGC-ρIIC)

From Sections 4.3.3 and 4.3.4 we know that, when operated under the EGC-NIIC or ES-EGC-NIIC fusion rule, once the state of a SE is estimated, the L elements corresponding to this state in the time-frequency matrix $\boldsymbol{R}$ are set to zero, resulting in full cancellation. However, there is a negative effect associated with this full cancellation. As seen in (4.9) of the transmitted signal or (4.11) for the specific example considered, there are cases where one time-frequency element in $\boldsymbol{R}$ conveys information for several SEs. Correspondingly, as seen in (4.9), this type of elements have relatively higher values than the others, that convey information only for one SE. Consequently, when the EGC-NIIC or ES-EGC-NIIC is used, the full cancellation may remove the information of the SEs not detected yet, and might degrade the achievable error performance.

Based on the above observations, in this chapter, we propose two partial cancellation fusion rules, namely, the EGC-ρIIC and ES-EGC-ρIIC, which are considered in this section and Section 4.3.6, respectively. Note that, the EGC-ρIIC and ES-EGC-ρIIC fusion rules are similar as the EGC-NIIC and ES-EGC-NIIC fusion rules. The differences include the above-mentioned partial cancellation and K number of detection stages, when a FH/MFSK WSN monitoring K SEs is considered. In detail, the EGC-ρIIC algorithm can be summarized as follows.

1. **Initialization**: $\boldsymbol{A}$, K, $0 < \rho \leq 1$, $\boldsymbol{R}^{(1)} = \boldsymbol{R}$.

2. **EGC-ρIIC detection**: for $i = 1, 2, \ldots, K$, the following steps are executed:

   (a) **Frequency de-hopping**: For those $(K - i + 1)$ SEs having not been detected, the detection matrices, $\boldsymbol{D}_1^{(i)}, \boldsymbol{D}_2^{(i)}, \ldots, \boldsymbol{D}_{K-i+1}^{(i)}$, are formed according to

   $$\boldsymbol{D}_k^{(i)} = \boldsymbol{R}^{(i)} \boxminus (\boldsymbol{1} \otimes \boldsymbol{a}_k^T), \; k = 1, 2, \ldots, K - i + 1 \tag{4.24}$$

   (b) **Forming decision variables**: For each of the $(K - i + 1)$ SEs, the M decision variables

are formed based on the EGC principles as

$$D_{k,m}^{(i)} = \sum_{l=1}^{L} D_{k,ml}^{(i)},\ m = 0,1,\ldots,M-1;\ k = 1,2,\ldots,K-i+1 \tag{4.25}$$

(c) **Reliability Measurement**: The reliabilities with respect to all the $(K-i+1)$ SEs are measured based on (4.16), and are expressed as $L_1^{(i)}, L_2^{(i)}, \ldots, L_{K-i+1}^{(i)}$.

(d) **Detecting the most reliable SE**: The most reliable SE is identified as

$$k' \leftrightarrow L_{k'}^{(i)} = \min\left\{L_1^{(i)}, L_2^{(i)}, \ldots, L_{K-i+1}^{(i)}\right\} \tag{4.26}$$

Correspondingly, the state of the most reliable SE of k' is detected as the m index of the largest in $\{D_{k';0}^{(i)}, D_{k';1}^{(i)}, \ldots, D_{k';M-1}^{(i)}\}$. Let the estimated state for the k'th SE be expressed as $\hat{m}_{k'}$.

(e) **Update $\boldsymbol{R}^{(i)}$ to $\boldsymbol{R}^{(i+1)}$**: When $i < K$, $\boldsymbol{R}^{(i)}$ is updated to $\boldsymbol{R}^{(i+1)}$ by changing the elements at $(\hat{m}_{k'} \oplus a_{k',l}, l)$ for $l = 1,2,\ldots,L$ as

$$R_{\hat{m}_{k'}\oplus a_{k',l},l}^{(i+1)} = R_{\hat{m}_{k'}\oplus a_{k',l},l}^{(i)} - \rho \times R_{\hat{m}_{k'}\oplus a_{k',l},l}^{(i)} \tag{4.27}$$

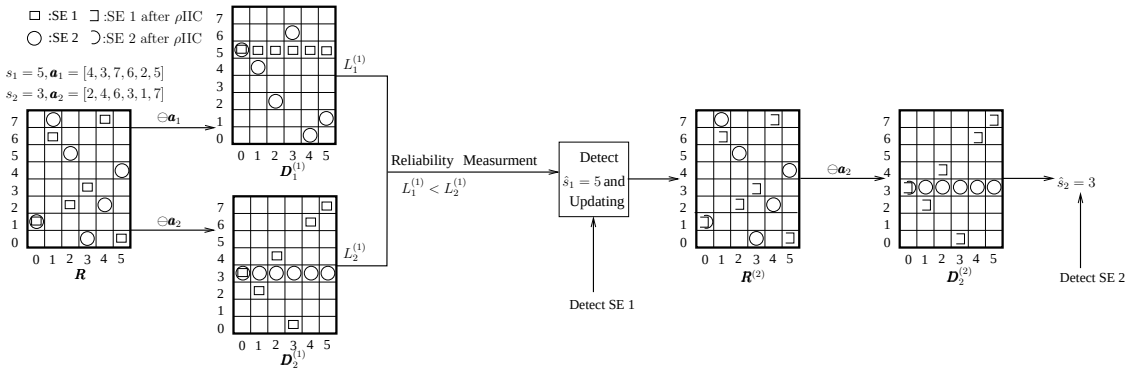

Figure 4.6: An example showing the operation of the EGC-ρIIC processing, where squares and circles represent the elements actived by SE 1 and 2, respectively. In the example, SE 1 is assumed to be more reliable than SE 2.

Fig 4.6 shows the principles of the EGC-ρIIC fusion detection. First, after the frequency dehopping, the detection matrices $\boldsymbol{D}_1^{(1)}$ and $\boldsymbol{D}_2^{(1)}$ are formed according to (4.24). Then, M decision variables for each of the two SEs are formed via EGC fusion rule. Then, the reliabilities of SE 1 and SE 2 are calculated according to (4.16), respectively. As SE 1 is assumed to be more reliable

than SE 2, SE 1 is first detected via EGC fusion rule, giving $\hat{s}_1 = 5$. Then, after cancelling the effect of SE 1, $\boldsymbol{R}$ is updated to $\boldsymbol{R}^{(2)}$ by reducing the corresponding elements' values ρ times of their original values. Finally, based on $\boldsymbol{R}^{(2)}$, SE 2 is detected, giving the estimate of $\hat{s}_2 = 3$.

In contrast to the EGC-NIIC fusion rule, which needs to optimize the value of N, in the EGC-ρIIC fusion rule, the value of ρ can also be optimized for achieving the best detection performance. However, the optimum value of ρ (as well as the optimum value of N) is depended on many factors, including the number of SEs and LSNs, detection performance of LSN, hypotheses about SEs, wireless channels between LSNs and FC, etc. It is in general very hard to find the optimum value of ρ by deriving the closed-form formulas. In practice, the optimum values in the context of various scenarios may be obtained via simulations.

4.3.6 ES-EGC Assisted ρ-Fraction Iterative Interference Cancellation (ES-EGC-ρIIC)

Straightforwardly, the ES-EGC-ρIIC is an improved version of the EGC-ρIIC by invoking the ES-EGC techniques. The algorithm can be described as follows.

1. **Initialization**: $\boldsymbol{A}$, K, $0 < \rho < 1$, $\boldsymbol{R}^{(1)} = \boldsymbol{R}$.

2. **ES-EGC-ρIIC detection**: for $i = 1, 2, \ldots, K$, the following steps are executed:

   (a) **Frequency de-hopping**: For those $(K - i + 1)$ SEs having not been detected, the detection matrices, $\boldsymbol{D}_1^{(i)}, \boldsymbol{D}_2^{(i)}, \ldots, \boldsymbol{D}_{K-i+1}^{(i)}$, are formed according to

   $$\boldsymbol{D}_k^{(i)} = \boldsymbol{R}^{(i)} \boxminus (\boldsymbol{1} \otimes \boldsymbol{a}_k^T),\ k = 1, 2, \ldots, K - i + 1 \tag{4.28}$$

   (b) **Erasure operation**: For each of the detection matrices, $\boldsymbol{D}_1^{(i)}, \boldsymbol{D}_2^{(i)}, \ldots, \boldsymbol{D}_{K-i+1}^{(i)}$, I $(0 \leq I < L)$ number of the largest entries in each row are set to zero, forming the modified detection matrices, $\bar{\boldsymbol{D}}_1^{(i)}, \bar{\boldsymbol{D}}_2^{(i)}, \ldots, \bar{\boldsymbol{D}}_{K-i+1}^{(i)}$.

   (c) **Forming decision variables**: For each of the $(K - i + 1)$ SEs, M decision variables are formed based on the EGC principles as

   $$\bar{D}_{k,m}^{(i)} = \sum_{l=1}^{L} \bar{D}_{k,ml}^{(i)},\ m = 0, 1, \ldots, M - 1;\ k = 1, 2, \ldots, K - i + 1 \tag{4.29}$$

(d) **Reliability measurement**: The reliabilities with respect to all the $(K-i+1)$ SEs are measured based on (4.20), and are expressed as $\bar{L}_1^{(i)}, \bar{L}_2^{(i)}, \ldots, \bar{L}_{K-i+1}^{(i)}$.

(e) **Detecting the most reliable SE**: The most reliable SE is identified as

$$k' \leftrightarrow \bar{L}_{k'}^{(i)} = \min\left\{\bar{L}_1^{(i)}, \bar{L}_2^{(i)}, \ldots, \bar{L}_{K-i+1}^{(i)}\right\} \tag{4.30}$$

Correspondingly, the state of the k'th SE is detected as the m index of the largest in $\{\bar{D}_{k';0}^{(i)}, \bar{D}_{k';1}^{(i)}, \ldots, \bar{D}_{k';M-1}^{(i)}\}$. Let the estimated state for the k'th SE be expressed as $\hat{m}_{k'}$.

(f) **Update $\boldsymbol{R}^{(i)}$ to $\boldsymbol{R}^{(i+1)}$**: When $i < K$, $\boldsymbol{R}^{(i)}$ is updated to $\boldsymbol{R}^{(i+1)}$ by changing the elements at $(\hat{m}_{k'} \oplus a_{k',l}, l)$ for $l = 1, 2, \ldots, L$ as

$$R_{\hat{m}_{k'} \oplus a_{k',l}, l}^{(i+1)} = R_{\hat{m}_{k'} \oplus a_{k',l}, l}^{(i)} - \rho \times R_{\hat{m}_{k'} \oplus a_{k',l}, l}^{(i)} \tag{4.31}$$

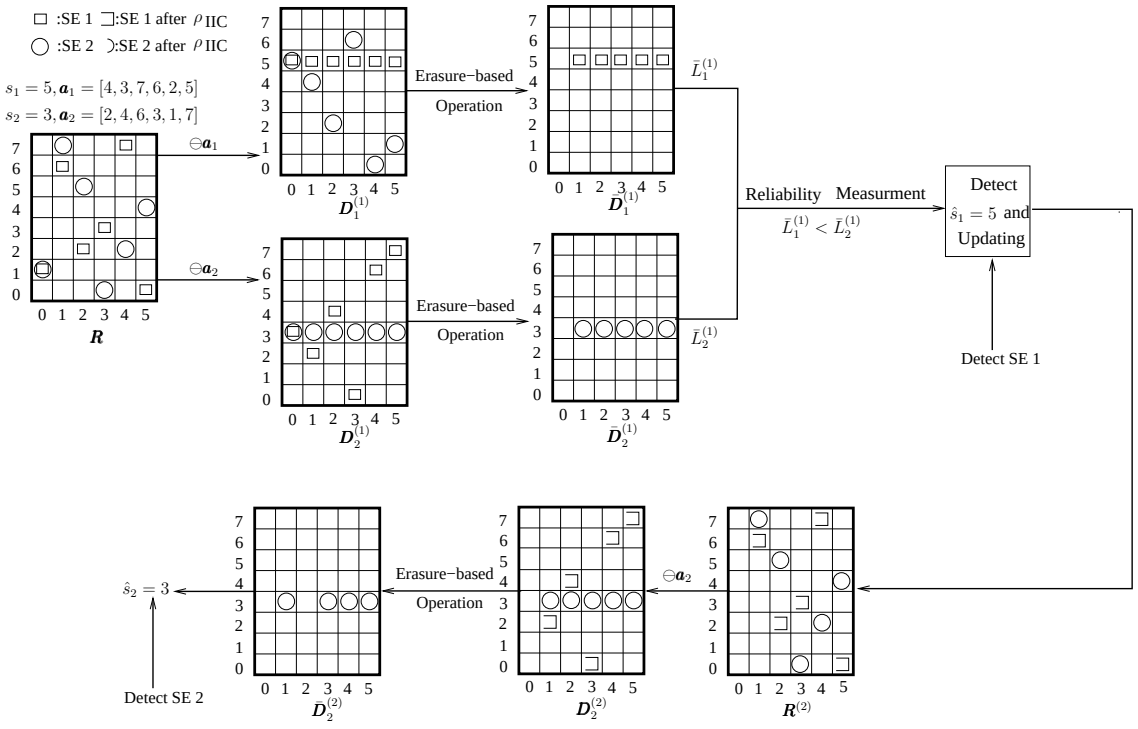

Figure 4.7: An example of ES-EGC-ρIIC processing, where squares and circles represent the elements actived by SE 1 and 2 respectively. SE 1 is assumed to be more reliable than SE 2, and $I = 1$ element per row is erasured.

As shown in Fig 4.7, the operation of the ES-EGC-ρIIC fusion rule is illustrated. As shown in Fig 4.7, after the frequency de-hopping, the detection matrices $\boldsymbol{D}_1^{(1)}$ and $\boldsymbol{D}_2^{(1)}$ are obtained. Then,

in each of the detection matrices, the largest entry in each row is removed, forming the modified detection matrices $\bar{\boldsymbol{D}}_1^{(1)}$ and $\bar{\boldsymbol{D}}_2^{(1)}$. Then, for each of the two SEs, M decision variables are formed based on the EGC principles. Then, the reliabilities for detection of SE 1 and SE 2 are measured based on (4.20). As the reliability of SE 1 is assumed to be higher than that of SE 2, SE 1 is first detected via the EGC fusion rule, yielding $\hat{s}_1 = 5$. Then, based on the decision of SE 1 and its FH address $\boldsymbol{a}_1$, $\boldsymbol{R}$ is updated to $\boldsymbol{R}^{(2)}$. Then, after the frequency de-hopping is operated on $\boldsymbol{R}^{(2)}$, the detection matrix $\boldsymbol{D}_2^{(2)}$ for SE 2 is obtained. Then, the largest entry in each row of $\boldsymbol{D}_2^{(2)}$ is removed, yielding the modified detection matrix $\bar{\boldsymbol{D}}_2^{(2)}$. Finally, SE 2 is detected based on $\bar{\boldsymbol{D}}_2^{(2)}$ via the EGC principles, yielding $\hat{s}_2 = 3$.

4.4 Analysis of Complexity

In this section, we analyze and compare the computational complexity of the six fusion rules, namely the EGC, ES-EGC, EGC-NIIC, ES-EGC-NIIC, EGC-ρIIC and ES-EGC-ρIIC, considered in this chapter. Our complexity analysis starts from the point when the FC forms the time-frequency matrix $\boldsymbol{R}$, as the number of computations required before this point is the same for all the six fusion rules. In our analysis, the complexity takes into account both the addition and comparison operations, while the complexity for frequency de-hopping is ignored. The reason for not including the frequency de-hopping is that the results of additions (or subtraction) in Galois field $GF(M)$ can be stored in a $(M \times M)$ table. With the aid of this table, frequency de-hopping is simply reading the values from $\boldsymbol{R}$ and writing them into the corresponding locations in $\boldsymbol{D}_k$, $k = 1, 2, \ldots, K$, where the locations are provided by the table.

EGC - First, in the context of the conventional EGC fusion rule, after $\boldsymbol{D}_k$, $k = 1, 2, \ldots, K$, is obtained, forming a decision variable needs $(L-1)$ additions. The number of comparisons for finding out the maximum one from M real numbers is $(M-1)$. Therefore, the total number of operations for detecting K SEs is $K[M(L-1)+M-1] = K(ML-1)$. Hence, the complexity of the EGC fusion rule is $\mathcal{O}(KML)$ for detection of the K SEs.

ES-EGC - For the ES-EGC fusion rule, starting from $\boldsymbol{D}_k$, $k = 1, 2, \ldots, K$, first, each row needs to implement the following operations: a) identifying the I maximal entries from the L entries, which requires $I(2L-I-1)/2$ number of comparisons when assuming $I \leq L/2$, and

b) adding together the entries of the rest $(L-I)$ entries, which requires $(L-I-1)$ additions. Finally, for each SE, selecting the maximum from the M decision variables requires $(M-1)$ comparisons. Hence, the total number of operations of the ES-EGC for detecting K SEs can be found to be $K[M(LI+L-I^2/2-3I/2)-1]$. Therefore, the complexity of the ES-EGC fusion rule is $\mathcal{O}(KMLI)$ for detecting K SEs.

EGC-NIIC - For the EGC-NIIC fusion rule, as shown in Section 4.3.3, N out of the K SEs are detected based on EGC and IIC in N iterations, while the rest $(K-N)$ SEs are detected based on EGC at the last iteration. Let us first consider the number of operations required by the ith, where $i \leq N$, iteration of detection. As seen in Section 4.3.3, after the frequency de-hopping, the ith iteration first implements the EGC for $(K-i+1)$ SEs, which requires in total $(K-i+1)[M(L-1)]$ operations. Then, associated with each of the $(K-i+1)$ SEs, the reliability of detection is measured based on (4.16), which needs to find the maximum and the second maximum from the decision variables $\left\{D_{k,0}^{(i)}, D_{k,1}^{(i)}, \cdots, D_{k,M-1}^{(i)}\right\}$ as well as compute their ratio, which requires in total $(2M-3)$ operations. Then, the most reliable SE is identified based on (4.19), which requires $(K-i)$ operations. Finally, the complexity of interference cancellation can be ignored. Hence, the total number of operations of the ith iteration is $(K-i+1)[M(L-1)+2M-3]+(K-i)$. When N iterations are considered, the number of operations can be expressed as

$$\begin{aligned}&\sum_{i=1}^{N}\{(K-i+1)[M(L-1)+2M-3]+(K-i)\}\\&\quad=N\left(K-\frac{N+1}{2}\right)[M(L-1)+2M-2]+N[M(L-1)+2M-3]\end{aligned} \tag{4.32}$$

After N iterations of detection based on the EGC and IIC, the rest $(K-N)$ SEs are detected based on the EGC alone, which requires $(K-N)[M(L-1)+M-1]$ number of operations. Therefore, the total number of operations required by the EGC-NIIC fusion rule is approximately given by

$$\begin{aligned}&N\left(K-\frac{N+1}{2}\right)[M(L-1)+2M-2]+N[M(L-1)+2M-3]\\&+(K-N)[M(L-1)+M-1]\\&=N\left(K-\frac{N+1}{2}\right)(ML+M-2)+N(ML+M-3)+(K-N)(ML-1)\end{aligned} \tag{4.33}$$

When considering only the dominate items in the above equation, we can see that the complexity of the EGC-NIIC is $\mathcal{O}(KMLN)$.

ES-EGC-*N*IIC - When comparing the ES-EGC-*N*IIC fusion rule described in Section 4.3.4 with the EGC-*N*IIC fusion rule described in Section 4.3.3, we can see that the only difference is the extra erasure operations for the ES-EGC-*N*IIC. Hence, from the above complexity analysis for the EGC and ES-EGC, we can readily know that the total number of operations required by the ES-EGC-*N*IIC fusion rule is approximately

$$\begin{aligned}
&N\left(K-\frac{N+1}{2}\right)\left[M\left(LI+L-\frac{I^2}{2}-\frac{3I}{2}-1\right)+2M-2\right]\\
&+N\left[M\left(LI+L-\frac{I^2}{2}-\frac{3I}{2}-1\right)+2M-3\right]\\
&+(K-N)\left[M\left(LI+L-\frac{I^2}{2}-\frac{3I}{2}-1\right)+M-1\right]\\
&=N\left(K-\frac{N+1}{2}\right)\left[M\left(LI+L-\frac{I^2}{2}-\frac{3I}{2}+1\right)-2\right]\\
&+N\left[M\left(LI+L-\frac{I^2}{2}-\frac{3I}{2}+1\right)-3\right]+(K-N)\left[M\left(LI+L-\frac{I^2}{2}-\frac{3I}{2}\right)-1\right] \quad (4.34)
\end{aligned}$$

Correspondingly, the complexity of the ES-EGC-*N*IIC is $\mathcal{O}(KMLNI)$.

EGC-ρIIC - As our previous discussion in Section 4.3.5 shows, when the EGC-ρIIC fusion rule is applied at the fusion center, $(K-1)$ SEs are detect according to the EGC-ρIIC fusion rule, while the last one is detected based on the EGC fusion rule. Hence, the number of operations required by the EGC-ρIIC fusion rule can be viewed as a special case of the EGC-*N*IIC fusion rule, where N equals $(K-1)$. Therefore, when the EGC-ρIIC fusion rule is employed, the number of operations required to detect all the K SEs is $K(K-1)(ML+M-2)/2+(K-1)(ML+M-3)+ML-1$, which yields the complexity of $\mathcal{O}(K^2ML)$.

ES-EGC-ρIIC - The total number of operations required by the ES-EGC-ρIIC fusion rule can be found from that of the ES-EGC-*N*IIC fusion rule associated with letting $N=K-1$, which can be expressed as

$$\begin{aligned}
&\frac{K}{2}(K-1)\left[M\left(LI+L-\frac{I^2}{2}-\frac{3I}{2}+1\right)-2\right]\\
&+(K-1)\left[M\left(LI+L-\frac{I^2}{2}-\frac{3I}{2}+1\right)-3\right]+M\left(LI+L-\frac{I^2}{2}-\frac{3I}{2}\right)-1 \quad (4.35)
\end{aligned}$$

Hence, the complexity of the ES-EGC-ρIIC fusion rule is $\mathcal{O}(K^2MLI)$.

The number of operations required by the various fusion rules considered in this chapter as well as the corresponding complexity are summarized in Table 4.1. As shown in Table 4.1, the conventional EGC fusion rule has the lowest complexity. The complexity of the ES-EGC fusion

Fusion rule	Number of operations	Complexity
EGC	$K(ML-1)$	$\mathcal{O}(KML)$
ES-EGC	$K[M(LI+L-\frac{I^2}{2}-\frac{3I}{2})-1]$	$\mathcal{O}(KMLI)$
EGC-NIIC	$N\left(K-\frac{N+1}{2}\right)(ML+M-2)+N(ML+M-3)$ $+(K-N)(ML-1)$	$\mathcal{O}(KMLN)$
ES-EGC-NIIC	$N\left(K-\frac{N+1}{2}\right)[M(LI+L-\frac{I^2}{2}-\frac{3I}{2}+1)-2]+N[M(LI+L-\frac{I^2}{2}-\frac{3I}{2}+1)-3]$ $+(K-N)[M(LI+L-\frac{I^2}{2}-\frac{3I}{2})-1]$	$\mathcal{O}(KMLNI)$
EGC-ρIIC	$\frac{K}{2}(K-1)(ML+M-2)+(K-1)(ML+M-3)+ML-1$	$\mathcal{O}(K^2ML)$
ES-EGC-ρIIC	$\frac{K}{2}(K-1)[M(LI+L-\frac{I^2}{2}-\frac{3I}{2}+1)-2]$ $+(K-1)[M(LI+L-\frac{I^2}{2}-\frac{3I}{2}+1)-3]+M(LI+L-\frac{I^2}{2}-\frac{3I}{2})-1$	$\mathcal{O}(K^2MLI)$

Table 4.1: Number of operations and complexity of the six fusion rules.

rule is slightly higher than that of the conventional EGC fusion rule, which is linearly dependent on the number of erasures per row. As shown in Table 4.1, the IIC based fusion rules demand relatively higher complexity than both the conventional EGC and the ES-EGC fusion rules. However, from the table we are implied that all the six fusion rules have relatively low complexity. The complexity for detecting K SEs is generally linearly proportional to the parameters M, L, N, I, or K, except the EGC-ρIIC and ES-EGC-ρIIC rules. However, the complexity of these two fusion rules is not related to the parameter N.

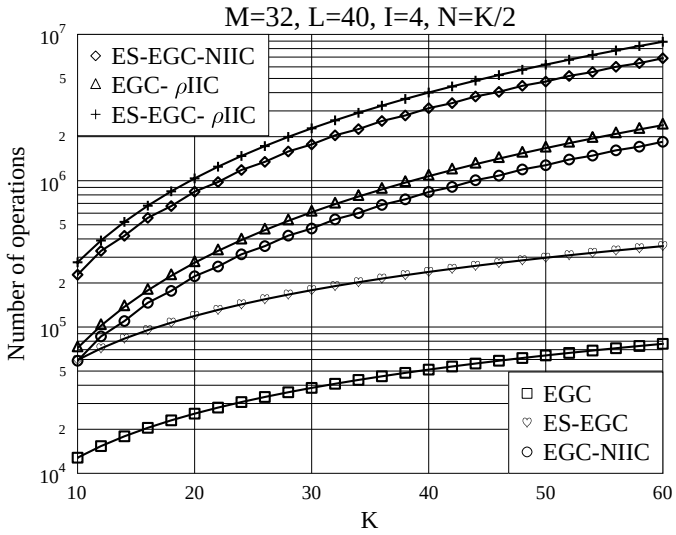

Figure 4.8: An example of Table 4.1: Number of operations versus number of SEs.

4.5 Characteristics of FH/MFSK WSN

Our proposed FH/MFSK WSN employs a range of characteristics, which can be summarized as follows. First, noncoherent detection is implemented at the FC, which does not consume extra energy for channel estimation. These energy-efficient and low-complexity detection strategies are beneficial to the life-time of battery-powered WSNs. Second, in addition to supporting multiple SEs, the FH/MFSK techniques employed are capable of providing frequency diversity for the fusion detection. This frequency diversity becomes especially important, when the LSNs are closely located, which may generate correlated fading in the space-domain. On the other hand, owing to the frequency diversity obtained from the FH/MFSK, the LSNs may be distributed within a relatively small space but still convey the FC independently faded signals, so that the detection performance of the FC is not degraded by the correlated fading experienced in the space-domain. Third, the proposed FH/MFSK WSN can simultaneously monitor multiple SEs of each with multiple states. Each LSN serves all the SEs and, hence, a FH/MFSK WSN does not have to use a big number of LSNs. However, the side effect of using one LSN to simultaneously transmit multiple frequency modulation signals is the possible high peak-to-average power ratio (PAPR), which is not power-efficient, if not treated appropriately. Forth, in the FH/MFSK WSN, in addition to the fusion rules considered in this chapter, other advanced noncoherent detection schemes [116] may also be implemented, which may further enhance the detection performance.

In this chapter, six different fusion rules, namely the EGC, ES-EGC, EGC-NIIC, ES-EGC-NIIC, EGC-ρIIC and the ES-EGC-ρIIC, are considered and compared. All of the six fusion rules are robust fusion rules of low-complexity. They have respectively different advantages and disadvantages. For example, the conventional EGC fusion rule has the lowest complexity and also the lowest detection delay. However, its detection performance is the worst, when multiple SEs interfering with each other are supported. By contrast, with a slight increase of complexity, the ES-EGC fusion rule is capable of achieving much better detection performance than the conventional EGC fusion rule. Furthermore, as our simulation results in the next section show, the single-user ES-EGC fusion rule employs certain capability to suppress MEI. Although the other four fusion rules invoke the concepts of multiuser detection, they are still low-complexity fusion rules designed based on the principles of interference cancellation. Additionally, in this chapter, the reliability measurement

scheme introduced is also a low-complexity scheme.

Finally, we note that the overall performance of the FH/MFSK WSN is jointly determined by the detection performance of the L LSNs, the wireless channels between the LSNs and FC, as well as the fusion rule employed by the FC. If the detection performance of the L LSNs is poor, then, the overall performance will most probably be poor, even when the wireless channels from LSNs to FC are perfect and the fusion detection is ideal. Similarly, the overall performance of the FH/MFSK WSN will degrade, when wireless channels become unreliable or when there exists MEI but the fusion rule is not efficient for MEI suppression. Therefore, when considering the optimization in the FH/MFSK WSN, the detection schemes at both the LSNs and FC need to be jointly considered. In general, in the FH/MFSK WSNs, the performance of LSNs may be improved by employing advanced sensing techniques, the fading of wireless channels can be compensated by making use of the frequency and space diversity, while the MEI may be mitigated with the aid of various noncoherent signal processing techniques, as shown in this chapter and [116].

Below we provide a range of simulation results, in order to characterize the achievable performance of the FH/MFSK WSNs.

4.6 Performance Results

In this section, error performance of the FH/MFSK WSNs employing various fusion rules as considered is investigated, when assuming that the wireless channels from LSNs to FC experience Rayleigh fading. We consider specifically the error classification probability (ECP) performance for the sake of unifying the WSN with the conventional one-hop communication schemes. Note that, in the following figures, the error detection probability of the LSNs is expressed as P_e, while the correct detection probability is hence $P_d = 1 - P_e$. The 'channel SNR per bit' is the average SNR per bit given by $\bar{\gamma}_b = \bar{\gamma}_s / b$, where $b = \log_2 M$ denotes the number of bits per M-ary symbol.

In Fig. 4.9, we compare the achievable ECP performance of the FH/MFSK WSN employing respectively the six fusion rules considered in this chapter, when the FH/MFSK WSN uses $L = 10$ LSNs to monitor $K = 2$ SEs and the LSNs send signals to the FC using 16FSK. Furthermore, as shown in Fig. 4.9, when the ES-EGC scheme is invoked, $I = 1$ entry is deleted from each of the rows of the detection matrix. In the context of the EGC-NIIC and ES-EGC-NIIC, we set

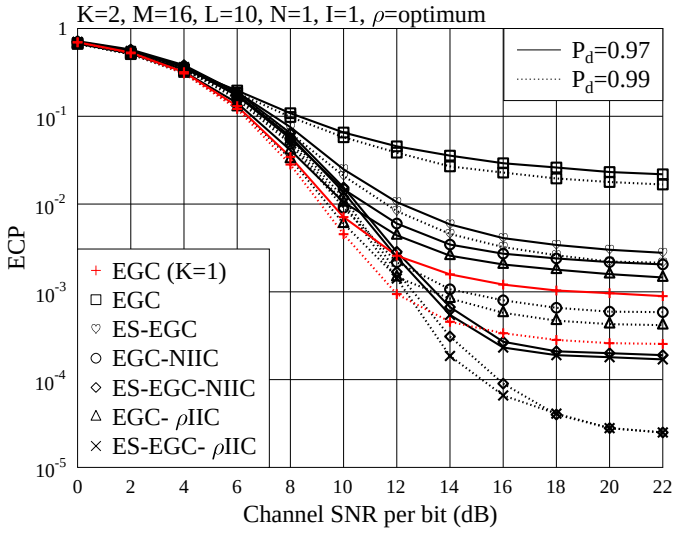

Figure 4.9: ECP versus channel SNR per bit performance of the FH/MFSK WSN monitoring $K = 2$ SEs using $L = 10$ LSNs, when communicating over Rayleigh fading channels.

$N = 1$. Furthermore, for the EGC-ρIIC and ES-EGC-ρIIC, an approximately optimum value for ρ is applied, which is found via simulations. From the performance results shown in Fig. 4.9, first, we can explicitly observe that both the reliability of the LSNs' detection and that of the wireless channels have a strong impact on the overall achievable detection performance of the FH/MFSK WSN. For any given fusion rule, the ECP performance of the FH/MFSK WSN degrades, as the correct detection probability P_d of the LSNs decreases from $P_d = 0.99$ to $P_d = 0.97$. Meanwhile, for any given P_d and any fusion rule, the ECP performance in general improves, as the wireless channels become more reliable, i.e., as the channel SNR increases.

As shown in Fig. 4.9, when the channel SNR is relatively low, such as $\bar{\gamma}_b < 12$ dB, the EGC-related fusion rules, including the EGC-NIIC and EGC-ρIIC, outperform the ES-EGC-related fusion rules, including the ES-EGC-NIIC and ES-EGC-ρIIC. By contrast, when the channel SNR is sufficiently high, such as $\bar{\gamma}_b > 12$ dB, then, the ES-EGC-NIIC and ES-EGC-ρIIC fusion rules outperform the EGC-NIIC and EGC-ρIIC fusion rules. The reason behind the above observations can be explained by remembering that EGC is an optimum diversity combining scheme over Gaussian channels, while ES-EGC has certain capability to suppress MEI. Hence, when the channel SNR is low and the Gaussian noise is dominant, the diversity gain from the EGC is critical for the achievable error performance. Consequently, the EGC-related fusion rules outperform the

ES-EGC-related fusion rules. As the channel SNR becomes higher, the Gaussian noise becomes less dominant. Instead, the MEI generates more impact, which dominates the achievable error performance of the FH/MFSK WSN. Therefore, when the channel SNR is sufficiently high, the EGC-related fusion rules are outperformed by the ES-EGC-related fusion rules.

As shown in Fig. 4.9, when the channel SNR is sufficiently high, we can observe that, comparing the detection performance from the worst to the best, the fusion rules are in the order EGC→ES-EGC→EGC-NIIC→EGC-ρIIC→ES-EGC-NIIC→ES-EGC-ρIIC. Furthermore, within the channel SNR region considered, except the ES-EGC-NIIC and ES-EGC-ρIIC, all the other four fusion rules yield error floors, implying that the MEI and/or the unreliable detection at the LSNs are unable to be fully removed by these fusion rules. By contrast, when the ES-EGC-NIIC or ES-EGC-ρIIC is employed, no error floors are present. Hence, these two fusion rules are capable of efficiently mitigating the effect of MEI as well as that of the errors generated by the LSNs' detections. Additionally, when the channel SNR is sufficiently high, the ES-EGC fusion rule may significantly outperform the EGC fusion rule, even though these two fusion rules have similar computational complexity, as the analysis in Section 4.4 shows. Note that, the ES-EGC fusion rule is capable of outperforming the EGC fusion rule, even when the scenario of monitoring one SE is considered, as shown in Fig. 4.10.

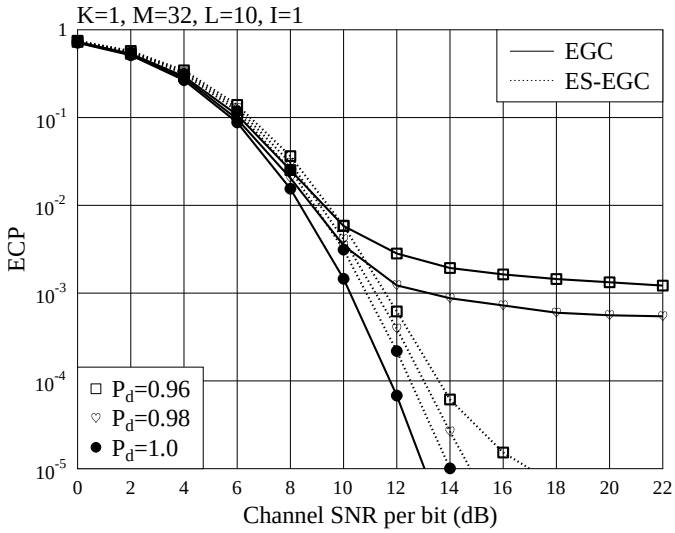

Figure 4.10: Comparison of ECP versus channel SNR per bit performance of the FH/MFSK WSN using the conventional EGC and ES-EGC fusion rules, when communicating over Rayleigh fading channels.

In Fig. 4.10, the ECP performance of the conventional EGC and that of the proposed ES-EGC are investigated and compared, when the correct detection probability of LSNs is $P_d = 0.96,\ 0.98$ or 1. Explicitly, when the LSNs' detections are unreliable, the ES-EGC scheme is capable of mitigating their negative effect, when the channel SNR is sufficiently large. As seen in Fig. 4.10, even for the case of $K = 1$, the ES-EGC rule may significantly outperform the conventional EGC in the relatively high SNR region. By contrast, when the channel SNR is low or when the LSNs' detections are ideal, erasures imposed by the ES-EGC rule reduce the information useful for detection, resulting in that the conventional EGC rule outperforms the ES-EGC rule.

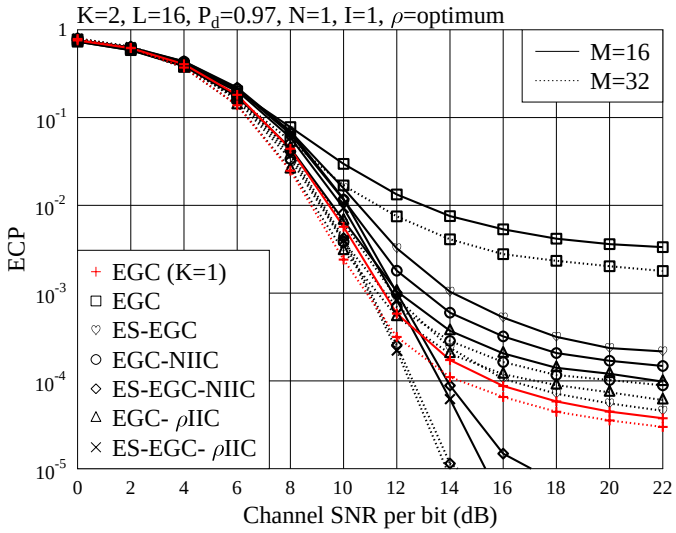

Figure 4.11: ECP versus channel SNR per bit performance of the FH/MFSK WSN monitoring $K = 2$ SEs using $L = 16$ LSNs, when communicating over Rayleigh fading channels.

In Fig. 4.11, we illustrate the ECP performance of the FH/MFSK WSN with various fusion rules, when communicating over Rayleigh fading channels. Both $M = 16$ and $M = 32$ are considered. The other parameters are shown associated with the figure. From the results of Fig. 4.11, we can draw similar conclusions as that drawn from Fig. 4.10 for comparison of the various fusion rules. Furthermore, when comparing the performance corresponding to $M = 16$ with that corresponding to $M = 32$, we can see that the detection performance of the FH/MFSK WSN using a given fusion rule improves, as the value of M increases. Therefore, in a FH/MFSK WSN with a relatively high number of LSNs for providing diversity, it is highly beneficial to use the MFSK modulation of high dimension. Fig. 4.11 shows that the ES-EGC is a high-efficiency low-complexity

fusion rule. First, it generates a big performance improvement over the conventional EGC fusion rule, which becomes more evident, when the value of M is increased from 16 to 32. Second, the ES-EGC-NIIC and ES-EGC-ρIIC fusion rules outperform all the other fusion rules. They are capable of efficiently mitigating the MEI as well as the unreliable detections at the LSNs, and generating no error-floors. Furthermore, most promisingly, when $M = 32$ and when the channel SNR is sufficiently high (about 15 dB), the low-complexity single-user ES-EGC scheme is capable of achieving better error performance than the more complicated multiuser EGC-NIIC and EGC-ρIIC fusion rules. This observation implies that the ES-EGC fusion rule employs a certain capability to mitigate MEI.

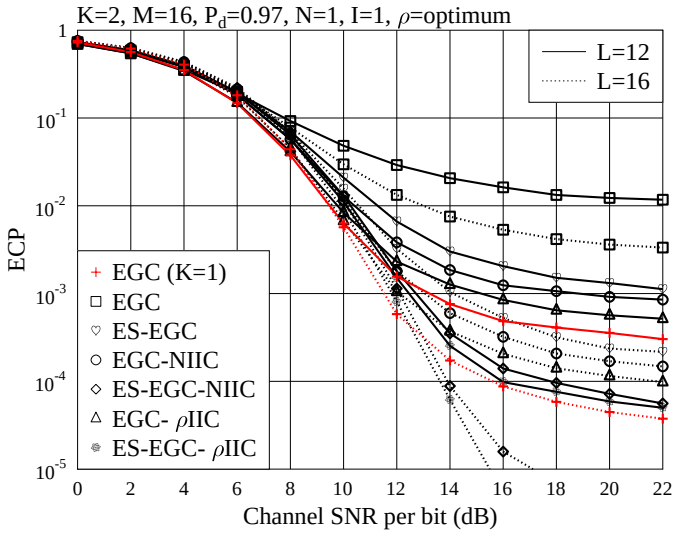

Figure 4.12: ECP versus channel SNR per bit performance of the FH/MFSK WSN monitoring $K = 2$ SEs using various number of LSNs, when communicating over Rayleigh fading channels.

Fig. 4.12 illustrates the impact of the number of LSNs on the error performance of the FH/MFSK WSN monitoring $K = 2$ SEs, when the correct detection probability at the LSNs is $P_d = 0.97$. Explicitly, the number of LSNs yields significant impact on the detection performance of the FH/MFSK WSN. In general, the ECP performance of the FH/MFSK WSN improves, as the number of LSNs increases, which generates higher space diversity. Specifically for the ES-EGC fusion rule, given $I = 1$, it becomes more efficient, as the value of L is increased from 12 to 16.

Fig. 4.13 shows the ECP versus channel SNR per bit performance of the FH/MFSK WSN supporting $K = 2$ or 3 SEs of each with $M = 32$ states. As seen in the figure, when $K = 2$ and

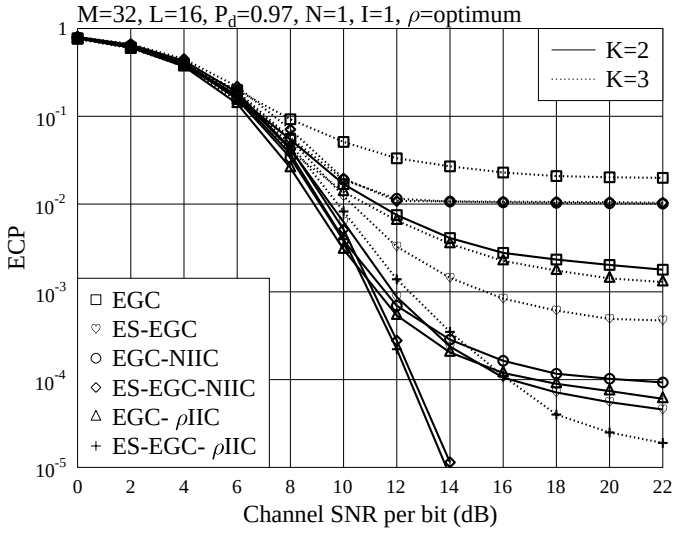

Figure 4.13: ECP versus channel SNR per bit performance of the FH/MFSK WSN monitoring $K = 2$ or 3 SEs using $L = 16$ LSNs, when communicating over Rayleigh fading channels.

the channel SNR is sufficiently large, both the ES-EGC-NIIC and the ES-EGC-ρIIC rules attain a similar ECP performance, which is the best among the six rules. By contrast, when $K = 3$ and the channel SNR is sufficiently large, the simple ES-EGC and ES-EGC-ρIIC rules attain the best ECP performance among the six. As seen in Fig. 4.13, the ES-EGC-NIIC cannot obtain any gain over the EGC-NIIC, when $K = 3$.

In Figs. 4.14 - 4.17, we investigate the effect of the parameter ρ, the fraction of cancellation, on the error performance of the FH/MFSK WSN systems, when various scenarios are considered. The details about the parameters used in the simulations can be found in the corresponding figures. First, as seen in these figures, for both the EGC-ρIIC and the ES-EGC-ρIIC, there exists an optimum value for ρ, which results in the lowest ECP. Second, the values of P_d, M and L seems do not have significant effect on the optimum value of ρ, although for some cases slight shifts are observed. By contrast, as shown in Fig. 4.17, the number of SEs invoked generates noticeable effect on the optimum value of ρ, which becomes lower as the number of SEs monitored increases. Finally, from Figs. 4.14 - 4.17 we can observe that the optimum value of ρ for the EGC-ρIIC is usually significantly higher than that for the ES-EGC-ρIIC, with the optimum value of ρ for the ES-EGC-ρIIC very close to 0.7. The reason behind the observation is that, for the EGC-ρIIC, the MEI suppression is dependent on the ρIIC alone. By contrast, for the ES-EGC-ρIIC, most of the MEI

has been removed by the ES-EGC scheme, before the ρIIC is executed. The results in Figs. 4.14 - 4.17 again reflect that the ES-EGC scheme is efficient for MEI suppression.

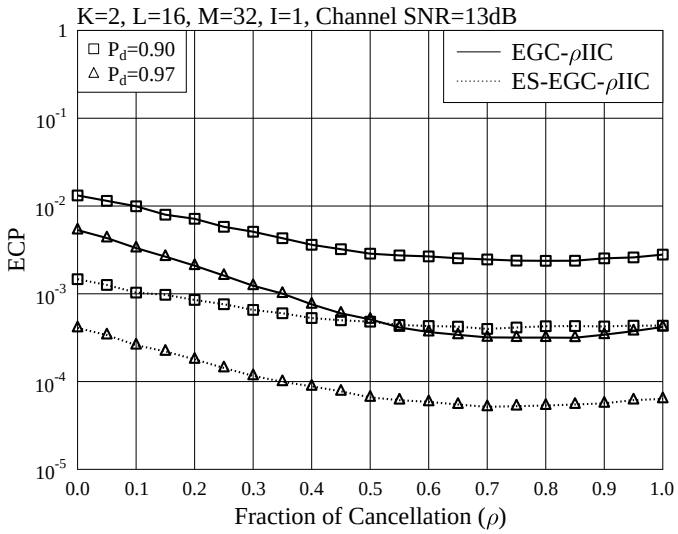

Figure 4.14: ECP versus ρ of the fraction of cancellation for the FH/MFSK WSN monitoring $K = 2$ SEs using $L = 16$ LSNs, when the EGC-ρIIC or ES-EGC-ρIIC is employed.

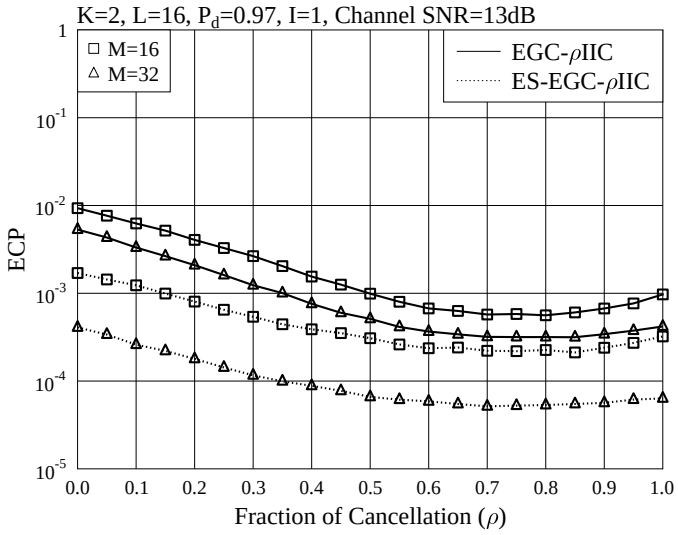

Figure 4.15: ECP versus ρ of the fraction of cancellation for the FH/MFSK WSN monitoring $K = 2$ SEs using $L = 16$ LSNs, when the EGC-ρIIC or ES-EGC-ρIIC is employed.

Fig.4.18 shows the ECP performance of the FH/MFSK WSN versus both the channel SNR per bit and the fraction of cancellation, when the FH/MFSK WSN employing EGC-ρIIC uses $L = 15$ LSNs to monitor $K = 2$ SEs of each with $M = 16$ states. We assume that the observations at the LSNs are perfect, yielding $P_d = 1$. From the figure, we can observe that, at a given channel

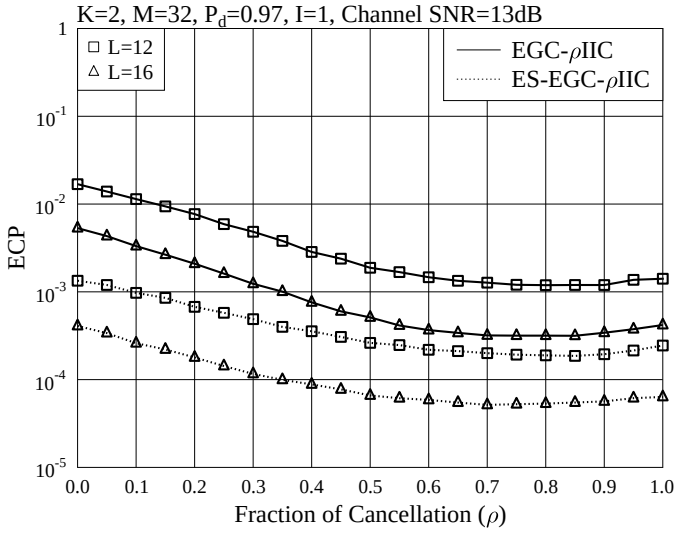

Figure 4.16: ECP versus ρ of the fraction of cancellation for the FH/MFSK WSN monitoring $K = 2$ SEs using $L = 12$ or 16 LSNs, when the EGC-ρIIC or ES-EGC-ρIIC is employed.

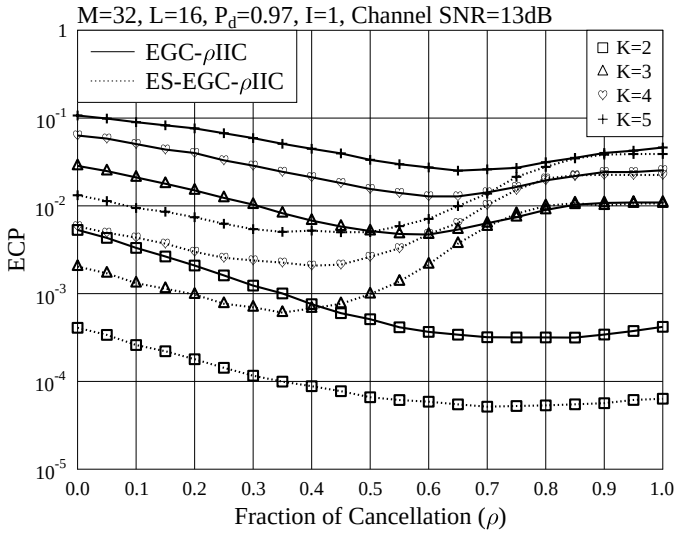

Figure 4.17: ECP versus ρ of the fraction of cancellation for the FH/MFSK WSN monitoring $K = 2$ or 3 SEs using $L = 16$ LSNs, when the EGC-ρIIC or ES-EGC-ρIIC is employed.

SNR, there is an optimum value of ρ for the fraction of cancellation, which yields the best ECP performance. As the channel SNR increases, the optimum value of ρ slightly increases, towards the value of one.

In Fig. 4.19, we study the effect of the number of iterations, expressed by N, used by the EGC-NIIC or ES-EGC-NIIC on the ECP performance of the FH/MFSK WSN. Note that, from

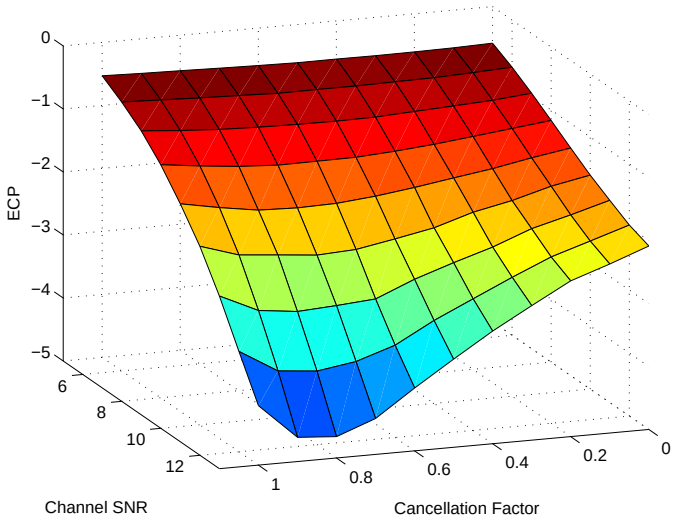

Figure 4.18: ECP versus channel SNR per bit and fraction of cancellation for the FH/MFSK WSN monitoring $K = 2$ SEs using $L = 15$ LSNs with $P_d = 1.0$, when communicating over Rayleigh fading channels.

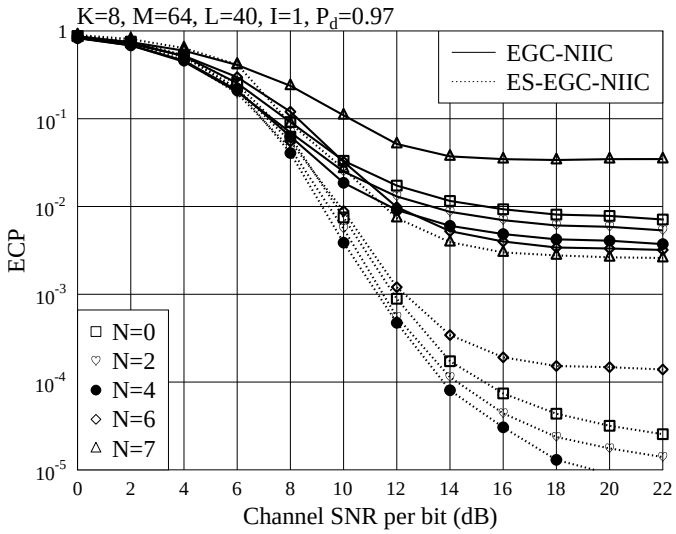

Figure 4.19: ECP versus channel SNR per bit performance of the FH/MFSK WSN monitoring $K = 8$ SEs using $L = 40$ LSNs with $P_d = 0.97$, when various orders of IIC are applied.

the principles of the (ES-)EGC-NIIC, we know that $N = 0$ corresponds to the pure (ES-)EGC fusion rule, while $N = K - 1$ corresponds to the full (ES-)EGC-IIC fusion rule, where K SEs are detected by involving the IIC operations. Generally, under the same simulation parameters, the ES-EGC-NIIC fusion rule always has a better ECP performance than the EGC-NIIC fusion rule. From the curves in Fig. 4.19, we can observe that, at a given channel SNR, there exists a value for

N, which yields the best ECP performance for the FH/MFSK WSN. The optimum value of N for the EGC-NIIC is not the same as that for the ES-EGC-NIIC. For example, at the channel SNR of 10 dB, the EGC-NIIC using $N = 4$ orders of IIC attains the lowest ECP. At the channel SNR of 16 dB, the EGC-NIIC using $N = 6$ orders of IIC achieves the lowest ECP. By contrast, for the ES-EGC-NIIC, the optimum value of N is always 4 for both the above cases.

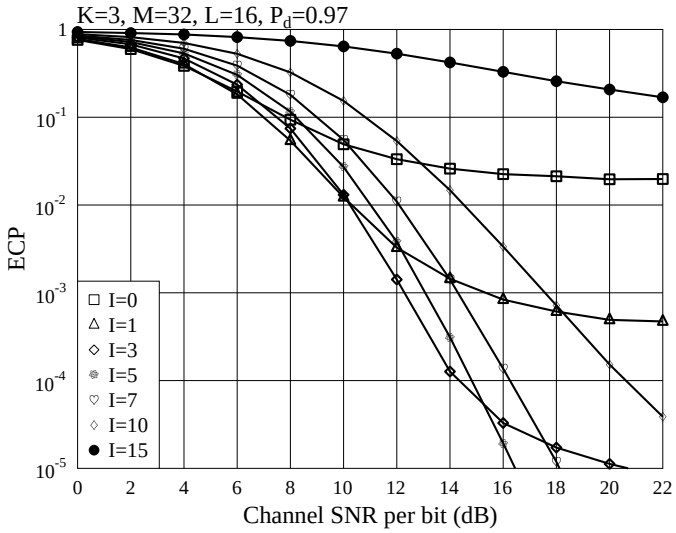

Figure 4.20: ECP versus channel SNR per bit for the FH/MFSK WSN monitoring $K = 3$ SEs using $L = 16$ LSNs, when communicating over Rayleigh fading channels.

Finally, in Fig 4.20, we show the impact of the number of deleted entries per row on the ECP performance of the FH/MFSK WSN employing the ES-EGC fusion rule. From the results of Fig. 4.20, we observe that, given a value for the channel SNR, there is an optimum value for I, which makes the ES-EGC fusion rule achieve the lowest ECP. Within the SNR range depicted, implicitly, the optimum value of I is in $[0, 5]$. When more than 5 entries per row are removed, the ECP performance degrades, resulted from the decrease of the diversity order due to too many erasures.

4.7 Conclusion

In this chapter, a FH/MFSK WSN has been studied, which uses a number of LSNs to monitor multiple SEs of each with multiple states. The FH/MFSK techniques are employed for transmitting signals from LSNs to FC in order to enhance the diversity gain, in addition to supporting com-

munications for multiple SEs. At the FC, the SEs' states are detected based on low-complexity noncoherent fusion rules. In this chapter, six noncoherent fusion rules have been investigated and compared, which include the conventional EGC fusion rule as the benchmark and five proposed fusion rules, namely the ES-EGC, EGC-NIIC, ES-EGC-NIIC, EGC-ρIIC and the ES-EGC-ρIIC fusion rules. The complexity of these fusion rules has been analyzed, which shows that all of them have relatively low complexity for implementation. The ECP performance of the FH/MFSK WSN associated with various fusion rules has been investigated by simulations, when assuming that the communication channels from LSNs to FC experience Rayleigh fading. Our studies and performance results show that the ES-EGC is a highly efficient fusion rule, which is a single-user fusion rule as the EGC, also has similar complexity as the EGC, but is capable of attaining much better ECP performance than the EGC, especially, when multiple SEs are simultaneously monitored by the FH/MFSK WSN. In general, the ES-EGC related fusion rules outperform the corresponding EGC related fusion rules. Furthermore, in some cases, the single-user ES-EGC rule may achieve better ECP performance than the EGC-NIIC and EGC-ρIIC rules, which are the multiuser fusion rules having much higher complexity than the ES-EGC rule.

Additionally, for the ES-EGC, EGC-NIIC, EGC-ρIIC, ES-EGC-NIIC and the ES-EGC-ρIIC, our studies show that there exist the optimum values for I, N and ρ, which result in the best ECP performance for the FH/MFSK WSN employing a corresponding fusion rule.

Chapter 5

Noncoherent Detection in FH/MFSK WSN with Soft-Sensing

5.1 Introduction

In Chapter 3, we have proposed and studied a the FH/MFSK WSN, which employs a number of LSNs to monitor one SE with multiple states. Furthermore, low-complexity fusion rules have been investigated and they are efficient to achieve frequency and spatial diversity. By contrast, in Chapter 4, we have proposed and studied the FH/MFSK WSN, which uses a number of LSNs to simultaneously monitoring multiple SEs of each with multiple states. In Chapter 4, we have also designed and studied a range of low-complexity single-user or multi-user noncoherent detectors. From our studies in Chapter 3 and 4, we can know that the single-user ES-EGC fusion rule is one of the highly promising noncoherent fusion rules for the FH/MFSK WSNs. However, in both Chapter 3 and Chapter 4, hard-decision based sensing is considered which may loss some information about the SE's states.

Therefore, in this chapter, our focus is on the performance improvement of the FH/MFSK WSN monitoring one SE with the aid of soft-sensing by a number of LSNs. Specifically, in the FH/MFSK WSNs considered in this chapter, after an observation, each of the LSNs calculates the probabilities (soft information) about all the states at which the SE might be. This soft information is then forwarded to the FC with the aid of the FH/MFSK techniques. As noncoherent fusion rule are employed at the FC, we propose a signalling scheme for conveying information from LSNs

to FC, which scales the transmission power of the frequency tones used by the FH/MFSK. At the FC, the SE's state is detected by a low-complexity noncoherent fusion rule. Owing to its high efficiency, in this chapter, we specifically study the ES-EGC fusion rule, in addition to the EGC fusion rule, which acts as a benchmark. In this chapter, the performance of the FH/MFSK WSN with EGC or ES-EGC fusion rule is investigated by assuming that the channels from LSNs to FC experience Rayleigh fading. Our studies and performance results show that, in comparison with the hard-decision based sensing, as shown in Chapter 3 and Chapter 4, using soft-sensing is able to enhance the performance of the FH/MFSK WSN. Furthermore, the ES-EGC fusion rule is robust to the errors made by LSNs, which may significantly outperform the EGC fusion rule, especially, when the sensing at LSNs is not very reliable.

The reminder of this chapter is organized as follows. In Section 5.2, we provide the details of the proposed FH/MFSK WSN, where the observed SE, soft-sensing and processing at LSNs are considered. In Section 5.3, signal detection at FC with EGC or ES-EGC fusion rule is analysed. The characteristics of FH/MFSK WSN system with soft-sensing are described in Section 5.4. Some simulation results and discussions are given in Section 5.5. Finally, in Section 5.6, conclusions of this chapter are drawn.

5.2 System Description

The framework of FH/MFSK WSN considered in this chapter is shown in Fig 5.1, which is the triple-layer WSN model [74, 76, 79, 80, 82, 117], has been considered in Chapter 3. As shown in Fig 5.1, the L number of LSNs simultaneously observe one SE with M states and then transmit their soft-sensing observations using FH/MFSK to the FC through wireless channels, which we assume to experience Rayleigh fading. Finally, the FC makes an estimation for the state of the SE using noncoherent approaches, based on the soft information sent by the L LSNs. Details of the components of the considered WSN framework as well as the operations are described as follows.

5.2.1 Source Event

As considered in Chapter 3, the SE to be observed is usually an analogue signal. For convenience of signal processing and transmission, this analogue signal can be digitalized to a finite number

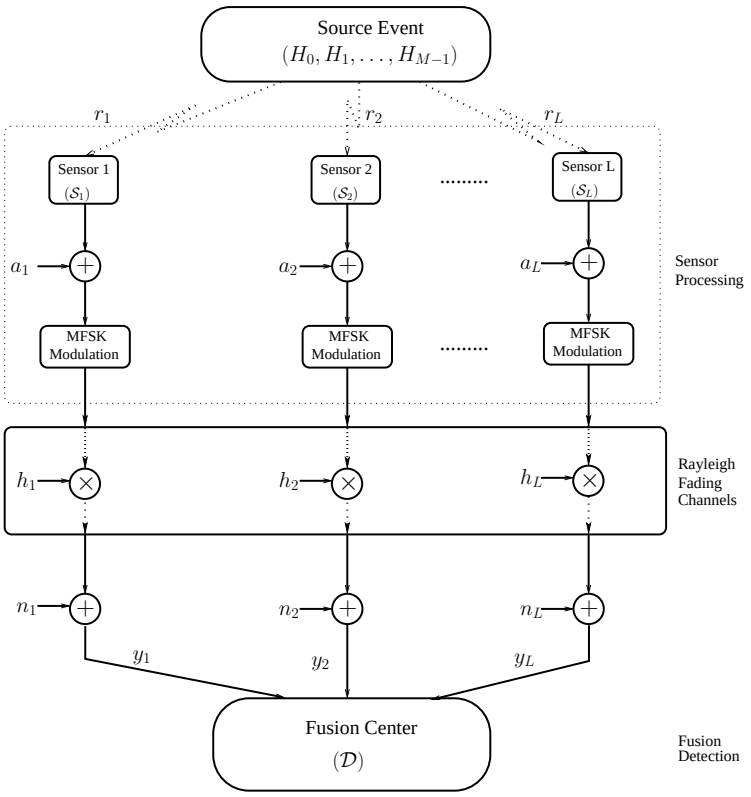

Figure 5.1: Triple-layer system model for the FH/MFSK WSN monitoring one event of M states.

states. In this chapter, we assume that the SE has M equal-probability states corresponding to M hypotheses, which are expressed as $H_0, H_1, \ldots, H_{M-1}$, as shown in Fig. 5.1. For example, the M hypothesises may represent M amplitudes, $A_0, A_1, \ldots, A_{M-1}$, obtained by quantizing a continuous event, such as temperature, pressure, etc. In this case, given at a state m, $m = 0, \ldots, M-1$, the event observed by the lth LSN can be represented as

$$r_l = A_m + n_l,\ l = 1, 2, \cdots, L \tag{5.1}$$

where n_l is the observation noise, which is assumed to be Gaussian distributed with zero mean and a variance σ^2.

5.2.2 Soft-Sensing and Processing at LSNs

LSNs used in WSNs are usually small, power-limited and low-cost. However, LSNs are prone to noise and erroneous hard decisions are likely made, especially, when observation noise is high. In order to improve the reliability of local observations and that of WSNs, soft-sensing techniques

may be employed. In this chapter, we propose a soft-sensing method in conjunction with our noncoherent FH/MFSK WSN.

When the lth, $l = 1, 2, \cdots, L$, LSN obtains an observation in the form of (5.1) for the state of the SE, it carries out the soft-sensing, which calculates the probabilities (soft information) for the M states at which the SE might be, based on the statistics of the observations. Specifically, for the lth LSN, the soft information corresponding to state m is given by

$$\begin{aligned} s_{ml} &= P(H_m|r_l) \\ &= \frac{P(H_m)p(r_l|H_m)}{P(r_l)} \\ &= \frac{p(r_l|H_m)}{\sum_{m=0}^{M-1} p(r_l|H_m)},\ m = 0, \ldots, M-1;\ l = 1, 2, \cdots, L \end{aligned} \tag{5.2}$$

where $P(H_m) = 1/M$ is the *a-priori* probability of H_m, $P(r_l)$ is the probability of receiving r_l, while $p(r_l|H_m)$ is the probability density function (PDF) of observing r_l, when given the state H_m of the SE, which can be expressed as

$$p(r_l|H_m) = \frac{1}{\sqrt{2\pi\sigma^2}} e^{-\frac{(r_l - A_m)^2}{2\sigma^2}} \tag{5.3}$$

Let us collect the soft-sensing information calculated by LSN l into a vector $\boldsymbol{s}_l = \left[s_{0l}, s_{1l}, \cdots, s_{(M-1)l}\right]^T$. Furthermore, let $\boldsymbol{S} = [\boldsymbol{s}_1, \boldsymbol{s}_2, \cdots, \boldsymbol{s}_L]$ holds all the soft information sensed by the L LSNs. Explicitly, $\boldsymbol{S}$ is an $(M \times L)$ matrix.

In order to achieve frequency diversity, FH is introduced so that the soft information observed by different LSNs is mixed in the frequency domain. In detail, the FH operations can be described as follows. Let the symbol duration be T_s seconds, which is evenly divided into L number of time-slots of duration T_h seconds. Each of the L LSNs uses one time-slot to transmit its soft information, which is achieved by scaling the transmission power of each of the M subcarriers using the corresponding probability calculated in (5.2). Let the WSN has M orthogonal frequency bands, whose center frequencies form a set $\mathcal{F} = \{f_0, f_1, \ldots, f_{M-1}\}$. Let $\boldsymbol{a} = [a_1, a_2, \ldots, a_L]^T$ be the FH address assigned to the lth LSN, where a_l is an element of the Galois field $GF(M)$, i.e., $a_l \in GF(M)$. Then, based on the matrix $\boldsymbol{S}$ and the FH address $\boldsymbol{a}$, the FH operations in the context of the L LSNs can be expressed as

$$\boldsymbol{Z} = \boldsymbol{S} \boxplus (\boldsymbol{1} \otimes \boldsymbol{a}^T) \tag{5.4}$$

where $\mathbf{1}$ denotes an all-one column vector of M-length and $\otimes$ denotes the Kronecker product operation between two matrices [116]. In (5.4), the operation of $\boldsymbol{S} \boxplus \boldsymbol{a}$ yields element shifts, resulting in $z_{ml} = s_{(m \oplus a_l)l}$ for $m = 0, 1, \cdots, M-1$ and $l = 1, 2, \cdots, L$, where $\oplus$ represents the addition operation in $GF(M)$ field. Consequently, considering all the M possible states of the SE, the signal transmitted by the lth $(1 \leq l \leq L)$ LSN during the ith symbol-duration, $iT_s < t \leq (i+1)T_s$, can be expressed in complex form as

$$\tilde{s}_{ml}(t) = \sum_{m=0}^{M-1} \sqrt{z_{ml}} \psi_{T_h}(t - iT_s - [l-1]T_h) \exp(j2\pi[f_c + f_m]t + j\phi_{ml}) \tag{5.5}$$

where f_c is the main carrier frequency, ϕ_{ml} is the initial phase introduced by carrier modulation, f_m is the frequency tone of the mth frequency band and, finally, $\psi_{T_h}(t)$ is the time-domain pulse for shaping signal's waveform, which is defined over the interval $[0, T_h)$ and satisfies $T_h^{-1} \int_0^{T_h} \psi_{T_h}^2(t)dt = 1$. Notice from (5.5) that the transmission power on the different frequency bands is scaled by the soft information obtained by the LSNs. The total transmission power per LSN for one symbol is normalized to one, as implied by (5.2).

We assume that the M frequencies used by the FH/MFSK WSN are sufficiently separated, resulting in that they experience independent flat Rayleigh fading. Then, the signal received by the FC from the lth $(1 \leq l \leq L)$ LSN during $iT_s < t \leq (i+1)T_s$ can be expressed as

$$\begin{aligned} r_l(t) &= \sum_{m=0}^{M-1} h_{ml} \tilde{s}_{ml}(t) + n_l(t) \\ &= \sum_{m=0}^{M-1} \sqrt{z_{ml}} h_{ml} \psi_{T_h}(t - iT_s - [l-1]T_h) \exp(j2\pi[f_c + f_m]t + j\phi_{ml}) + n_l(t) \end{aligned} \tag{5.6}$$

where h_{ml} denotes the channel gain experienced by the mth frequency activated by the lth LSN, h_{ml} obeys the complex Gaussian distribution with zero mean and a variance of 0.5 per dimension. Furthermore, in (5.6), $n_l(t)$ represents the Gaussian noise process presenting at the FC, which has zero mean and a single-sided power-spectral density (PSD) of N_0 per dimension.

5.3 Signal Detection at Fusion Center

When the FC received the signals in the form of (5.6), the SE's state is estimated using noncoherent detection as follows. In our FH/MFSK WSN, the FC starts the detection by forming a time-frequency (TF) matrix $\boldsymbol{R}$ of $(M \times L)$-dimensions, where M explains the M frequencies while L

corresponds to the L time-slots used by the L number of LSNs. Assuming that the square-law noncoherent detection is employed [116], then, it can be shown that the elements of $\boldsymbol{R}$ have the values

$$R_{ml} = \left| \frac{1}{T_h} \int_{iT_s+(l-1)T_h}^{iT_s+lT_h} r_l(t) \psi_{T_h}^*(t - iT_s - [l-1]T_h) \exp(-j2\pi[f_c + f_m]t) dt \right|^2, \tag{5.7}$$

where $m = 0, 1, \ldots, M-1$ and $l = 1, 2, \cdots, L$. Since the M frequency bands invoked are assumed to be orthogonal with each other, there is no interference between any two frequency bands. Consequently, when substituting (5.6) into (5.7) and absorbing the carrier phase ϕ_{ml} into h_{ml}, we obtain

$$R_{ml} = |\sqrt{z_{ml}} h_{ml} + N_{ml}|^2, \;\; m = 0, 1, \ldots, M-1; \; l = 1, 2, \cdots, L \tag{5.8}$$

where N_{ml} is a complex Gaussian noise sample corresponding to the mth frequency band and the lth time-slot, which can be expressed as

$$N_{ml} = \left(\sqrt{\Omega} T_h \right)^{-1} \int_{iT_s+(l-1)T_h}^{iT_s+lT_h} n(t) \psi_{T_h}^*(t - iT_s - [l-1]T_h) \exp(-j2\pi[f_c + f_m]t) dt \tag{5.9}$$

It can be shown that N_{ml} has zero mean and variance of $LN_0/E_s = L/\bar{\gamma}_s$, where E_s represents the total energy for transmitting one M-ary source symbol with each sensor's transmitted energy being $E_h = E_s/L$ per symbol, while $\bar{\gamma}_s = E_s/N_0$ denotes the average SNR per symbol.

Based on the TF matrix $\boldsymbol{R}$, the FC can then carry out the required processing and make the final detection, which are analyzed in the following two subsections.

5.3.1 EGC Fusion Rule

In the context of the EGC fusion rule, the FC detects the SE's state by first carrying out the frequency de-hopping operations, forming the detection matrix

$$\boldsymbol{D} = \boldsymbol{R} \boxminus (\boldsymbol{1} \otimes \boldsymbol{a}^T) \tag{5.10}$$

where $\boldsymbol{A} \boxminus \boldsymbol{B}$ is defined as the element-shift operation in $GF(M)$, which is the reversing operation used in (5.4). Specifically, after the operation of (5.10), we have the element $D_{(m \ominus a_l)l} = R_{ml}$, where $\ominus$ is the minus operation in $GF(M)$. In other words, the (m, l)th element in $\boldsymbol{R}$ is mapped to the $(m \ominus a_l, l)$th element in $\boldsymbol{D}$, after the frequency de-hopping operations of (5.10)

Following the frequency de-hopping, the M decision variables for detecting the SE's state are formed based on the detection matrix $\boldsymbol{D}$ in EGC principles, which can be expressed as

$$D_m = \sum_{l=1}^{L} D_{ml},\ m = 0, 1, \ldots, M-1 \tag{5.11}$$

Finally, the largest of $\{D_0, D_1, \ldots, D_{M-1}\}$ is selected, whose subscript index is a value in $\{0, 1, \ldots, M-1\}$, which represents the estimate to the SE's state.

5.3.2 ES-EGC Fusion Rule

As the EGC fusion rule, the ES-EGC fusion rule is low-complexity. However, as our performance results in Section 5.5 show, the ES-EGC fusion rule has certain capability to mitigate the effect from the unreliable sensing made by LSNs.

When the ES-EGC fusion rule is employed, the same operations as the EGC fusion rule are first carried out at the FC to form the detection matrix $\boldsymbol{D}$ as shown in (5.10). Then, in each of the M rows of $\boldsymbol{D}$, I $(0 \leq I < L)$ elements corresponding to the I largest values are replaced by a value of zero. Note that, when $I = 0$, it means that no elements is erased from each of the M rows. In this case, the proposed ES-EGC fusion rule is reduced to the EGC fusion rule, as described in Section 5.3.1.

Let us denote the modified detection matrix after the erasure operation as $\bar{\boldsymbol{D}}$ and its elements as $\bar{\boldsymbol{D}}_{ml}$. Then, based on this modified detection matrix $\bar{\boldsymbol{D}}$, M decision variables formed in EGC principles can be expressed as

$$\bar{D}_m = \sum_{l=1}^{L} \bar{D}_{ml},\ m = 0, 1, \ldots, M-1 \tag{5.12}$$

Finally, the largest one of the M decision variables of $\{\bar{D}_0, \bar{D}_1, \cdots, \bar{D}_{M-1}\}$ is selected and its index value in terms of m represents the estimate to the state of the monitored SE.

5.4 Analysis of Characteristics

Our proposed FH/MFSK WSN with soft-sensing LSNs employs a range of characteristics, which may be summarized as follows. First, soft-sensing technique is employed by the LSNs to monitor the SE. In comparison with the hard-decision based sensing techniques, where LSNs have to make

decisions about the SE's state, the LSNs using soft-sensing convey soft information about the SE's state to the FC. Hence, the FC detection of the FH/MFSK WSN with soft-sensing is more reliable than that with hard-decision based sensing [117]. Second, noncoherent detection is implemented at the FC of the FH/MFSK WSN, which does not require to consume extra energy for channel estimation. This energy-efficient and low-complexity detection strategy is beneficial to the life-time of battery-powered WSNs. Third, the FH/MFSK techniques employed are capable of providing frequency diversity for the FC detection. This frequency diversity becomes more important, when the LSNs are distributed close to each other, which may generate correlated fading in the space-domain. In our FH/MFSK WSN, owing to the FH operation, the LSNs may be distributed within a relatively small space but still convey sufficiently independently faded signals to the FC, so that frequency diversity is achieved and the detection performance of the FC is not seriously affected by the correlated fading experienced in the space-domain.

In this chapter, two types of fusion rules, namely EGC and ES-EGC, are considered and compared. Both of them are low-complexity and low detection delay fusion rules. They have respectively different advantages and disadvantages. More specifically, the EGC fusion rule has the lowest complexity and also the lowest detection delay among all the FC rules considered so far. Unfortunately, the EGC fusion rule is sensitive to the errors made by LSNs. The detection performance of the EGC fusion rule degrades significantly, as the power of the observation noise at LSNs increases. By contrast, having a similar complexity and also a similar detection delay as the EGC fusion rule, the proposed ES-EGC fusion rule is capable of achieving better detection performance than the EGC fusion rule, especially, when the detection at LSNs becomes less reliable.

5.5 Performance Results

In this section, the ECP performance of the soft-sensing assisted FH/MFSK WSN employing either EGC or ES-EGC fusion rule is investigated. We assume that signals observed by the LSNs only conflict Gaussian noise, while the wireless channels from the LSNs to the FC experience Rayleigh fading and each subband sent by any LSN experiences independent Rayleigh fading. In the figures considered below, two types of SNR are used, one is called the sensor SNR per bit, which is the SNR per bit of the signals observed at the LSNs. The other one is referred to as the channel SNR

per bit, which is the average SNR per bit of the signals observed by the FC.

Fig. 5.2 shows the ECP performance of the FH/MFSK WSN employing, respectively, $L = 6, 8, 12, 16$ LSNs, which monitor a SE with $M = 32$ states (hypotheses). The sensor SNR for the signals observed by all the LSNS is the same and is 10dB per bit. From the performance results, we can explicitly observe that both the number of LSNs and the channel SNR have strong impact on the overall achievable performance of the FH/MFSK WSN. The ECP performance of the FH/MFSK WSN improves, as the number of LSNs is increased from $L = 6$ to 8, to 12 and, finally, to $L = 16$. This is because the achieved diversity gain increases, as the number of LSNs increases. From Fig. 5.2, we can see that, when the channel SNR is sufficiently high, the ES-EGC fusion rule may significantly outperform the EGC fusion rule. However, when the channel SNR is low, such as, lower than 12 dB, the EGC fusion rule may slightly outperform the ES-EGC fusion rule. The explanation behind the above observation is as follow. As mentioned previously, the EGC fusion rule is optimum in Gaussian channels but sensitive to the errors made by the LSNs. By contrast, the ES-EGC fusion rule is robust to the errors made by the LSNs, but at the cost of removing some useful information. Consequently, when channel SNR is low, making background noise dominates the overall performance, the EGC fusion rule may slightly outperform the ES-EGC fusion rule. By contrast, when channel SNR is high, resulting in that the errors made by LSNs dominate the overall performance, as seen in Fig. 5.2, the ES-EGC fusion rule significantly outperforms the EGC fusion rule. Furthermore, in comparison with the case of hard-sensing as shown in Fig 5.2b, soft sensing is capable of enhencing the overall detection performance of our FH/MFSK WSN for either EGC fusion rule or ES-EGC fusion rule under the same simulation factors as shown in Fig 5.2b.

In Fig. 5.3, we illustrate the effect of the value of M on the ECP performance of the FH/MFSK WSN employing $L = 12$ LSNs operated at a sensor SNR of 10dB per bit. First, as observed in Fig. 5.3, we observe that the ES-EGC fusion rule outperforms the EGC fusion rule, provided that the channel SNR is sufficiently high. However, if the channel SNR is too sufficient, the ES-EGC fusion rule may be outperformed by the EGC fusion rule. The above observation becomes more explicit, as the value of M is relatively large, such as $M = 16$ or 32. In addition, the results of Fig. 5.3 show that the ECP performance of the FH/MFSK WSN improves, as the value of M increases from $M = 4$ to $M = 32$. Compared Fig 5.3a with Fig 5.3b, it is clear that soft sensing is able to improve the detection performance of the FH/MFSK WSN significantly.

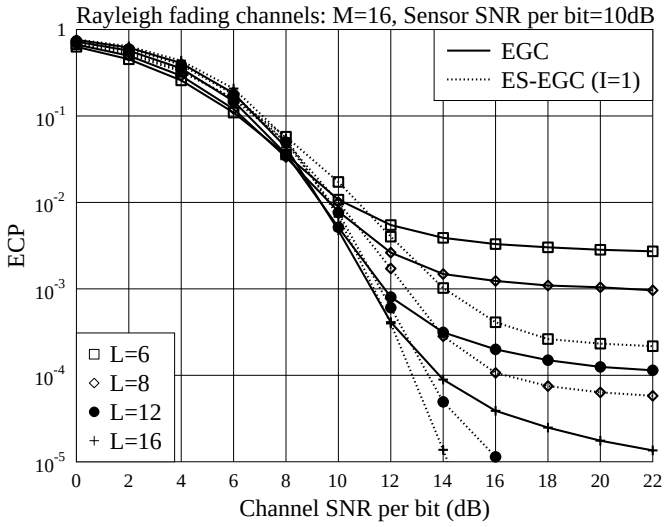

(a) Soft-sensing

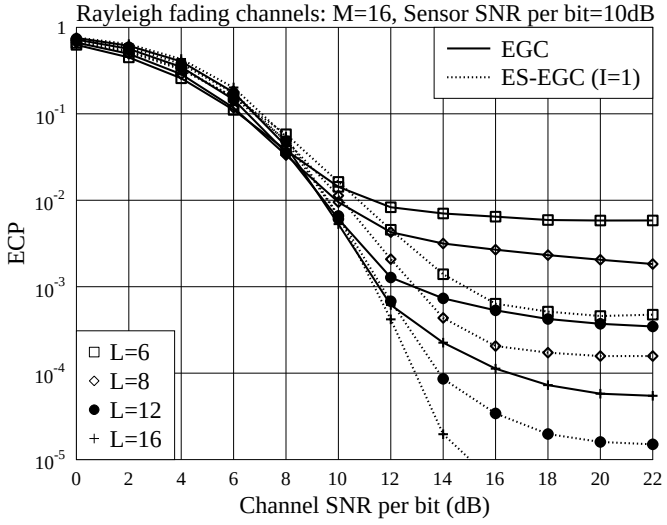

(b) Hard-Sensing

Figure 5.2: ECP versus channel SNR per bit performance of the FH/MFSK WSN with soft-sensing or hard-sensing LSNs monitoring a SE of 16 states.

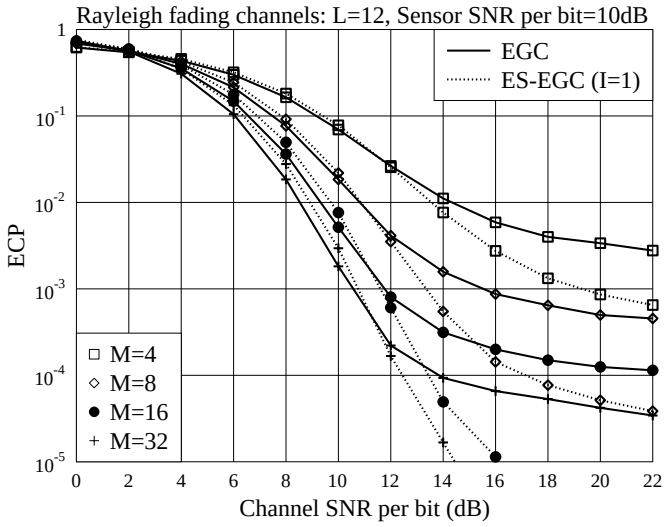

(a) Soft-sensing

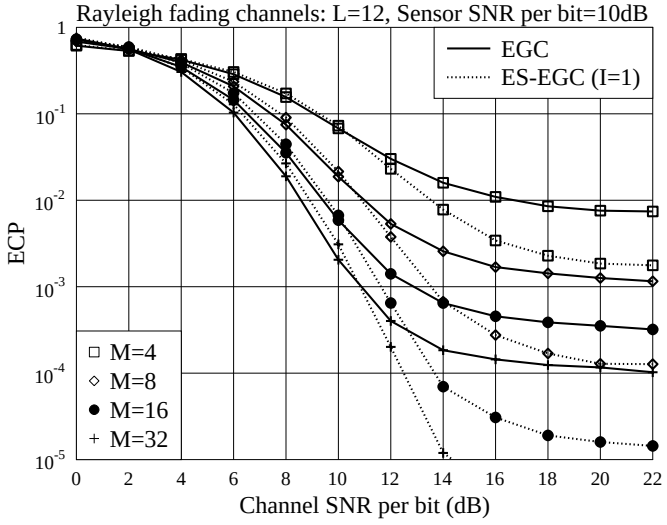

(b) Hard-sensing

Figure 5.3: ECP versus channel SNR per bit performance of the FH/MFSK WSN employing $L = 12$ LSNs with a sensor SNR 10dB per bit.

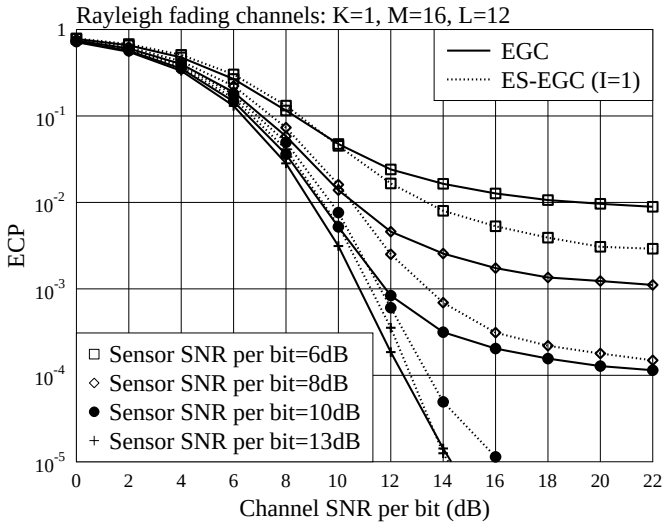

(a) Soft-sensing

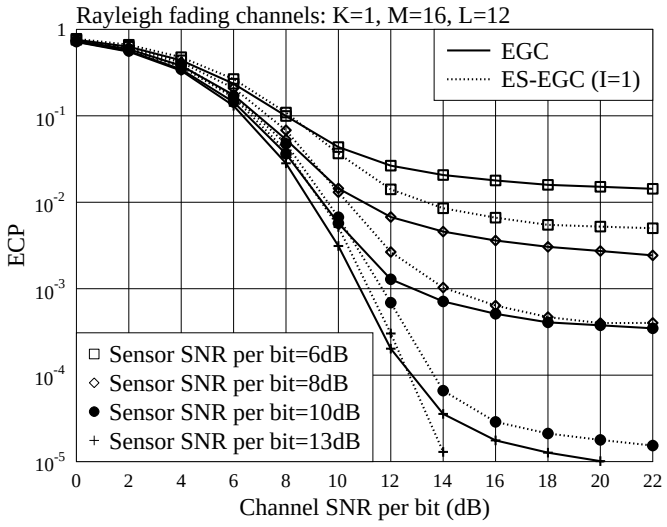

(b) Hard-sensing

Figure 5.4: ECP versus channel SNR per bit performance of the FH/MFSK WSN employing $L = 12$ LSNs with respect to various sensor SNR values.

In Fig. 5.4, the ECP performance of the FH/MFSK WSNs with, respectively, the EGC and ES-EGC fusion rules is investigated and compared, when various values for the sensor SNR are considered. Explicitly, when the sensor SNR increases, the overall error performance of the FH/MFSK WSNs improves. As shown in Fig. 5.4, when the sensor SNR is low, such as at 6dB or 8dB, the ES-EGC fusion rule is capable of achieving much better detection performance than the EGC fusion rule, when the channel SNR is sufficiently high. By contrast, the advantage of the ES-EGC over the EGC becomes less as the sensor SNR increases, meaning that the detection at LSNs becomes more reliable. In comparison of Fig 5.4a and Fig 5.4b, it can be seen that, given reasonable channel SNR, soft-sensing is able to enhance the ECP performance of either EGC or ES-EGC for all the values of sensor's SNR.

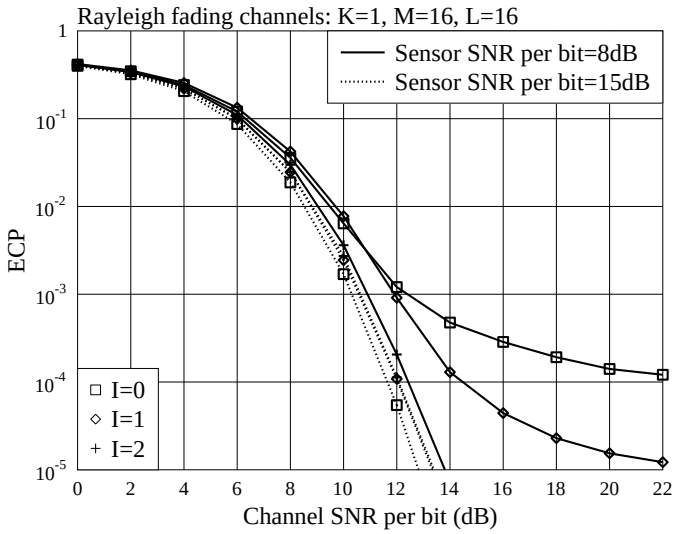

Figure 5.5: ECP versus channel SNR per bit performance of the FH/MFSK WSN employing $L = 16$ LSNs, when various number of TF elements are deleted from each of the M rows of the detection matrix.

Finally, in Fig. 5.5, we study the effect of the number erased elements, expressed by I, used by the ES-EGC fusion rule on the ECP performance of the FH/MFSK WSN. Note again that, $I = 0$ corresponds to the conventional EGC fusion rule. From Fig. 5.5, we can observe that, both the sensor SNR and channel SNR have a big impact on the detection performance of FH/MFSK WSN with soft-sensing LSNs. When the sensor SNR is low and equal to 8dB, the ES-EGC fusion rule with $I = 2$ yields the best detection performance, while the EGC fusion rule results in the worst ECP performance. By contrast, when the sensor SNR is 15dB per bit, which makes the detection

at the LSNs very reliable, the EGC fusion rule outperforms the ES-EGC fusion rule, regardless of $I = 1$ or $I = 2$. Again, from the observations we are implied that, when the detection at LSNs is unreliable, the erasure operation employed by the ES-EGC is capable of mitigating the effect from the errors made by the LSNs, yielding better detection performance than the EGC fusion rule. On the other hand, when the detection at LSNs is highly reliable, the erasure operation will remove useful information, resulting in that the ES-EGC fusion rule is outperformed by the EGC

5.6 Conclusions

In this chapter, we have proposed a noncoherent FH/MFSK WSN, which employs a range of LSNs monitoring one SE. The LSNs carry out soft-sensing and forward the FC soft information about the SE's state. At FC, the SE's state is detected by the low-complexity EGC fusion rule or the proposed ES-EGC fusion rule, which also has low-complexity. The detection performance of the proposed FH/MFSK WSN has been investigated by assuming that the channels from LSNs to FC experience Rayleigh fading. Our studies and performance results show that, when the sensor SNR is low, resulting in unreliable detection at LSNs, and the channel SNR is relatively high, the ES-EGC fusion rule may significantly outperform the EGC fusion rule. Therefore, the ES-EGC fusion rule is robust to the errors made by LSNs. By contrast, when the detection at LSNs is highly reliable, making the channel noise dominate the FC's detection performance, then, we may simply use the EGC fusion rule. In fact, the ES-EGC fusion rule may be regarded as an extension of the EGC fusion rule. The number of erasures per row may be determined according to the specific environment that the FH/MFSK WSN is deployed. Furthermore, compared with the hard-sensing scenario considered in Chapter 3, soft-sensing is capable of enhancing the overall detection performance of our proposed FH/MFSK WSN with either EGC or ES-EGC fusion rule.

Chapter 6

Energy-Based Cooperative Spectrum Sensing of SC-FDMA Systems

6.1 Introduction

In wireless communications, the need for high data rate services is increasing as a result of the transition from voice-only communications to multimedia applications [176]. Given the limit of natural frequency spectrum, it has been recognized that the current static frequency allocation schemes are unable to accommodate the increasing number of high data rate devices. Cognitive radio with the capability to sense and exploit unoccupied channels or frequencies has therefore become a promising candidate for mitigating the problem of spectrum shortage [156]. According to Federal Communication Commission (FCC) [158], cognitive radio is defined as a radio or system that can sense its operational electromagnetic environment and can dynamically and autonomously adjust its radio operating parameters to modify system operation, such as maximize throughput, mitigate interference, facilitate interoperability, access secondary markets.

In cognitive radio terminology, primary radios (PRs) have higher priority or legacy rights on the usage of specific parts of spectrum allocated to them, while cognitive radios (CRs) can access these spectrums in such a way that they do not cause interference on the PRs or degrade the performance of the PRs. The studies with CRs show that the efficiency of CR systems depends mainly on the CRs' capability to sense the PR users' states (on/off) and to respond correspondingly and quickly. Hence, it is critical that CR systems can make quick and reliable decisions during spectrum

sensing [177].

Depending on the knowledge available to the CRs, a range of spectrum sensing methods have been proposed and studied. As some examples, energy detection has been considered in [148, 176, 178, 179], matched filter detection in [148, 151], cyclostationary feature detection in [148, 151, 180, 181], etc. Each of these spectrum sensing techniques has some unique advantages and disadvantages, as detailed as follows. First, energy detection, also known as radiometry or periodogram, is the first way of spectrum sensing coming to our mind, owing to its low computation and implementation complexities [176]. In principle, an energy detector simply treats PR signals as noise and decides about their presence or absence based on the energy levels of the observed signals. Since it does not require any *a-priori* knowledge of PR signals, energy detection is viewed as a type of blind detection method. In energy detection, if the noise power is unable to be accurately estimated, its performance may significantly degrade. Furthermore, the noise-uncertainty in energy detection may lead to the so-called SNR wall phenomena [146]. Unlike the energy detector, matched filter detector and cyclostationary feature detector rely on the *a-priori* knowledge of PR signals' parameters, such as, the knowledge of waveforms, which is impractical for certain applications [177]. In a little more detail, matched filter detector makes coherent detection based on the *a-priori* knowledge of modulation type and carrier frequency of the PR signals. By contrast, cyclostationary feature detection belongs to a noncoherent spectrum sensing approach, which may distinguish various modulation signals. However, cyclostationary feature detector requires some parameters of PR signals, such as, symbol rate. In comparison with the above three types of spectrum sensing approaches, eigenvalue detection [156–158, 177, 182–185] does not depend on the *a-priori* information as well as noise power, and it has the advantage of simultaneously achieving a high detection probability and a low false-alarm probability. However, the eigenvalue detection is highly dependent on the correlation of PR signals, it becomes less efficient when PR signals become less correlated. In this contribution, energy detection is employed to sense- an low peak-to-average power ratio (PAPR) and low complexity interleaved frequency-division multiple access (IFDMA) PR system [186]. Note that, in some references IFDMA is also referred as the distributed frequency-division multiple access (DFDMA) [187, 187].

In this chapter, we propose and study a spectrum sensing scheme for CR systems, where a number of cognitive radio sensing nodes (CRSNs) distributively sense a PR system with multiple

PR users. We assume that the PR system is the interleaved frequency-division multiple access (IFDMA) system for the LTE [186], which supports a number of synchronous PR users. To attain fast and low-complexity spectrum sensing, energy detection is employed by the CRSNs. Specifically, local decisions for the presence of multiple PR users are made by the CRSNs separately based on one of the *three types of energy detection schemes* considered, under the constraints of one of the *four synchronization scenarios* assumed between the PR signals and the CRSNs. By this way, every CRSN obtains a binary local decision vector, which is sent to the FC with the aid of frequency-hopping (FH) and M-ary frequency-shift keying (MFSK). In this chapter, two types of noncoherent fusion rules are employed by the FC for making the final decision, which include the EGC fusion rule and ES-EGC fusion rule, as shown in previous chapters. The performance of the FH/MFSK assisted spectrum sensing system with EGC or ES-EGC fusion rule is investigated via simulation, under the assumptions that the channels from PR users to CRSNs and the channels from CRSNs to FC experience independent Rayleigh fading. Our studies and performance results show that, our proposed FH/MFSK assisted spectrum sensing system constitutes one highly reliable spectrum sensing scheme, which is capable of exploiting the space diversity provided by CRSNs as well as the frequency diversity provided by the subcarriers of the IFDMA systems. Additionally, in comparison with the conventional EGC fusion rule, the ES-EGC fusion rule is robust to the errors made by CRSNs, yielding better detection performance.

The reminder of this chapter is organized as follows. In Section 6.2, we provide the details of the proposed FH/MFSK assisted spectrum sensing system. Section 6.3 considers the fusion detection with either EGC or ES-EGC fusion rule. Section 6.4 demonstrates the simulation results for the detection performance. Finally, in Section 6.5, conclusions of this chapter are derived.

6.2 System Model

The framework for our cognitive spectrum sensing system is shown as Fig. 6.1. In our proposed spectrum sensing system, we assume that the primary radio (PR) system is a LTE/LTE-A uplink SC-FDMA system, which supports K PR users. Each of the K PR users has two states: H_0 (off) and H_1 (on). We assume that the SC-FDMA system employs N subcarriers. As shown in reference [116], there are typically two strategies for allocation of N subcarriers to K users, yielding the so-called

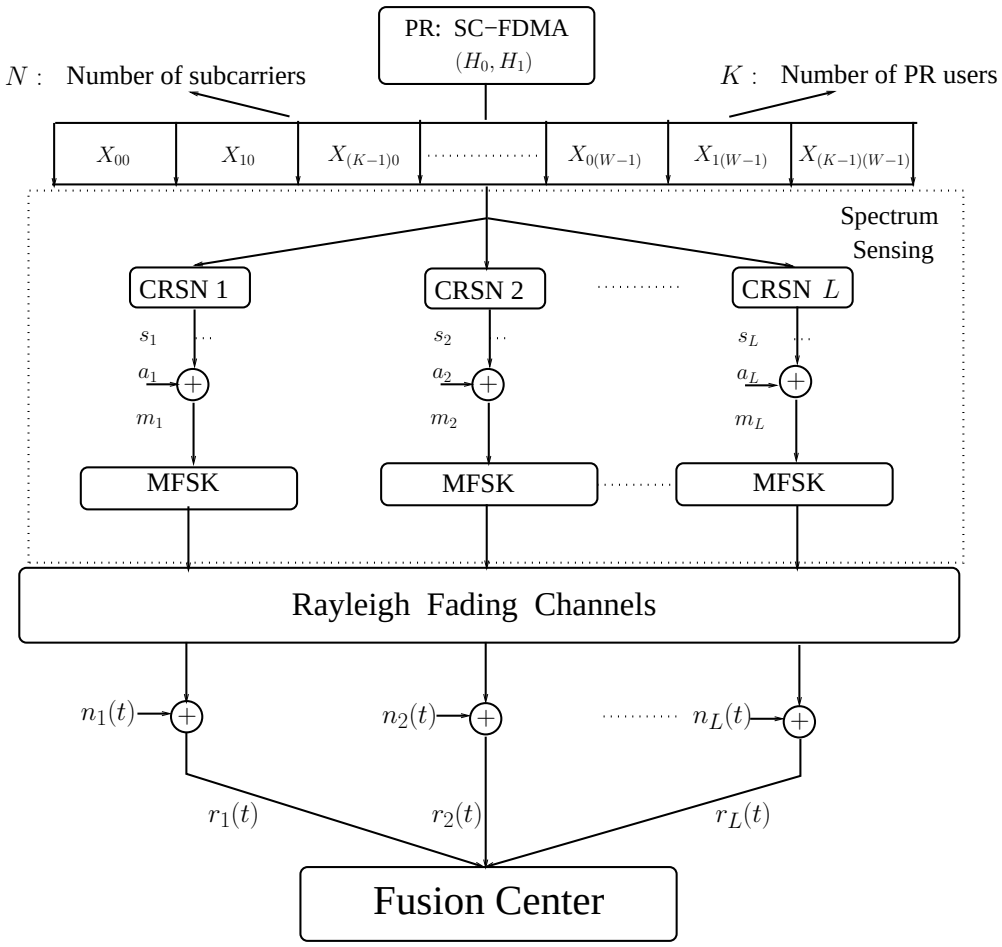

Figure 6.1: System model for IFDMA system's spectrum sensing with FH/MFSK technique.

interleaved FDMA (IFDMA) and localized FDMA (LFDMA). The PAPR problem in LFDMA system is significantly less severe than that in the conventional OFDM systems. Furthermore, in the IFDMA system there is only one subcarrier activated for transmission at any time, the IFDMA signals conflict no PAPR problem at all [116]. In this chapter, we consider only the IFDMA scheme. For convenience of our description, we assume that the N subcarriers are equally assigned to the K PR users. Hence, each of the K PR users occupies $W = N/K$ interleaved subcarriers. When the kth, $k = 1, 2, \ldots, K$, PR user is present to communicate, it occupies all the W subcarriers corresponding to its assignment. As the subcarriers are orthogonal with each other in SC-FDMA systems, we assume that every cognitive radio sensing node (CRSN) is capable of sensing all the N subcarriers simultaneously without interference.

In this chapter, energy sensing (detection) is employed by the L CRSNs, as seen in Fig. 6.1, to sense which PR user(s) is on/off or which subcarriers are available for the CR system. After the

local sensing, each of the CRSNs obtains a binary vector of length K, indicating the on/off states of the K PR users. Then, the K-length binary vector is conveyed to an M-ary number and transmitted to the fusion center (FC) in the principles of FH/MFSK. In this chapter, we assume that the number of frequency bands, expressed as M, used for FH/MFSK is equal to or larger than 2^K. Finally, at the FC, the on/off states of the K PR users are noncoherently classified based on the signals received from the L CRSNs. In this chapter, two types of fusion classification schemes are considered, which are based on the conventional equal gain combining (EGC) [188] and the erasure-supported equal gain combining (ES-EGC) [189], respectively. Below, we provide the details about the operations carried out at the CRSNs and FC.

6.2.1 Spectrum Sensing at CRSNs

For convenience, the main parameters used in this chapter are summarized as follows.

- N: number of subcarriers of SC-FDMA PR system;
- K: number of uplink PR users;
- $W = N/K$: number of subcarriers per PR user;
- L: number of CRSNs;
- M: number of frequency bands used by FH/MFSK;
- $U+1$: number of multipaths of communications channels.

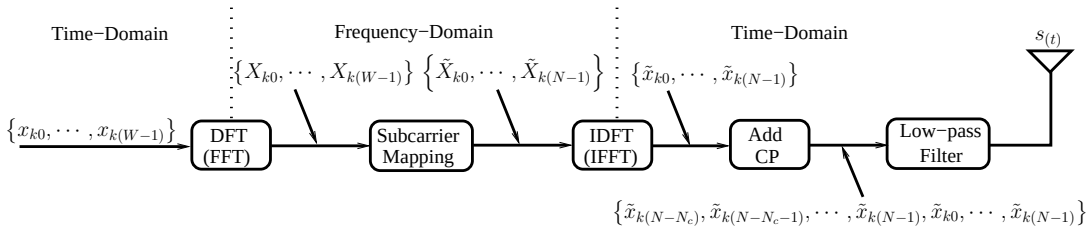

Figure 6.2: Transmitter schematic for the kth user supported by the SC-FDMA uplink.

The transmitter schematic of the SC-FDMA uplink is shown in Fig. 6.2. Let the W symbols transmitted by the kth PR user in time-domain be expressed as

$$\boldsymbol{x}_k = [x_{k0},\ x_{k1},\cdots,x_{k(W-1)}]^T,\ \ k=0,\ 1,\cdots,K-1 \tag{6.1}$$

As shown in Fig. 6.2, first, $\boldsymbol{x}_k$ is transformed to the frequency-domain with the aid of the W-point DFT, yielding the W-length vector $\mathbf{X}_k$, which can be expressed as

$$\mathbf{X}_k = \boldsymbol{\mathcal{F}}_W \boldsymbol{x}_k = [X_{k0},\ X_{k1}, \cdots, X_{k(W-1)}]^T \tag{6.2}$$

where $\boldsymbol{\mathcal{F}}_W$ denotes an W-point FFT matrix [116]. More specifically, the W entries in the vector $\mathbf{X}_k$ are given by

$$X_{kl} = \frac{1}{\sqrt{W}} \sum_{w=0}^{W-1} x_{kw} \exp\left(-j\frac{2\pi l w}{W}\right),\ \ l = 0,\ 1, \cdots, W-1 \tag{6.3}$$

Following the DFT operation, the W elements in $\mathbf{X}_k$ are mapped to W out of the $N = WK$ subcarriers, according to the principles of IFDMA [116]. After the subcarrier mapping, the W-length vector $\mathbf{X}_k$ is extended to an N-length vector $\tilde{\mathbf{X}}_k$, which can be represented as

$$\tilde{\mathbf{X}}_k = [\tilde{X}_{k0},\ \tilde{X}_{k1}, \cdots, \tilde{X}_{k(N-1)}]^T \tag{6.4}$$

In more detail, under the IFDMA strategy for mapping, the elements of $\tilde{\mathbf{X}}_k$ are given by

$$\begin{aligned} &\tilde{X}_{kn} = X_{kw},\ \text{if } n = wK + k \\ &\tilde{X}_{kv} = 0,\ \text{otherwise} \end{aligned} \tag{6.5}$$

where $w = 0,\ 1, \cdots, W-1;\ k = 0,\ 1, \cdots, K-1$. After the subcarrier mapping, as shown in Fig. 6.2, $\tilde{\mathbf{X}}_k$ is transformed to the time-domain by carrying out the IDFT operation, yielding an N-length vector

$$\tilde{\boldsymbol{x}}_k = \boldsymbol{\mathcal{F}}_N^H \tilde{\mathbf{X}}_k \tag{6.6}$$

where $\boldsymbol{\mathcal{F}}_N$ denotes the an N-point FFT matrix.

According to [116], upon submitting (6.3) and (6.5) into (6.6), the vth, $v = 0,\ 1, \cdots, N-1$, element of $\tilde{\boldsymbol{x}}_k$ can be expressed as

$$\begin{aligned} \tilde{x}_{k(v=qW+i)} =& \frac{1}{\sqrt{N}} \sum_{n=0}^{N-1} \tilde{X}_{kn} \exp\left(j\frac{2\pi v n}{N}\right) \\ =& \frac{1}{\sqrt{K}} \exp\left[j\frac{2\pi(qW+i)k}{N}\right] x_{ki} \end{aligned} \tag{6.7}$$

where the values of q, $q = 0,\ 1, \cdots, K-1$, and i, $i = 0,\ 1, \cdots, W-1$, are uniquely determined by the value of v. From (6.7) we can see that the W symbols of $\boldsymbol{x}_k$ of the kth PR user are repeatedly

transmitted on the kth subcarrier, and all the W symbols are transmitted K times within one IFDMA symbol duration [116].

Following the N-point IDFT operation, as shown in Fig. 6.2, a cyclic prefix (CP) is added in the front of $\tilde{\boldsymbol{x}}_k$ in order to eliminate intersymbol interference (ISI). Explicitly, the N_c-length CP for $\tilde{\boldsymbol{x}}_k$ is $\left[\tilde{x}_{k(-N_c)},\ \tilde{x}_{k(-N_c+1)}, \cdots \tilde{x}_{k(-1)}\right] = \left[\tilde{x}_{k(N-N_c)},\ \tilde{x}_{k(N-N_c-1)}, \cdots \tilde{x}_{k(N-1)}\right]$, which consists of the last N_c elements of vector $\tilde{\boldsymbol{x}}_k$. Let us express the time-domain vector after the CP as $\tilde{\boldsymbol{x}}'_k$, which is

$$\begin{aligned}\tilde{\boldsymbol{x}}'_k &= \left[\tilde{x}_{k(-N_c)},\ \tilde{x}_{k(-N_c+1)}, \cdots \tilde{x}_{k(-1)},\ \tilde{x}_{k0}, \tilde{x}_{k1}, \cdots, \tilde{x}_{k(N-1)}\right] \\ &= \left[\tilde{x}_{k(N-N_c)},\ \tilde{x}_{k(N-N_c-1)}, \cdots \tilde{x}_{k(N-1)},\ \tilde{x}_{k0}, \tilde{x}_{k1}, \cdots, \tilde{x}_{k(N-1)}\right]\end{aligned} \tag{6.8}$$

Based on (6.8), finally, as shown in Fig. 6.2, we can form the complex baseband equivalent signal transmitted by the kth PR user, which is

$$s_k(t) = \sum_{v=0}^{N+N_c-1} \sqrt{2P}\tilde{x}'_{kv}\psi(t - vT_c) \tag{6.9}$$

where P is the transmission power per dimension, $\tilde{x}'_{kv}$ is the vth element of $\tilde{\boldsymbol{x}}'_k$ and $\psi(t)$ is a unit-power chip-waveform impulse defined in $(0,\ T_c]$, where T_c is the chip duration, determined by the bandwidth used by the SC-FDMA system.

In our proposed spectrum sensing system, each of the CRSNs is capable of simultaneously sensing all the K PR users. In this case, when the K uplink PR users' signals in the form of (6.9) are transmitted through wireless channels, the received complex baseband equivalent signal at the lth $(0 < l \leq L)$ CRSN can be written as

$$R_l(t) = \sum_{k=0}^{K-1} s_k(t) * h_{kl}(t) + n_l(t) \tag{6.10}$$

where $h_{kl}(t)$ denotes the channel impulse response (CIR) between the lth CRSN and the kth PR user, while $n_l(t)$ is the Gaussian noise process presenting at the lth CRSN, with zero mean and single-sided power-spectral density (PSD) of N_0 per dimension.

At the lth, $l = 1, \ldots, L-1$, CRSN, the received signal $R_l(t)$ is first filtered by a filter matched to the chip waveform $\psi(t)$. Then, the filter's output signal is sampled at the chip rate of $1/T_c$. After the normalization using $1/\sqrt{2P}T_c$, it can be shown that the vth, $(0 \leq v \leq N + N_c - 1)$, sample

can be expressed as

$$\begin{aligned}\tilde{y}'_{l,v} &= \frac{1}{\sqrt{2P}T_c}\int_{vT_c}^{(v+1)T_c} R_l(t)\psi(t-vT_c)dt \\ &= \sum_{k=0}^{K-1}(h_{l,kv} * \tilde{x}'_{kv}) + \tilde{n}_{l,v} \\ &= \sum_{k=0}^{K-1}\sum_{u=0}^{U} h_{l,ku} \times \tilde{x}'_{k(v-N_c-u)} + \tilde{n}_{l,v} \end{aligned} \tag{6.11}$$

where we assumed that the CIR has $(U+1)$ taps, i.e., $\boldsymbol{h}_{kl} = [h_{l,k0}, \cdots, h_{l,kU}]^T$. In the above equation, the Gaussian noise sample $\tilde{n}_{l,v}$ is expressed as

$$\tilde{n}_{l,v} = \frac{1}{\sqrt{2P}T_c}\int_{vT_c}^{(v+1)T_c} n_l(t)\psi(t-vT_c)dt \tag{6.12}$$

which has zero mean and a variance $2\sigma^2 = N_0/E_c$ with $E_c = PT_c$ representing the chip energy.

From the outputs of $\tilde{y}'_{l,v}$, we can form an N-length vector $\tilde{\boldsymbol{y}}_l$ at the lth CRSN. Furthermore, in the cases when the CRSNs do not know the beginning of an IFDMA symbol, they have to use an N-length vector having a random starting point. In this case, the N samples may span two consecutive IFDMA symbols. In order to consider this scenario, in this chapter, we use the superscript '0' to indicate the current IFDMA symbol, while the superscript '-1' to indicate the previous IFDMA symbol. In this chapter, four scenarios will be addressed. In the first scenario, namely, *synchronous sensing*, we consider the case of perfect synchronisation between the PR users and CRSNs. In the second and the third scenarios, we assume quasi-synchronisation between the PR users and the CRSNs, where the N samples used by a CRSN all come from one IFDMA symbol. However, we assume that there is no inter-(IFDMA) symbol interference in the second scenario, but there is in the third scenario. Correspondingly they are referred to as the *quasi-synchronous sensing without ISI* and *quasi-synchronous sensing with small ISI*, respectively. Finally, in the context of the fourth scenario, we assume that the N samples used by one CRSN are contributed by two consecutive IFDMA symbols, hence, it is an asynchronous scenario, giving the name of *asynchronous sensing*. Below we detail the representations corresponding to these operational scenarios.

6.2.1.1 Synchronous Sensing

When a CRSN perfectly synchronises with the incoming IFDMA signals, the CP added in the transmitted signals can be removed, yielding an N-length vector $\tilde{\boldsymbol{y}}_l$, as seen in Fig. 6.3. The value

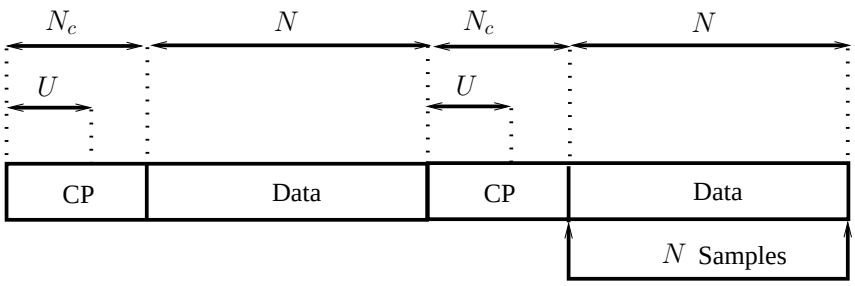

Figure 6.3: Illustration for the scenario of synchronous sensing.

of the nth element of $\tilde{\boldsymbol{y}}_l$ with its elements given by

$$\tilde{y}_{l,n} = \tilde{y}'_{l,(n+N_c)}, \;\; n = 0,\, 1, \cdots, N-1 \tag{6.13}$$

Furthermore, it can be shown that $\tilde{\boldsymbol{y}}_l$ can be expressed based on matrix representation as

$$\tilde{\boldsymbol{y}}_l = \begin{bmatrix} \tilde{y}_{l,0} \\ \tilde{y}_{l,1} \\ \vdots \\ \tilde{y}_{l,(N-1)} \end{bmatrix} = \sum_{k=0}^{K-1} \begin{bmatrix} h^0_{l,kU} & h^0_{l,k(U-1)} & \cdots & h^0_{l,k0} & 0 & \cdots & 0 \\ 0 & h^0_{l,kU} & \cdots & h^0_{l,k1} & h^0_{l,k0} & \cdots & 0 \\ \vdots & \vdots & \ddots & \ddots & \ddots & \ddots & \vdots \\ 0 & \cdots & 0 & h^0_{l,kU} & \cdots & h^0_{l,k1} & h^0_{l,k0} \end{bmatrix} \begin{bmatrix} \tilde{x}^0_{k,(-U)} \\ \vdots \\ \tilde{x}^0_{k,(-1)} \\ \tilde{x}^0_{k,0} \\ \vdots \\ \tilde{x}^0_{k,(N-1)} \end{bmatrix} + \begin{bmatrix} \tilde{n}_{l,N_c} \\ \tilde{n}_{l,(N_c+1)} \\ \vdots \\ \tilde{n}_{l,(N+N_c-1)} \end{bmatrix} \tag{6.14}$$

6.2.1.2 Quasi-Synchronous Sensing without ISI

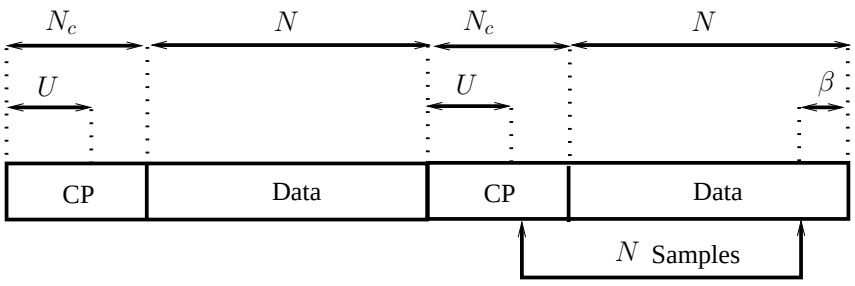

Figure 6.4: Illustration for the scenario of quasi-synchronous sensing without ISI, where $0 \leq \beta \leq N_c - U$.

As an example, Fig. 6.4 shows a case corresponding to the scenario of quasi-synchronous sensing without ISI. In this scenario, the sampling of a CRSN starts β chips before the first symbol $\tilde{x}^0_{k0}$, where $\beta \in (0, N_c - U)$. From Fig. 6.4 we can see that, when $\beta \in (0, N_c - U)$, there is no interference from the previous IFDMA symbol on the current IFDMA symbol. Furthermore, from Fig. 6.4, we can readily know that the nth element of $\tilde{\boldsymbol{y}}_l$ is given by

$$\tilde{y}_{l,n} = \tilde{y}'_{l,(n+N_c-\beta)}, \ \ n = 0,\ 1, \cdots, N-1 \tag{6.15}$$

When expressed in matrix form, we have

$$\tilde{\boldsymbol{y}}_l = \begin{bmatrix} \tilde{y}_{l,0} \\ \tilde{y}_{l,1} \\ \vdots \\ \tilde{y}_{l,(N-1)} \end{bmatrix} = \sum_{k=0}^{K-1} \begin{bmatrix} h^0_{l,kU} & h^0_{l,k(U-1)} & \cdots & h^0_{l,k0} & 0 & \cdots & 0 \\ 0 & h^0_{l,kU} & \cdots & h^0_{l,k1} & h^0_{l,k0} & \cdots & 0 \\ \vdots & \vdots & \ddots & \ddots & \ddots & \ddots & \vdots \\ 0 & \cdots & 0 & h^0_{l,kU} & \cdots & h^0_{l,k1} & h^0_{l,k0} \end{bmatrix} \begin{bmatrix} \tilde{x}^0_{k,(-U-\beta)} \\ \vdots \\ \tilde{x}^0_{k,(-1)} \\ \tilde{x}^0_{k,0} \\ \vdots \\ \tilde{x}^0_{k,(N-1-\beta)} \end{bmatrix}$$
$$+ \begin{bmatrix} \tilde{n}_{l,(N_c-\beta)} \\ \tilde{n}_{l,(N_c+1-\beta)} \\ \vdots \\ \tilde{n}_{l,(N+N_c-\beta-1)} \end{bmatrix} \tag{6.16}$$

6.2.1.3 Quasi-Synchronous Sensing with Small ISI

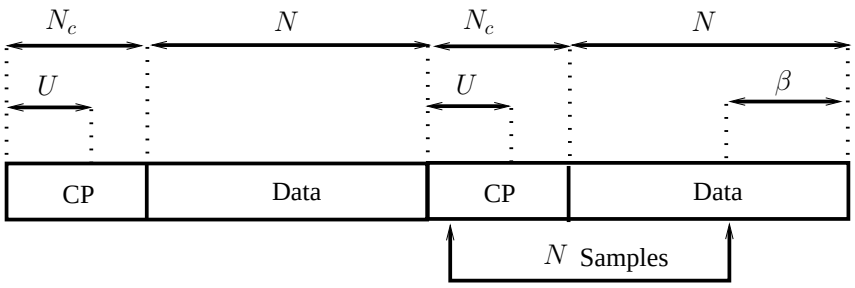

Figure 6.5: Illustration for the scenario of quasi-synchronous sensing with small ISI, where $N_c - U \leq \beta \leq N_c$.

The scenario considered is similar as the one considered in Section 6.2.1.2, except that now $(N_c - U \leq \beta \leq N_c)$. In this case, the samples used for sensing are affected by both the -1th IFDMA symbol and the 0th IFDMA symbol, as seen in Fig. 6.5.

From Fig. 6.5, we can know that the nth element of $\tilde{\boldsymbol{y}}_l$ is given by

$$\tilde{y}_{l,n} = \tilde{y}'_{l,(n+N_c-\beta)}, \;\; n = 0,\, 1, \cdots, N-1 \tag{6.17}$$

Furthermore, it can be shown that $\tilde{\boldsymbol{y}}_l$ can be expressed in matrix form as

$$\tilde{\boldsymbol{y}}_l = \begin{bmatrix} \tilde{y}_{l,0} \\ \tilde{y}_{l,1} \\ \vdots \\ \tilde{y}_{l,(N-1)} \end{bmatrix} = \sum_{k=0}^{K-1} \begin{bmatrix} h_{l,kU}^{-1} & h_{l,k(U-1)}^{-1} & \cdots & h_{l,k0}^{-1} & 0 & \cdots & 0 \\ 0 & h_{l,kU}^{-1} & \cdots & h_{l,k1}^{-1} & h_{l,k0}^{-1} & \cdots & 0 \\ \vdots & \vdots & \ddots & \ddots & \ddots & \ddots & \vdots \\ 0 & \cdots & 0 & h_{l,kU}^{0} & \cdots & h_{l,k1}^{0} & h_{l,k0}^{0} \end{bmatrix} \begin{bmatrix} x_{N+N_c-U-\beta}^{-1} \\ \vdots \\ x_{N-1}^{-1} \\ x_{-N_c}^{0} \\ \vdots \\ x_{0}^{0} \\ \vdots \\ x_{N-1-\beta}^{0} \end{bmatrix}$$
$$+ \begin{bmatrix} \tilde{n}_{l,(N_c-\beta)} \\ \tilde{n}_{l,(N_c+1-\beta)} \\ \vdots \\ \tilde{n}_{l,(N+N_c-\beta-1)} \end{bmatrix} \tag{6.18}$$

6.2.1.4 Asynchronous Sensing

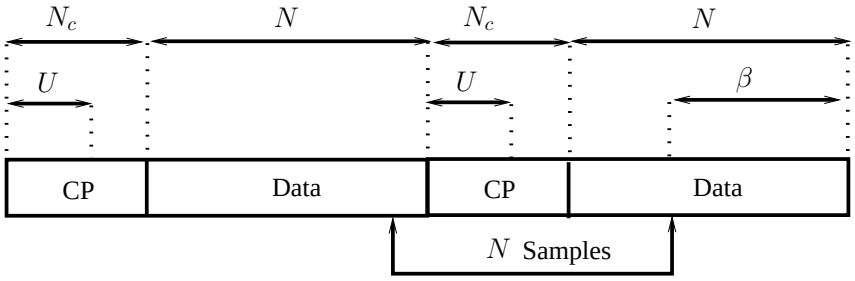

Figure 6.6: Illustration for the scenario of asynchronous sensing, where $N_c \leq \beta < N$.

Finally, for the scenario of asynchronous sensing, the situation can be seen in Fig. 6.6, where $N_c \leq \beta < N$. Hence, the samples used for spectrum sensing depend on two consecutive IFDMA symbols. The nth entry of $\tilde{\boldsymbol{y}}_l$ can be expressed as

$$\tilde{y}_{l,n} = \tilde{y}'_{l,(n+N_c-\beta)}, \;\; n = 0,\, 1, \cdots, N-1 \tag{6.19}$$

which, when in matrix form, can be represented as

$$\tilde{\boldsymbol{y}}_l = \begin{bmatrix} \tilde{y}_{l,0} \\ \tilde{y}_{l,1} \\ \vdots \\ \tilde{y}_{l,(N-1)} \end{bmatrix} = \sum_{k=0}^{K-1} \begin{bmatrix} h_{l,kU}^{-1} & h_{l,k(U-1)}^{-1} & \cdots & h_{l,k0}^{-1} & 0 & \cdots & 0 \\ 0 & h_{l,kU}^{-1} & \cdots & h_{l,k1}^{-1} & h_{l,k0}^{-1} & \cdots & 0 \\ \vdots & \vdots & \ddots & \ddots & \ddots & \ddots & \vdots \\ 0 & \cdots & 0 & h_{l,kU}^{0} & \cdots & h_{l,k1}^{0} & h_{l,k0}^{0} \end{bmatrix} \begin{bmatrix} x_{N+N_c-U-\beta}^{-1} \\ \vdots \\ x_{N-1}^{-1} \\ x_{-N_c}^{0} \\ \vdots \\ x_{0}^{0} \\ \vdots \\ x_{N-1-\beta}^{0} \end{bmatrix} + \begin{bmatrix} \tilde{n}_{l,(N_c-\beta)} \\ \tilde{n}_{l,(N_c+1-\beta)} \\ \vdots \\ \tilde{n}_{l,(N+N_c-\beta-1)} \end{bmatrix} \tag{6.20}$$

which has the same form as (6.18). However, we should note that in (6.18), $N_c - U \leq \beta \leq N_c$, while in (6.20) $N_c \leq \beta < N$.

After obtaining the N observation samples, as shown in (6.14), (6.16), (6.18) or (6.20), the DFT operation is carried out to transform the time-domain observations $\tilde{\boldsymbol{y}}_l$ to the frequency-domain, yielding an N-length vector

$$\tilde{\boldsymbol{Y}}_l = \boldsymbol{\mathcal{F}}_N \tilde{\boldsymbol{y}}_l = [\tilde{Y}_{l,0},\ \tilde{Y}_{l,1}, \cdots, \tilde{Y}_{l,(N-1)}],\ l = 1, 2, \ldots, L \tag{6.21}$$

where the vth $(0 \leq v \leq N-1)$ element of $\tilde{\boldsymbol{Y}}_l$ can be expressed as

$$\begin{aligned} \tilde{Y}_{l,v} &= \frac{1}{\sqrt{N}} \sum_{n=0}^{N-1} \tilde{y}_{l,n} \exp\left(-j\frac{2\pi v n}{N}\right) \\ &= \frac{1}{\sqrt{N}} \sum_{n=0}^{N-1} \tilde{y}'_{l,(n+N_c)} \exp\left(-j\frac{2\pi v n}{N}\right) \end{aligned} \tag{6.22}$$

In correspondence to the subcarrier mapping operated at the transmitter side, at the CRSN, subcarrier de-mapping is carried out to execute the inverse operation of (6.5). The corresponding outputs for the kth PR user can be collected into an W-length vector as

$$\tilde{\boldsymbol{Y}}_l^k = [\tilde{Y}_{l,0}^k,\ \tilde{Y}_{l,1}^k, \cdots, \tilde{Y}_{l,(W-1)}^k] \tag{6.23}$$

in which the wth $(0 \leq w \leq W-1)$ element is

$$\tilde{Y}_{l,w}^{k} = \tilde{Y}_{l,(wK+k)} \tag{6.24}$$

With the aid of (6.23), a CRSN can now detect the on/off state of a PR user occupying a certain set of subcarriers. As for the purpose of CR sensing a CR system only needs to know which subcarriers are active or inactive, low-complexity noncoherent detection can be employed. In this chapter, noncoherent energy detection is employed to detect the K PR users' states. Specifically, three types of local detection rules are investigated, which are referred to as the *average power assisted detection (APD)*, *majority vote assisted detection (MVD)* and the *maximum selection assisted detection (MSD)*. Their details are as follows.

In the context of the APD, the decision rule for detection of the kth PR user by the lth CRSN is given by

$$\delta_{(l,k)} = \frac{1}{W} \sum_{w=0}^{W-1} |\tilde{Y}_{l,w}^{k}|^2 \underset{H_1}{\overset{H_0}{\lessgtr}} \lambda_{AP} \tag{6.25}$$

where λ_{AP} is a preset threshold for the APD, which is chosen to satisfy a fixed false alarm probability of P_f.

When the MVD is employed, we first set a threshold $\lambda_{mv} > 0$. By comparing with this threshold, whenever an element $\tilde{Y}_{l,w}^{k}$ in $\tilde{\boldsymbol{Y}}_{l}^{k}$ exceeds λ_{mv}, the corresponding entry of a newly formed vector $\tilde{\boldsymbol{Y}}_{l}^{'k}$ is flagged by a logical one. Otherwise, it gives a logical zero. Based on $\tilde{\boldsymbol{Y}}_{l}^{'k}$, the local detection is made in the principles of MVD. Specifically, if the number of ones is equal to or more than λ_{MV} of the preset threshold, the CRSN renders that the corresponding PR user is on (H_1). Otherwise, it decides that the PR is off (H_0). In summary, the decision rule is described as

$$\delta_{(l,k)} = \sum_{w=0}^{W-1} |\tilde{Y}_{l,w}^{'k}|^2 \underset{H_1}{\overset{H_0}{\lessgtr}} \lambda_{MV} \tag{6.26}$$

where λ_{MV} is an integer threshold for the MVD.

Finally, when MSD is employed, the largest one of $\tilde{\boldsymbol{Y}}_{l}^{k}$ is chosen for making the local decision. The decision rule can be expressed as

$$\delta_{(l,k)} = \max\{|\tilde{Y}_{l,0}^{k}|^2,\ |\tilde{Y}_{l,1}^{k}|^2, \cdots, |\tilde{Y}_{l,(W-1)}^{k}|^2\} \underset{H_1}{\overset{H_0}{\lessgtr}} \lambda_{MS} \tag{6.27}$$

where λ_{MS} is the threshold for the MSD, which is chosen for satisfying a fixed false alarm probability P_f.

After the on/off states of all the K PR users are detected, the lth CRSN obtains an K-length binary vector giving the on/off states of the K PR users, which is expressed as $\boldsymbol{s}_l^{(B)} = [s_{l,0}^{(B)}, s_{l,1}^{(B)}, \cdots, s_{l,(K-1)}^{(B)}]$. This vector is then mapped to an M-ary number expressed as $s_l^{(M)}$, which is then transmitted in the FH/MFSK principles, as shown in Fig. 6.1 and detailed in the next subsection.

6.2.2 Signal Processing and Transmission at CRSNs

Let the estimated states by the L CRSNs are collected into a vector $\boldsymbol{s}^{(M)} = [s_1^{(M)}, s_2^{(M)}, \cdots, s_L^{(M)}]$, where $s_l^{(M)} \in [0, M-1]$. Following the local spectrum sensing, the L CRSNs convey their local detected states to the FC with the aid of the FH/MFSK techniques. Let the total transmission time of $\boldsymbol{s}^{(M)}$ to the FC be T_s seconds, which is referred to as the symbol duration. This symbol duration is equally divided into L portions referred to as *time-slots* having the duration $T_h = T_s/L$. Each CRSN uses one time-slot to send its detected states to the FC. As previously mentioned, the FH/MFSK scheme has M orthogonal sub-frequency bands, their center frequencies are represented by $\boldsymbol{F} = \{f_0, f_1, \ldots, f_{M-1}\}$. These M frequencies are used for both FH and MFSK modulation, which are implemented as follows. Let $\boldsymbol{a} = [a_1, a_2, \cdots, a_L]$ be a FH address used for FH operation, where $a_l \in \{0, 1, \cdots, M-1\}$, $l = 1, 2, \ldots, L$. With the aid the FH operation, different CRSNs will convey their signals on different sub-frequency bands. The operation enhances the diversity capability for final signal detection at the FC, especially, when some of the CRSNs are close to each other, resulting in correlation in the space domain.

After processing $\boldsymbol{s}^{(M)}$ using the FH address $\boldsymbol{a}$, we obtain

$$\begin{aligned} \boldsymbol{m} &= [m_1, m_2, \cdots, m_L] = \boldsymbol{s}^{(M)} \oplus \boldsymbol{a} \\ &= \left[s_1^{(M)} \oplus a_1, s_2^{(M)} \oplus a_2, \cdots, s_L^{(M)} \oplus a_L\right] \end{aligned} \tag{6.28}$$

where $\oplus$ represents the addition operation in the Galois field of $GF(M)$. Therefore, the value of m_l $(l = 1, 2, \ldots, L)$ is within $[0, M-1]$ and is suitable for MFSK modulation. Following the FH operation, as shown in Fig. 6.1, the components of $\boldsymbol{m}$ are mapped to the MFSK's sub-frequencies $\boldsymbol{F}_m = \{f_{m1}, f_{m2}, \ldots, f_{ml}\}$, where $f_{m_l} \in \boldsymbol{F}$. Finally, the MFSK signals of the L CRSNs are transmitted one-by-one to the FC in a time-division fashion using L time-slots of duration T_h. Specifically, the signal transmitted by the lth CRSN during $iT_s < t \leq (i+1)T_s$ can be expressed

in complex form as

$$s_l(t) = \sqrt{P}\psi_{T_h}[t - iT_s - (l-1)T_h]\exp[j2\pi(f_c + f_{m_l})t + j\phi_l],\ \ l = 1, 2, \ldots, L \tag{6.29}$$

where P denotes the transmission power, which is assumed the same for all the L CRSNs, f_c is the main carrier frequency and ϕ_l is the initial phase introduced by carrier modulation. In (6.29), $\psi_{T_h}(t)$ is the pulse-shaped signalling waveform, which is defined over the interval $[0, T_h)$ and satisfies the normalization of $\int_0^{T_h} \psi^2(t)dt = T_h$.

Assuming that the signals as shown in (6.29) are transmitted via flat Rayleigh fading channels to the FC, the received signal during $iT_s < t \leq (i+1)T_s$ can then be expressed as

$$\begin{aligned} r_l(t) =& h_l s_l(t) + n_l(t) \\ =& \sqrt{P}h_l\psi_{T_h}[t - iT_s - (l-1)T_h]\exp[j2\pi(f_c + f_{m_l})t + j\phi_l] + n(t), \\ & l = 1, 2, \ldots, L, \end{aligned} \tag{6.30}$$

where $h_l = \alpha_l \exp(j\theta_l)$ denotes the channel gain with respect to the lth CRSN, which is assumed constant over one symbol-duration. In (6.29), $n(t)$ is the Gaussian noise process presenting at the FC, which has zero mean and single-sided power-spectral density (PSD) of N_0 per dimension.

6.3 Fusion Processing

When the FC receives the signal $r_l(t)$, $l = 1, 2, \cdots, L$, final decision is made with the aid of one of the two noncoherent fusion rules, namely the conventional EGC fusion rule and the ES-EGC fusion rules, which are detailed as follows.

First, for both the fusion rules, M decision variables are formed for every of the L CRSNs, which are

$$\begin{aligned} R_{ml} =& |(\sqrt{\Omega P}T_h)^{-1} \int_{iT_s + lT_h}^{iT_s + (l+1)T_h} r_l(t)\psi^*_{T_h}[t - iT_s - (l-1)T_h]\exp[-j2\pi(f_c + f_m)t]dt|^2, \\ & m = 0, 1, \ldots, M-1;\ l = 1, 2, \ldots, L \end{aligned} \tag{6.31}$$

where $\Omega = E[|h_l|^2]$ denotes the average channel power. Since the M sub-frequency bands used for FH/MFSK are assumed to be orthogonal to each other, there is no interference between any two sub-frequency bands. Consequently, upon substituting (6.30) into (6.31) and absorbing the carrier

phase ϕ_l into h_l, we obtain

$$R_{ml} = \left| \frac{\mu_{mm_l} h_l}{\sqrt{\Omega}} + N_{ml} \right|^2, \; m = 0, 1, \ldots, M-1; \; l = 1, 2, \ldots, L \tag{6.32}$$

where, by definition, $\mu_{mm} = 1$, while $\mu_{mm_l} = 0$, if $m \neq m_l$. In (6.32), N_{ml} is a complex Gaussian noise sample collected from the mth sub-frequency band during the lth time-slot, which is given by

$$N_{ml} = (\sqrt{\Omega P} T_h)^{-1} \int_{iT_s + lT_h}^{iT_s + (l+1)T_h} n(t) \psi^*_{T_h}[t - iT_s - (l-1)T_h] \exp[-j2\pi(f_c + f_m)t] dt \tag{6.33}$$

It can be shown that N_{ml} has mean zero and a variance of $LN_0/(\Omega E_s) = L/\bar{\gamma}_s$, where $E_s = PT_s$ represents the total energy with each CRSN's transmitted energy per symbol being $E_h = E_s/L$, while $\bar{\gamma}_s = \Omega E_s / N_0$ denotes the average SNR per symbol.

Using the ML values shown in (6.32), we can form a time-frequency matrix $\boldsymbol{R}$ of $(M \times L)$, where each column holds M decision variables in the form of (6.32). Based on $\boldsymbol{R}$ the FC carries out the final detection in the principles of EGC or ES-EGC fusion rule.

6.3.1 EGC Fusion Rule

In the context of the EGC fusion rule, the FC makes the final decision based on the time-frequency matrix as follows.

1. **Frequency de-hopping to form a detection matrix**:

$$\boldsymbol{D} = \boldsymbol{R} \boxminus (\mathbf{1} \otimes \boldsymbol{a}^T) \tag{6.34}$$

where $\mathbf{1}$ denotes an all-one column vector of M-length and $\otimes$ denotes the Kronecker product operation between two matrices [116]. In (6.34), the operation of $\boldsymbol{A} \boxminus \boldsymbol{B}$ shifts the elements in $\boldsymbol{A}$ based on the values provided by $\boldsymbol{B}$. Specifically, after the operation in (6.34), a detection matrix $\boldsymbol{D}$ is formed as

$$D_{(m \ominus a_l)l} = R_{ml}, \; m = 0, 1, \ldots, M-1, \;\; l = 1, 2, \ldots, L \tag{6.35}$$

where $\ominus$ denotes the subtraction operation in the Galois field of $GF(M)$. The operation in Equation (6.35) means that the element indexed by m in $\boldsymbol{R}$ is changed to the one indexed by $m' = m \ominus a_l$ in $\boldsymbol{D}$.

2. **EGC detection**: Based on the detection matrix $\boldsymbol{D}$, M decision variables for final spectrum sensing are formed under the EGC principles [116] as

$$D_m = \sum_{l=1}^{L} D_{ml}, \quad m = 0, 1, \ldots, M-1 \tag{6.36}$$

Finally, the largest one of $\{D_0, D_1, \cdots, D_{M-1}\}$ is selected and its index is mapped to an integer in the range $[0, M-1]$, which represents the M-ary estimation of the K PR users' on/off states. Then, the M-ary integer is converted to a binary vector of K-length, whose K elements give the on/off states of the K PR users.

6.3.2 ES-EGC Fusion Rule

In our spectrum sensing scheme, there are mainly two sources resulting in that the FC makes erroneous decisions. The first one is the incorrect detection made by the CRSNs. In this case, the CRSNs directly send the FC incorrect information. Secondly, the wireless channels between CRSNs and FC are no-ideal, which also introduce errors. Statistically, we can know that, when an element in the detection matrix $\boldsymbol{D}$ contains both signal and noise, its energy will be higher than that of the element containing only noise. This implies that, if an element in the undesired rows (the rows not matching to the states of the PR users) has high energy, then, it might be an erroneous element introduced by what the above-mentioned. Straightforwardly, this types of elements in the undesired rows may significantly degrade the detection performance of the FC.

Based on the above observation, in this chapter, the ES-EGC fusion rule is employed. When operated under this fusion rule, in each of the M rows of the detection matrix $\boldsymbol{D}$, a given number of entries with the highest values are removed before forming the M decision variables based on the EGC principles. As the result, the errors transmitted by the CRSNs might be removed, especially, when the signal-to-noise ratio (SNR) is relatively high. As our performance results in Section 6.4 show, this error-erasing process will significantly enhance the detection performance of the FC.

In detail, the ES-EGC fusion rule is operated as follows.

1. **Frequency de-hopping to form the detection matrix $\boldsymbol{D}$**, which is the same as that done by the EGC fusion rule.

2. **Erasure operation**: After obtaining $\boldsymbol{D}$, the ES-EGC fusion rule carries out the erasure oper-

ations. In each of the M rows of $\boldsymbol{D}$, I $(0 \leq I < L)$ elements corresponding to the I largest values are replaced by the value of zero, which results in a new matrix $\bar{\boldsymbol{D}}$.

3. **EGC detection**: M decision variables are formed based on the matrix $\bar{\boldsymbol{D}}$ in EGC principles [116] as

$$\bar{D}_m = \sum_{l=1}^{L} \bar{D}_{ml}, \quad m = 0, 1, \ldots, M-1 \tag{6.37}$$

Finally, the largest of $\{\bar{D}_0, \bar{D}_1, \cdots, \bar{D}_{(M-1)}\}$ is selected and its index value in terms of m represents the M-ary estimation of value conveyed by the CRSNs. Furthermore, after mapping the M-ary value to the binary representation, the on/off states of the K PR suers can be estimated.

6.4 Spectrum Sensing Performance

In this section, both the local spectrum sensing at CRSNs and the overall detection performance at the FC are investigated via simulation results. Specifically, we consider the missing probability, P_m, of the sensing at CRSNs and the missing probability, P_M, of the detection at the FC, for demonstrating the impact of collision between PR users and CR users. At the CRSNs, we assume that the signals received from the PR users experience multipath Rayleigh fading. We compare the local missing probability of different detection approaches via simulation results and show the influence of the threshold applied for detection. At the FC, the overall spectrum sensing performance of our proposed cooperative spectrum sensing system employing either EGC or ES-EGC fusion rule is investigated, when assuming that random FH addresses are used for transmitting the local decisions made by the CRSNs to the FC, and that the wireless channels from the CRSNs to the FC experience independent Rayleigh fading.

In our simulations, local decisions are made based on the energy-based spectrum sensing. The parameters used in our simulations for each of the figures are detailed associated with the corresponding figure. In the figures, the 'Observation SNR at each CRSN' is the average SNR per PR user received at a CRSN. The false-alarm probability of all the CRSNs is assumed the same, which is expressed as P_f. The 'channel SNR per bit' is the average received SNR at the FC per bit given by $\bar{\gamma}_b = \bar{\gamma}_s / b$, where $b = \log_2 M$ denotes the number of bits required to represent a M-ary number.

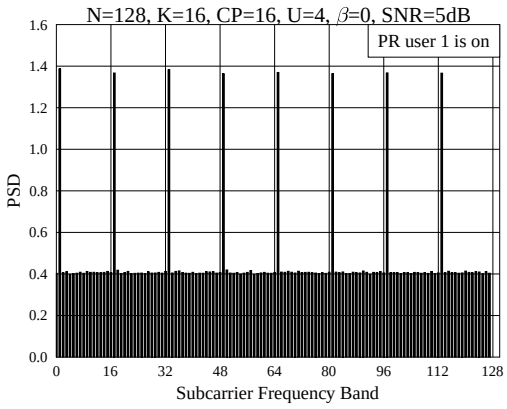

(a) Case 1: Synchronous sensing.

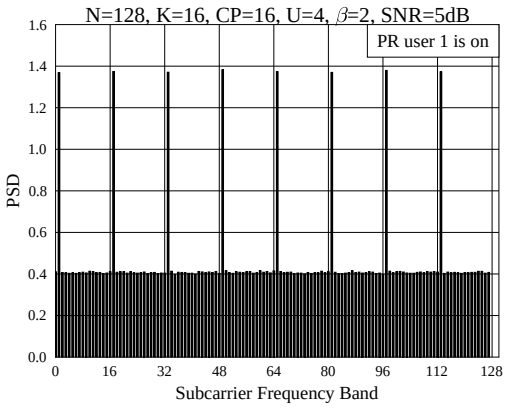

(b) Case 2: Quasi-synchronous sensing without ISI.

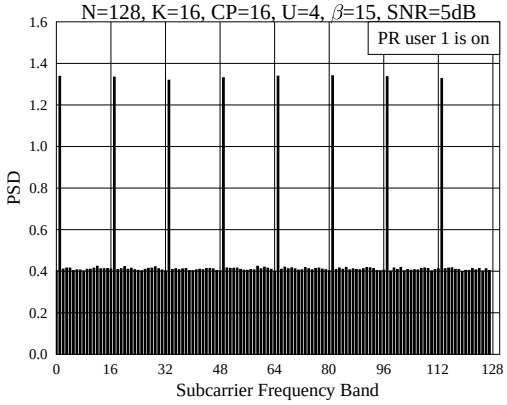

(c) Case 3: Quasi-synchronous sensing with small ISI.

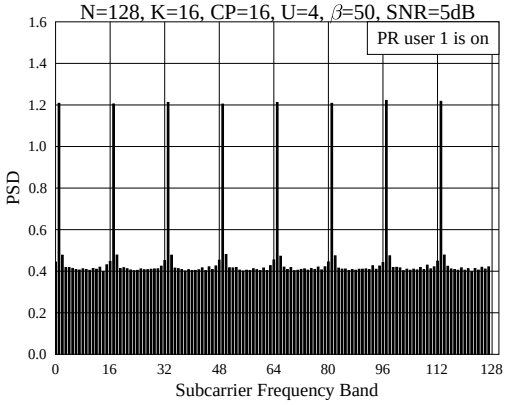

(d) Case 4: Asynchronous sensing.

Figure 6.7: Power spectral density presenting at the CRSNs in a IFDMA system using 128 subcarriers to support 16 users, when communicating over multipath Rayleigh fading channels having 5 time-domain resolvable paths. The results were obtained from 10000 realizations.

Fig. 6.7 shows the impacts of the four scenarios, as shown in Section 6.2.1, which address the synchronization between the received signals from PR users and the sensing, on the PSDs of the received signals. As shown on the top of the figure, we consider an IFDMA PR system, which employs $N = 128$ subcarriers to support maximum $K = 16$ uplink users. Hence, each PR user occupies $W = 8$ subcarriers evenly distributed over the 128 subcarriers, as indicated by the eight dominant spectral lines in each of the four figures. We assume that, in the PR system, only user 1 is on, while all the other PR users are idle. Signals received by CRSNs from the PR users are assumed to experience multipath Rayleigh fading having $(U + 1) = 5$ time-domain resolvable paths. As shown in Section 6.2.1, the value of the parameter β reflects the synchronization level between the PR signals and the local sensing. Specifically, we set the values of β as $\beta = 0,\ 2,\ 15$ and 50, respectively, for the scenarios of synchronous sensing, quasi-synchronous sensing without ISI, quasi-synchronous sensing with small ISI and asynchronous sensing. From the results shown in the figures, we can clearly see that, when the sensing becomes more asynchronous with the arrival PR signals, inter-carrier interference increases, i.e., more power leaks from the activated subcarriers to their neighbouring subcarriers. However, at 5 dB of the SNR, the activated subcarriers stand out explicitly and have significantly higher power than the other idle subcarriers.

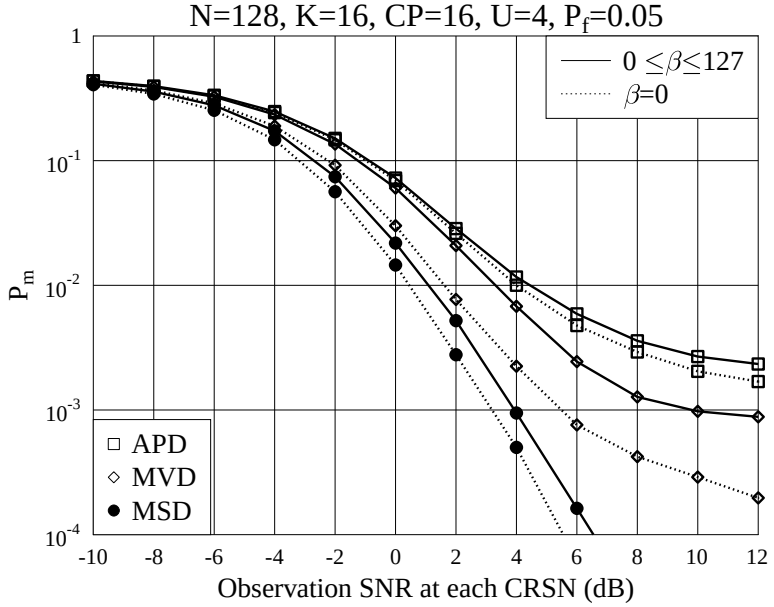

Figure 6.8: Missing probability of the local CRSNs sensing the spectrum of an IFDMA system using 128 subcarriers to support maximum 16 users, when communicating over multipath Rayleigh fading channels having 5 time-domain resolvable paths.

In Fig. 6.8, we investigate the performance of the three types of energy-based detections schemes, namely, the APD, MVD and the MSD, when the false-alarm probability of local CRSNs is set as $P_f = 0.05$. In the figure, $\beta = 0$ stands for the scenario of synchronous sensing, as shown in Section 6.2.1. By contrast, $0 \leq \beta \leq 127$ means that β is a random variable taking integer values uniformly in $[0, 127]$, which provides the average performance achieved by the four synchronization scenarios considered. From Fig. 6.8, we can have the following observations. First, we can see that the MVD outperforms the APD, and that the MSD achieves the best sensing performance among the three local detection schemes. Second, the synchronous sensing provides the best local sensing performance, as there is no inter-carrier interference.

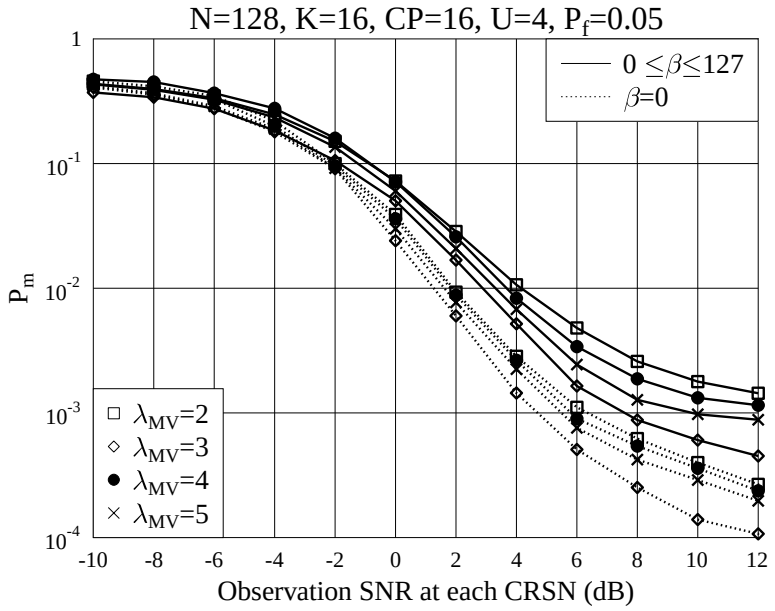

Figure 6.9: Missing probability of the local CRSNs sensing the spectrum of an IFDMA system with 128 subcarriers to support maximum 16 users, when the MVD associated with various values for λ_{MV} is employed.

In Fig. 6.9, we illustrate the local sensing performance of the CRSNs employing MVD, when the thresholds are $\lambda_{MV} = 2,\ 3,\ 4$ and 5. Similarly to Fig. 6.8, in Fig. 6.9 both the synchronous sensing $(\beta = 0)$ and the random asynchronous sensing $(0 \leq \beta \leq 127)$ are considered. From the results of Fig. 6.9, again, we observe that the synchronous sensing outperforms the asynchronous sensing. For both the cases, we see that $\lambda_{MV} = 3$ results in the lowest missing probability, when the SNR is relatively high, which implies that there exists an optimal value for the threshold, which makes the MVD-assisted local sensing attain the lowest missing probability.

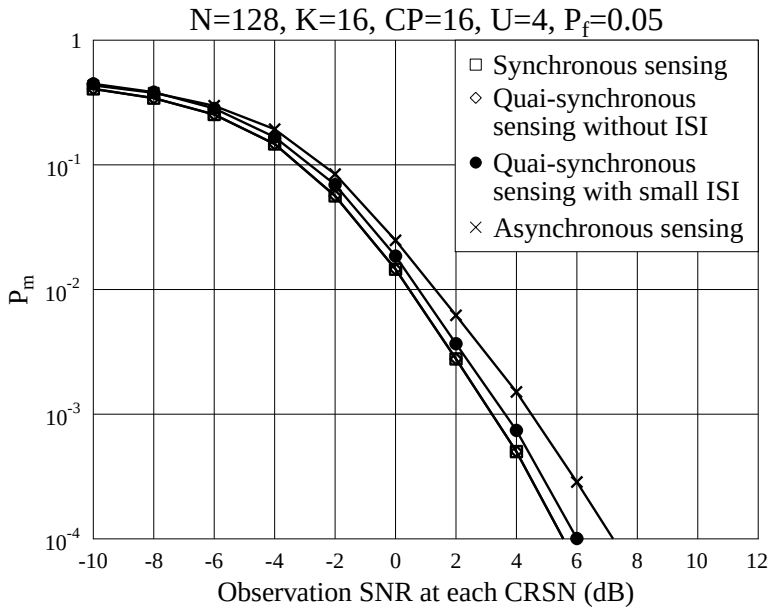

Figure 6.10: Missing probability of the CRSNs sensing an IFDMA system using 128 subcarriers for supporting maximum 16 users with MSD local detection, when four sensing scenarios are considered.

Fig. 6.10 depicts the sensing performance of the MSD local detection in the context of the four scenarios considered in Section 6.2.1. As our discussion in Section 6.2.1 shows, when the CRSNs are operated in the scenarios of synchronous sensing or quasi-synchronous sensing without ISI, there is no interference from a previous IFDMA symbol on the current IFDMA symbol. As shown in Fig. 6.10, we are unable to distinguish between the performance of these two scenarios. By contrast, when there is small or large ISI, corresponding to the scenarios of quasi-synchronous sensing with small ISI and asynchronous sensing, the performance of local CRSNs degrades explicitly, in comparison with that of the scenarios of synchronous sensing and quasi-synchronous sensing without ISI. Furthermore, the missing probability achieved under the scenario of asynchronous sensing is higher than that achieved under the scenario of quasi-synchronous sensing with small ISI.

Fig. 6.11 shows the overall missing probability of the cognitive spectrum sensing systems with various numbers of CRSNs, when the local CRSNs employs the MSD. In the studies, we assume an IFDMA system which has in total $N = 128$ subcarriers and supports maximum $K = 16$ users. Hence, each active user uses $W = 8$ subcarriers for uplink communications. At the FC, both the EGC fusion rule (Fig. 6.11a) and ES-EGC fusion rule (Fig. 6.11b) are considered. Furthermore, when the ES-EGC fusion rule is employed, we assume that an optimum number of entries per row

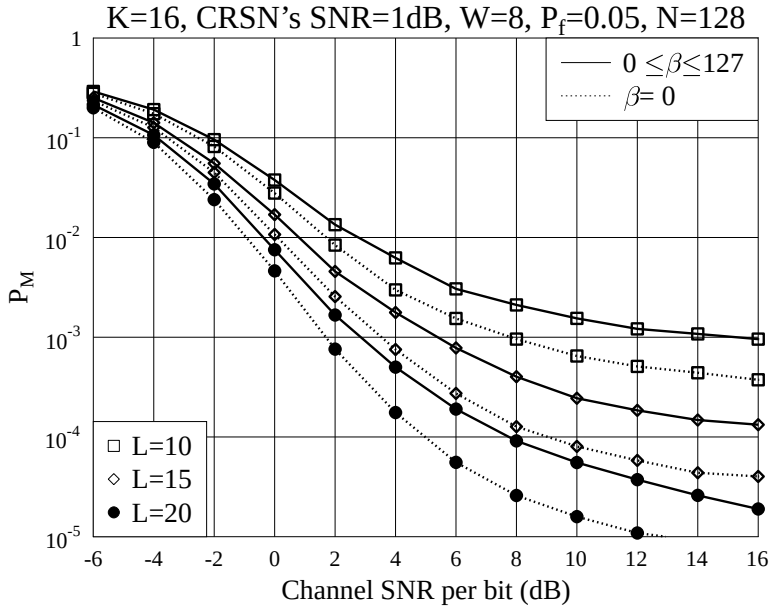

(a) Local detection: MSD; Fusion detection: EGC

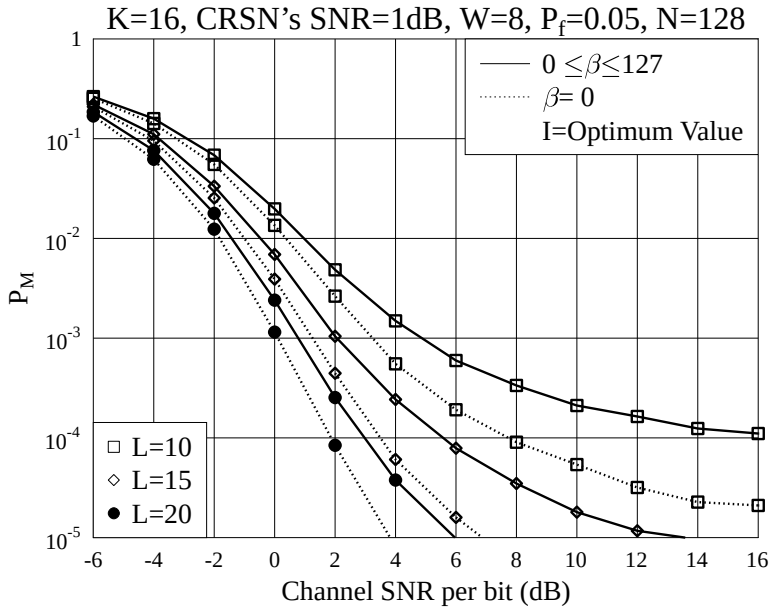

(b) Local detection: MSD; Fusion detection: ES-EGC

Figure 6.11: Overall missing probability of the cognitive spectrum sensing systems with different numbers of CRSNs, when the MSD local detection and the EGC or ES-EGC assisted fusion detection are employed.

are erased, which yields the best overall detection performance. From the results of Fig. 6.11a and Fig. 6.11b, first, we can explicitly see that the overall missing probability decreases, as the number of CRSNs increases from $L = 10$ to $L = 15$ and to $L = 20$, owing to the improvement of spatial diversity. Second, similar as the detection at the CRSNs, the overall detection performance of the system with synchronous sensing corresponding to $(\beta = 0)$ is better than that achieved by the systems using asynchronous sensing. Finally, when comparing Fig. 6.11b with Fig. 6.11a, we can clearly see that the ES-EGC fusion rule outperforms the EGC fusion rule, which becomes more significant, when the channel SNR increases.

Finally, in Fig. 6.12, the overall missing probability performance of the cognitive spectrum sensing system, when different observation SNR is assumed for the CRSNs. From Fig. 6.12, we can have similar observations as that from Fig. 6.11. Furthermore, from Figs. 6.11 and 6.12, we can find that the ES-EGC fusion rule outperforms the EGC fusion rule, which becomes more explicit, as the SNR of the channels from CRSNs to FC increases.

6.5 Conclusion

In this chapter, we have proposed a FH/MFSK assisted cognitive spectrum sensing system monitoring, specifically, a IFDMA PR system supporting multiple users. Local decisions for the presence of multiple PR users are made by the CRSNs separately based on one of the three types of energy detection schemes considered, under the constraints of one of the four synchronization scenarios assumed between the PR signals and the CRSNs. After each of the CRSNs obtains the on/off states of all the PR users, this binary local decision vector is conveyed into an M-ary number, and then transmitted to the FC with the aid of FH/MFSK. At the FC, overall decision is made based on either the EGC fusion rule or ES-EGC fusion rule. Both the local spectrum sensing at CRSNs and the overall detection performance at the FC are investigated via simulation results. At the CRSNs, we assume that the signals received from the PR users experience multiple Rayleigh fading channels. Our simulation results show that reliable local sensing is achievable at the very low SNR. Both the synchronization and the local detection approach, as well as the threshold has significant influence on the local detection performance. At the FC, the overall spectrum sensing performance is investigated, when assuming that random FH addresses are used for transmitting

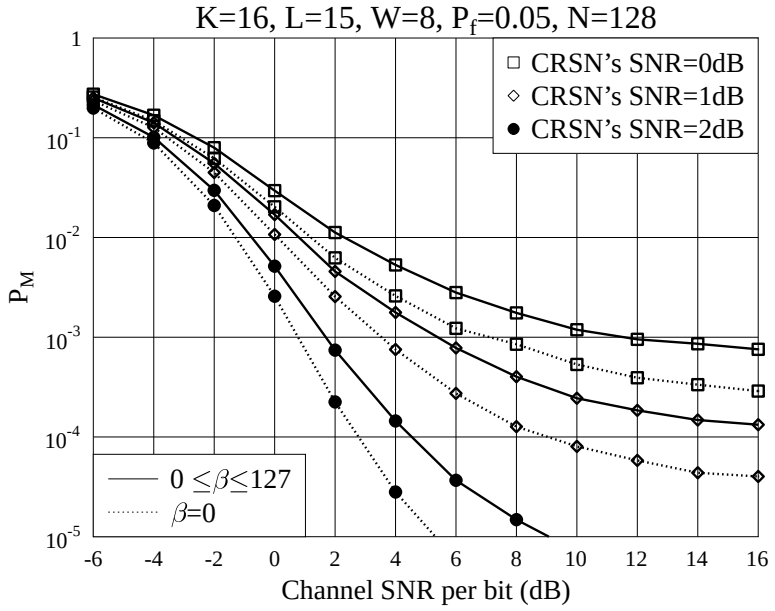

(a) Local detection: MSD; Fusion detection: EGC

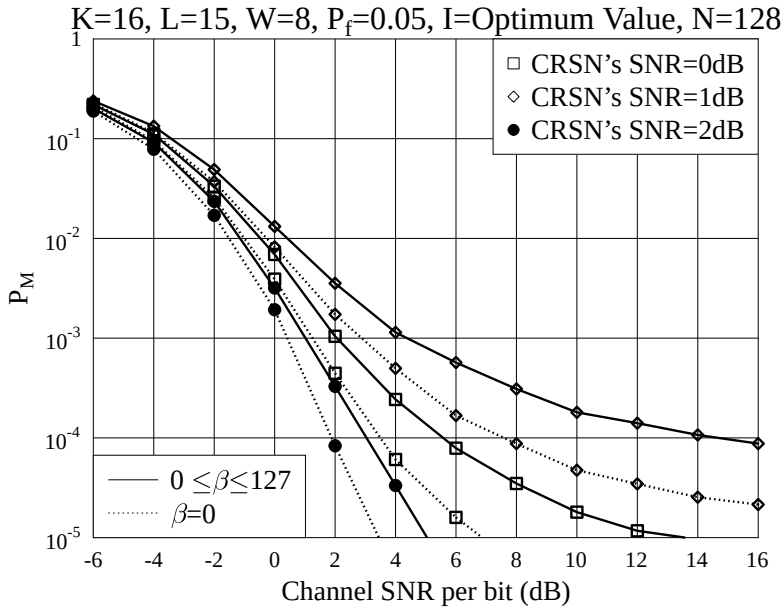

(b) Local detection: MSD; Fusion detection: ES-EGC

Figure 6.12: Overall missing probability of the cognitive spectrum sensing system with the MSD for local detection and EGC or ES-EGC assisited fusion detection, when the CRSNs have various observation SNRs.

the local decisions through independent Rayleigh fading channels. From the simulation results, we can clearly see that the ES-EGC fusion rule outperforms the ES-EGC fusion rule, which becomes more significant, when the channel SNR increase.

Chapter 7

Conclusions and Future Work

In this final concluding chapter, we first provide a summary of the thesis in Section 7.1. Then a range of issues requiring further research are provided in Section 7.2.

7.1 Summary of Conclusions

In this thesis, we have proposed and investigated a novel triple-layer wireless sensor network (WSN) framework known as the FH/MFSK WSN system. Generally, our proposed FH/MFSK WSN employs two typical characteristics as follows. First, low-complexity noncoherent detection is employed at the FC, which does not depend on energy-greedy channel estimation. These energy-efficient and low-complexity detection strategies are beneficial to the life-time of power-limited WSNs. Second, in the proposed FH/MFSK WSN, the FH/MFSK techniques have been introduced for supporting single/multiple SE(s). The FH/MFSK techniques are also capable of enhancing the detection performance of the FH/MFSK WSN system, which is achieved by reducing the correlation among the signals transmitted by the different LSNs, so that the detection at the FC can benefit from both the space diversity provided by the LSNs and the frequency diversity yielded by the FH/MFSK operations. As our analysis shows, the frequency diversity becomes more important to the WSNs, when their LSNs are closely distributed, resulting in that the signals transmitted by different LSNs experience correlation in the space domain.

Each of the chapters in the thesis has its own emphases. In brief, Chapter 2 gives an overview of local detections and fusion rules. In Chapter 3, the proposed FH/MFSK WSN is employed

for monitoring single SE with multiple states. In Chapter 4, the FH/MFSK WSN is proposed to monitor multiple SEs of each having multiple states. Chapter 5 addresses soft-sensing, which is implemented to enhance the detection performance of the FH/MFSK WSN with single SE. Finally, as an example for the applications of the FH/MFSK WSN, in Chapter 6, spectrum sensing in cognitive radios is studied. More details concerning the contribution of the thesis are provided as follows.

We have commenced in Chapter 2 with a detailed review of local detections and fusion rules. According to the references, a lot of research has been done with WSNs in order to attain reliable signal detection through the optimization at FC level or/and at LSN level. Specifically, the principles of the classical binary hypothesis test at LSNs and the fusion rules used by FC, as well as some local spectrum sensing approaches are summarized as follows.

- **Classical binary local detections**: In the context of binary local detection, a LSN makes local decision of the observed SE based on its own observation. Bayesian detection is made to achieve the average cost as small as possible, which requires the knowledge of the *a-priori* probability and the cost of all decisions. When the cost functions are unavailable, MAP detection may be employed to choose the most possible hypothesis based on local observations. When neither the cost functions nor the *a-priori* probabilities are achievable, but a false-alarm probability P_F is available, NP detection may be designed to maximize the detection probability P_D or minimize the missing probability P_M.

- **Optimum and sub-optimum channel-aware fusion rules**: With the channel state information (CSI) of the channels from LSNs to FC, as well as noise variance, optimum likelihood-ratio (LR) fusion rule can be derived. In order to reduce the complexity and the requirements from channels, CV fusion rule is derived based on the approximation of the optimum LR-based fusion rule within high channel SNR region. In low channel SNR region, MRC fusion rule approximates the optimum LR-based fusion rule. EGC fusion rule can be viewed as a trade-off between the MRC fusion rule and CV fusion rule, which is robust in a wide channel SNR range.

- **Noncoherent M-ary fusion rules**: In Section 2.3, some existing noncoherent fusion detection schemes are summarised, which require neither channel estimation nor LSN's detection performance. All our discussion about noncoherent M-ary fusion rules are based on a frame-

work of MFSK WSN, specifically, based on a so-called detection matrix $\boldsymbol{D}$. It can be seen that each of these noncoherent fusion detections has its unique advantages and disadvantages, as well as some unique requirements.

- **Spectrum sensing approaches**: In Section 2.4, three typical spectrum sensing approaches have been addressed, which include the energy detection, matched filter (MF) detection and the feature based detection approaches. Energy detection is the simplest spectrum sensing approach with wide applications. However, its performance is highly susceptible to noise power uncertainty, as well as shadowing and fading environments. MF detection is the optimum spectrum sensing approach in stationary Gaussian noise, when the required *a-priori* information is available. By contrast, if the knowledge about the PR users is not perfect known, the detection performance of the MF degrades significantly. Cyclostationary detection is one of the feature detections, which make use of the periodic patterns of the PR signals. Compared with energy detection, cyclostationary detection is less sensitive to the noise uncertainty, but, at the cost of complexity increasing. Eigenvalue-based detection is another type of feature detection relying on the correlation of the received PR signals. It is effective for blind implementation, when the PR signals are highly correlated.

In Chapter 3, our exploration has been focused on a novel FH/MFSK WSN framework, which monitors an M-ary SE and conveys observations from LSNs to FC with the aid of FH/MFSK techniques through either AWGN or Rayleigh fading channels. The FH/MFSK techniques are employed for gaining diversity, especially, when LSNs are closely distributed. At the FC, the SE's state is detected based on low-complexity noncoherent fusion rules. The simulation results in Chapter 3 show that our proposed FH/MFSK WSN is a promising scheme for operating in different environments. In comparison with the conventional EGC fusion rule, our proposed novel ES-EGC fusion rule may significantly improve the detection performance of the FH/MFSK WSN. In this chapter, three noncoherent fusion rules have been investigated and compared, which include the EGC, ES-EGC and the optimum fusion rules. In more detail, our findings can be summarized as follows.

- **Noncoherent fusion rules**:

  1. **EGC**: EGC fusion rule has the lowest-complexity and yields lowest-delay among the

three noncoherent fusion rules considered. However, EGC fusion rule is sensitive to the LSNs' sensing errors, yielding very poor detection performance, when the LSNs are not reliable.

2. **ES-EGC**: ES-EGC fusion rule has similar complexity and processing delay as the EGC fusion rule. However, our studies and simulation results show that, when the detection in LSNs are unreliable and when the channel SNR is relatively high, ES-EGC fusion rule may significant outperform the EGC fusion rule. In the ES-EGC, the optimum number of erasures per row is determined by the specific environment where the FH/MFSK WSN is deployed.

3. **Optimum fusion rule**: The optimum fusion rule has been investigated based on the MAP principles. However, the complexity of the optimum fusion rule increases exponentially with the number of states M, which is extreme for practical applications. Hence, a sub-optimum fusion rule has been considered, in which EGC is first operated to reduce then number of candidates. From the candidates, final decision is made using the MAP principles. In order to further reduce the computation complexity, the SLD-SMAP fusion rule has been introduced. From (3.23) we can see that the complexity of the SLD-SMAP is related to the threshold λ, which can be controlled at a reasonable level according to the practical requirements.

- **Detection performance of FH/MFSK WSNs with single SE**: In the study of the detection performance, all the M states are assumed to have equal probability.

1. **Error floor of EGC fusion rule**: When error floor is derived, the transmission from LSNs to FC is assumed to be ideal, without noise and fading. In this case, floor for the average error classification probability (ECP) is given by

$$P_E = \sum_{i=0}^{\lfloor L/2 \rfloor} \binom{L}{i} P_d^i P_e^{L-i} \sum_{k=i}^{L-i} \left(\frac{1}{M-1}\right)^{k-1} \left(\frac{M-2}{M-1}\right)^{L-i-k} \tag{7.1}$$

where $\lfloor L/2 \rfloor$ denotes the integer smaller or equal to $L/2$.

2. **Error floor of ES-EGC fusion rule**: Similar as the case of using EGC fusion rule, no fading and noise are considered, when error floor is analysed for the ES-EGC fusion

rule. Assuming that I erasures are used in each row, the error floor is

$$P_E = \sum_{i=0}^{I} \binom{L}{i} P_d^i P_e^{L-i} + \sum_{i=I+1}^{\lfloor L/2 \rfloor} \binom{L}{i} P_d^i P_e^{L-i} \sum_{k=i-I}^{L-i-I} \left(\frac{1}{M-1}\right)^{k-1} \left(\frac{M-2}{M-1}\right)^{L-i-k-I},$$

$$\text{if } 1 \leq I \leq \lfloor L/2 \rfloor \tag{7.2}$$

$$P_E = \sum_{i=0}^{I} \binom{L}{i} P_d^i P_e^{L-i},$$

$$\text{if } \lfloor L/2 \rfloor < I < L \tag{7.3}$$

3. **Error probability of ES-EGC over Rayleigh fading channels**: After erasure operation in the ES-EGC, the decision variables become correlated, making the analysis of the detection performance of the ES-EGC fusion rule highly involved. For this sake, in our analysis, the LSNs are assumed to be perfect, which results in a lower-bound for the ECP of the ES-EGC fusion rule. In our analysis, the PDF of the decision variable after erasure operation is derived with the aid of moment generating function (MGF). After the inverse Laplace transform, with the aid of the residue theorem, we derived the PDF of the decision variable $\bar{D}_m$. Finally, we have derived the expression of ECP with single integral. Additionally, a closed-form union-bound for the ECP has been derived.

In Chapter 4, the FH/MFSK WSN has been employed to monitor multiple M-ary SEs, where L number of LSNs are used to simultaneously observe K SEs and, meanwhile, all these K SEs are observed by each of the L LSNs without observation interference. In this chapter, wireless channels from LSNs to FC are assumed to experience independent Rayleigh fading. We find that in the FH/MFSK WSN, there are two types of interference, in addition to the background Gaussian noise, which are the MEI and the interference generated by erroneous decisions at LSNs. At the FC, six low-complex noncoherent fusion rules have been considered, which include the EGC, ES-EGC, EGC-NIIC, ES-EGC-NIIC, EGC-ρIIC and the ES-EGC-ρIIC. The characteristics of these six fusion rules as well as their computation complexity are summarized as follows.

1. **EGC fusion rule**: In this chapter, the EGC fusion rule is considered as a benchmark, which is low-complexity and low detection delay. The complexity of the EGC fusion rule is $\mathcal{O}(KML)$, where K is the number of SEs, M is number of states of each SE and L is the number of LSNs. However, EGC fusion rule is a very deficient scheme for signal detection in

interference environments, yielding significant loss in detection performance as the number of SEs increases.

2. **ES-EGC fusion rule**: Under the ES-EGC fusion rule, in each of the rows in the decision matrix $\boldsymbol{D}$, I $(0 \leq I < L)$ elements corresponding to the I largest values are removed, yielding the modified detection matrix $\bar{\boldsymbol{D}}$. Then, decision variables are formed via EGC principle based on $\bar{\boldsymbol{D}}$. The complexity of the ES-EGC fusion rule is $\mathcal{O}(KMLI)$ for detecting K SEs. It is a single-user fusion rule However, it is a high-efficiency fusion rule, which, for some cases, may achieve even better detection performance than some of the noncoherent multiuser fusion rules, such as, the EGC-NIIC fusion rule.

3. **EGC-NIIC fusion rule**: When the EGC-NIIC fusion rule is employed, the IIC is operated associated with the first N most reliable SEs, whose states are detected one-by-one iteratively from the most reliable ones to the less reliable ones. Then, the rest $(K-N)$ SEs are simultaneously detected via EGC principle. For the EGC-NIIC, a low-complexity reliability measurement method has been proposed, which measures the reliability of the states detected by the EGC-based detection. The complexity of the EGC-NIIC fusion rule is $\mathcal{O}(KMLN)$. We find that there is a trade-off between the number of IIC iterations and the detection performance, showing that, for a given set of parameters, there usually exists a value for N, which results in the best fusion detection performance.

4. **ES-EGC-NIIC fusion rule**: The ES-EGC-NIIC fusion rule carries out the IIC operation based on the modified detection matrices $\{\bar{\boldsymbol{D}}_k^{(i)}\}$, which are obtained after the ES-EGC operations. The reliabilities are measured based on the decision variables provided by the ES-EGC. As the EGC-NIIC, with ES-EGC-NIIC, the N most reliable SEs are first detected iteratively and, then, the rest $(K-N)$ SEs are detected simultaneously using the ES-EGC fusion rule. In the ES-EGC-NIIC, the IIC operations at one iteration impose effect on the following iterations of detection and the effect is accumulative. By contrast, the erasure operations are independent iteration-by-iteration, which does not directly propagate to the following detection. The complexity of the ES-EGC-NIIC is $\mathcal{O}(KMLNI)$. For a FH/MFSK WSN with a fixed set of parameters, there usually exists an optimum value for N, which yields the best detection performance.

5. **EGC-ρIIC fusion rule**: When carrying out the IIC operations, full cancellation may remove the information of the SEs having not detected yet, and might degrade the overall detection performance. In order to mitigate the effect of the full IIC, in the EGC-ρIIC principle, partial cancellation has been proposed. The EGC-ρIIC has the complexity of $\mathcal{O}(K^2ML)$. The value of ρ can be optimized for achieving the best detection performance.

6. **ES-EGC-ρIIC fusion rule**: The ES-EGC-ρIIC has the same principle as the EGC-ρIIC, except that the EGC associated wit the EGC-ρIIC is replaced by the ES-EGC in the ES-EGC-ρIIC. The complexity of the ES-EGC-ρIIC is $\mathcal{O}(K^2MLI)$. Both I and ρ may be optimized to achieve better detection performance.

The studies in Chapter 4 show that, in general, the ES-EGC related fusion rules outperform the EGC related fusion rule, when detection performance is considered.

In Chapter 5, we have aimed at the performance improvement of the FH/MFSK WSN monitoring single SE with the aid of soft-sensing by LSNs. Specifically, after an observation, each of the LSNs calculates the probabilities about all the states at which the SE might be. This soft information is then forwarded to the FC with the aid of the FH/MFSK techniques. In this chapter, a signalling scheme has been proposed for transmitting information from LSNs to FC, which scales the transmission power of frequency tones used by the FH/MFSK. At the FC, the SE's state is detected either by EGC or by ES-EGC fusion rule. Our simulation results show that, in comparison with the hard-decision based sensing, as shown in Chapter 3 and Chapter 4, using soft-sensing is able to enhance the overall detection performance of the FH/MFSK WSN. Furthermore, the ES-EGC fusion rule is robust to the errors made by LSNs, which may significantly outperform the EGC fusion rule, especially, when the soft-sensing at LSNs is not very reliable.

In Chapter 6, a FH/MFSK assisted cognitive spectrum sensing scheme has been proposed for spectrum sensing, specifically, a IFDMA PR system supporting multiple users. In our studies, three types of energy-based detection schemes have been considered, so that the CRSNs can make quick and low-complexity local detection. In this chapter, four synchronization scenarios have been considered, which include the synchronous sensing, quai-synchronous sensing without ISI, quai-synchronous sensing with small ISI and asynchronous sensing. After each of the CRSNs obtains the on/off states of the PR users, it sends the detected states to the FC with the aid of the FH/MFSK.

Finally, at the FC, noncoherent detection is carried out, which is based on either the EGC or the ES-EGC fusion rule, as done in Chapter 3, Chapter 4 and Chapter 5. In this chapter, both the local spectrum sensing at CRSNs and the overall detection performance at the FC are investigated via simulation results. Our studies and performance results show that, our proposed FH/MFSK assisted spectrum sensing system constitutes one highly reliable spectrum sensing scheme, which is capable of exploiting the space diversity provided by CRSNs as well as the frequency diversity provided by the subcarriers of the IFDMA systems. At the CRSNs, we assume that the signals received from the PR users experience multiple Rayleigh fading channels. Our simulation results show that reliable local sensing is achievable at the very low SNR. Both the synchronization and the local detection approach, as well as the threshold has significant influence on the local detection performance. At the FC, the overall spectrum sensing performance is investigated, when assuming that random FH addresses are used for transmitting the local decisions through independent Rayleigh fading channels. From the simulation results, we can clearly see that the ES-EGC fusion rule outperforms the ES-EGC fusion rule, which becomes more significant, when the channel SNR increase.

7.2 Future Work

In this thesis, we have proposed and investigated a range of noncoherent fusion rules in the content of the FH/MFSK WSNs. Our research may be extended in different properties.

This thesis has focused mainly on the low-complexity high-efficiency noncoherent fusion rules, in addition to the cognitive spectrum sensing as one of the applications of the proposed FH/MFSK WSN framework. There are many related issues requiring further investigation.

First, as mentioned previously in the thesis, we generally assumed that local sensing and fusion detection are independent. In other words, the optimization at LSNs and that at FC are carried out independently, which implies that both the local sensing and the fusion detection should be as reliable as possible. However, in our considered triple-layer WSNs, if local sensing sensing is unreliable, the overall performance of the WSNs might be poor, no matter how reliable is the fusion detection. On the other hand, when the fusion detection is unreliable, the overall performance of the WSNs will be poor, even the local sensing is ideal. Hence, in the FH/MFSK WSNs, joint optimization of local sensing and fusion detection constitutes one of the future research topics.

With the aid of joint optimization, we may maximize the overall detection reliability, maximize the lifetime, or/and minimize the overall energy consumed, etc., of the FH/MFSK WSNs.

Second, in our studies, we assumed that the SEs are independent events, which can be observed without interfering with each other, for the sake of focusing our attention mainly on the fusion rules. This is the case for some applications, such as, the example of environment monitoring. However, in practice, there are the SEs which are highly correlated and the observations of these correlated SEs may interfere with each other. For example, in a WSN used for identifying battleships, fight planes, etc., the observations may interfere each other, resulting in that it is difficult to distinguish between different types of them. Hence, when the SEs monitored by our FH/MFSK WSNs are correlated SEs, it is important to design high-efficiency local sensing algorithms. Furthermore, although our proposed fusion rules can be directly employed by the FH/MFSK WSNs monitoring correlated SEs, the effectiveness of these fusion rules is not clear and requires further studies.

Third, except in Chapter 5 where soft-sensing is considered, for simplicity, we mainly assumed that once an erroneous observation occurs, it has the same probability to one of the other $(M-1)$ erroneous states. This assumption may be too strong for some applications. In fact, in many practical applications, an erroneous state often has high probabilities to be the ones closer to the correct state. This uneven error probabilities may be exploited for designing novel signalling schemes for conveying information from LSNs to FC as well as for designing novel high-efficiency fusion rules.

Fourth, in our thesis, as one of the examples to demonstrate the applications of the FH/MFSK WSNs, cognitive spectrum sensing of LTE IFDMA systems has been investigated. In the future research, the FH/MFSK WSNs associated with the various noncoherent fusion rules as proposed may be invoked in the specific application scenarios. We not only need to investigate the achievable performance of the FH/MFSK WSNS employing the proposed noncoherent fusion rules in the specific application scenarios, but also to modify and improve the local sensing and fusion rules according to the specific application environments.

Fifth, in the soft-sensing scenario considered in Chapter 5, the transmission power on the different frequency bands are scaled by the probabilities of the states obtained by the LSNs. However, these probabilities do not equal the useful information of the states, especially when the probabilities of the states are the same or similar. Hence, the improved soft-forward modulation would

use information rather than probability to scale the power on each frequency band. This novel information-based forwarding may improve our WSNs' performance significantly.

Sixth, in our FH/MFSK spectrum sensing system, all the CRSNs are assumed to be equally distributed from the PR users with the same received power. In our future work, more practical scenarios may be considered to assume that the CRSNs are randomly distributed and the received power at the CRSNs from different PR users is different. In this case, an energy threshold may be pre-set to decide whether a CRSN should forward information to the FC. Or a CRSN may be played as a relay to forward informations from the other CRSNs to the FC.

Finally, in this thesis, the FH/MFSK WSNs associated with the proposed fusion rules have only been investigated with the triple-layer type of WSNs. As shown in Chapter 1, there are many other types of WSN structures. Hence, it is highly important to investigate the efficiency of the FH/MFSK WSNs as well as that of the proposed noncoherent fusion rules, when they are applied to the other types of WSNs.

Glossary

$GF(M)$	Galois field
AWGN	additive white Gaussian noise
BFSK	binary frequency-shift-keying
CIR	channel impulse response
CR	cognitive radio
CSI	channel state information
CSMA	carrier sense multiple-access
CV	Chair-Varshney
DTFT	discrete time Fourier transformation
ECP	error classification probability
EGC	equal gain combining
EMAC	energy efficient MAC
ES-EGC	erasure-supported equal gain combining
FC	fusion center
FCC	Federal Communications Commission

FFH fast frequency-hopping

FFT fast Fourier transform

FH frequency-hopping

FH/MFSK frequency-hopping M-ary frequency shift keying

FLAMA flow-aware medium access

G-MAC gateway MAC

IC interference cancellation

ID identification

IIC iterative interference cancellation

LLR log-likelihood ration

LR likelihood-ratio

LRT likelihood ratio test

LSN local sensor node

MAC medium access control

MEMS micro-electromechanical systems

MF matched filter

MFSK M-ary frequency-shift keying

MGF moment generating function

ML maximum likelihood

MMAC mobility adaptive MAC

MMSN multi-frequency MAC for WSNs

MRC maximum ratio combining

MV majority vote

NNC noise-normalization combing

NP Neyman-Pearson

NTIA	National Telecommunication and Information Administration
PAPR	low peak-to-average power ratio
PBPO	person-by-person optimization
PC	product combing
PDF	probability density function
PMAC	position-enabled MAC
PR	primary radio
PSD	power-spectral density
SC	selection combing
SE	source event
SLC	soft-limiting combining
SLD-SMAP	shrink local decisions aided sub-optimum MAP
SMACS	self-organizing MAC for sensor networks
SNC	self-normalization combing
SNR	signal-to-noise ratio
TDMA	time-division multiple-access
TRAMA	traffic adaptive medium access
WSN	wireless sensor network

Bibliography

[1] R. Rajagopalan and P. K. Varshney, "Data-aggregation techniques in sensor networks: A survey," *IEEE Communications Surveys Tutorials*, vol. 8, pp. 48 – 63, 4th Quarter 2006.

[2] N. Kimura and S. Latifi, "A survey on data compression in wireless sensor networks," in *International Conference on Information Technology: Coding and Computing (ITCC'05)*, vol. 2, pp. 8 – 13, April 2005.

[3] T. Q. S. Quek, M. Z. Win, and D. Dardari, "Energy efficiency of dense wireless sensor networks: To cooperate or not to cooperate," in *IEEE International Conference on Communications (ICC'06)*, vol. 10, pp. 4479 – 4484, June 2006.

[4] S. Appadwedula, V. V. Veeravalli, and D. L. Jones, "Energy-efficient detection in sensor networks," *IEEE Journal on Selected Areas in Communications*, vol. 23, pp. 693 – 702, April 2005.

[5] T. Q. S. Quek, D. Dardari, and M. Z. Win, "Energy efficiency of dense wireless sensor networks: To cooperate or not to cooperate," *IEEE Journal on Selected Areas in Communications*, vol. 25, pp. 459 – 470, February 2007.

[6] C. Yao, P.-N. Chen, T.-Y. Wang, Y. Han, and P. K. Varshney, "Performance analysis and code design for minimum hamming distance fusion in wireless sensor networks," *IEEE Transactions on Information Theory*, vol. 53, pp. 1716 – 1734, May 2007.

[7] H. Wang, Y. Yang, M. Ma, J. He, and X. Wang, "Network lifetime maximization with cross-layer design in wireless sensor networks," *IEEE Transactions on Wireless Communications*, vol. 7, pp. 3759 – 3768, October 2008.

[8] A. Kalis and A. G. Kanatas, "Cooperative beam forming in smart dust: Getting rid of multihop communications," *IEEE Pervasive Computing*, vol. 9, pp. 47 – 53, July-September 2010.

[9] P. F. Gorder, "Sizing up smart dust," *Computing in Science Engineering*, vol. 5, pp. 6 – 9, November-December 2003.

[10] R. Viswanathan and P. K. Varshney, "Distributed detection with multiple sensors I. Fundamentals," *IEEE Proceedings*, vol. 85, pp. 54 – 63, January 1997.

[11] P. Sun, X. Zhang, Z. Dong, and Y. Zhang, "A novel energy efficient wireless sensor mac protocol," in *Fourth International Conference on Networked Computing and Advanced Information Management (NCM'08)*, vol. 1, pp. 68 – 72, September 2008.

[12] A. Bachir, M. Dohler, T. Watteyne, and K. K. Leung, "Mac essentials for wireless sensor networks," *IEEE Communications Surveys Tutorials*, vol. 12, pp. 222 – 248, Quarter 2010.

[13] A. C. V. Gummalla and J. O. Limb, "Wireless medium access control protocols," *IEEE Communications Surveys Tutorials*, vol. 3, pp. 2 – 15, Quarter 2000.

[14] I. Stojmenovic and X. Lin, "Power-aware localized routing in wireless networks," *IEEE Transactions on Parallel and Distributed Systems*, vol. 12, pp. 1122 – 1133, November 2001.

[15] D. Wang, B. Xie, and D. P. Agrawal, "Coverage and lifetime optimization of wireless sensor networks with Gaussian distribution," *IEEE Transactions on Mobile Computing*, vol. 7, pp. 1444 – 1458, December 2008.

[16] N. Moreira, M. Venda, C. Silva, L. Marcelino, and A. Pereira, "@sensor - mobile application to monitor a WSN," in *6th Iberian Conference on Information Systems and Technologies (CISTI'11)*, pp. 1 – 6, June 2011.

[17] J.-Q. Xu, H.-C. Wang, F.-G. Lang, P. Wang, and Z.-P. Hou, "Study on WSN topology division and lifetime," in *IEEE International Conference on Computer Science and Automation Engineering (CSAE'11)*, vol. 1, pp. 380 – 384, June 2011.

[18] E. Ding, Y. Huang, H. Huang, W. Yu, and X. Liu, "A linear-hierarchy WSN topology used in coal face," in *4th International Conference on New Trends in Information Science and Service Science (NISS'10)*, pp. 159 – 163, May 2010.

[19] P. K. Varshney, *Distributed Detection and Data Fusion*. Springer-Verlag, 1997.

[20] H. Takagi and L. Kleinrock, "Throughput analysis for persistent CSMA systems," *IEEE Transactions on Communications*, vol. 33, pp. 627 – 638, July 1985.

[21] C. Guo, L. C. Zhong, and J. M. Rabaey, "Low power distributed MAC for ad hoc sensor radio networks," in *IEEE Global Telecommunications Conference (GLOBECOM'01)*, vol. 5, pp. 2944 – 2948, 2001.

[22] M. I. Brownfield, K. Mehrjoo, A. S. Fayez, and N. J. Davis, "Wireless sensor network energy-adaptive mac protocol," in *IEEE Consumer Communications and Networking Conference (CCNC'06)*, vol. 2, pp. 778 – 782, January 2006.

[23] K.-H. Kwong, T.-T. Wu, C. Michie, and I. Andonovic, "A self-organizing multi-channel medium access control (SMMAC) protocol for wireless sensor networks," in *2nd International Conference on Communications and Networking in China (CHINACOM'07)*, pp. 845 – 849, August 2007.

[24] T. O. Walker, M. Tummala, J. McEachen, and J. B. Michael, "Medium access for hybrid, large-scale wireless networks for missile defense," in *IEEE International Conference on System of Systems Engineering (SoSE'09)*, vol. 30, pp. 1 – 5, June 2009.

[25] V. Rajendran, J. J. Garcia-Luna-Aveces, and K. Obraczka, "Energy-efficient, application-aware medium access for sensor networks," in *IEEE International Conference on Mobile Adhoc and Sensor Systems*, pp. 1 – 8, November 2005.

[26] V. Hoesel, T. Nieberg, H. J. Kip, and P. J. M. Havinga, "Advantages of a TDMA based, energy-efficient, self-organizing mac protocol for WSNs," in *IEEE Conference on Vehicular Technology (VTC'04-Spring)*, vol. 3, pp. 1598 – 1602, May 2004.

[27] N. P. Khan and C. Boncelet, "PMAC: Energy efficient medium access control protocol for wireless sensor networks," in *IEEE Conference on Military Communications (MILCOM'06)*, pp. 1 – 5, October 2006.

[28] M. Ali, T. Suleman, and Z. A. Uzmi, "MMAC: A mobility-adaptive, collision-free MAC protocol for wireless sensor networks," in *IEEE International Performance, Computing, and Communications Conference (IPCCC'05)*, pp. 401 – 407, April 2005.

[29] G. Zhou, C. Huang, T. Yan, T. He, J. A. Stankovic, and T. F. Abdelzaher, "MMSN: Multi-frequency media access control for wireless sensor networks," in *Proceedings of IEEE International Conference on Computer Communications (INFOCOM'06)*, pp. 1 – 13, April 2006.

[30] H. Fattah and C. Leung, "An overview of scheduling algorithms in wireless multimedia networks," *IEEE Wireless Communications*, vol. 9, pp. 76 – 83, October 2002.

[31] Q. Wang and W. Yang, "Energy consumption model for power management in wireless sensor networks," in *IEEE Communications Society Conference on Sensor, Mesh and Ad Hoc Communications and Networks (SECON'07)*, pp. 142 – 151, June 2007.

[32] W. Ye, J. Heidemann, and D. Estrin, "Medium access control with coordinated adaptive sleeping for wireless sensor networks," *IEEE/ACM Transactions on Networking*, vol. 12, pp. 493 – 506, June 2004.

[33] Y. Ding, C. Wang, and L. Xiao, "An adaptive partitioning scheme for sleep scheduling and topology control in wireless sensor networks," *IEEE Transactions on Parallel and Distributed Systems*, vol. 20, pp. 1352 – 1365, September 2009.

[34] Y. Chen and Q. Zhao, "On the lifetime of wireless sensor networks," *IEEE Communications Letters*, vol. 9, pp. 976 – 978, November 2005.

[35] M. Bhardwaj, T. Garnett, and A. P. Chandrakasan, "Upper bounds on the lifetime of sensor networks," in *IEEE International Conference on Communications (ICC'01)*, vol. 3, pp. 785 – 790, 2001.

[36] M. Bhardwaj and A. P. Chandrakasan, "Bounding the lifetime of sensor networks via optimal role assignments," in *Proceedings of 21st Annual Joint Conference of the IEEE Computer and Communications Societies (INFOCOM'02)*, vol. 3, pp. 1587 – 1596, 2002.

[37] V. Shah-Mansouri and V. W. S. Wong, "Bounds for lifetime maximization with multiple sinks in wireless sensor networks," in *IEEE Pacific Rim Conference on Communications, Computers and Signal Processing (PacRim'07)*, pp. 82 – 85, August 2007.

[38] Z. Hu and B. Li, "On the fundamental capacity and lifetime limits of energy-constrained wireless sensor networks," in *Proceedings of IEEE Real-Time and Embedded Technology and Applications Symposium (RTAS'04)*, pp. 2 – 9, May 2004.

[39] T. Harms, S. Sedigh, and F. Bastianini, "Structural health monitoring of bridges using wireless sensor networks," *IEEE Instrumentation Measurement Magazine*, vol. 13, pp. 14 – 18, December 2010.

[40] D. Ye, D. Gong, and W. Wang, "Application of wireless sensor networks in environmental monitoring," in *2nd International Conference on Power Electronics and Intelligent Transportation System (PEITS'09)*, vol. 1, pp. 205 – 208, December 2009.

[41] A. Hu, "Applications of environmental security monitoring based on WSN in substation," in *4th International Congress on Image and Signal Processing (CISP'11)*, vol. 5, pp. 2806 – 2808, October 2011.

[42] M. Dunbabin and L. Marques, "Robots for environmental monitoring: Significant advancements and applications," *IEEE Robotics Automation Magazine*, vol. 19, pp. 24 – 39, March 2012.

[43] C. Alippi, R. Camplani, C. Galperti, and M. Roveri, "A robust, adaptive, solar-powered WSN framework for aquatic environmental monitoring," *IEEE Sensors Journal*, vol. 11, pp. 45 – 55, January 2011.

[44] J. A. Fraile, J. Bajo, J. M. Corchado, and A. Abraham, "Applying wearable solutions in dependent environments," *IEEE Transactions on Information Technology in Biomedicine*, vol. 14, pp. 1459 – 1467, November 2010.

[45] G. D. Abowd, G. R. Hayes, G. Iachello, J. A. Kientz, S. N. Patel, M. M. Stevens, and K. N. Truong, "Prototypes and paratypes: Designing mobile and ubiquitous computing applications," *IEEE Pervasive Computing*, vol. 4, pp. 67 – 73, October-December 2005.

[46] M. Akay, M. Sekine, T. Tamura, Y. Higashi, and T. Fujimoto, "Unconstrained monitoring of body motion during walking," *IEEE Engineering in Medicine and Biology Magazine*, vol. 22, pp. 104 – 109, May-June 2003.

[47] A. A. Freitas, D. C. Wieser, and R. Apweiler, "On the importance of comprehensible classification models for protein function prediction," *IEEE/ACM Transactions on Computational Biology and Bioinformatics*, vol. 7, pp. 172 – 182, January-March 2010.

[48] S. Wernicke, "Efficient detection of network motifs," *IEEE/ACM Transactions on Computational Biology and Bioinformatics*, vol. 3, pp. 347 – 359, October-December 2006.

[49] J. Paradiso, G. Borriello, and P. Bonato, "Implantable electronics," *IEEE Pervasive Computing*, vol. 7, pp. 12 – 13, January-March 2008.

[50] Y.-M. Chen, W. Shen, H.-W. Huo, and Y.-Z. Xu, "A smart gateway for health care system using wireless sensor network," in *International Conference on Sensor Technologies and Applications (SENSORCOMM'10)*, pp. 545 – 550, July 2010.

[51] E. Strommer, J. Kaartinen, J. Parkka, A. Ylisaukko-oja, and I. Korhonen, "Application of near field communication for health monitoring in daily life," in *IEEE Conference of the Engineering in Medicine and Biology Society (EMBS'06)*, pp. 3246 – 3249, September 2006.

[52] K. Hung and Y.-T. Zhang, "Implementation of a WAP-based telemedicine system for patient monitoring," *IEEE Transactions on Information Technology in Biomedicine*, vol. 7, pp. 101 – 107, June 2003.

[53] C.-C. Lin, P.-Y. Lin, P.-K. Lu, G.-Y. Hsieh, W.-L. Lee, and R.-G. Lee, "A healthcare integration system for disease assessment and safety monitoring of dementia patients," *IEEE Transactions onInformation Technology in Biomedicine*, vol. 12, pp. 579 – 586, September 2008.

[54] J. M. Corchado, J. Bajo, and A. Abraham, "Gerami: Improving healthcare delivery in geriatric residences," *IEEE Intelligent Systems*, vol. 23, no. 2, pp. 19 – 25, 2008.

[55] A. Dogandzic and B. Zhang, "Distributed estimation and detection for sensor networks using hidden Markov random field models," *IEEE Transactions on Signal Processing*, vol. 54, pp. 3200 – 3215, August 2006.

[56] F. Kelly, "Charging and rate control for elastic traffic," *European Transactions on Telecommunications*, vol. 8, pp. 33 – 37, 1999.

[57] S. H. Low and D. E. Lapsley, "Optimization flow control. I. Basic algorithm and convergence," *IEEE/ACM Transactions on Networking*, vol. 7, pp. 861 – 874, December 1999.

[58] M. Chiang, S. H. Lowand, A. R. Calderbank, and J. C. Doyle, "Layering as optimization decomposition: A mathematical theory of network architectures," *Proceedings of the IEEE*, vol. 95, pp. 255 – 312, January 2007.

[59] R. J. La and V. Anantharam, "Utility-based rate control in the internet for elastic traffic," *IEEE/ACM Transactions on Networking*, vol. 10, pp. 272 – 286, April 2002.

[60] M. Chiang, "Balancing transport and physical layers in wireless multihop networks: Jointly optimal congestion control and power control," *IEEE Journal on Selected Areas in Communications*, vol. 23, pp. 104 – 116, January 2005.

[61] X. Wang and K. Kar, "Cross-layer rate optimization for proportional fairness in multihop wireless networks with random access," *IEEE Journal on Selected Areas in Communications*, vol. 24, pp. 1548 – 1559, August 2006.

[62] X. Lin and N. B. Shroff, "Joint rate control and scheduling in multihop wireless networks," in *IEEE Conference on Decision and Control (CDC'04)*, vol. 2, pp. 1484 – 1489, December 2004.

[63] L. Chen, S. H. Low, and J. C. Doyle, "Joint congestion control and media access control design for ad hoc wireless networks," in *Proceedings of the 24th Annual Joint Conference of the IEEE Computer and Communications Societies (INFOCOM'05)*, vol. 3, pp. 2212 – 2222, March 2005.

[64] S. Eswaran, A. Misra, and T. L. Porta, "Utility-based adaptation in mission-rriented wireless sensor networks," in *IEEE Communications Society Conference on Sensor, Mesh and Ad Hoc Communications and Networks (SECON'08)*, pp. 278 – 286, June 2008.

[65] L. Pescosolido and C. Petrioli, "Wireless sensor networks for spectrum sensing to support opportunistic spectrum access networks: Protocol design and fundamental trade-offs," in

IEEE Wireless Communications and Networking Conference (WCNC'11), pp. 422 – 427, March 2011.

[66] A. A. Sreesha, S. Somal, and I.-T. Lu, "Cognitive radio based wireless sensor network architecture for smart grid utility," in *IEEE Long Island Systems, Applications and Technology Conference (LISAT'11)*, pp. 1 – 7, May 2011.

[67] B. M. *et al*., "Sensor networks for cognitive radio: Theory and system design," in *ICT-MobileSummit*, pp. 10 – 12, June 2008.

[68] V. Fodor, I. Glaropoulos, and L. Pescosolido, "Detecting low-power primary signals via distributed sensing to support opportunistic spectrum access," in *IEEE International Conference on Communications (ICC'09)*, pp. 1 – 6, June 2009.

[69] A. S. Zahmati, S. Hussain, X. Fernando, and A. Grami, "Cognitive wireless sensor networks: Emerging topics and recent challenges," in *IEEE Toronto International Conference Science and Technology for Humanity (TIC-STH'09)*, pp. 593 – 596, 2009.

[70] M. Naraghi-Pour and T. Ikuma, "Autocorrelation-based spectrum sensing for cognitive radios," *IEEE Transactions on Vehicular Technology*, vol. 59, pp. 718 –733, February 2010.

[71] Z. Han, R. Fan, and H. Jiang, "Replacement of spectrum sensing in cognitive radio," *IEEE Transactions on Wireless Communications*, vol. 8, no. 6, pp. 2819 – 2826, 2009.

[72] N. Shankar, C. Cordeiro, and K. Challapali, "Spectrum agile radios: Utilization and sensing architectures," in *IEEE International Symposium on New Frontiers in Dynamic Spectrum Access Networks (DySPAN'05)*, pp. 160 – 169, 2005.

[73] A. Nahvi, V. Fodor, and I. Glaropoulos, "Performance of deterministic local sensing aggregation under interference," in *Proceedings of the 5th International Conference on Cognitive Radio Oriented Wireless Networks Communications (CROWNCOM'10)*, pp. 1 – 5, 2010.

[74] R. Niu, B. Chen, and P. K. Varshney, "Fusion of decisions transmitted over Rayleigh fading channels in wireless sensor networks," *IEEE Transactions on Signal Processing*, vol. 54, pp. 1018 – 1027, March 2006.

[75] B. Chen, L. Tong, and P. K. Varshney, "Channel-aware distributed detection in wireless sensor networks," *IEEE Signal Processing Magazine*, vol. 23, pp. 16 – 26, July 2006.

[76] B. Chen, R. Jiang, T. Kasetkasem, and P. K. Varshney, "Channel aware decision fusion in wireless sensor networks," *IEEE Transactions on Signal Processing*, vol. 52, pp. 3454 – 3458, December 2004.

[77] I. Y. Hoballah and P. K. Varshney, "An information theoretic approach to the distributed detection problem," *IEEE Transactions on Information Theory,*, vol. 35, pp. 988 – 994, September 1989.

[78] W. Li and H. Dai, "Distributed detection in wireless sensor networks using a multiple access channel," *IEEE Transactions on Signal Processing*, vol. 55, pp. 822 – 833, March 2007.

[79] Y. Lin, B. Chen, and P. K. Varshney, "Decision fusion rules in multi-hop wireless sensor networks," *IEEE Transactions on Aerospace and Electronic Systems*, vol. 41, pp. 475 – 488, April 2005.

[80] T.-Y. Wang, Y. S. Han, B. Chen, and P. K. Varshney, "A combined decision fusion and channel coding scheme for distributed fault-tolerant classification in wireless sensor networks," *IEEE Transactions on Wireless Communications*, vol. 5, pp. 1695 – 1705, July 2006.

[81] R. Jiang and B. Chen, "Fusion of censored decisions in wireless sensor networks," *IEEE Transactions on Wireless Communications*, vol. 4, pp. 2668 – 2673, November 2005.

[82] S. A. Aldosari and J. M. F. Moura, "Detection in sensor networks: The saddlepoint approximation," *IEEE Transactions on Signal Processing*, vol. 55, pp. 327 – 340, January 2007.

[83] R. R. Tenney and N. R. Sandell, "Detection with distributed sensors," *IEEE Transactions on Aerospace and Electronic Systems*, vol. AES-17, pp. 501 – 510, July 1981.

[84] Z. Chair and P. K.Varshney, "Optimal data fusion in multiple sensor detection systems," *IEEE Transactions on Aerospace and Electronic Systems*, vol. 19, pp. 98 – 101, January 1986.

[85] C. Rago, P. Willett, and Y. Bar-Shalom, "A low communication rate scheme for distributed detection," in *American Control Conference*, pp. 166 – 170, June 1993.

[86] F. Gini, F. Lombardini, and L. Verrazzani, "Decentralised detection strategies under communication constraints," *IEE Proceedings of Radar, Sonar and Navigation*, vol. 145, pp. 199 – 208, August 1998.

[87] C.-T. Yu and P. K. Varshney, "Bit allocation for discrete signal detection," *IEEE Transactions on Communications,*, vol. 46, pp. 173 – 175, February 1998.

[88] J. Hu and R. S. Blum, "On the optimality of finite-level quantizations for distributed signal detection," *IEEE Transactions on Information Theory*, vol. 47, pp. 1665 – 1671, May 2001.

[89] J.-F. Chamberland and V. V. Veeravalli, "Decentralized detection in sensor networks," *IEEE Transactions on Signal Processing*, vol. 51, pp. 407 – 416, February 2003.

[90] L.-L. Yang, K. Yen, and L. Hanzo, "A Reed-Solomon coded DS-CDMA system using noncoherent M-ary orthogonal modulation over multipath fading channels," *IEEE Journal on Selected Areas in Communications*, vol. 18, pp. 2240 – 2251, November 2000.

[91] K. C. Teh, A. Kot, and K. H. Li, "Partial-band jamming rejection of FFH/BFSK with product combining receiver over a Rayleigh-fading channel," *IEEE Communications Letters*, vol. 1, pp. 64 – 66, May 1997.

[92] R. C. Robertson and T. T. Ha, "Error probabilities of fast frequency-hopped MFSK with noise-normalization combining in a fading channel with partial-band interference," *IEEE Transactions on Communications*, vol. 40, pp. 404 – 412, February 1992.

[93] K. C. Teh, A. C. Kot, and K. H. Li, "Multitone jamming rejection of FFH/BFSK spread-spectrum system over fading channels," *IEEE Transactions on Communications*, vol. 46, pp. 1050 – 1057, August 1998.

[94] B. Chen, R. Jiang, T. Kasetkasem, and P. K. Varshney, "Fusion of decisions transmitted over fading channels in wireless sensor networks," in *36th Asilomar Conference on Signals, Systems and Computers*, vol. 2, pp. 1184 – 1188, November 2002.

[95] A. Nandi and S. Kundu, "Optimal transmit power in wireless sensor networks using MRC space diversity in Rayleigh fading channel," in *International Conference on Industrial and Information Systems (ICIIS'10)*, pp. 19 – 24, 29 July-1 August 2010.

[96] S. C. A. Thomopoulos and L. Zhang, "Distributed decision fusion with networking delays and channel errors," *Information Science*, vol. 66, pp. 91 – 118, December 1992.

[97] G. Zhao, J. Ma, G. Y. Li, T. Wu, Y. Kwon, A. Soong, and C. Yang, "Spatial spectrum holes for cognitive radio with relay-assisted directional transmission," *IEEE Transactions onWireless Communications*, vol. 8, pp. 5270 – 5279, October 2009.

[98] B. Chen and P. K. Varshney, "A Bayesian sampling approach to decision fusion using hierarchical models," *IEEE Transactions on Signal Processing*, vol. 50, pp. 1809 – 1818, August 2002.

[99] A. D. Whalen, *Detection of Signals in Noise*. New York, USA: Academic Press, 1971.

[100] C. W. Helstrom, *Statistical Theory of Signal Detection*. Pergamon, 1960.

[101] M. Barkat, *Signal Detection and Estimation*. Boston, Mass: Artech House, 1991.

[102] L. L. Scharf, *Statistical Signal Processing : Detection, Estimation, and Time Series Analysis*. Addison-Wesley, 1991.

[103] A. Swami, Q. Zhao, Y.-W. Hong, and L. Tong, *Wireless Sensor Networks: Signal Processing and Communications Perspectives*. England: John Wiley & Sons, 2006.

[104] Q. Tian and E. J. Coyle, "Optimal distributed detection in clustered wireless sensor networks," *IEEE Transactions on Signal Processing*, vol. 55, pp. 3892 – 3904, July 2007.

[105] Z. Chair and P. K. Varshney, "Neyman-Pearson hypothesis testing in distributed networks," in *26th IEEE Conference on Decision and Control, 1987*, vol. 26, pp. 1842 – 1843, December 1987.

[106] H. L. V. Trees, *Detection, Estimation, and Modulation Theory*. Wiley, 1968.

[107] I. Y. Hoballah and P. K. Varshney, "Neyman-Pearson detection wirh distributed sensors," in *25th IEEE Conference on Decision and Control*, vol. 25, pp. 237 – 241, December 1986.

[108] R. S. Blum, "Necessary conditions for optimum distributed sensor detectors under the Neyman-Pearson criterion," *IEEE Transactions on Information Theory*, vol. 42, pp. 990 – 994, May 1996.

[109] J. Plata-Chaves, M. Lazaro, and A. Artes-Rodriguez, "Optimal Neyman-Pearson fusion in two-dimensional sensor networks with serial architecture and dependent observations," in *Proceedings of the 14th International Conference on Information Fusion (FUSION'11)*, pp. 1 – 6, July 2011.

[110] R. S. Blum, "Necessary conditions for N distributed sensor detectors connected in parallel under the Neyman-Pearson criterion," in *Proceedings of IEEE International Symposium on Information Theory*, p. 254, June-July 1994.

[111] N. C. Beaulieu and X. Dong, "Level crossing rate and average fade duration of MRC and EGC diversity in Ricean fading," *IEEE Transactions on Communications*, vol. 51, pp. 722 – 726, May 2003.

[112] F. Altman and W. Sichak, "A simplified diversity communication system for beyond-the-horizon links," *IRE Transactions on Communications Systems*, vol. 4, pp. 50 – 55, March 1956.

[113] A. Ramesh, A. Chockalingam, and L. B. Milstein, "SNR estimation in Nakagami-*m* fading with diversity combining and its application to turbo decoding," *IEEE Transactions on Communications*, vol. 50, pp. 1719 – 1724, November 2002.

[114] D. G. Brennan, "Linear diversity combining techniques," *Proceedings of the IEEE*, vol. 91, pp. 331 – 356, February 2003.

[115] J. G. Proakis, *Digital Communications, 4th edn.* USA: Mc Graw Hill, 2006.

[116] L.-L. Yang, *Multicarrier Communications*. United Kingdom: John Wiley, 2009.

[117] F. Yang, L.-L. Yang, H. Wei, and L. Sun, "Frequency-hopping/M-ary frequency-shift keying for wireless sensor networks: Noncoherent detection and performance," in *7th International Symposium on Wireless Communication Systems (ISWCS'10)*, pp. 135 – 139, September 2010.

[118] M. Z. Win and R. K. Mallik, "Error analysis of noncoherent M-ary FSK with postdetection EGC over correlated Nakagami and Rician channels," in *IEEE International Conference on Communications (ICC'01)*, vol. 7, pp. 2241 – 2245, 2001.

[119] M. K. Slimon and M.-S. Alouini, *Digital Communication over Fading Channles, 2nd edn*. Wiley-IEEE Press, 2005.

[120] J. Proakis, "On the probability of error for multichannel reception of binary signals," *IEEE Transactions on Communication Technology*, vol. 16, no. 1, pp. 68 – 71, 1968.

[121] W. C. Lindsey, "Error probabilities for Rician fading multichannel reception of binary and n -ary signals," *IEEE Transactions on Information Theory*, vol. 10, no. 4, pp. 339 – 350, 1964.

[122] U. Charash, "Reception through Nakagami fading multipath channels with random delays," *IEEE Transactions on Communications*, vol. 27, no. 4, pp. 657 – 670, 1979.

[123] C.-H. Chu, C.-H. Wang, C.-K. Liang, W. Ouyang, J.-H. Cai, and Y.-H. Chen, "High-accuracy indoor personnel tracking system with a zigbee wireless sensor network," in *7th International Conference on Mobile Ad-hoc and Sensor Networks (MSN'11)*, pp. 398 – 402, December 2011.

[124] B. Moslem, M. Khalil, M. O. Diab, and C. Marque, "Classification of multichannel uterine EMG signals by using a weighted majority voting decision fusion rule," in *16th IEEE Mediterranean Electrotechnical Conference (MELECON'12)*, pp. 331 – 334, March 2012.

[125] S. Zhang, L.-L. Yang, and Y. Zhang, "Fast frequency-hopping dynamic multiple-access for cognitive radios: Noncoherent interference cancellation," in *7th International Symposium on Wireless Communication Systems (ISWCS'10)*, pp. 1051 – 1055, September 2010.

[126] H. Peng, C. Lin, L. Luo, and Q. Zhou, "Accuracy of classifier combining based on majority voting," in *IEEE International Conference on Control and Automation (ICCA'07)*, pp. 2654 – 2658, 2007.

[127] L. Lam and C. Y. Suen, "Application of majority voting to pattern recognition: An analysis of its behavior and performance," *IEEE Transactions on Systems, Man and Cybernetics*, vol. 27, no. 5, pp. 553 – 568, 1997.

[128] J. Kittle, M. Hatef, R. P. W. Duin, and J. Matas, "On combining classifiers," *IEEE Transactions on Pattern Analysis and Machine Intelligence*, vol. 20, no. 3, pp. 226 – 239, 1998.

[129] M.-S. Alouini and M. Simon, "An MGF-based performance analysis of generalized selection combining over Rayleigh fading channels," *IEEE Transactions on Communications*, vol. 48, pp. 401 – 415, March 2000.

[130] R. Viswanathan and K. Taghizadeh, "Diversity combining in FH/BFSK systems to combat partial band jamming," *IEEE Transactions on Communications*, vol. 36, pp. 1062 – 1069, September 1988.

[131] C. M. Keller and M. B. Pursley, "Diversity combining for channels with fading and partial-band interference," *IEEE Journal on Selected Areas in Communications*, vol. 5, no. 2, pp. 248 – 260, 1987.

[132] S. Ahmed, L.-L. Yang, and L. Hanzo, "Diversity combining for fast frequency hopping multiple access systems subjected to Nakagami-*m* fading," in *IEE International Conference on 3G and Beyond*, pp. 1 – 5, 2005.

[133] R. Viswanathan and K. Taghizadeh, "Diversity combining in FH/BFSK systems to combat partial band jamming," *IEEE Transactions on Communications*, vol. 36, no. 9, pp. 1062 – 1069, 1988.

[134] K. Teh, A. C. Kot, and K. H. Li, "Performance analysis of an FFH/BFSK product-combining receiver under multitone jamming," *IEEE Transactions on Vehicular Technology*, vol. 48, no. 6, pp. 1946 – 1953, 1999.

[135] K. C. Teh, A. C. Kot, and K. H. Li, "Performance analysis of an FFH/BFSK product-combining receiver with multitone jamming over Rician-fading channels," in *IEEE Vehicular Technology Conference Proceedings (VTC'00-Spring)*, vol. 2, pp. 1508 – 1512, 2000.

[136] J. Lee, L. Miller, and R. French, "The analyses of uncoded performances for certain ECCM receiver design strategies for multihops/symbol FH/MFSK waveforms," *IEEE Journal on Selected Areas in Communications*, vol. 3, pp. 611 – 621, September 1985.

[137] J. S. Lee, R. H. French, and L. E. Miller, "Error-correcting codes and nonlinear diversity combining against worst case partial-band noise jamming of frequency-hopping MFSK systems," *IEEE Transactions on Communications*, vol. 36, pp. 471 – 478, April 1988.

[138] J. Lee, L. Miller, and Y. Kim, "Probability of error analyses of a BFSK frequency-hopping system with diversity under partial-band jamming interference–Part II: Performance of square-law nonlinear combining soft decision receivers," *IEEE Transactions on Communications*, vol. 32, pp. 1243 – 1250, December 1984.

[139] L. ping Zhu, Y. Yao, and Y.-S. Zhu, "Antijam performance of FFH/BFSK with noise-normalization combining in a Nakagami-m fading channel with partial-band interference," *IEEE Communications Letters*, vol. 10, no. 6, pp. 429 – 431, 2006.

[140] L. Miller, J. Lee, and A. Kadrichu, "Probability of error analyses of a BFSK frequency-hopping system with diversity under partial-band jamming interference–Part III: Performance of a square-law self-normalizing soft decision receiver," *IEEE Transactions on Communications*, vol. 34, pp. 669 – 675, July 1986.

[141] R. C. Robertson and T. T. Ha, "Error probabilities of fast frequency-hopped FSK with self-normalization combining in a fading channel with partial-band interference," *IEEE Journal on Selected Areas in Communications*, vol. 10, pp. 714 – 723, May 1992.

[142] O.-C. Yue, "Maximum likelihood combining for noncoherent and differentially coherent frequency-hopping multiple-access systems," *IEEE Transactions on Information Theory*, vol. 28, no. 4, pp. 631 – 639, 1982.

[143] C. P. Hung and Y.-T. Su, "Diversity combining considerations for incoherent frequency hopping multiple access systems," *IEEE Journal on Selected Areas in Communications*, vol. 13, no. 2, pp. 333 – 344, 1995.

[144] D. Cabric, A. Tkachenko, and R. W. Brodersen, "Spectrum sensing measurements of pilot, energy, and collaborative detection," in *IEEE Military Communications Conference (MILCOM'06)*, pp. 1 – 7, October 2006.

[145] S. Haykin, "Cognitive radio: brain-empowered wireless communications," *IEEE Journal on Selected Areas in Communications*, vol. 23, pp. 201 – 220, February 2005.

[146] R. Tandra and A. Sahai, "SNR walls for signal detection," *IEEE Journal of Selected Topics in Signal Processing*, vol. 2, pp. 4 – 17, February 2008.

[147] R. Tandra and A. Sahai, "Fundamental limits on detection in low SNR under noise uncertainty," in *International Conference on Wireless Networks, Communications and Mobile Computing*, vol. 1, pp. 464 – 469, June 2005.

[148] E. Axell, G. Leus, and E. G. Larsson, "Overview of spectrum sensing for cognitive radio," in *2nd International Workshop on Cognitive Information Processing (CIP'10)*, pp. 322 – 327, June 2010.

[149] D. Bhargavi and C. R. Murthy, "Performance comparison of energy, matched-filter and cyclostationarity-based spectrum sensing," in *IEEE Eleventh International Workshop on Signal Processing Advances in Wireless Communications (SPAWC'06)*, pp. 1 – 5, June 2006.

[150] W. Wang, "Spectrum sensing for cognitive radio," in *International Symposium on Intelligent Information Technology Application Workshops (IITAW '09)*, pp. 410 – 412, November 2009.

[151] J. Ma, G. Y. Li, and B. H. Juang, "Signal processing in cognitive radio," *Proceedings of the IEEE*, vol. 97, pp. 805 – 823, May 2009.

[152] Z. Quan, S. Cui, H. V. Poor, and A. H. Sayed, "Collaborative wideband sensing for cognitive radios," *IEEE Signal Processing Magazine*, vol. 25, pp. 60 – 73, November 2008.

[153] H.-S. Chen, W. Gao, and D. G. Daut, "Signature based spectrum sensing algorithms for IEEE 802.22 WRAN," in *IEEE International Conference on Communications (ICC'07)*, pp. 6487 – 6492, June 2007.

[154] A. V. Dandawate and G. B. Giannakis, "Statistical tests for presence of cyclostationarity," *IEEE Transactions on Signal Processing*, vol. 42, pp. 2355 – 2369, September 1994.

[155] K. Letaief and W. Zhang, "Cooperative communications for cognitive radio networks," *Proceedings of the IEEE*, vol. 97, pp. 878 – 893, May 2009.

[156] A. Kortun, T. Ratnarajah, M. Sellathurai, C. Zhong, and C. B. Papadias, "On the performance of eigenvalue-based cooperative spectrum sensing for cognitive radio," *IEEE Journal of Selected Topics in Signal Processing*, vol. 5, pp. 49 – 55, February 2011.

[157] T. J. Lim, R. Zhang, Y.-C. Liang, and Y. Zeng, "GLRT-based spectrum sensing for cognitive radio," in *IEEE Global Telecommunications Conference (GLOBECOM'08)*, pp. 1 – 5, November 2008.

[158] Y. Zeng and Y.-C. Liang, "Eigenvalue-based spectrum sensing algorithms for cognitive radio," *IEEE Transactions on Communications*, vol. 57, pp. 1784 – 1793, June 2009.

[159] F. Penna, R. Garello, and M. Spirito, "Cooperative spectrum sensing based on the limiting eigenvalue ratio distribution in Wishart matrices," *IEEE Communications Letters*, vol. 13, pp. 507 – 509, July 2009.

[160] V. V. Veeravalli and J.-F. Chamberland, *Detection in Sensor Networks*. England: John Wiley & Sons, 2007.

[161] P. V. Sukhatme, "Tests of significance for samples of the χ^2 population with two degrees of freedom," *Ann.Eugenics*, vol. 8, pp. 52 – 56, 1937.

[162] D. S. Mitrinović and J. D. Keckic, *The Cauchy Method of Residues : Theory and Applications, 1st edn*. Holland: D. Reidel Publishing Company, 1984.

[163] A. Lei and R. Schober, "Coherent max-log decision fusion in wireless sensor networks," *IEEE Transactions on Communications*, vol. 58, May 2010.

[164] A. Lei and R. Schober, "Multiple-symbol differential decision fusion for mobile wireless sensor networks," *IEEE Transactions on Wireless Communications*, vol. 9, February 2010.

[165] V. Kanchumarthy, R. Viswanathan, and M. Madishetty, "Impact of channel errors on decentralized detection performance of wireless sensor networks: A study of binary modulation, Rayleigh fading and nonfading channels, and fusion-combiners," *IEEE Transactions on Signal Processing*, vol. 56, May 2008.

[166] S. Verdú, *Multiuser Detection*. United Kingdom: Cambridge University Press, 1998.

[167] D. Divsalar, M. K. Simon, and D. Raphaeli, "Improved parallel interference cancellation for CDMA," *IEEE Transactions on Communications*, vol. 46, no. 2, pp. 258–268, 1998.

[168] N. Miridakis and D. Vergados, "A survey on the successive interference cancellation performance for single-antenna and multiple-antenna ofdm systems," *Communications Surveys Tutorials, IEEE*, vol. 15, no. 1, pp. 312–335, 2013.

[169] J. G. Andrews, "Interference cancellation for cellular systems: a contemporary overview," *IEEE Wireless Communications*, vol. 12, no. 2, pp. 19–29, 2005.

[170] Z. Yu, T. T. Tjhung, and C. C. Chai, "Performance of MC-MFSK systems with IIC-based multiuser detection over Rayleigh fading channels," in *IEEE Global Telecommunications Conference (GLOBECOM'04)*, vol. 2, pp. 893 – 897, December 2004.

[171] D. J. Goodman, P. S. Henry, and V. K. Prabhu, "Frequency-hopped multilevel FSK for mobile radio," *Bell System Technical Journal*, vol. 59, pp. 1257 – 1275, September 1980.

[172] G. Einarsson, "Address assignment for a time-frequency-coded, spread-spectrum system," *Bell System Technical Journal*, vol. 59, pp. 1241 – 1255, September 1980.

[173] L. Hanzo, L.-L. Yang, E.-L. Kuan, and K. Yen, *Single and Multi-Cariier DS-CDMA: Multiuser Detection, Space Time Spreading, Synchronisation and Standards*. United Kingdom: John Wiley and Sons, 2005.

[174] L.-L. Yang and L. Hanzo, "Low complexity erasure insertion in RS-coded SFH spread-spectrum communications with partial-band interference and Nakagami-*m* fading," *IEEE Transactions on Communications*, vol. 50, pp. 914 – 925, June 2002.

[175] L.-L. Yang and L. Hanzo, "Performance analysis of coded M-ary orthogonal signaling using errors-and-erasures decoding over frequency-selective fading channels," *IEEE Journal on Selected Areas in Communications*, vol. 19, pp. 211 – 221, February 2001.

[176] T. Yucek and H. Arslan, "A survey of spectrum sensing algorithms for cognitive radio applications," *IEEE Communications Surveys Tutorials*, vol. 11, pp. 116 – 130, First Quarter 2009.

[177] L. Wei and O. Tirkkonen, "Cooperative spectrum sensing of OFDM signals using largest eigenvalue distributions," in *IEEE International Symposium on Personal, Indoor and Mobile Radio Communications*, pp. 2295 – 2299, September 2009.

[178] F. F. Digham, M.-S. Alouini, and M. K. Simon, "On the energy detection of unknown signals over fading channels," *IEEE Transactions on Communications*, vol. 55, pp. 21 – 24, January 2007.

[179] J. J. Lehtomaki, M. Juntti, H. Saarnisaari, and S. Koivu, "Threshold setting strategies for a quantized total power radiometer," *IEEE Signal Processing Letters*, vol. 12, pp. 796 – 799, November 2005.

[180] A. V. Dandawate and G. B. Giannakis, "Statistical tests for presence of cyclostationarity," *IEEE Transactions on Signal Processing*, vol. 42, pp. 2355 – 2369, September 1994.

[181] W. A. Gardner and C. M. Spooner, "Signal interception: Performance advantages of cyclic-feature detectors," *IEEE Transactions on Communications*, vol. 40, pp. 149 – 159, January 1992.

[182] S. Wang and R. Nazanin, "Eigenvalue-based cooperative spectrum sensing with finite samples/sensors," in *46th Annual Conference on Information Sciences and Systems (CISS'12)*, pp. 1 – 5, March 2012.

[183] A. Kortun, M. Sellathurai, T. Ratnarajah, and C. Zhong, "Distribution of the ratio of the largest eigenvalue to the trace of complex Wishart matrices," *IEEE Transactions on Signal Processing*, vol. 60, pp. 5527 – 5532, October 2012.

[184] B. Nadler, F. Penna, and R.Garello, "Performance of eigenvalue-based signal detectors with known and unknown noise level," in *IEEE International Conference on Communications (ICC'11)*, pp. 1 – 5, June 2011.

[185] P. Bianchi, M. Debbah, M. Maida, and J. Najim, "Performance of statistical tests for single-source detection using random matrix theory," *IEEE Transactions on Information Theory*, vol. 57, pp. 2400 – 2419, April 2011.

[186] W. Zhang and Y. Sanada, "Cyclostationarity feature matched detection and application to IFDMA system," in *4th International Conference on Cognitive Radio Oriented Wireless Networks and Communications (CROWNCOM'09)*, pp. 1 – 5, 2009.

[187] Z. Chao, W. Zhaocheng, Y. Zhixing, W. Jun, and S. Jian, "Frequency domain decision feedback equalization for uplink SC-FDMA," *IEEE Transactions on Broadcasting*, vol. 56, no. 2, pp. 253–257, 2010.

[188] F. Yang and L.-L. Yang, "Frequency-hopping/M-ary frequency-shift keying wireless sensor network monitoring multiple source events," in *IEEE 75th Vehicular Technology Conference (VTC'12 Spring)*, pp. 1 – 5, 2012.

[189] F. Yang and L.-L. Yang, "Frequency-hopping/M-ary frequency-shift keying wireless sensor networks with soft-sensing," in *1st IEEE International Conference on Communications in China (ICCC'12)*, pp. 751 – 756, 2012.

Subject Index

Author Index

W

Z